Universitat Autònoma de Barcelona

GENETIC AND PROTEOMIC STUDY OF ERCC4/XPF IN DNA REPAIR AND HUMAN DISEASES

Maria Marín Vilar

Universitat Autònoma de Barcelona

Faculty of Biosciences
Department of Genetics and Microbiology
Genome Instability and DNA Repair group

GENETIC AND PROTEOMIC STUDY OF *ERCC4*/XPF IN DNA REPAIR AND HUMAN DISEASES

DOCTORAL THESIS

Maria Marín Vilar

Universitat Autònoma de Barcelona

Faculty of Biosciences

Department of Genetics and Microbiology

Genome Instability and DNA Repair group

GENETIC AND PROTEOMIC STUDY OF *ERCC4*/XPF IN DNA REPAIR AND HUMAN DISEASES

Dissertation respectfully submitted by

MARIA MARÍN VILAR

To Universitat Autònoma de Barcelona in partial fulfilment of the requirements for the degree of Doctor of Philosophy, as per the Doctorate Program in Genetics with the International Degree Mention.

Thesis Director and Tutor,	Thesis Director,	Author,
		
Dr. Jordi Surrallés Calonge, PhD	Dr. Massimo Bogliolo, PhD	Maria Marín Vilar
Full Professor of Genetics	Associated professor of Genetics	

“There is a driving force more powerful than steam, electricity and nuclear power: the will.”

Albert Einstein

ACKNOWLEDGEMENTS

M’agradaria agrair aquest treball al meu director, Jordi Surrallés, per donar-me l’oportunitat de formar part del seu equip i per les encertades correccions, i al meu co-director, Massimo Bogliolo, per tots aquests anys que t’he tingut a la meva vora i he après de tu, que m’has fet créixer com a científica i que m’has donat la confiança per poder discutir-te obertament. T’agraeixo totes les converses sobre ciència i metaciència i mai et podré agrair prou que confiares en mi i en aquesta tesi en els trams més delicats. Per totes les partides de Scrabble que hauríem jugat en un univers alternatiu.

Agraeixo també a la resta del grup i Departament per tots aquests anys de convivència; per ajudar-me a aconseguir-ho però més especialment per formar família, per les converses extracientífiques sobre la “revolució d’octubre”, per compartir somriures i neguits i per tot el suport rebut durant els meus tetris temporals.

Òbviament, agraeixo especialment a l’equip cafè de les escales, amb totes les seves renovacions, per les converses, interessants o absolutament intranscendents, que trencaven la rutina. I a tu, Cristian, t’agraeixo “*un miler de vegades*” que també “*cantes a la vida*” com si fos una “*cançò total*”. Et desitjo que continues sempre ballant la teva pròpia banda sonora.

I would like to put into words my gratitude towards Dr Tomoo Ogi and his team at Nagoya University; for taking me in in his lab during three months and for giving me the chance to understand how science works at the other side of the world, which has provided me a wider sight on being a scientist. Thank you very much especially to Dr Nan Jia, Dr Chaowan Guo and Dr Yasuyoshi Oka for making the effort of helping me with the technical and everyday Japanese life stuff. **どうもありがとうございます.**

I am grateful to my Erasmus friends for their support along all my PhD period, for their determination and for their contagious eagerness of never stop learning no matter where they are.

A les companyes de Precàries els agraeixo haver caminat juntes amb el cap ben alt i amb dignitat i haver compartit la lluita per unes condicions laborals més justes malgrat les dificultats predoctorals.

A les de ConCiencias Barcelona, l'estimat exèrcit d'escèptiques, us agraeixo que entre tot allò que és urgent trobeu el temps per lluitar també per allò que és important. Us agraeixo compartir aquesta passió per la ciència i per creure possible una ciència deslligada dels interessos neoliberals del mercat. Us agraeixo que no claudiqueu i no us aparteu del sistema, sinó que tracteu de buscar fórmules per combatre'l. Moltes gràcies pel suport amb la tesi durant l'època més complicada i per cuidar-nos unes a altres en temps de revolta.

A totes les tesistes d'arreu amb qui he compartit els camins sinuosos dels finals de tesis i m'han fet sentir que no estava sola, a vosaltres més que a ningú, milers de gràcies. Hem fet de l'empatia la nostra arma més poderosa.

A Carles, amb qui porto creixent des de fa quasi 25 anys, i amb qui també tinc el plaer de compartir curiositats, dubtes, frustracions i emocions de la ciència; tu que sempre m'arreplegues l'ànima dels peus, gràcies per ser-hi.

Voldria dedicar aquesta tesi a Nettie Stevens (1861-1912), Charlotte Auerbach (1899-1994), Barbara McClintock (1902-1992), Rosalind Franklin (1920-1958), Anne McLaren (1927-2007), Lynn Margulis (1938-2011), Tsuneko Okazaki (1933) i a la resta de genetistes i biòlogues moleculars que el patriarcat ha volgut menysprear al llarg de la història.

I a la meva coetània Alexandra Elbakyan, creadora del Sci-Hub, per posar a l'abast de tota la comunitat científica el gruix del coneixement publicat i per la seva lluita incessant contra els gegants de les editorials. Sense tu no hauria estat possible. Gràcies per ser exemple.

"*La ciencia avanza de verdad sólo cuando desobedece, sólo cuando es rebelde."*
(Delegada zapatista de los Caracoles, 2a edición ConCiencias por la Humanidad, 2017)

"Instruïu-vos, perquè necessitarem tota la nostra intel·ligència. Emocioneu-vos, perquè necessitarem tot el nostre entusiasme. I organitzeu-vos, perquè necessitarem tota la nostra força." (Antonio Gramsci, *L'ordine Nuovo,* 1919)

ABBREVIATIONS

6-4 PPs	*6-4 photoproducts*
aa	*Amino-acid*
a-EJ	*Alternative end joining*
ATM	*Ataxia-telangiectasia*
ATR	*ATM and Rad3-related*
ATRIP	*ATR interacting protein*
BER	*base excision repair*
BLM	*Bloom syndrome RecQ-like helicase*
bp	*Base pair*
CBP	*Calmodulin binding protein*
C. elegans	*Caenorhabditis elegans*
C-NHEJ	*Canonical nonhomologous end joining*
CDK	*Cyclin-dependent kinase*
CoIP	*Coimmunoprecipitation*
CPDs	*Cyclobutane-pyrimidine dimers*
CRISPR	*Clustered Regularly Interspaced Short Palindromic Repeats*
CS	*Cockayne Syndrome*
CSA	*Cockayne syndrome WD repeat protein A*
CSB	*Cockayne syndrome protein B*

DEB	*Diepoxybutane*
DDR	*DNA damage repair*
DMEM	*Dulbecco's Modified Eagle Medium*
DTT	*Dithiothreitol*
DUBs	*Deubiquitylases*
D. *melanogaster*	*Drosophila melanogaster*
DNA2	*DNA replication helicase/nuclease 2*
DNA-PK	*DNA-dependent protein kinase*
DSB	*Double strand break*
dsDNA	*Double strand DNA*
E. coli	*Escherichia coli*
EdU	*5-ethynyl-2'-deoxyuridine*
EMA	*Ethidium Monoazyde Bromide*
EU	*5-ethynyluridine*
EV	*Empty vector*
FA	*Fanconi anemia*
FAN1	*Fanconi Associated Nuclease 1*
FBOC	*Familiar breast and ovarian cancer*
FBS	*Fetal Bovine Serum*
GFP	*Green fluorescence protein*
GG-NER	*Global genome repair of NER*
GGR	*Global genome repair*

HEK293T	*Human embryonic kidney 293T*
HhH	*Helix-hairpin-helix*
HJ	*Holliday junction*
HMGN1	*High mobility group nucleosome-binding domain-containing protein 1*
HR	*Homologous recombination*
ICL	*Interstrand crosslink*
ICLR	*Interstrand crosslink repair*
Lig1	*Ligase I*
Lig3	*Ligase III*
MH	*Microhomologies*
MMC	*Mitomycin C*
MMEJ	*Microhomology-mediated end joining*
MMR	*Mismatch repair*
MN	*Micronucleus*
NBS1	*Nijmegen Breakage Syndrome 1*
NER	*Nucleotide-excision repair*
NHEJ	*Nonhomologous end joining*
PAM	*Protospacer Adjacent Motif*
PARP1	*Poly (ADP-ribose) polymerase 1*
PCNA	*Proliferating cell nuclear antigen*
PEI	*Polyethylenimine*

EU	*5-ethynyluridine*
Pol θ	*Polymerase theta*
Polη	*Polymerase eta*
RIR	*Replication-independent repair*
RPA	*Replication protein A*
SBP	*Streptavidine binding protein*
S. cerevisiae	*Saccharomyces cerevisiae*
SILAC	*Stable isotope labeling by amino acids in cell culture*
S. pombe	*Schizosaccharomyces pombe*
SSA	*Single strand annealing*
ssDNA	*Single strand DNA*
SD	*Standard deviation*
SDSA	*Synthesis dependent strand annealing*
SEM	*Standard error of the mean*
TALEN	*Transcription activator-like effector nuclease*
TAP	*Tandem affinity purification*
TC-NER	*Transcription-couple repair of NER*
TCR	*Transcription-coupled repair*
T-loop	*Telomeric loop*
TLS	*Translesion synthesis*
TFIIH	*Transcription initiation factor IIH*
TOP1	*Topoisomerase I*

UBZ	*Ubiquitin-binding*
USP7	*Ubiquitin-specific-processing protease 7*
USP11	*Ubiquitin Carboxyl-terminal hydrolase 11*
UV	*Ultraviolet*
UV-DDB	*UV radiation-DNA damage-binding protein*
UVSSA	*UV-stimulated scaffold protein A*
vs	*Versus*
WB	*Western blot*
WCE	*Whole cell extract*
XAB2	*XPA-binding protein 2*
XFE	*Segmental Progeria*
X. laevis	*Xenopus laevis*
XP	*Xeroderma Pigmentosum*
XP-F	*Xeroderma Pigmentosum complementation group F*

Abstract

A change in an organism's DNA can affect all the aspects of its life, until the point of compromising it. To overcome this, cells have evolved sophisticated machineries of DNA damage repair. Thus, our DNA contains the necessary information to produce proteins that participate in damage recognition, binding, excision and in the reestablishment of correct genetic information. One of these proteins is the XPF endonuclease, which is the catalytic subunit of the stable heterodimer XPF-ERCC1, able to incise at the 5' side at different DNA damages. This essential protein is encoded by *ERCC4* gene and participates in multiple genome maintenance pathways including nucleotide excision repair (NER), interstrand crosslink (ICL) repair, double strand break (DSB) repair pathways such as microhomology-mediated end joining (MMEJ) and single strand annealing (SSA). XPF has also been suggested to have possible backup roles in repairing oxidative damage and in telomere maintenance besides to have a role in the response of cancer cells to chemotherapy. Considering its wide involvement in multiple DNA repair pathways, it is not surprising that *ERCC4* mutations are associated to a range of human diseases including Xeroderma Pigmentosum (XP), Segmental Progeria (XFE), Fanconi Anemia (FA), Cockayne Syndrome (CS) and several cases combined diseases of Xeroderma and Cockayne syndromes (XPCSCD). A better understanding of (i) the correlation between the pathogenic mutations and patients' phenotype and (ii) the essential DNA repair mechanisms is expected to promote a faster development of possible treatments. Here we report a detailed overview of functional studies performed with a set of cells containing pathogenic XPF mutations in a genetically homogeneous background. The selected XPF mutants, located in different domains of the protein, and the resulting human syndromes, were the following: XPF^{R153P} (XFE), XPF^{I225M} (XP), XPF^{L230P} (FA), XPF^{C236R} (CS), XPF^{R589W} (XP/XPCSCD), XPF^{R689S} (FA), XPF^{R799W} (XP/XFE-CS). Detailed functional studies include the analyses of NER pathway (UVC sensitivity, UDS and RRS) and ICLR pathway (ICL sensitivity, ICL-induced G2/M arrest and

ICL-induced chromosome fragility). Our results emphasize the importance of other factors, beyond protein position of the variant, such as protein levels, cell localization and the molecular interactions, in order to associate any XPF mutant to a clinical phenotype. In this framework, and to increase our knowledge about XPF interactions that can regulate XPF functions in the distinct DNA repair pathways, we investigated the XPF interactome. The implementation of the most advanced proteomic techniques including tandem affinity purification, co-immunoprecipitation and SILAC, coupled to mass spectrometry led us to identify a new XPF interactor involved in genome maintenance: USP11, a deubiquitinase that is known to regulate the activity of functionally related proteins such as BRCA2 or XPC. Here we prove XPF-USP11 interaction occurs irrespective of DNA damage and is DNA–independent. We also demonstrate that USP11 regulates DSB repair by SSA and possibly NER but is not involved in HR or ICLR.

Table of Contents

Table of Contents

I. INTRODUCTION 1

I.1- GENOMIC INSTABILITY AND DNA REPAIR 1

I.2- XPF PROTEIN 2

I.2.1 EVOLUTION OF XPF PROTEIN 4

I.2.2 XPF INTERACTIONS 6

I.3- XPF ROLE IN GENOMIC INSTABILITY SYNDROMES 8

I.3.1 NUCLEOTIDE EXCISION REPAIR AND PHOTOSENSITIVE SYNDROMES 8

I.3.1.1 XERODERMA PIGMENTOSUM (XP) 11

I.3.1.2 SEGMENTAL PROGERIA CASES (XFE) 11

I.3.1.3 COCKAYNE SYNDROME (CS) 12

I.3.2 INTERSTRAND CROSSLINKS REPAIR AND FANCONI ANEMIA 12

I.3.2.1 GROUP I: FA CORE COMPLEX 14

I.3.2.2 GROUP II: ID COMPLEX 16

I.3.2.3 ICL INCISION 17

I.3.2.3.1 SLX proteins: SLX1-SLX4 19

I.3.2.3.2 XPF-ERCC1 20

I.3.2.3.3 MUS81-EME1 21

I.3.2.3.4 FAN1 22

I.3.2.3.5 SNM1 nucleases: SNM1A AND SNM1B 23

I.3.2.4 GROUP III: TRANSLESION SYNTHESIS AND RECOMBINATION PROTEINS 24

I.3.3 REPLICATION-INDEPENDENT ICL REPAIR 29

I.3.4 OTHER DOUBLE STRAND BREAK SUBPATHWAYS 30

I.3.5 TELOMERE STABILITY 35

II. OBJECTIVES 37

III. MATERIALS AND METHODS 38

III.1- CELL LINES AND CULTURE 38

III.2- ESTABLISHING OF THE HEK 293T TALEN *ERCC4*-KNOCKED OUT AS THE XPF-KO BACKGROUND CELL LINE 39

III.2.1 GENERATION OF THE HEK XPF-KNOCKED OUT CELL LINE 39

III.2.2 WESTERN BLOT VALIDATION OF THE KNOCKED OUT CLONES 40

III.2.3 CHARACTERIZATION AND SELECTION OF THE XPF-KNOCKED OUT CLONE 40

III.3- GENERATION OF XPF CELL LINES 42

III.3.1 GENERATION OF THE XPF-Wt LENTIVIRAL VECTOR 42

III.3.2 GENERATION OF THE XPF-LENTIVIRAL PARTICLES AND GENETIC COMPLEMENTATION OF HEK XPF-KO CELLS 44

III.3.3 GENERATION OF THE XPF MUTANT VARIANTS 46

III.3.3.1 GENERATION OF XPF VARIANTS BY SUBCLONING 46

III.3.3.2 GENERATION OF XPF VARIANTS BY SITE DIRECTED MUTAGENESIS 47

III.4- GENERATION OF *USP11* KNOCKED OUT AND *ERCC4/USP11* DOUBLE KNOCKED OUT BY CRISPR/Cas9 TECHNOLOGY 49

III.4.1 TARGET SEQUENCE SELECTION 49

III.4.2 PRIMERS ANNEALING AND VECTOR CONSTRUCTION 50

III.4.3 CELL TRANSFECTION AND CLONE SELECTION 51

III.4.4 GENOTYPING 52

III.5- FUNCTIONAL STUDIES 53

III.5.1 UVC SENSITIVITY SURVIVAL ASSAY 53

III.5.2 UNSCHEDULED DNA SYNTHESIS ASSAY 54
III.5.3 RECOVERY OF RNA SYNTHESIS ASSAY 55
III.5.4 DEB SENSITIVITY SURVIVAL ASSAY 55
III.5.5 DEB-INDUCED G2/M CELL CYCLE ARREST 56
III.5.6 MICRONUCLEI- FRAGILITY TEST 56
III.6- PROTEIN PURIFICATION 58
III.6.1 TANDEM AFFINITY PURIFICATION 58
III.6.2 HA-PURIFICATION 58
III.6.2.1 PROTEIN BAND EXTRACTION FROM SDS GEL 60
III.7- STABLE ISOTOPE LABELING WITH AMINO ACIDS IN CELL CULTURE 61
III.8- COIMMUNOPRECIPITATIONS 63
III.9- *IN VIVO* DOUBLE STRAND BREAKS REPAIR ASSAYS 64
III.9.1 HOMOLOGOUS RECOMBINATION REPAIR ASSAY 64
III.9.2 SINGLE STRAND ANNEALING REPAIR ASSAY 66
IV. RESULTS AND DISCUSSION 68
PROJECT 1 68
IV.1- ESTABLISHING OF THE HEK 293T TALEN *ERCC4*-KNOCKED OUT AS THE XPF-KO BACKGROUND CELL LINE 68
IV.2- ANALYSES OF DIFFERENT XPF VARIANTS IN AN XPF-KO BACKGROUND 74
IV.2.1 SELECTION OF THE XPF SINGLE NUCLEOTIDE VARIANTS TO STUDY 74
IV.2.2 EXPRESSION OF THE XPF MUTANT VARIANTS IN AN XPF-KO BACKGROUND 77
IV.2.3 FUNCTIONAL ANALYSES OF XPF VARIANTS 78
IV.2.3.1 NER PATHWAY 78
IV.2.3.2 ICLR PATHWAY 84
IV.2.3.2.1 ICL- Induced G2/M arrest 85
IV.2.3.2.2 Analysis of ICL-induced chromosome fragility 87
IV.3- OVERVIEW OF THE ANALYZED XPF VARIANTS CELLULAR PHENOTYPES 89
PROJECT 2 94

IV.4- PROTEOMIC STUDY OF XPF INTERACTOME 94

IV.5- GENERATION OF THE HEK *USP11*-KO AND THE DOUBLE KO HEK *XPF/USP11* BY CRISPR TECHNOLOGY 100

IV.6- ANALYSIS OF XPF AND USP11 ROLES IN *IN VIVO* DOUBLE STRAND BREAKS REPAIR 104

IV.6.1 STUDY OF HOMOLOGOUS RECOMBINATION REPAIR 105

IV.6.2 STUDY OF SINGLE STRAND ANNEALING REPAIR 108

IV.7- UNDERSTANDING THE BIOLOGICAL IMPACT OF XPF-USP11 INTERACTION 114

V. CONCLUSIONS 116

VI. BIBLIOGRAPHY 118

ANNEX 127

Introduction

I. INTRODUCTION

I.1- GENOMIC INSTABILITY AND DNA REPAIR

The maintenance of genome integrity is crucial for the survival of cells because it ensures the faithful transmission of genetic information to the progeny and safeguards the proper functioning and survival of all the organisms. DNA is by far the most prone subcellular molecule to be threatened by lesions and yet the one that can deal better with them due to multiple DNA repair systems. The different DNA repair pathways are essential to identify DNA damage and correct it, therefore investing in genome maintenance (Hoeijmakers 2009).

Human cells have around 24,000 genes confined in 3 billion base pairs (bp). It is estimated that DNA damage occurs at a rate of 10,000 to 100,000 molecular lesions per cell per day (Vermeij et al. 2014). Thanks to the DNA repair pathways most of these lesions can be fixed but permanent changes in the DNA may occur and they are defined as mutations. If these unrepaired lesions affect critical genes, the integrity of the genome will be compromised and hence the cells' stability.

Genome instability can be induced by different DNA damage sources: exogenous physical and chemical agents and endogenous chemical genotoxic agents which are products of metabolism (Hoeijmakers 2009). Accumulation of cellular damage can lead to two different processes: ageing and cancer (Lopez-Otin et al. 2013). Ageing is produced when damage interferes with the vital processes of the cell and drives it to apoptosis or senescence, while the hallmark of cancer is the accumulation of damage that confers aberrant proliferation advantages to certain cells which become immortal.

DNA repair mechanisms have evolved to detect the damage and remove it, therefore ensuring the integrity of the genome by several multiple protein pathways such as base-

excision repair (BER), nucleotide-excision repair (NER), transcription-coupled repair (TCR), nonhomologous end joining (NHEJ), homologous recombination (HR) and interstrand cross-link (ICL) repair. This wide machinery evidences the importance of investment in genome maintenance and cell survival.

I.2- XPF PROTEIN

XPF is a protein encoded by *ERCC4* gene and also receives the alias of FANCQ. It was identified as the defective gene in Xeroderma Pigmentosum complementation group F (XP-F) (Sijbers et al. 1996) and its cDNA complemented the human XPF cells and the deficient rodent NER cells *Ercc4* and *Ercc11* (Yagi et al. 1998). The human *ERCC4* is located in 16p13.1-p13.2 and encodes for a 916 amino-acid (aa) protein (Brookman et al. 1996) which forms a stable heterodimer with ERCC1 in order to constitute a structure-specific endonuclease that incises in the 5' side of DNA damage. This dependent stabilization is reciprocal; the heterodimer is found to be formed stechiometrically 1:1 and it is essential for life, since the complete inactivation of the *ERCC4* gene in humans seems to be incompatible with postnatal survival (Osorio et al. 2013; Tian et al. 2004).

XPF is organized in three different domains: a N-terminal helicase domain (residues 15-647), a central nuclease domain (residues 667-824) and a C-terminal helix-hairpin-helix (HhH) domain (residues 848-916) (Klein Douwel et al. 2017) (Figure 1).

Figure 1: Domain organization of XPF and ERCC1 (adapted from (McNeil and Melton 2012)).

The N-terminal helicase domain is homologous to superfamily II helicases and contributes to DNA binding activity, the nuclease domain of XPF is responsible for the catalytic activity of the protein (Tsodikov et al. 2005), and the C-terminal HhH domain works as a scaffold for the correct folding of ERCC1 to form a functional endonuclease (Tripsianes et al. 2005) besides to be also involved in DNA substrate binding. Residues confined in 224-297 from ERCC1 protein and 825-916 from XPF are the regions responsible for the stable heterodimer formation (de Laat et al. 1998).

From the two components of the heterodimer, XPF specifically recognizes single strand DNA (ssDNA) through the N-terminal helicase domain, while ERCC1 rather binds to dsDNA through its hairpin region. This different substrate specificity allows the heterodimer to bind to ss/double strand DNA (dsDNA) substrate and dictates the incision position during the DNA repair (Das et al. 2017).

Previously, a time-consistent model proposed that the two HhH domains of the two proteins were binding to ssDNA and the central domain of ERCC1 bound ssDNA/dsDNA junctions with a preference for 5' single-stranded overhang (Tsodikov et al. 2005). Notwithstanding, it has been recently elucidated that ERCC1 specifically recognizes dsDNA through its HhH domain, and that the C-terminal heterodimer complex binds more tightly to the sites with a ss-dsDNA junction, such as bubble and splayed arm substrates than to either dsDNA or ssDNA alone. In fact, the two motifs of the HhH domain form a cavity where a guanine base can be bound. Apparently, there is a sequence dependence in the recognition of the damaged DNA, being guanine the most prone to be recognized, followed by cytosine and thymidine, and leaving adenine as the less recognized one.

The two HhH domains of XPF and ERCC1 have been solved by crystallography and the dimer structure consists of a wide network of hydrophobic interactions between the two proteins that make them to mutually stabilize one another (Croteau et al. 2008) (Figure 2).

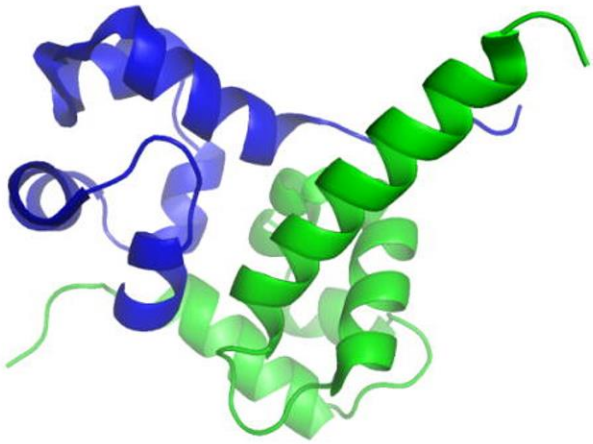

Figure 2: Crystal structure of the human C-terminal HhH_2 domain complex of XPF (blue) and ERCC1 (green) (adapted from (Croteau et al. 2008)).

Considering this ss-dsDNA junction, XPF would bind to the 5' site of the ssDNA and this ssDNA would be linked by the 3' to the dsDNA that ERCC1 would recognize. Putting this all together, an important idea to emphasize would be that the XPF-ERCC1 would be positioned according to the DNA structure and in a sequence dependent way, which would moreover dictate the cleavage efficiency of the endonuclease heterodimer (Das et al. 2017).

I.2.1 EVOLUTION OF XPF PROTEIN

XPF protein seems to be highly conserved during evolution; its structure reveals similarities in archaeal (Rouillon and White 2011) and in eukarya (Barve et al. 2013), proving its essential role for the cell maintenance. Mammalian XPF shares a degree of homology with Rad1, a protein of 1,100 aa from *Saccharomyces cerevisiae (S. cerevisiae)*; Rad16, a protein of 892 aa from *Schizosaccharomyces Pombe (S.pombe)* and MEI-9, a 946 aa *Drosophila melanogaster (D. melanogaster)* protein that ranges from 28% homology with Rad1 to 40% of MEI-9 (Brookman et al. 1996) (Figure 3).

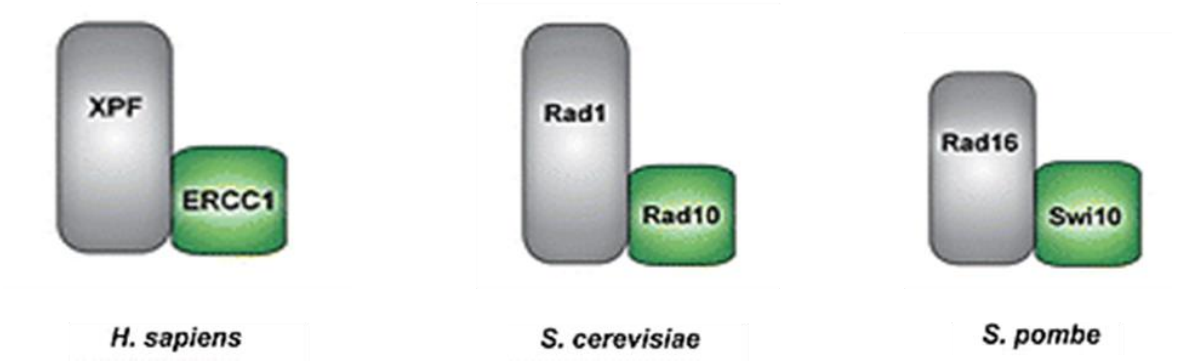

Figure 3: Heterodimeric associations of mammalian XPF and its homologous in yeast (adapted from (Ciccia et al. 2008)).

Rad1 and Rad16 are essential components in yeast. Rad1 activity requires to be bound in a heterodimer to Rad10 by its C-terminal regions (809-997 aa of Rad1 and 90-210 aa of Rad10). This complex would be the homologous to the mammalian XPF-ERCC1 and it shows ssDNA endonuclease activity, cleaving at 3' of the ssDNA at the junction with dsDNA, with a clear preference for splayed-arm DNA substrates (Ciccia et al. 2008). This complex is an essential component of NER in yeast, it interacts with Rad14, the homologous of mammalian XPA protein from NER (de Laat et al. 1998), and it has also been proved to be involved in the removal of the two non-homologous 3'-ended ssDNAs that are formed as intermediates in single strand annealing (SSA) (Prakash and Prakash 2000). Despite all these similarities, the XPF interaction site of ERCC1 is different from the Rad1-binding site of Rad10. XPF interaction site in ERCC1 comprises aa 224-297, which would be out of the homologous region in Rad10; the correspondent region of XPF-binding in Rad10 comprises aa 98-214. This shows an extended C-terminal region in mammalian ERCC1, which is composed by the double HhH motif (residues 236-289). This HhH motifs have been found in many DNA break processing enzymes like in UvrC NER protein of *Escherichia coli* (*E. coli*) or *S. pombe* and contribute to DNA binding (de Laat et al. 1998).

Rad16 is the ortholog of XPF in *S. pombe* and it forms a complex with Swi10/Rad23 (ERCC1). Rad16 promotes recombination repair of broken replication forks without using sister chromatids repair, but ectopic donor sequences, thus contributing to genome stability.

Rad1 and Rad16 seem to not have any role in meiosis while Mei-9, the XPF NER-homologue in *D. melanogaster* is also essential for resolution of meiotic chiasmata. In *Caenorhabditis elegans* (*C. elegans*), XPF shares roles with other nucleases involved in meiosis such as Mus81 and SLX-1 (Mastro and Forsburg 2014).

I.2.2 XPF INTERACTIONS

Besides the already explained interaction of XPF with ERCC1, the nuclease heterodimer is able to stablish temporal interactions with other proteins to participate in the different damage repair pathways in which it is seen to be involved. XPF interactome had not been deeply investigated but some important interactor partners are already unrevealed and, considering the relevance they can have to understand the different pathways where XPF works, potentially more will arise.

One of these important interactions is established with SLX4, a protein involved in repairing the damage produced by ICL causing agents, topoisomerase I (TOP1) inhibitors and in Holliday junction (HJ) resolution. This protein works as a platform for several nucleases in ICL repair (ICLR). Two interaction sites are described between XPF and SLX4 (Figure 4): the BTB domain and the MUS312/MEI9 interaction-like, or MLR domain, one ensuring the recruitment of XPF to the damage sites and another one enhancing its nuclease activity (Y. Kim 2014). The BTB domain of SLX4 is not essential for the SLX4 and XPF interaction, the binding is established through the SLX4 N-terminal segment MLR domain (Y. Kim et al. 2013). Recent studies performed in *Xenopus laevis* (*X. laevis*) suggest the interaction takes place most likely between the MLR domain and the 230 leucine of human XPF aa sequence but there is a second interaction site in BTB domain of SLX4 and the residues 323-326 of XPF, which is transient but important to promote XPF nuclease activity (Klein Douwel et al. 2017).

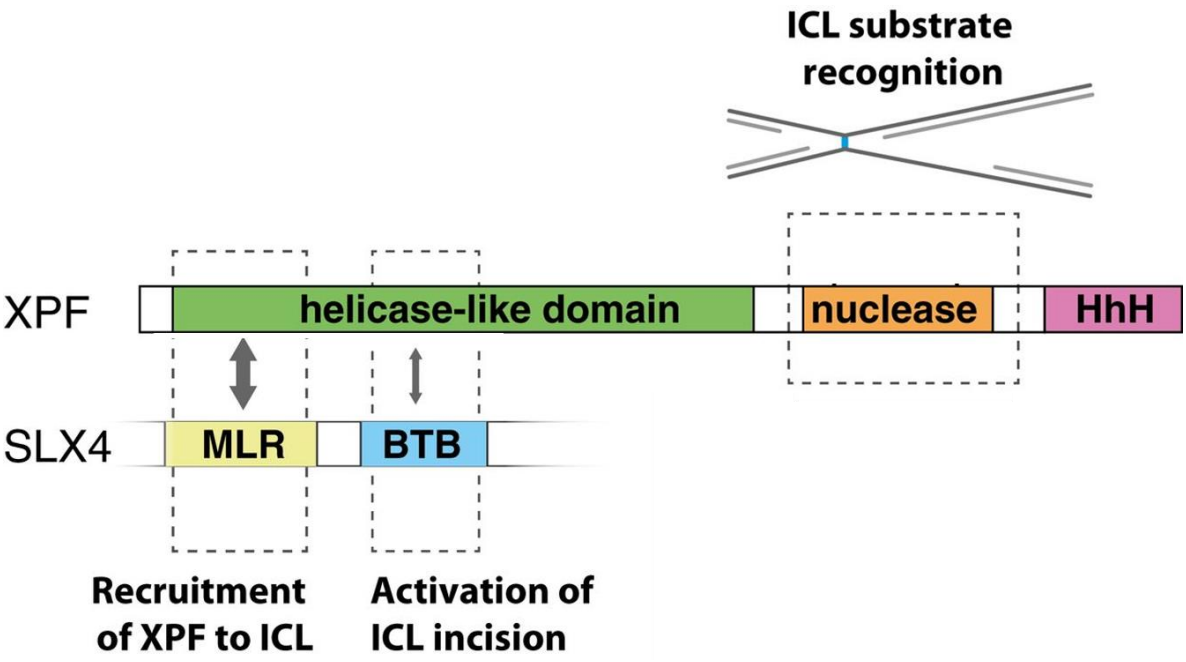

Figure 4: Model of XPF-SLX4 domains interactions for ICLR (adapted from (Klein Douwel et al. 2017)).

SLX4 is a SUMO E3 ligase able to SUMOylate itself and XPF, although this post translational modification does not seem to interfere in any of these two proteins ICLR ability (Guervilly et al. 2015).

The replication protein A (RPA) is the major protein that binds to ssDNA in eukaryotic cells. It prevents the ssDNA from winding back on itself or forming secondary structures during replication. RPA recruitment to ssDNA stimulates XPF-ERCC1 activity and selectively permits the endonuclease to incise at 5' of the fork junction when there is a nascent leading strand (Matsunaga et al. 1996). Therefore, RPA is considered an XPF interactor partner (Abdullah et al. 2017). In fact, a direct interaction between XPF and RPA has been proved in the presence of DNA bubble substrates (Bessho et al. 1997) which explains how RPA orientates properly XPF-ERCC1 on the DNA substrate.

The XPF-ERCC1 heterodimer physically interacts with XPA, another protein from NER pathway, but in this case it does it through ERCC1 instead of XPF subunit. The central

domain of ERCC1 is structurally homologous to the XPF nuclease domain but it differs with it in the presence of a grooved lined with basic aromatic residues that interact with XPA protein. Consequently, ERCC1, and therefore, XPF heterodimer, is connected to the NER machinery through XPA (Su et al. 2012).

Due to the wide range of processes where XPF is involved, it is reasonable that more interacting partners will come out.

I.3- XPF ROLE IN GENOMIC INSTABILITY SYNDROMES

The XPF-ERCC1 heterodimer participates in multiple genome maintenance pathways, such as NER (Sijbers et al. 1996), ICLR (Damia et al. 1996), an alternative end joining (a-EJ) also known as microhomology-mediated end joining (MMEJ) (Ahmad et al. 2008), the SSA branch of double strand breaks (DSB) repair (Ahmad et al. 2008) and telomere maintenance (Zhu et al. 2003). Moreover, XPF has been found to have possible backup roles in repairing oxidative damage and DNA breaks with damaged ends (Scharer 2017). Considering its wide involvement in DNA repair machinery, it is not surprising the range of human diseases which are associated with mutations in XPF-ERCC1 heterodimer.

I.3.1 NUCLEOTIDE EXCISION REPAIR AND PHOTOSENSITIVE SYNDROMES

NER is one of the most versatile DNA damage repair pathways. It is involved in the removal of lesions caused by ultraviolet (UV) radiation like cyclobutane-pyrimidine dimers (CPDs) and 6-4 photoproducts (6-4 PPs), several natural and induced bulky chemical adducts, intrastrand crosslinks caused by some drugs and ROS-generated cyclopurines. All of these lesions distort the DNA double helix and must be removed to allow a proper DNA replication (Marteijn et al. 2014).

NER is divided in two subpathways (Figure 5): global genome repair (GGR) and TCR, which differ in the damage recognition process but share the same mechanism to incise at both sides of the lesion, repair and ligate the DNA gap.

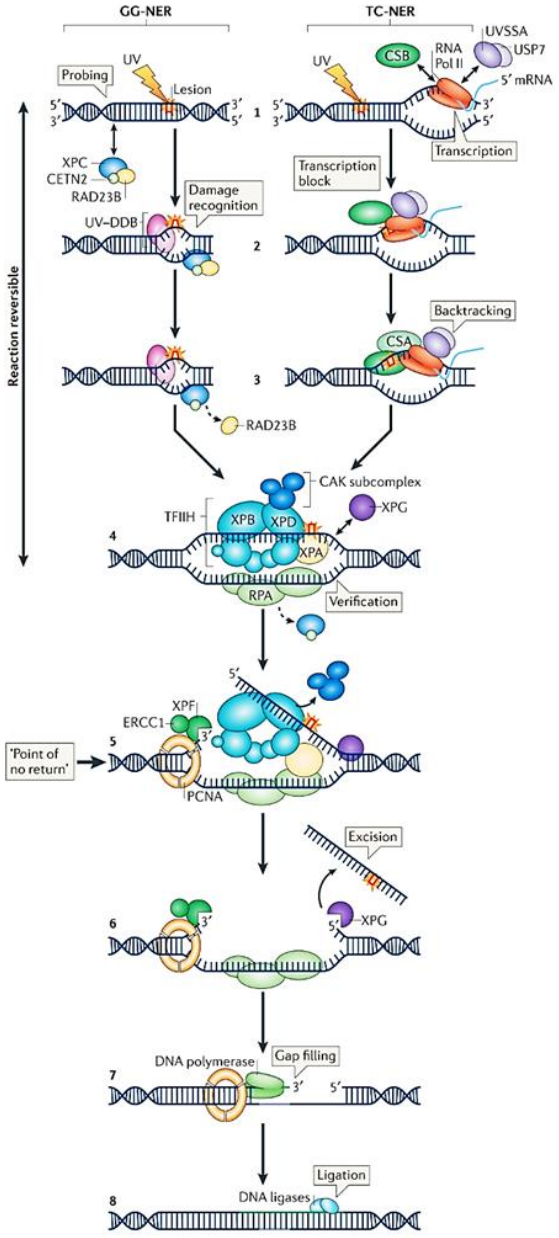

Figure 5: NER pathway (Marteijn et al. 2014).

In GGR subpathway, the entire genome is probed by the protein sensor XPC in association with RAD23B and CETN2 to find any helix distortion (Sugasawa et al. 1998). As some of the UV induced lesions just mildly destabilize the DNA helix, the XPC sensor is unable to detect them and requires the help of the UV radiation-DNA damage-binding protein (UV-DDB) complex, which comprises DDB1 and DDB2 (Chu and Chang 1988). In contrast, TCR subpathway is activated when the UV-induced lesions arrest the transcriptional machinery; the RNA Pol II stalls at the damaged site and recruits the proteins Cockayne syndrome WD repeat protein A (CSA or ERCC8) and the Cockayne syndrome protein B (CSB or ERCC6) (Fousteri et al. 2006). Both proteins are required for the recruitment of NER factors and some TCR-specific proteins such as UV-stimulated scaffold protein A (UVSSA), ubiquitin-specific-processing protease 7 (USP7) (X. Zhang et al. 2012), XPA-binding protein 2 (XAB2) (Kuraoka et al. 2008) and high mobility group nucleosome-binding domain-containing protein 1 (HMGN1) (Fousteri et al. 2006). It is thought that CSB is the protein involved in the backtracking that the RNA Pol II experiences when it is stalled at the lesion site, leaving it accessible for the rest of the complexes to be recruited for the damage repair (Sigurdsson et al. 2010).

Once the damage is recognized, the two molecular subpathways converge into a single one and the transcription initiation factor IIH (TFIIH or XPB) complex is recruited. The two helicases of this protein complex, XPB and XPD, extend the open DNA around the lesion in opposite directions. XPA protein binds to them and is able to detect distortions in the ssDNA, contributing to the damage verification. Following damage verification, the unwound DNA strand gets covered by ssDNA binding RPA and XPA recruits XPF-ERCC1 heterodimer by binding to ERCC1 (Tsodikov et al. 2007; Volker et al. 2001). This endonuclease complex, whose specificity is stimulated by RPA (Matsunaga et al. 1996), binds to the damaged strand to create an incision 5’ to the lesion. Right after the lesion the trimeric proliferating cell nuclear antigen (PCNA) ring is loaded (Hutton et al. 2010) and recruits the polymerases which will fill the gap from the excision. The 5’ incision sets the machinery in a “point of no return”, as the damaged DNA strand is already cleaved by one site and the process must move onwards to avoid the creation of damaging intermediates. Next step is the XPG 3’ incision to the lesion which leaves a gap in the damaged strand of 22-30 nucleotides. The

gap filling is provided by the DNA Pol δ, DNA Pol ε or DNA Pol κ and the process ends with the sealing of the nick by the DNA ligase 1 or DNA ligase 3 (A. R. Lehmann 2011).

I.3.1.1 XERODERMA PIGMENTOSUM (XP)

ERCC4 is also known as *XPF* because it was identified as the defective gene in complementation group F of Xerodema Pigmentosum (XP) (Sijbers et al. 1996), an autosomal recessive syndrome with 100% penetrance characterized by extreme photosensitivity and a 10,000-fold increased risk of skin cancers due to failure to repair DNA lesions produced by UV light (Gregg et al. 2011). Ocular abnormalities and increased risk of cancers of the oral cavity are also very common among the patients (A. R. Lehmann et al. 2011). Despite XP is more frequently diagnosed in Asian patients (Imoto et al. 2013), there are few Caucasians cases with mild UV sensitivity and no skin cancer but presenting acute neurological syndromes such as recessive cerebellar ataxia and chorea (Carre et al. 2017). There have been described eight XP complementation groups (XP-A to XP-G and XPV); proteins from XP-A to XP-G are involved in the repair of the UV lesions while XPV is involved in DNA replication bypassing the UV-damage. XP patients of group F have mild XP symptoms and a reduced level of nuclear XPF indicating that its mutations promote mislocalization of the heterodimer XPF-ERCC1 to the cytoplasm of cells (Ahmad et al. 2010) and lead to insufficient levels of the endonuclease to complete NER functions.

I.3.1.2 SEGMENTAL PROGERIA CASES (XFE)

Few cases described patients characterized by a progeria-like phenotype produced by a characteristic failure of the mutant XPF protein to properly translocate to the nucleus, likely through aggregation of the protein in the cytoplasm, and being avoided to be recruited to sites of active NER. The very low levels of nuclear XPF were apparently insufficient to support either NER or ICL. The patients presented severe photosensitivity, neurological and musculoskeletal abnormalities and hematopoietic symptoms (Mori et al. 2018; Niedernhofer et al. 2006).

I.3.1.3 COCKAYNE SYNDROME (CS)

Some XPF mutations can produce Cockayne Syndrome (CS), a recessive disorder characterized by neurological and developmental abnormalities, growth and mental retardation, microcephaly, premature ageing and abnormal skin photosensitivity that does not lead to pigmentation changes or skin cancer (Kleijer et al. 2008).

Four subtypes of CS have been discriminated according to the type of onset and rate of progression. Molecularly, CS patients are diagnosed by a reduction of recovery of RNA and DNA synthesis in absence of UV sensitivity in fibroblasts following UV irradiation (He et al. 2017).

There are rare CS variants that combine features of CS and XP and receive the nomenclature of XPCSCD. These cases present severe UV sensitivity and cancer predisposition typical from XP and developmental abnormalities which are common in CS patients (Kashiyama et al. 2013; Natale and Raquer 2017).

I.3.2 INTERSTRAND CROSSLINKS REPAIR AND FANCONI ANEMIA

One of the most dangerous DNA lesions are the ICLs, since they covalently link the two strands of the DNA. These ICL block the DNA molecular machinery by inhibiting the strand separation which leads to the block of replication, transcription and segregation of DNA. About 40 unrepaired ICLs can kill a mammalian cell (Dronkert and Kanaar 2001). ICLs provoke a challenge for the DNA repair mechanisms because of the involvement of the two strands (McHugh et al. 2001), and, aside from leading to the cell death, they can induce mutations and DNA rearrangements which could drive to uncontrolled cell growth and tumor formation.

ICLs can be produced by the products of the cellular metabolism or by external agents like mitomycin C (MMC), diepoxybutane (DEB), cisplatin, nitrogen mustard and psoralens (Muniandy et al. 2010).

The detection and repair of these lesions require strictly organized multiple DNA repair pathways such as Fanconi anemia (FA) pathway, HR, translesion synthesis (TLS) and NER.

FA is a genetically and phenotypically heterogeneous disorder caused by germ-line mutations in genes that cooperate in the repair of DNA ICL. It is a rare disease with an incidence of 1-9 in 1,000,000 live births and an estimated carrier frequency of 1 in 250 in most populations (Mathew 2006). It was first reported by Guido Fanconi (1927) and its clinical features (all of incomplete penetrance) include bone marrow failure, pancytopenia, hyperpigmentation, skeletal malformations, small stature and urogenital abnormalities and cancer predisposition. FA cellular phenotype is characterized by extreme sensitivity to DNA cross-linking agents and chromosomal fragility (Bogliolo and Surralles 2015) and it is caused by mutations in any of the, until the date hereof, 22 identified complementation groups: *FANCA, FANCB, FANCC, FANCD1 (BRCA2), FANCD2, FANCE, FANCF, FANCG (XRCC9), FANCI, FANCJ (BRIP1), FANCL (PHF9), FANCM, FANCN (PALB2), FANCO (RAD51C), FANCP (SLX4), FANCQ (XPF), FANCR (RAD51), FANCS (BRCA1), FANCT (UBE2T), FANCU (XRCC2), FANCV (REV7)* and *FANCW (RFWD3)* (Gueiderikh et al. 2017; Knies et al. 2017) from which twenty-one shows autosomal inheritance while *FANCB* maps to the X chromosome. It is expected that more associated genes will arise, although there is a controversy about whether its designation as FA genes comes along with the initial requirement of its association with a clinical case, bone marrow failure, chromosome fragility and malformations to be called FA genes. FA genes which mutations do not lead to bone marrow failure would be confined into FA-like genes while genes which biallelic mutations carriers are not linked to FA disease phenotype would be designated as FA-associated genes (Bogliolo and Surralles 2015) (Figure 6).

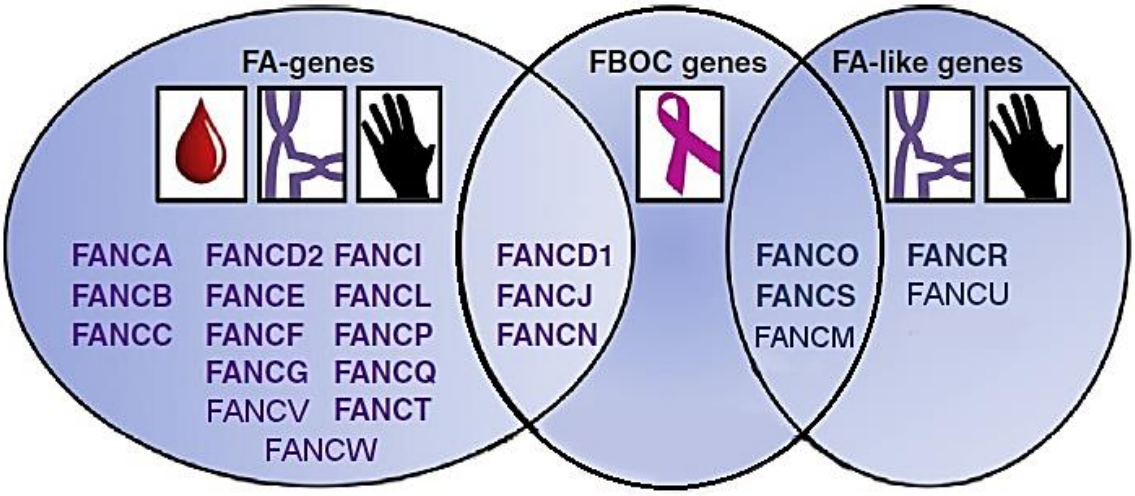

Figure 6: Diagram of the relationship of FA-genes (biallelic mutations in these genes produce bone marrow failure, chromosome fragility and malformations), familiar breast and ovarian cancer (FBOC) genes and FA-like genes (biallelic mutations in these genes do not cause bone marrow failure) (Bogliolo et al. 2017; Catucci et al. 2017) (adapted from (Bogliolo and Surralles 2015)).

I.3.2.1 GROUP I: FA CORE COMPLEX

FA proteins from the twenty-two complementation groups reported have been divided in three functional groups.

Seven FA proteins (FANCA, FANCB, FANCC, FANCE, FANCF, FANCG, and FANCL) and six FA-associated proteins (FANCM/FAAP250, FAAP100, FAAP24, FAAP20, FAAP16 and FAAP10) constitute the nuclear FANCore complex. The core complex forms a high molecular weight E3 ubiquitin ligase complex, based on the ubiquitin ligase domain of FANCL. This complex function is to activate through monoubiquitination a second heterodimer formed by FANCD2 and FANCI (ID complex). The key event in initiating ICLs repair lies on the monoubiquitination of FANCD2, which is achieved through the functions of the gene product of *FANCT*, an E2 enzyme that connects the ubiquitin to the substrate, the gene product of *FANCL,* an E3 ubiquitin ligase, and the E1 ubiquitin-activating enzyme that activates the ubiquitin (van Twest et al. 2017). A mutation in any of the components of the FANCore or FANCT drives to an impairment in the monoubiquitination of the ID complex,

with the exception of mutations in FANCM, whose cells still show a residual FANCD2 monoubiquitination (Singh et al. 2009) (Figure 7).

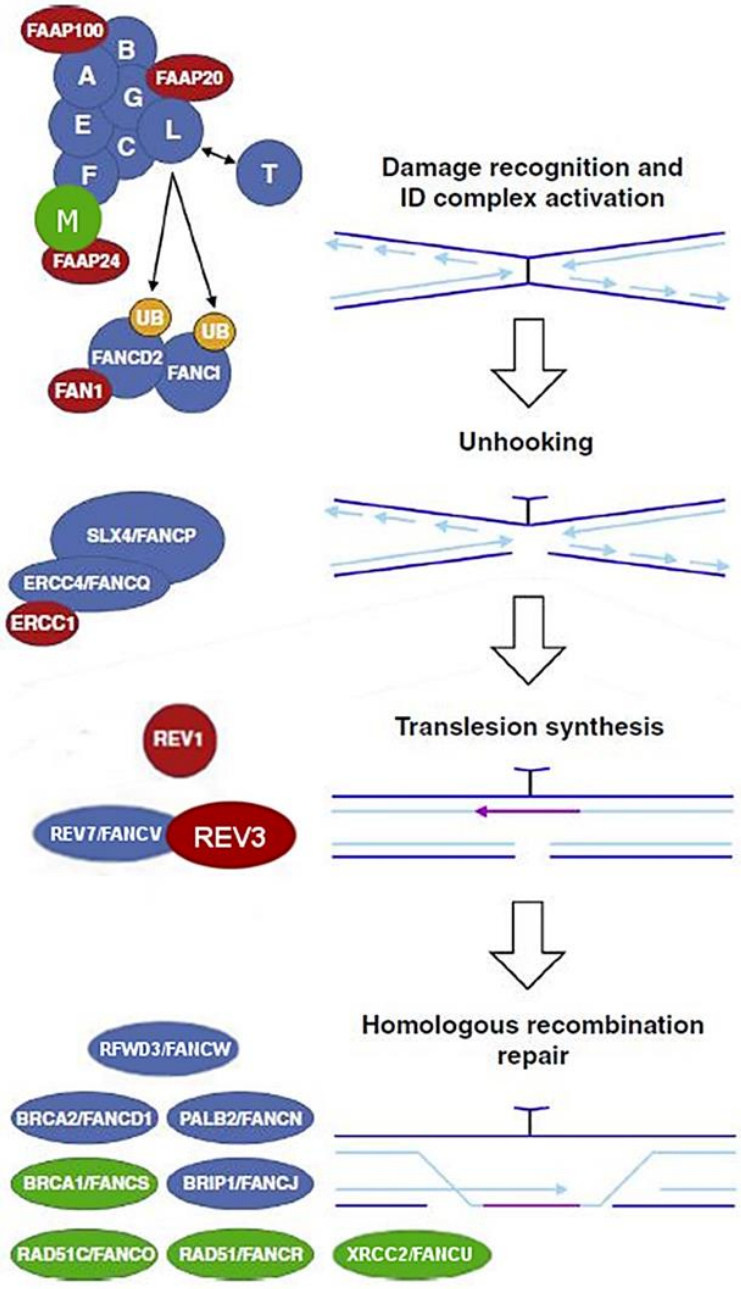

Figure 7: The FA pathway of ICLR. Blue: proteins encoded by FA genes; green: proteins encoded by FA-like genes; red: FA-associated proteins (adapted from (Bogliolo and Surralles 2015)).

I.3.2.2 GROUP II: ID COMPLEX

As already mentioned, group II is formed by FANCD2 and FANCI proteins associated in the so called ID complex, activated upon DNA damage by interdependent monoubiquitination. A recently discovered Tower domain of FANCD2 is crucial for a direct interaction with the DNA from the arrested replication fork, being this interaction the one that triggers the subsequently monoubiquitination (C. C. Liang et al. 2016).

Multiple constituents of the FA pathway (FANC-A, -G, -M, -D1 and the two components of ID complex) are phosphorylated by both ataxia-telangiectasia (ATM) and ATM and Rad3-related (ATR) kinases. While ATM coordinates the cellular response to DNA DSBs by phosphorylating substrates to halt cell cycle progression and proceed to damage repair, ATR kinase is activated in response to replicative stress. The activation of the FA/BRCA pathway starts with disassociation of the ID2 heterodimer, which is enhanced by ATM/ATR-mediated phosphorylation of FANCI (Boisvert and Howlett 2014).

The monoubiquitinated form of FANCD2 relocates in nuclear foci that colocalize with γH2AX in response to damage: ATR phosphorylates H2AX at stalled replication forks to recruit FANCD2 to DNA damage (Bogliolo et al. 2007).

The USP1:UAF1 protein dimer is required then for the ID deubiquitination, a crucial step to complete the DNA repair process and the rescue of the stalled replication forks (Gueiderikh et al. 2017; Q. Liang et al. 2014). UAF1 protein binds and activates the ubiquitin-specific protease USP1 (Cohn et al. 2009). When the DNA damage repair is completed, the ID complex must be deubiquitinated in a critical step for the ICLR executed by USP1 deubiquitinase (Figure 8). USP1 levels are regulated at transcription level and they are highest when cells exit S phase or when the cell cycle is restored after DNA damage (Nijman et al. 2005). The lack of de-ubiquitination of the ID complex also produces ICL sensitivity, therefore suggesting that both monoubiquitination and deubiquitination of the complex are crucial steps for the pathway (J. M. Kim et al. 2009).

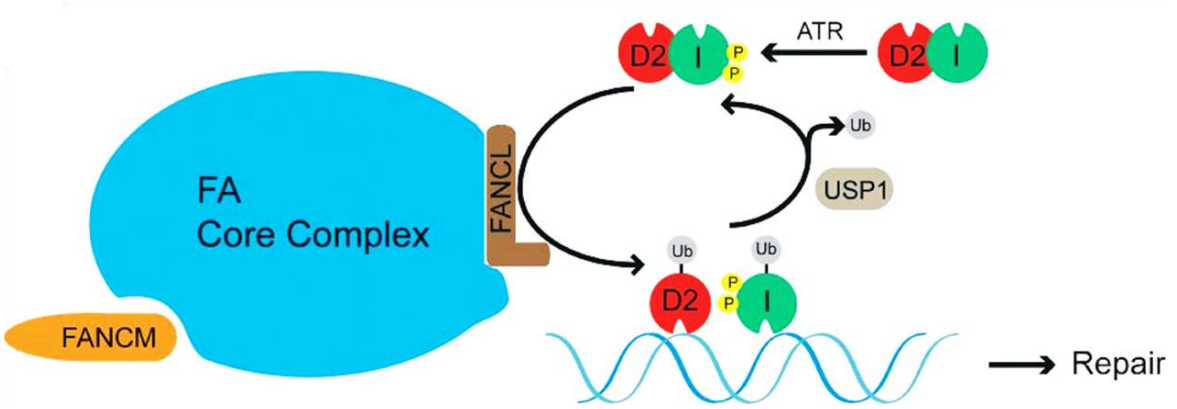

Figure 8: After the DNA damage, FANCI is phosphorylated and the ID complex is monoubiquitinated by FANCL. The ID complex is then able to be recruited to the chromatin to promote DNA repair. After its action, ubiquitination is removed by USP1 to recycle the ID complex (adapted from (Crossan and Patel 2012)).

I.3.2.3 ICL INCISION

The principal ICLR pathway takes place in S phase of the cell cycle. Current models propose that the mechanism is initiated when two DNA replication fork collide with the linked strands and generate a new structure in which the leading strands stall about 20-40 nucleotides from the crosslink (Raschle et al. 2008) (Figure 9). One of the forks then advances up to a one nucleotide from the crosslinked base and stalls again (Knipscheer et al. 2009). The process is followed by the action of endonucleases involved in dual incisions on either side of the crosslink and “unhooks” it.

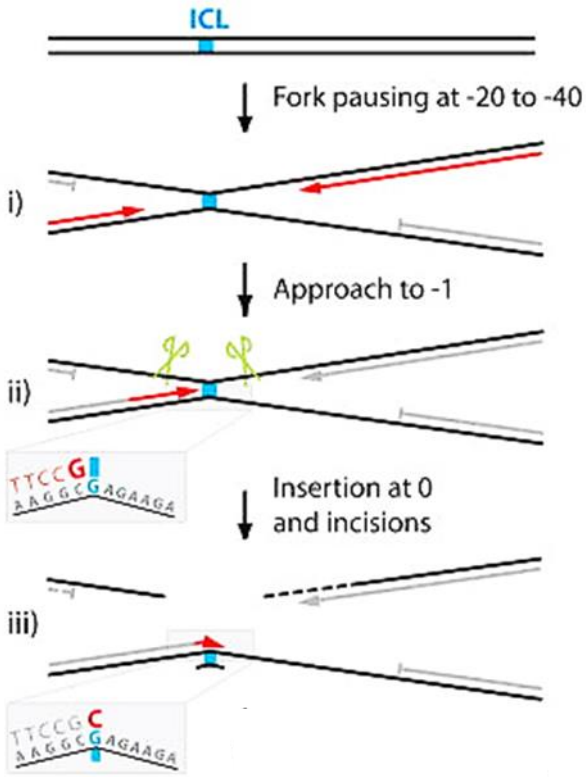

Figure 9: Representation of fork collision and incisions in ICL. The replication fork collides with the linked strands and gets initially arrested at -20 to -40 from the crosslink. Then approaches to it while one strand is incised at both sides of the crosslink. Insertion at 0 allows the extension of the nascent strand (adapted from (Knipscheer et al. 2009)).

The Unhooking step performed by proteins involved in dual incisions on either side is a fundamental step in ICLR of FA/BRCA pathway. Following the monoubiquitination of the ID complex six different endonucleases are involved in ICLR: SLX1-SLX4, XPF-ERCC1, MUS81-EME1, FAN1, SNM1A and SNM1B. These nucleases have different preferences for the different X-shape incisions substrates that the crosslink causes when the replication forks are stalled.

I.3.2.3.1 SLX PROTEINS: SLX1-SLX4

SLX4 is a large protein of about 200 KDa described as a platform where FANCQ/XPF-ERCC1, MUS81-EME1 and SLX1 nucleases can dock (Figure 10) to perform their roles in repairing DNA damage induced by ICLs or TOP1 inhibitors, in HJ resolution and telomere maintenance (Sarkar et al. 2015).

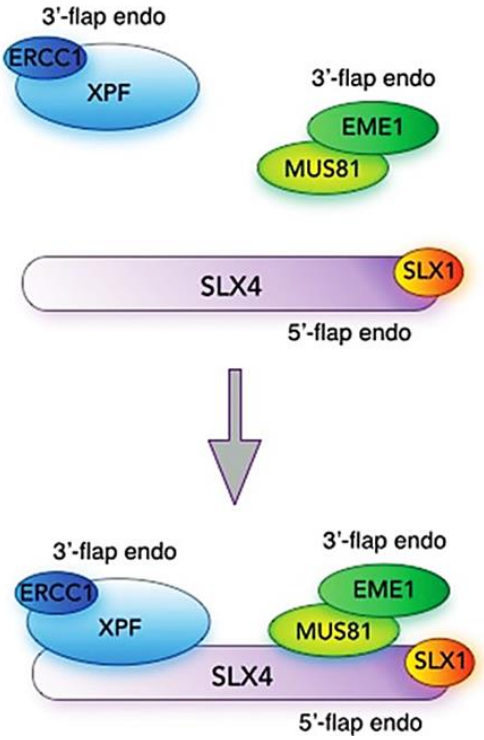

Figure 10: SLX4 is a platform for the formation of the SLX1-SLX4-MUS81-EME1-XPF-ERCC1 complex (adapted from (West et al. 2015)).

HJ are defined as four branched DNA structures that arise as intermediates of HR resolution. These intermediates must be correctly repaired to allow proper segregation during mitotic division (West et al. 2015). SLX4 contains two tandem UBZ4-type domains: UBZ-1 and UBZ-2. UBZ-1 is the required domain to recognize a poly-ubiquitylated protein at DNA damage sites and the proper recruitment of the protein to these sites, while UBZ-2 is needed for the resolution of HJ (Lachaud et al. 2014). It is the protein in charge of orchestrating the cooperation of the involved nucleases (SLX1, MUS81 and XPF) and this structure specific selective endonuclease is called SMX (Wyatt et al. 2017).

SLX1 is the catalytic subunit of the SLX4-SLX1 structure-specific endonuclease. Studies were SLX1 was depleted showed a very mild sensitivity to cross-linking agents, therefore showing that the SLX1-SLX4 heterodimer is not the crucial endonuclease for the unhooking but acts as a platform recruiting other nucleases. Despite being a promiscuous endonuclease able to cut a wide variety of DNA substrates like splayed arms, 5' flaps, 3' flaps and HJ, it has a preference for 5' flaps generated on the 5' side of the crosslink (Saito et al. 2012), and it incises them at the ssDNA-dsDNA junction when the leading strand has been extended to the -1 position.

I.3.2.3.2 XPF-ERCC1

Cells lacking FANCQ/XPF-ERCC1 showed a strong ICLR impairment that was restored after genetic complementation with wild type cDNA (Bogliolo et al. 2013). The physical interaction between the N-terminus of SLX4 and XPF is critical for the unhooking (Crossan et al. 2011; Hodskinson et al. 2014) and almost the entire SF2 helicase-like domain of XPF is required for the interaction (K. Hashimoto et al. 2015). Loading of XPF-ERCC1 to the crosslink was reduced in the absence of SLX4, but this did not occur in the other way around, indicating that SLX4 leads XPF-ERCC1 to the stalled replication forks (Klein Douwel et al. 2014). Some mutations found in XPF disrupt the function of this selective endonuclease in the repair of ICL without compromising its role in NER, suggesting that different mutations in the same nuclease can lead to malfunction in the different DNA repair mechanisms (Bogliolo et al. 2013).

The most efficient substrate incision structure from XPF-ERCC1 is the "splayed arm" (Figure 11). XPF cuts the DNA duplex at the base of the 3' arm. It also cuts other structures like 3' flap but its efficiency is considerably reduced especially when the leading strand is present in the junction.

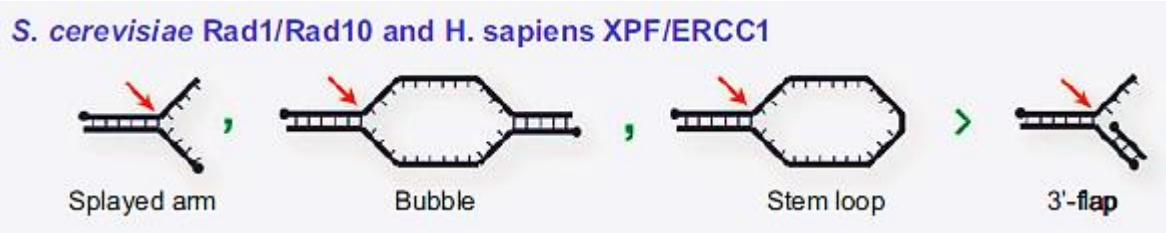

Figure 11: Substrate specificity of XPF/ERCC1. The preferential structures of the endonuclease are splayed arms, bubbles and stem loops, following by 3'-flap structures. Red arrows indicate the sites of cleavage (modified from (Ciccia et al. 2008)).

Apparently, incisions on both sides of the crosslink would be necessary for its correct removal, therefore another nuclease needs to cut at the 3' side, unless XPF-ERCC1 is able to cut at both sides. The presence of a nascent leading strand, or a lagging strand or both strands inhibits the action of the XPF-ERCC1 but it is now unrevealed how RPA protein selectively stimulates XPF-ERCC1 to overcome its inhibition in the presence of the nascent leading strand. Notwithstanding, RPA does not stimulate XPF-ERCC1 cleavage on fork substrates containing a nascent lagging strand; on the contrary, RPA occupation of the 3'-flap region of the fork while there is a nascent lagging strand at the 5'-flap region prevents XPF-ERCC1 to recognize the fork junction (Abdullah et al. 2017).

XPF-ERCC1 is a member of the XPF/MUS81 protein family and regarding their structure and function similarities there is probably a competition between XPF and MUS81 endonucleases to bind to SLX4 (I. M. Munoz et al. 2009). It has been argued about the importance of the individual contributions of the endonucleases and although this issue is still not completely solved, XPF-ERCC1 seems to be the main endonuclease for the unhooking (Klein Douwel et al. 2017). It has recently been discovered that the ubiquitin-like protein UHRF1 is involved in the recruitment of MUS81-EME1 and XPF-ERCC1 for the unhooking although the complete picture is still unclear (S. Hashimoto et al. 2016).

I.3.2.3.3 MUS81-EME1

MUS81 is the catalytic subunit of the MUS81-EME1 heterodimer that belongs to the XPF/MUS81 nuclease family. It has a preference for the 3' flap structures that contain a 5'

end within 4 nucleotides of the flap junction; if the 5' end is located more than 5 nucleotides away from the ICL, MUS81 cannot cleave this DNA structure (Figure 12) (Ciccia et al. 2008). Mutations in MUS81-EME1 were less sensitive to ICLs than those in XPF-ERCC1 heterodimer and this sets aside the action of MUS81 to a particular subset of ICL DNA intermediates and demonstrates that this heterodimer endonuclease plays a secondary role in crosslinks repair (J. Zhang and Walter 2014).

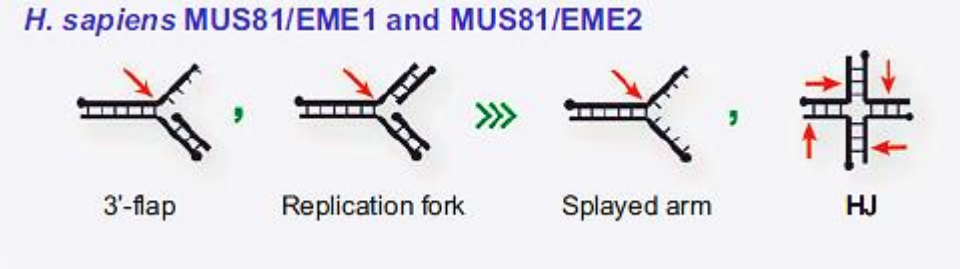

Figure 12: Substrate specificity of MUS81/EME1. Its preferential substrates are 3'-flap structures and replication forks followed by far by splayed arms and HJ structures. Red arrows indicate the sites of cleavage (modified from (Ciccia et al. 2008)).

I.3.2.3.4 FAN1

Fanconi Associated Nuclease 1 (FAN1) is another nuclease of the family XPF/MUS81 that is recruited to ICLs by its ubiquitin-binding (UBZ) domain to the monoubiquitinated FANCD2. Despite mutations in FAN1 do not cause severe ICL sensitivity, they still produce chromosome abnormalities due to the block of replication forks even without the presence of crosslinks (Lachaud et al. 2016; Segui et al. 2015; Trujillo et al. 2012). FAN1 preferred substrates are 5' flap DNA (Figure 13), like SLX1 does, but it cleaves 2-4 nucleotides 3' to the branch point instead of cutting at the ssDNA-dsDNA junction and it complements the cleavage activity of MUS81 by subsequently incising the lagging strand, for which MUS81 has no affinity (O'Donnell and Durocher 2010).

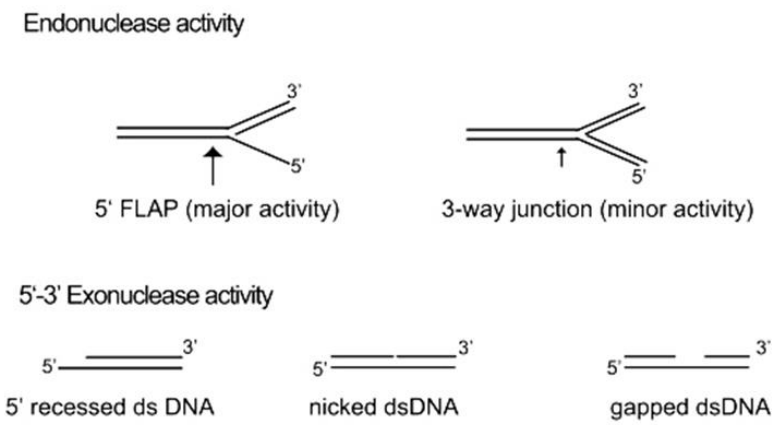

Figure 13: FAN1 nuclease activities and possible specific substrates. Its endonuclease activity has mainly affinity for 5'-flap structures and a weaker affinity for 3-way junction structures. The arrows indicate the double-stranded site of cleavage. FAN1 5'-3' exonuclease activity is performed in 5' recessed ds DNA, nicked dsDNA and gapped dsDNA structures (adapted from (O'Donnell and Durocher 2010)).

Studies performed by Knipscheer group in *X. laevis* eggs in order to discriminate which endonucleases are responsible for the unhooking of ICL showed that immunodepletion of MUS81 or FAN1 did not affect the repair pathway while removing of XPF-ERCC1 impaired the repairing efficiency, therefore pushing XPF-ERCC1 heterodimer to be the most crucial endonuclease recruited to SLX4 for the crosslinks unhooking (Klein Douwel et al. 2014).

I.3.2.3.5 SNM1 NUCLEASES: SNM1A AND SNM1B

SNM1 nucleases are processing enzymes involved in ICLs repair. SNM1A works as an exonuclease and it loads in a nascent leading strand stalled fork substrate to digest in 5'->3' direction past the ICL, continues several nucleotides beyond the junction and completes the unhooking. SNM1A exonucleolytic action might replace the 3' incisions when the 3' side of the ICL is not ideal for cleavage by other nucleases like XPF or MUS81. Therefore, when a 5' incision takes place, SNM1A can complete the unhooking without the need for the 3' endonucleolytic cleavage. Furthermore, SNM1A could also eliminate some of the nucleotides between the incision points to a residual mono-adduct that can be detected as a substrate for the downstream TLS bypass of ICL (J. Zhang and Walter 2014).

On the other side, SNM1B is a 5' to 3' dsDNA nuclease that participates in the nucleolytic processing of ICLR intermediates; it does not seem to be important for the unhooking step but it is sought to be required for the proper localization of other repair factors such as FANCD2 (SNM1B is crucial for efficient assembly of FANCD2 into subnuclear foci), BRCA1 and RAD51. Its exonuclease activity generates single-strand regions at collapsed replication forks after XPF-ERCC1 unhooks the ICL lesion (Mason and Sekiguchi 2011).

New approaches will be necessary to completely understand the combined action of XPF-ERCC1, FAN1, MUS81, RPA and SNM1A, but it seems demonstrated that there are different ways to fix ICLs depending on the temporal and substrate context in which they are detected (A. T. Wang et al. 2011).

I.3.2.4 GROUP III: TRANSLESION SYNTHESIS AND RECOMBINATION PROTEINS

This group consists of a group of proteins whose alteration do not alter FANCD2 monoubiquitination levels in response of DNA damage, as they play their role downstream ID complex and following to the incisions performed by the nucleases.

After the unhooking processes, the 3' end will be extended from the nascent leading strand previously arrested at the -20 to -40 position from the ICL by the TLS DNA polymerases REV1 and Pol-ζ, therefore the nascent leading strand becomes a template for the repair of the opposite strand (Abdullah et al. 2017). Pol-ζ consists in polymerases REV3 and REV7 (which has been recently identified as *FANCV* gene of FA pathway) (Bluteau et al. 2017) and the accessory subunits POLD2 and POLD3 (Tomida et al. 2015) that are recruited to the stalled replication forks through their interaction with mono-ubiquitinated PCNA) and the extended strand turns into a template for the repair of the opposite strand. REV1 is a cytidine-transferase which incorporates single cytosines opposite to the crosslinks, that usually occurs between guanines (Crossan and Patel 2012).

The duplication of the parental strand that has been incised from the ICL by the endonucleases produces a DSB in the daughter duplex. Meanwhile the opposite parental strand still keeps the crosslink attached and requires the polymerases from TLS to bypass it in its daughter duplex. After this step, the daughter strand gets completely filled by ligation

and a model suggests that unhooked DNA mono-adduct might be removed by NER. The repaired daughter strand becomes then the template for repair of DSB by HR (Figure 14) (Roy and Scharer 2016).

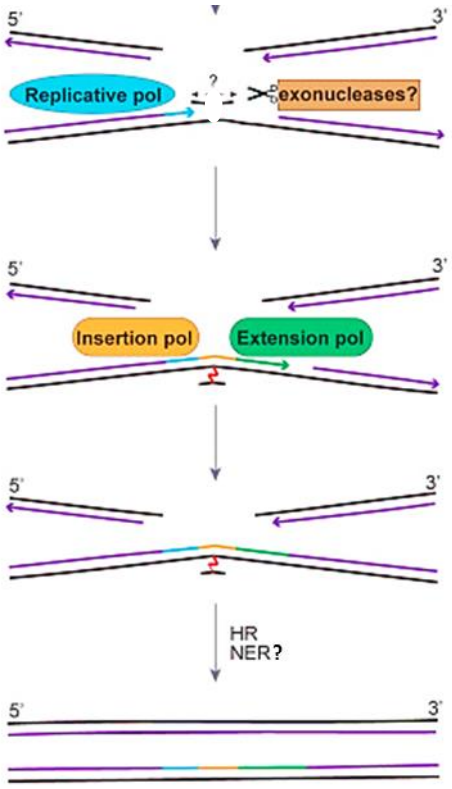

Figure 14: Representation of lesion bypass in ICL. After the unhooking the crosslink remains attached to the other parental strand and the duplication of it requires the TLS polymerases to bypass it. Finally the ligases will complete the daughter strand and the crosslink will be removed. This daughter duplex will be the template for the repair of the DSB (adapted from (Roy and Scharer 2016)).

HR and NHEJ are the two basic mechanisms by which a DSB can be fixed. NHEJ links two DNA end ligation without any homology requirement neither end resection and it is active during the whole cell cycle. It is also known as canonical NHEJ (C-NHEJ) and it requires the action of the DNA-dependent protein kinase (DNA-PK) (which comprises the Ku70/80 heterodimer and the catalytic subunit DNA-PKcs), XRCC4 and ligase IV proteins. It can restore DNA sequence but often causes insertions or deletions. In contrast to NHEJ

(Bhargava et al. 2016), the HR requires the presence of a sister chromatid as an homologous intact template to faithfully copy the genetic information, and therefore is confined to S/G2 phases of the cell cycle (Katsuki and Takata 2016).

Certain genes of HR and involved in the FA pathway have been revealed, furthermore, to be involved in FBOC susceptibility. Homozygous mutations of *FANCD1 (BRCA2), FANCN (PALB2), FANCO (RAD51C), FANCJ (BRIP1), FANCS (BRCA1),* cause FA, while heterozygous or monoallelic mutations predispose to breast and ovarian cancer. While *FANCS/BRCA1* and *FANCO/RAD51C* are considered FA-like genes involved in FBOC, *FANCR/RAD51* and *FANCU/XRCC2* are identified as FA-like genes without connection to breast and ovarian cancer predisposition (Bogliolo and Surralles 2015). Additionally, *FANCM* gene, which is involved in HR as part of the complex with BLM/RM1/Topo3A (dissolvasome complex) also contributes to FBOC (Kiiski et al. 2014; Peterlongo et al. 2015).

During HR, the DNA duplex generated by TLS is used as a template to repair the DSB originated by the unhooking. FANCS/BRCA1 forms a complex with Abraxas and RAP80 proteins to detect damage through recognition of ubiquitinated proteins (Sawyer et al. 2015; B. Wang et al. 2007). 5' sites of the DSB must be firstly processed to generate 3' ssDNA substrates for the binding of the repair proteins.

MRN complex reaches the lesion site; it is formed by MRE11, RAD50 and Nijmegen Breakage Syndrome 1 (NBS1). This endonuclease, together with CtIP endonuclease that works associated to FANCS/BRCA1, cleaves at 5' to generate a ssDNA overhang. This process is called DNA end resection and allows the following search of homology on the sister chromatid (Figure 15) (Katsuki and Takata 2016).

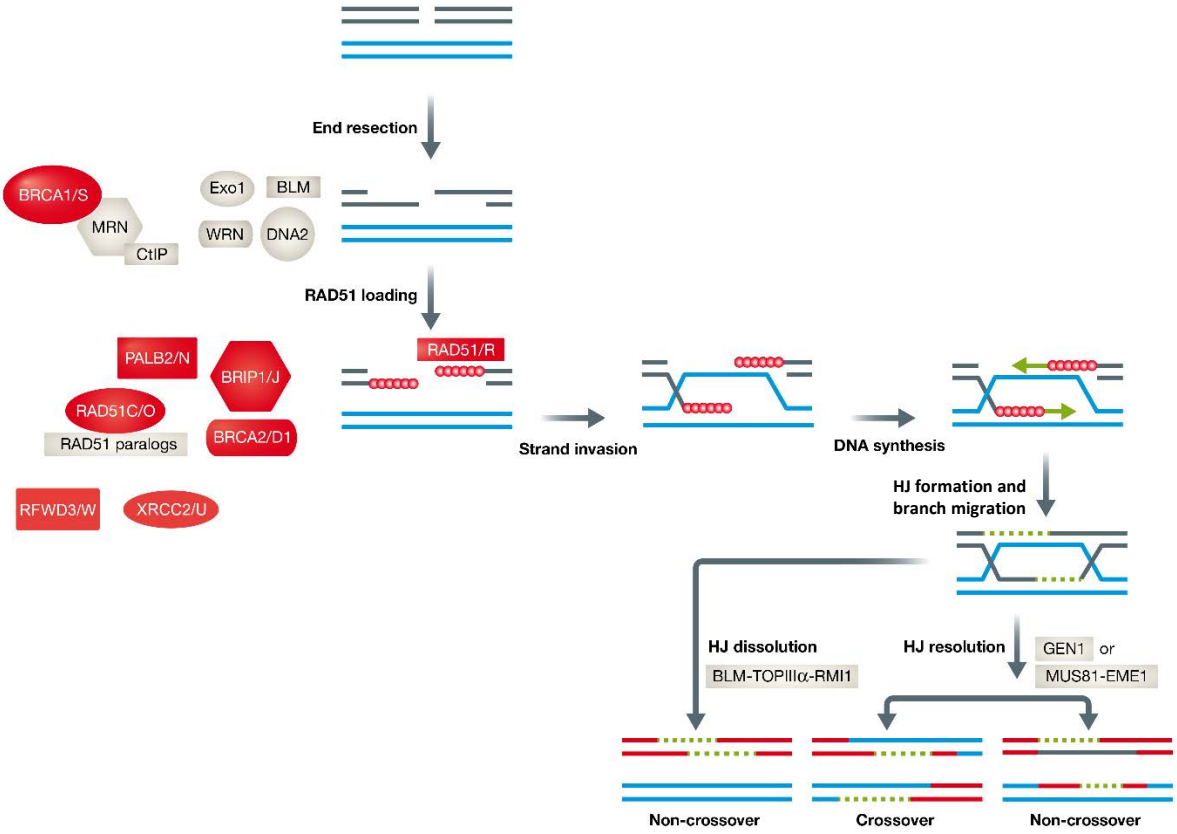

Figure 15: The HR pathway of DSB repair (adapted from (Michl et al. 2016)).

Resection is necessary for HR but not for NHEJ and CtIP acts as a regulator promoting HR instead of NHEJ (Huertas and Jackson 2009). The 3' ssDNA generated during this resection step is then covered and protected by RPA. The last HR protein identified to be associated to FA is FANCW/RFWD3 (Knies et al. 2017). RFWD3 ubiquitinates RPA so that it can leave the ssDNA and go towards the proteasome (Feeney et al. 2017; Inano et al. 2017). The recruiting of RPA to ssDNA attracts ATR and its partner ATR interacting protein (ATRIP) complex to turn on the S-phase checkpoint that leads to cell cycle arrest. The ATR-ATRIP activation is mediated by TopBP1 protein and it phosphorylates FANCJ/BRIP1 helicase for its proper G2 checkpoint function (Andreassen and Ren 2009). Therefore, the formation of ssDNA-RPA requires cyclin-dependent kinase (CDK) protein activity. This CDK

forms a complex with a cyclin that directs its phosphorylative activity and restricts it to S and G2 phases to monitor the timing of the repair mechanism (Zhao et al. 2017).

RPA is then replaced by FANCR/RAD51 thanks to a new complex formed by FANCS/BRCA1, FANCN/PALB2 and FANCD1/BRCA2. FANCD1/BRCA2 was identified as the first core HR gene involved in FA (Howlett et al. 2002) and the loading of FANCR/RAD51 stimulated by this protein is required for strand invasion. FANCN/PALB2 association to FANCS/BRCA1 is enhanced by ATR to promote HR. FANCN/PALB2 stabilizes FANCD1/BRCA2 and links together FANCD1/BRCA2 with FANCS/BRCA1 (Orthwein et al. 2015).

Five FANCR/RAD51 paralogs (RAD51B, FANCO/RAD51C (Somyajit et al. 2012), RAD51D, FANCU/XRCC2 (Park et al. 2016), and XRCC3) organized in two different complexes have been identified as FANCR/RAD51 mediators (Katsuki and Takata 2016); they are positive regulators at different steps of HR through facilitating the invasion of the sister chromatid, although the molecular mechanism of this stimulation is still unknown (Taylor et al. 2015)

The last step of HR involves extension of the filament by polymerase eta (Polη), resolution of the HJ or synthesis dependent strand annealing (SDSA) mechanism. In this last mechanism a D-loop migrates while DNA is synthetized at 3' of the invading ssDNA tail ensuring that a copy of the homologous DNA template is replaced without chromosome crossover (Miura et al. 2012). HR finishes with the ligation of the DNA strand.

During last years the idea of the two replication forks stalling at the crosslink point as a requirement to initiate ICLR has been put to spotlight and a traverse model has won attention. This other replication coupled model would require the translocase activity of FANCM, and it would recruit RPA to an ICL duplex DNA, which could enhance XPF-ERCC1 to make the 5' incision (Figure 16). In summary, both ICL traverse and fork convergence events would ultimately lead to an X-shaped structure that would be post-replicatively repaired by similar unhooking and TLS mechanisms (Roy and Scharer 2016; J. Zhang and Walter 2014).

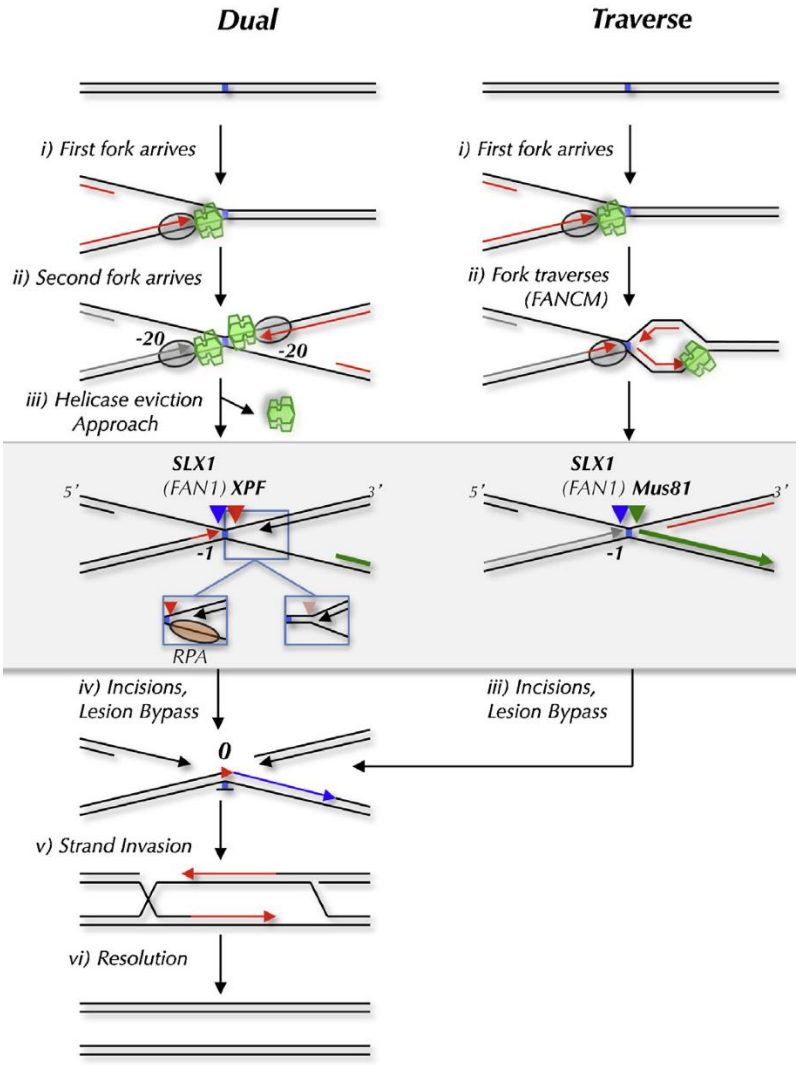

Figure 16: Possible mechanisms of replication-coupled ICLR (adapted from (J. Zhang and Walter 2014)).

I.3.3 REPLICATION-INDEPENDENT ICL REPAIR

DNA crosslinks are especially damaging during replication in S-phase, however the replication-independent repair (RIR) during G0/G1 plays an important role in post-mitotic cells. Once mitosis is ended, endogenous crosslinks could block transcription of crucial genes. Moreover, ICLR in G1 reduces considerably the damage before the cells enter S-

phase (Roy and Scharer 2016). This replication and recombination-independent ICLR involves NER proteins to recognize and incise the crosslinks, but as cells with mutations in NER factors are only mildly sensitive to crosslinker agents, this pathway could be secondary in the ICLR context, and be activated only when the transcription of an essential gene is compromised (Enoiu et al. 2012). Unlike replication-dependent ICL, which starts when a replication fork is stalled and needs the orchestrated action of the FA pathway proteins, RIR does not rely on FA pathway. The starting point could be a collision between a RNA polymerase and the crosslink, from where NER or mismatch repair (MMR) proteins could recognize ICLs depending on the structural nature of the ICL (Williams et al. 2013).

Actually, most of the endonucleases involved in the replication-dependent ICLR unhooking would take part in this pathway (XPF-ERCC1 with RPA, SNM1A and FAN1) and especially SNM1A is thought to be recruited to CSB during TC-NER complexes to process these transcription-dependent ICLR (Iyama et al. 2015). DSBs are not generated in RIR but they are generated in replication-dependent ICL in response to crosslinker agents, and they last much longer in cells deficient for XPF-ERCC1, which would suggest that XPF-ERCC1 is involved in something else apart from the incision, possibly in the resolution of the DSB through recombinational repair (Williams et al. 2013) which could explain the possible contribution of the heterodimer in RIR but the exact knowledge of how the ICLR pathway works independent from replication is still unclear.

I.3.4 OTHER DOUBLE STRAND BREAK SUBPATHWAYS

Any DSB that takes place in S phase may be resected; in the absence of a sister chromatid it will be processed by MMEJ or by SSA (Figure 17).

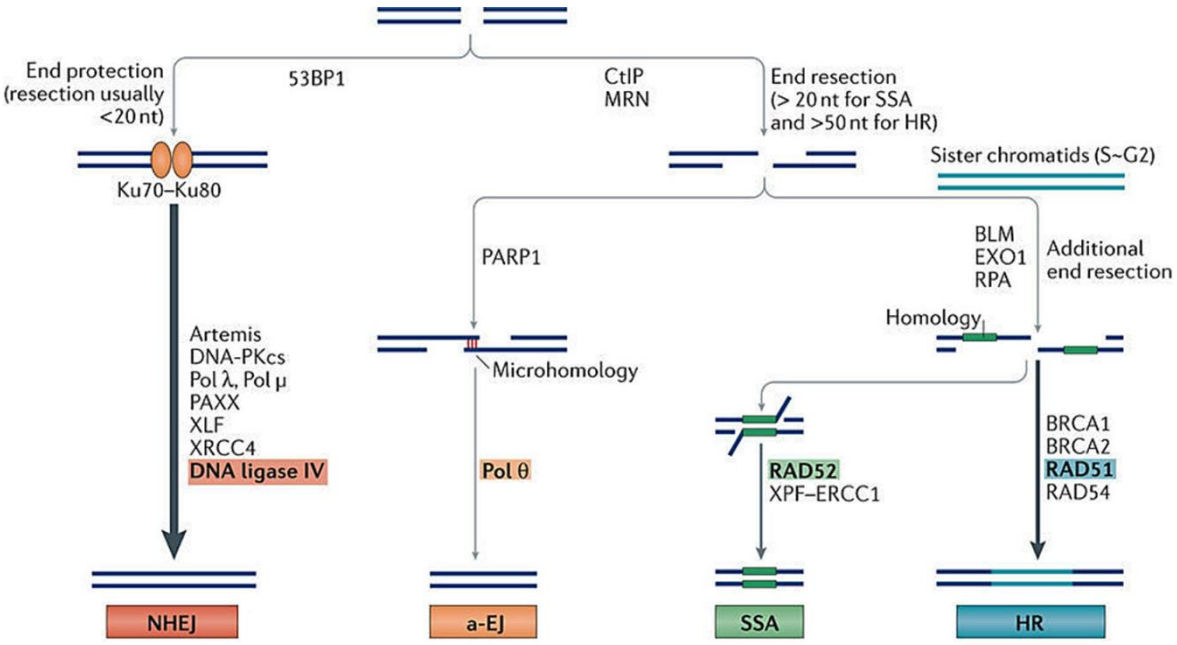

Figure 17: Diagram of the different DSB repair pathways (adapted from (Chang et al. 2017)).

MMEJ, which is an a-EJ pathway that takes place when any of the two canonical DSB pathways cannot work or simply at 10-20% cells levels when the other two pathways are available, probably because MMEJ produces a deletion, and therefore it is a more error-prone and mutagenic pathway. MMEJ consists of the alignment of microhomologous sequences near the DSB before joining and is inherently associated with deletions flanking the breaks (Sfeir and Symington 2015).

MMEJ starts with 5' end resection through MRN complex stimulated by phosphorylated CtIP action. This complex generates 15-100 nucleotides 3' overhangs. In mammalian cells, the extension of short complementary base pairing called microhomologies (MH) is required for the MMEJ and their stretch can be as few as 1 nucleotide. MMEJ operates differently depending on the size of MH and the types of DNA breaks. Poly (ADP-ribose) polymerase 1 (PARP1) is involved in joining the linear DNA fragments through their complementary sequences after the resection. When the ends are incompatible, insertions of nucleotides at break sites copied from other chromosomes or added *de novo* generate MH that are used

to pair the DNA ends and promote diversity and increase mutagenicity (Sfeir and Symington 2015).

ERCC1-XPF is not part of the core NHEJ machinery and there are evidences that HR occurs in the absence of XPF-ERCC1. Rad10-rad1, its yeast ortholog, is required to remove the nonhomologous sequence from the 3' ends to allow the synthesis and/or ligation. In mammals, the mechanism is not totally clear but some studies demonstrate that in the absence of XPF-ERCC1, joining of homologous 3' overhangs is impaired and drives to large deletions. Furthermore, this endonuclease cleaves unprotected telomeric ends, promotes telomeric fusion through end joining and it is important for end joining in c-NHEJ deficient cells (Bhargava et al. 2016). These observations support the hypothesis that XPF-ERCC1 plays a role in MMEJ analogous to yeast Rad10-rad1 (Ahmad et al. 2008; Manandhar et al. 2015). If the homology does not naturally occurs flanking the broken end, XPF/ERCC1 removes the 3' flap and forms DNA ends which are available for the DNA synthesis and ligation, and as a consequence provokes the deletion of inter-MH sequence (Sinha et al. 2016).

The TLS polymerase theta (Pol θ) is shown to be necessary in mammals for the synthesis of nucleotides during joining. It might be involved in the displacing of RPA from the ssDNA and it interacts with RAD51 and downregulates its role as an intermediate of HR, thereby enhancing MMEJ instead (Ceccaldi et al. 2015). Pol θ is able to stabilize annealing of two 3' ssDNA overhangs with as little as 2 bp homology, simply using the annealing partner as a template. The polymerase activity contributes to prevent long resection of ends which would shunt to other DSB repair mechanisms (Chang et al. 2017). The pathway concludes with the sealing of the ends; Ligase III (Lig3) is the main protein involved in the ligation step and Ligase I (Lig1) acts as a back-up enzyme (Sfeir and Symington 2015) (Figure 18).

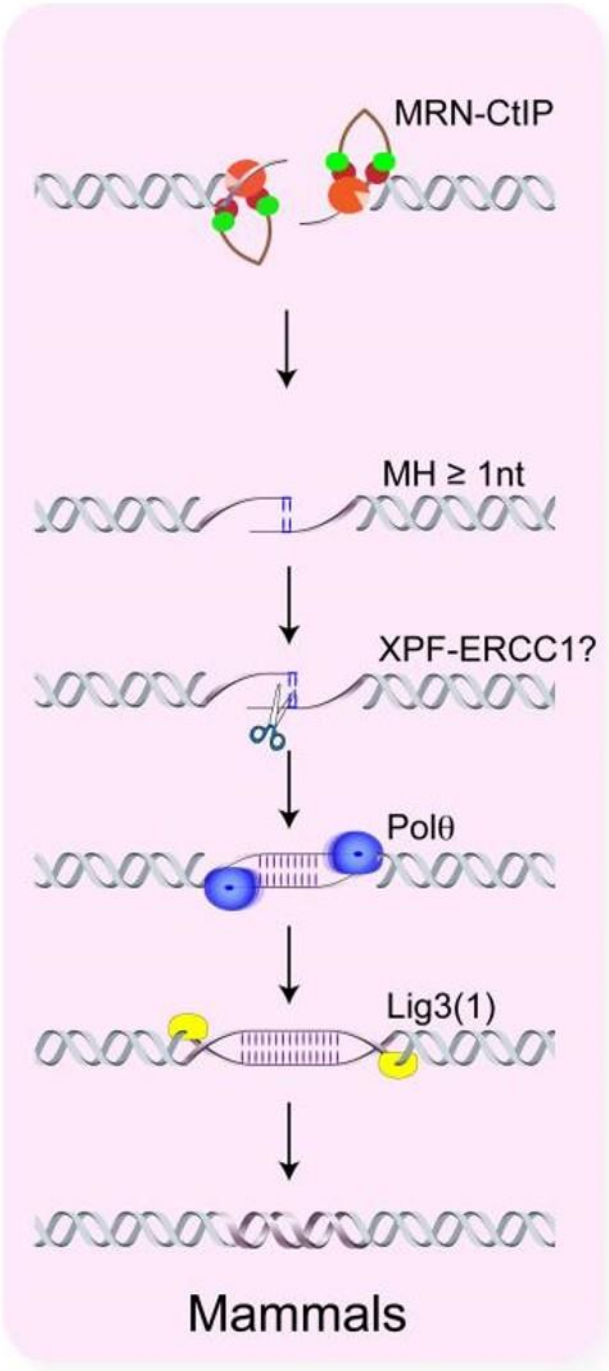

Figure 18: Mechanistic model for MMEJ in mammals (adapted from (Sfeir and Symington 2015)).

MMEJ is an extremely versatile mechanism, when MH are shorter than 5-6 bp, it resembles NHEJ, but when the homologies are larger than 15 bp, it operates more similarly to SSA (Sinha et al. 2016). Although the role of PARP1 is not precisely clarified in MMEJ, its activity, together with Pol θ role, seem to be the main directors of this pathway (Bhargava et al. 2016).

SSA is a DSB pathway that requires longer homologies than MMEJ to initiate the repair of the break. It shares the initiation step with other DSB pathways such as MMEJ and HR because it requires MRN and CtIP to generate the ssDNA tails, but the resection is more extensive and needs additional nucleases like EXO1 or Bloom syndrome RecQ-like helicase (BLM) or DNA replication helicase/nuclease 2 (DNA2). End resection is a crucial step of SSA and factors that inhibit end resection suppress this pathway (Bhargava et al. 2016).

After end resection, RPA quickly covers the single strand to prevent the formation of secondary structures and the unannealed non-homologous portions of the 3' ssDNA are cleaved by XPF-ERCC1 endonuclease and the MMR complex MSH2-MSH3, whose role is not totally understood yet. Finally, the annealing of the homologies is mediated by RAD52 (Chang et al. 2017) a DNA binding protein that specifically works in SSA mediating annealing of the 3' tails and enhancing the endonucleolytic activity of XPF-ERCC1 (McNeil and Melton 2012).

Following to the annealing, some DNA polymerases will fill the gaps and some ligases will produce the junction, but the nature of which specific proteins are involved in this step is still unclear.

When sequence repeats are close to a DSB, SSA can be activated and produce a deletion of sequences between the repeats, which constitutes an important source of mutagenesis. Although SSA is an error-prone mechanism, it is needed for the survival of cells with DNA damage that could not be repaired in any other way (Stark et al. 2004). Consequently, SSA and MMEJ are deletion-inducers error-prone mechanisms unlike HR, which requires a sister chromatid as a template to generate a loyal copy of the strand. However, some deletions can occur while HR repair pathway when DNA tandem repeats provoke the resolution by crossing over. These deletions would be similar to the ones

produced by SSA but the key distinction element in this case would be RAD51, which is essential in HR for the strand-invasion but does not participate in SSA.

SSA could also participate in gene targeting, a process also called homology-directed gene editing that is defined by a site-specific modification of genomic DNA using an exogenous donor template that is homologous to the target site. This uncommon event might be promoted by a DSB at a target site (Bhargava et al. 2016).

I.3.5 TELOMERE STABILITY

Telomeres are protein-DNA complexes at the ends of linear chromosomes that are important for genome stability. They are composed by TTAGGG DNA repeats that end in a single-stranded 3'-overhang of the G-strand which are protected by TRF2, a dimeric protein that binds along the duplex telomeric repeat tract. Inhibition of TRF2 activates a DNA damage response that leads to induction of apoptosis or senescence. These unprotected telomeres are processed by NHEJ, which produces mutations through telomeres fusion and multicentric chromosomes formation. TRF2 can promote telomeric loop (T-loop) formation. T loops are large duplex loops formed through the strand invasion of the single-stranded telomeric overhang. If the 3' overhang is confined into the duplex part of the telomere it remains protected from degradation and prevents fusion by NHEJ. These overhangs disappear gradually as a consequence of DNA replication, but even when cells do not progress to S phase overhang loss is observed in TRF2 inhibited cells, which suggests the activity of a nuclease cleaving these overhangs. XPF-ERCC1 is the endonuclease involved in 3' overhang telomeric cleavage (Zhu et al. 2003) (Figure 19).

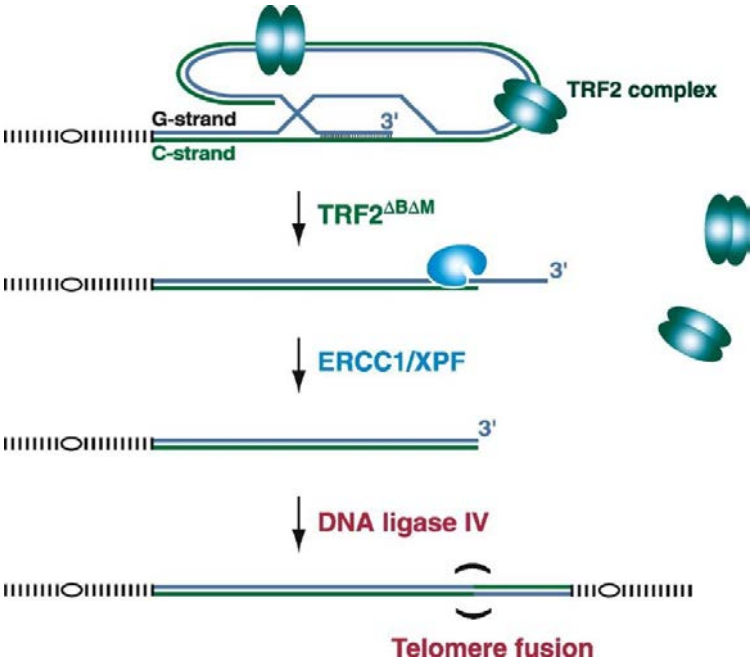

Figure 19: Model for telomere processing (adapted from (Zhu et al. 2003)).

XPF shows interaction with TRF2 via SLX4 and cleaves 3' overhangs from uncapped telomeres, which results in telomeres shortening and ageing (Manandhar et al. 2015). SLX4 associates with telomeres in late S phase or under genotoxic stress, interacts to TRF2 by its TMB domain. The main protective role of TRF2 is to prevent overhang loss, but the mechanism by which it blocks XPF-ERCC1 from removing the 3' overhang is not yet unrevealed.

Objectives

II. OBJECTIVES

Concerning the wide range of diseases associated with changes in XPF protein and the amount of DNA repair pathways in which it plays a crucial role, the objective of this thesis was to better understand the role of *ERCC4*/XPF in DNA repair and human diseases.

The specific objectives of this work were:

- To analyze the genotype-phenotype correlation of *ERCC4* pathogenic variants.
- To uncover new XPF partners and study their role in DNA repair.

Materials and Methods

III. MATERIALS AND METHODS

III.1- CELL LINES AND CULTURE

Human cell lines HEK 293T (Human Embryonic Kidney 293T cells, ATCC CRL-11268) and human osteosarcoma U2OS were used in this study.

HEK 293T *ERCC4* knocked out (HEK XPF-KO) created by TALENs (Transcription Activator-Like Effector Nuclease) technology were generated and used as the knocked *ERCC4* background in which all the mutant versions of XPF were generated.

HEK 293T *USP11* knocked out (HEK USP11-KO) and double knocked out HEK *ERCC4-USP11* (HEK XPF/USP11) were created by Clustered Regularly Interspaced Short Palindromic Repeats (CRISPR) technology.

Human osteosarcoma cell line U2OS DR-GFP was kindly provided by Dr Maria Jasin (New York). U2OS SA-GFP was previously developed by members of our laboratory using SA-GFP plasmid (Addgene Nº 41594).

All the cell lines were cultured in DMEM (Dulbecco's Modified Eagle Medium, Biowest) complemented with 10% FBS (Fetal Bovine Serum, Biowest) and 0.1 µg/mL Plasmocin (IBIAN Technologies). Cells were cultured at a controlled temperature of 37º C in 5% CO_2 atmosphere. All the cell lines were kept in liquid N_2 in a Biobank from our group.

III.2- ESTABLISHING OF THE HEK 293T TALEN *ERCC4*-KNOCKED OUT AS THE XPF-KO BACKGROUND CELL LINE

III.2.1 GENERATION OF THE HEK XPF-KNOCKED OUT CELL LINE

HEK 293T *ERCC4*-KO was generated by TALEN. *ERCC4* exon 2 (Figure 20) was targeted by a pair of designed plasmids fused to a FokI nuclease domain that excised the sequence producing an early truncated protein completely unfunctional.

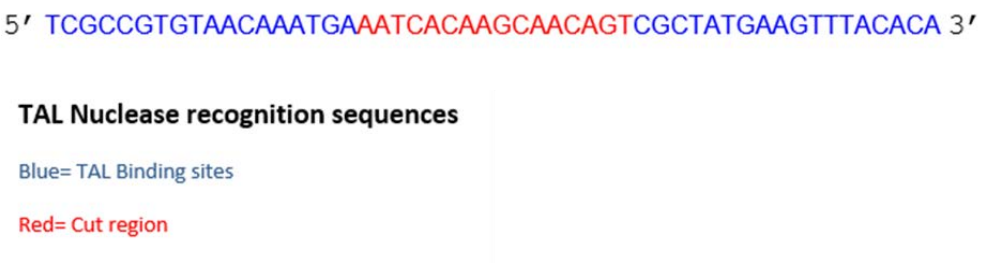

Figure 20: *ERCC4* TALEN recognition sequence. The fragment corresponds to exon 2. Blue region represents TALEN binding sites and red region represents FokI endonuclease cutting sites.

Additionally, another plasmid was used: a reporter-based plasmid containing the same *ERCC4* recognition sequence, a red fluorescent protein sequence and an out of frame green fluorescent protein (GFP) that could be restored when the DSB produced by FokI was repaired by NHEJ. After 48 h post transfection the fluorescence was visible.

Double fluorescent (red and green) cells were selected by flow cytometry using the FACSAria II (BD Bioscience). Single cell cloning of these cells was performed by limit dilution (3 cells/mL), plating 3 plates of 96 wells with 100 µL of complete medium to ensure just one clone was plated per well. After 2-3 weeks three individual clones grown and were picked to check the lack of XPF protein by Western Blot (WB).

III.2.2 WESTERN BLOT VALIDATION OF THE KNOCKED OUT CLONES

50 µL of RIPA 1x lysis buffer (Millipore 20-188) with Benzonase nuclease (10 U/mL final) (VWR International 7074-6-3) was added for each million of cells. Samples were incubated at 37ºC during 10 min and then centrifuged at 13,000 rpm. The total protein concentration of the supernatant was determined by Bio-Rad Protein Assay (Biorad) according to manufacturer's instructions and 50 µg of total proteins with Laemmli 1x (Sigma S3401-10VL) were denaturalized for 10 min at 96ºC and loaded in an SDS-PAGE 8% acrylamide. Proteins were transferred from the gel to the nitrocellulose membrane in the iBLOT2 (Invitrogen, ThermoFisher Scientific), blocking of the membrane was achieved by incubation with blocking solution (5% of milk in TBS+ Tween) during 1h at RT, immunodetection was performed by incubating the membranes with diluted primary antibodies in blocking solution during 16h at 4ºC. Primary antibodies used were: anti-XPF (mouse monoclonal, Ab-1 219 Thermo Scientific) 1:200 and anti-Actin (rabbit polyclonal, ab1801, Abcam) 1:1,000. The following day, membranes were incubated in secondary antibodies conjugated to peroxidase during 1h at RT and revealed with Pierce ECL Western Blotting Substrate (Pierce) and digital images of the membranes were captured with the GeneGnome apparatus (Syngene Bio imaging).

III.2.3 CHARACTERIZATION AND SELECTION OF THE XPF-KNOCKED OUT CLONE

Genomic DNA was extracted from 5 x 10^6 clonal HEK XPF-KO cells using the DNeasy Blood & Tissue Kit (QIAGEN) according to manufacturer's instructions and DNA concentration was measured by spectrophotometry using NanoDrop ND-1000 (NanoDrop Technologies).

PCR to identify mutations inserted by TALEN was performed using the following primers (Table I):

ERCC4-Ex2-F	TGTAGACTGGTTGGCTGAAGT
ERCC4-Ex2-R	CGCCTATGTGCTTCCCAAGA

Table I: Primers sequences used to identify the mutations inserted by TALEN.

PCR conditions are schematized in (Table II):

Segment	Cycles	Temperature	Time
1	1	94º C	1 min
2	35	94º C	30 sec
		58º C	30 sec
		72º C	4 min
3	1	72º C	4 min

Table II: PCR conditions to amplify XPF modified region by TALEN.

The product size was checked by loading the sample into a 1.5% agarose gel, the DNA band was purified and subcloned by TOPO TA cloning (Thermo Fisher) according to manufacturer's, transformed in One Shot TOP10 Chemically Competent *E.coli* cells (Life Technologies) following manufacturer's instructions, amplified by performing Minipreps with NucleoSpin Plasmid (Macherey-Nagel) and sent to Sanger sequencing of Macrogen with the ERCC4_Ex2-F primer to check the sequence mutations in the individual alleles. Sequences results were analyzed by Sequencher (Gene Codes Corporation) bioinformatics software.

III.3- GENERATION OF XPF CELL LINES

III.3.1 GENERATION OF THE XPF-Wt LENTIVIRAL VECTOR

The retroviral pBABE vector (pBABE puro IRES-EGFP, Addgene 14430) with the cDNA of *ERCC4* insert was already built in our lab. *ERCC4* cDNA was modified by cloning the HA-tag epitope in C-terminal, and with two N-terminal epitopes: streptavidin binding protein (SBP) and calmodulin binding protein (CBP) (TAP tag). (From now onwards referred as pBABE XPF). Modified *ERCC4* cDNA was subcloned into a 3rd generation lentiviral vector pUltra (Addgene, 24129) downstream of the EGFP-P2A site, to produce a bi-cistronic expression of EGFP and ERCC4. P2A site, similar to IRES, is a peptide with a motif associated with cleavage-like activity through a ribosomal skip mechanism that impairs normal peptide bond formation between ERCC4 and EGFP without affecting the translation of EGFP, ensuring both proteins can be translated from a single sequence to two individual proteins. To do that, two primers were designed in order to amplify and modify the insert TAPtag-XPF-HA by including a restriction site compatible with the restriction enzymes used to cut the pUltra vector (Table III).

TAPTAG-XPF-HA_S	CCCTCTAGAATGAAGCGACGATGGAAAAAG
TAPTAG-XPF-HA_AS	ATGTGATCATCAAGCGTAATCTGGAACATCG

Table III: Primers sequences used to amplify and modify the insert from pBABE plasmid making compatible with the pULTRA lentiviral plasmid.

The PCR was carried out with the following conditions (Table IV):

Segment	Cycles	Temperature	Time
1	1	94º C	1 min
2	35	94º C	30 sec
		57º C	30 sec
		72º C	4 min
3	1	72º C	2 min

Table IV: PCR conditions to amplify the insert from pBABE plasmid.

The PCR product was then digested first with XbaI (Roche) restriction enzyme during 2h at 37ºC and second with BclI (Roche) restriction enzyme during 2h at 55ºC.

The pUltra vector was digested first with XbaI (Roche) as the insert and secondly with BamHI (Roche) restriction enzyme during 2h at 37ºC. The vector was loaded in a 0.7% agarose gel, purified, dephosphorylated with FastAP (Thermo Fisher Scientific) and ligated to the digested PCR product of the insert TAPtag-XPF-HA with the Quick Ligation Kit (New England Biolabs) overnight on ice. The ligation product was then transformed using One Shot Stbl3 Chemically competent *E.coli* (Thermo Fisher Scientific), amplified by standard Miniprep and Maxiprep procedures and sent to Sanger sequencing of Macrogen for a primer walking (Table V).

FOR1-XPF-pULTRA	TGGAAAAAGAATTTCATAGCCG
FOR2-XPF-pULTRA	TTCTCCAGCTGCACTGCC
FOR3-XPF-pULTRA	TGAGAAATCTTTTTGTGAGGAAA
FOR4-XPF-pULTRA	AAGCTTTTGGTCAGAATTCAGGT
FOR5-XPF-pULTRA	TGGATGAAATTTAGGAAGGAAGA
FOR6-XPF-pULTRA	GAGCTAACCTTTGTTCGGCA
FOR7-XPF-pULTRA	TCACTCCAGAAATGTGCGTG
FOR8-XPF-pULTRA	CTTGTTAAAAATGCCAGGGG
REV1-XPF-pULTRA	TACCGCTACCGCTTCCAAGT

Table V: Primers sequences used to perform a primer walking of the pULTRA plasmid ligated to the PCR amplified insert.

III.3.2 GENERATION OF THE XPF-LENTIVIRAL PARTICLES AND GENETIC COMPLEMENTATION OF HEK XPF-KO CELLS

Production of Lentiviral particle was achieved with the CalPhos Tranfection kit (Clonetech). 5x 10^6 packaging cells HEK293T (passages between 3 and 8) were seeded in 10 cm plates with complete medium. Three plates were needed for the production of each type of lentiviral particles. 24h hours later the medium was changed for new one and 3 µL of chloroquine 100 mM were added per plate and the transfection solution (Table VI) was prepared per each plate.

Volume (µL)	Component
10	pUltra- TAP-XPF-HA (1 µg/µL)
6.5	Packaging plasmid (PAX) (1 µg/µL)
3.5	Lenti VSVG plasmid (ENV) (1 µg/µL)
87	Calcium Solution ($CaCl_2$) (Clontech)
593	Sterile MQ water

Table VI: Components of the transfection solution used to produce the lentiviral particles.

One volume of Solution B (2x, HBS Calphos, Clontech) was then added while gently vortexing the transfection solution. After 15 min at RT, this solution was added dropwise to the three dishes which remain at 37ºC and 5% of CO_2 overnight. The third day medium was replaced with fresh complete medium. The day after the medium containing the lentiviral particles was collected and stored at 4ºC and new medium was added to the plates. The fifth day the supernatant was collected again and filtered through a 0.45 µm filter together with the supernatant volume collected the previous day. The supernatants were then centrifuged with Beckman JS-24.38 rotor at 19,500 rpm during 1.5h at 4ºC or using Amicon-Ultra15 centrifugal filter units (Millipore) during 1h at 3,220 RCF. After the centrifugation the medium was carefully discarded and the lentiviral pellet was resuspended with PBS 1x up to 150 µL, by warming them at 32ºC during 2h shaking at 1,000 rpm.

180,000 HEK XPF-KO cells were seeded in a 12-wells plate, 24h later cells were infected with 40 µL of pULTRA-TAP-XPF-HA lentiviral particles and 1.5 µL Polybrene (Sigma-Aldrich). Three days after the infection, green fluorescence was detectable and cells that had integrated the virus with the XPF cDNA were selected by flow cytometry using the FACSAria II (BD Bioscience). Single cell cloning of these cells was performed as previously detailed and a single clone confirmed by WB was determined as HEK XPF-KO + XPF-Wt cell line.

III.3.3 GENERATION OF THE XPF MUTANT VARIANTS

The following table summarizes the XPF-single nucleotide variants generated (Table VII):

Aminoacidic change	Nucleotidic change
p.R153P	c.458G>C
p.I225M	c.675A>G
p.L230P	c.689T>C
p.C236R	c.706T>C
p.R589W	c.1765C>T
p.R689S	c.2065C>A
p.R799W	c.2395C>T

Table VII: Aminoacidic changes and single nucleotide changes of the *XPF* variants generated.

The generation of the XPF mutant variants was achieved by two different methodologies: by subcloning of the XPF inserts from the retroviral vector pBABE to the lentiviral vector pUltra or by site directed mutagenesis from the pUltra +TAP-XPF-HA.

III.3.3.1 GENERATION OF XPF VARIANTS BY SUBCLONING

Two XPF variants, C236R and R589W, were moved from pBABE to pUltra following the same protocol described above for the generation of the wild type TAP-XPF-HA .The pUltra C236R and pUltra R589W vectors were sent to Sanger sequencing (Macrogen) to check the introduced variants. The primers used are detailed in Table IV.

III.3.3.2 GENERATION OF XPF VARIANTS BY SITE DIRECTED MUTAGENESIS

The XPF variants: R153P, I225M, L230P, R689S and R799W were generated by site directed mutagenesis from the lentiviral vector carrying the wild type version of XPF (pUltra + TAP-XPF-HA) by designing with the software from Agilent Technologies the mutagenic primers that contained the desired single nucleotide variant (Table VIII).

Mutation	Primers
p.Arg153Pro	CATCTTGCGCCTCTTTCCCCAGAAAAACAAACGTG CACGTTTGTTTTTCTGGGGAAAGAGGCGCAAGATG
p.Ile225Met	CCTACCATGCTTGCTATGCAGACTGCTATACTGG CCAGTATAGCAGTCTGCATAGCAAGCATGGTAGG
p.Leu230Pro	TAGACATGCATTTAAAATGTCCGGTATAGCAGTCTGTATAGCAAG CTTGCTATACAGACTGCTATACCGGACATTTTAAATGCATGTCTA
p.Arg689Ser	GAAGCTCACTTCGAAATTCACTCATATCCACAACTATGCTTTG CAAAGCATAGTTGTGGATATGAGTGAATTTCGAAGTGAGCTTC
p.Arg799Trp	CTTCACTTCCCCAGACTATGGATTCTCTGGTGC GCACCAGAGAATCCATAGTCTGGGGAAGTGAAG

Table VIII: Primers sequences used to introduce the exact single nucleotide variant of *XPF* by site directed mutagenesis.

The QuickChange II XL Site-Directed Mutagenesis Kit (Agilent Technologies) was used to introduce the variants in the wt cDNA of *XPF* by a PCR amplification (Table IX).

5 *µ*L of 10x reaction buffer
***X µ*L (10 ng) of dsDNA template**
***X µ*L (125 ng) of oligonucleotide primer #1**
***X µ*L (125 ng) of oligonucleotide primer #2**
1 *µ*L of dNTP mix
3 *µ*L of QuickSolution
ddH_2O to a final volume of 50 *µ*L

Table IX: Parameters used for the amplification and introduction of the nucleotide variants.

And ideal cycling parameters appear in table X:

Segment	Cycles	Temperature	Time
1	1	95º C	1 min
2	18	95º C	50 sec
		60º C	50 sec
		68º C	12 min
3	1	68º C	7 min

Table X: Cycling parameters used for the PCR of the site directed mutagenesis.

After amplification DpnI restriction enzyme was added during 1h at 37ºC to digest the dsDNA template, as this enzyme is able to cleave at methylated sites, therefore cutting the template plasmid, methylated by the bacteria, though leaving the PCR product intact.

The PCR product was transformed by XL10-Gold Ultracompetent Cells (Agilent Technologies), plated in LB Agar with Ampicillin (100 µg/mL), DNA from single colony minipreps was controlled by Sanger sequencing (Macrogen) with primers from Table XI to check if the variants were correctly introduced.

Variant	Primer name	Sequence
R153P	c.458G>C(p.R153P)	GGAGTTGAACACCTCCCTCG CTGCTACATGGAACCTTGGC
I225M	c.675A>G(p.I225M)	GGCCAAGGTTCCATGTAGCA CCGTTGCTCTCAGAGATTCCA
L230P	c.689T>C(p.L230P)	CTGTGGCCAAGGTTCCATGT TCCGTTGCTCTCAGAGATTCC
C236R	c.689T>C(p.L230P)	CTGTGGCCAAGGTTCCATGT TCCGTTGCTCTCAGAGATTCC
R589W	c.1765C>T (p.R589W)	ATCCATCCGCTTCTGGGTTG TGCAGATGCTGTGCCTCTTA
R689S	c.2065C>A(p.R689S)	GCAAGCATGGTTGTCCCTGA AGGCTTGCTAGGGTCAAACTC
R799W	R799W-S786F	AAAACTCATAAGGGAAAAAGCAAGC CTCTGACTCGGGAAGGGTTT

Table XI: Primers sequences used to check the single nucleotide variants introduced by site directed mutagenesis.

The CalPhos-Clontech transfection Kit (Clontech) was used to generate the lentiviral particles with all the XPF variants following the same steps as for the XPF-wt and HEK XPF-KO cells were transduced with each individual variant as described in section III.3.2.

III.4- GENERATION OF *USP11* KNOCKED OUT AND *ERCC4/USP11* DOUBLE KNOCKED OUT BY CRISPR/Cas9 TECHNOLOGY

III.4.1 TARGET SEQUENCE SELECTION

The selected plasmid to generate the USP11 knocked out was PX458 (pSpCas9(BB)-2A-GFP (PX458), Addgene 48138) (Ran et al. 2013). This is a mammalian expression vector

containing an U6 promoter, a sgRNA scaffold site next to the oligo cloning site, the coding sequence of the humanized *S. pyogenes* Cas9 endonuclease and a fused 2A-GFP to allow screening of the transfected cells.

This plasmid needed to be ligated to a specific sequence of 20 nucleotides to guide the Cas9 endonuclease to the complementary sequence of USP11 genomic DNA. The selected sgRNA sequence was obtained from bioinformatics analyses carried out by Cong (Cong et al. 2013) that were optimized to minimize the off-target modifications. The selected sgRNA sequence for USP11 was 5'GCAGTGGGAGGCATACGTGC3' (Sigma-Aldrich) and it targets the exon 2 of *USP11*. sgRNA sequences showed in the Cong table have a PAM (Protospacer Adjacent Motif) motif (a 5'-NGG -3'motif) that was deleted from the selected sequence to design the pair of oligos. This PAM motif is present in the target gene next to the DNA sequence corresponding to the sgRNA sequence and allows Cas9 to bind and cut properly. Its removal from the designed oligos avoids the nuclease to cut the sgRNA sequence of the plasmid.

The two sgRNA (sense and antisense) needed to be 5' phosphorylated to insert in the PX458 linearized with *BbsI* (New England Biolabs) and dephosphorylated (see below). The final sequences (5' to 3') are in Table XII.

CRISPR USP11_S	[Phos]**CACC**GCAGTGGGAGGCATACGTGC
CRISPR USP11_AS	[Phos]**AAAC**GCACGTATGCCTCCCACTGC

Table XII: sgRNA sequences for *USP11*.

III.4.2 PRIMERS ANNEALING AND VECTOR CONSTRUCTION

10 µL of both selected primers mixed at a final concentration of 100 µM were annealed by three sequential incubations of 30 min at 37ºC, 5 min at 95ºC and 10 min at RT. 10 µg of PX458 plasmid were digested with 10 units of *BbsI* restriction enzyme (New England Biolabs) during 3.5 h at 37ºC in buffer 2.1 1x (New England Biolabs), followed by its loading in a 0.8% agarose gel run at 100 V.

The corresponding band was cut and purified using NucleoSpin Gel and PCR Clean-up kit (Macherey-Nagel) and dephosphorylated by FastAP Thermosensitive Alkaline Phosphatase (1U/µL) (ThermoFisher Scientific).

50 ng of the digested PX458 were ligated with 1 µL of diluted 1:200 annealed sgRNA by 1 µL of Quick Ligase (New England Biolabs) and Quick Ligation Reaction Buffer 1x (Quick Ligation Kit, New England Biolabs) on ice overnight.

From this ligation product, 5 µL was used to transform One Shot TOP10 Chemically Competent *E.coli* cells (Life Technologies) following manufacturer's instructions and plating them overnight in LB agar with Ampicillin.

Minipreps from these transformed colonies were carried out using NucleoSpin Plasmid purification kit (Macherey-Nagel) according to manufacturer's instructions, the final product was quantified by NanoDrop ND- 1,000 (NanoDrop Technologies) and sent to Sanger sequencing (Macrogen) using the primer 5' – TTTCTTGGGTAGTTTGCAG – 3'.

After confirming the sequences, Maxiprep was carried out using NucleoBond PC 500 Kit (Machenerey- Nagel) according to manufacter's instructions, the DNA concentration was quantified by NanoDrop ND- 1,000 and sent to Sanger sequencing service of Macrogen using the same primer as the one used for the Minipreps sequencing.

III.4.3 CELL TRANSFECTION AND CLONE SELECTION

500,000 HEK 293T clonal cells and 500,000 HEK XPF-KO cells were seeded in a well of a 6-wells plate with 2 mL of complete medium. Six hours later cells transfections were carried out using 7.5 µL of Lipofectamine 2,000 (Life Technologies) in 250 µL of Opti-MEM (Gibco, Life Technologies) and mixing these with 2.5 µg of the CRISPR vector in 250 µL of Optimem. Transfection medium (2.5 mL) was changed for complete medium after incubation overnight. 48 h after transfections cells were detached and analyzed by flow cytometry using the FACSAria II (BD Bioscience) to select those that have included the plasmid based on the fluorescence emission conferred by the GFP protein encoded by the PX458 vector. Single sorted cells were seeded in three 96-wells plates with 200 µL of complete medium.

After 2-3 weeks individual grown clones were checked by WB to confirm the absence of USP11 protein in HEK and in HEK XPF-KO cell lines

III.4.4 GENOTYPING

Genomic DNA was extracted from 5 x 10^6 cells of each cell line following the lack of USP11 confirmation by WB using the DNeasy Blood & Tissue Kit (QIAGEN) according to manufacturer's instructions and DNA concentration was measured by spectrophotometry using NanoDrop ND-1,000 (NanoDrop Technologies).

PCR to identify mutations in the target region of CRISPR clones was performed. Primers to amplify a *USP11* region in the genomic DNA were designed (Table XIII) and ordered to Sigma-Aldrich.

USP11_KO_Clones_S	TTGGGCATGGGAAGTTGTAT
USP11_KO_Clones_AS	GCACACAGAATGGGCTTATG

Table XIII: Primers sequences used for the PCR to amplify a USP11 region in the genomic DNA.

Ideal parameters for the reaction are summarized in table XIV.

1x Reaction Buffer (Bioron GmbH)
50 ng of genomic DNA
10 µM of primer USP11_KO_Clones_S
10 µM of primer USP11_KO_Clones_AS
10 mM of dNTP mix
25 mM of $MgCl_2$
0,5 Units of Taq DNA Polymerase (Bioron GmbH)
ddH_2O to a final volume of 25 µL

Table XIV: PCR reaction components.

PCR cycling conditions used are shown here (Table XV).

Segment	Cycles	Temperature	Time
1	1	94º C	1 min 30 sec
2	35	94º C	45 sec
		54º C	45 sec
		72º C	45 sec
3	1	72º C	7 min

Table XV: PCR cycling conditions to amplify a *USP11* region of the genomic DNA.

PCR amplified product was loaded in a 1.5% agarose and purified using ExoSAP-IT for PCR Product Cleanup (Affymetrix) as indicated by manufacturer's instructions. The product was subcloned by TOPO TA cloning (Thermo Fisher) following protocol instructions and sent to Sanger sequencing to check the sequence mutations in the individual alleles.

III.5- FUNCTIONAL STUDIES

III.5.1 UVC SENSITIVITY SURVIVAL ASSAY

In order to determine the sensitivity of the cell lines to the nucleotide dimers lesions produced by UVC irradiation, HEK 293T cells of each transduced line were seeded in 2 mL of complete medium per duplicate in a 6-well plate. 24h afterwards, medium was removed, cells were washed with PBS and UVC irradiated (254 nm; 15 W UVC Lamp G15-T18 Philips) at the doses of 0, 2, 5, 10 and 15 J/m^2. Complete medium was then added and survival cells were counted after 72 h by the Beckman-Coulter Cell Counter. At least three independent assays were performed and results were expressed as a percentage of irradiated viable cells versus (vs) viability of the untreated controls.

III.5.2 UNSCHEDULED DNA SYNTHESIS ASSAY

In order to evaluate the repair activity of the GGR subpathway of NER (GG-NER), Unscheduled DNA Synthesis (UDS) assays were performed. A mix of poly-L and poly-D Lysine (Sigma-Aldrich) was used to coat 96-well plates to improve cell attachment. Afterwards, 8 x 10^4 cells of each transduced cell line were seeded in 100 µL of complete medium, seeding 10 replicate wells per cell line, from which half of them are UVC irradiated (254 nm) at 20 J/m^2 after 16 h while the other half remains as non-treated controls. After UV irradiation cells were incubated in DMEM without FBS with 5-ethynyl-2'-deoxyuridine (EdU) (Invitrogen) conjugated with fluorescent-azide. After 2h of incubation at 37ºC, cells are fixed in 100 µL of Fixation Buffer (Table XVI) and incubated for 20 min on ice. EdU is detected by adding 41 µL/well of EdU Detection Solution (Table XVI) that exposes it to Alexa Fluor 488-azide coupling solution (Invitrogen) and nuclei were counterstained with DAPI (Dojindo) during 1h. Then, cells were washed in PBS 0.05% Tween-20 during 40 min, fixed with 100 µL Formalin/PBS (1:10) during 20 min and image acquisition and data processing achieved using a high content screening (HCS) system, the ARRAY^{SCAN}VTI (Thermo Scientific) Plates were scanned with a CCD camera-equipped fluorescence microscope and the images were processed with the software Cellomics Scan (Cellomics). At least three independent UDS assays were performed and results are represented as fluorescence intensity of treated and non-treated cells.

Fixation Buffer	
Final Conc.	Component
300 mM	Sucrose
2%	Formalin
0.5%	Triton X-100
	PBS

Detection Buffer	
Final Conc.	Component
50 mM	Tris-HCl pH 7.3
4 mM	$CuSO_4$
10 mM	Ascorbate (Na)
10 µM	Alexa 488 azide
	MQ H_2O
20 ng/mL	DAPI

Table XVI: Fixation and Detection Buffers detailed components used in the UDS assay.

III.5.3 RECOVERY OF RNA SYNTHESIS ASSAY

To evaluate the repair activity of the TCR subpathway of NER (TC-NER), Recovery of RNA synthesis (RRS) assays were performed with all the transduced cell lines. Coating and seeding of the cells were performed as for the UDS assay. After 16h, half of the cells were UVC irradiated (20 J/m^2) and incubated during 8h at 37ºC in DMEM with 1% FBS serum (to allow RRS) before incubation during 2h at 37ºC in 60 µL/well of serum-free DMEM supplemented with 5-ethynyluridine (EU) (100 µM). Afterwards, cells were fixed, EU was detected and image acquisition was done as in the UDS assay. At least three independent RRS assays were performed and results are represented as fluorescence intensity of treated and non-treated cells. Detailed UDS and RRS methodologies were provided by Dr Ogi group (Jia et al. 2015).

III.5.4 DEB SENSITIVITY SURVIVAL ASSAY

To evaluate the sensitivity of the cell lines to ICL, 2 x 10^5 HEK 293T cells of each transduced line were seeded in 2 mL of complete medium per duplicate in a 6-well plate. 24h afterwards, DEB was added at a final concentration of 0, 0.025, 0.05, 0.1 and 0.2 µg/mL.

Cells were grown during the time needed by the untreated to perform at least three population doublings. Afterwards cells were harvested by trypsinization and counted with a Beckman-Coulter Cell Counter. At least three independent assays were performed and results are expressed as a percentage of treated viable cells vs the untreated controls.

III.5.5 DEB-INDUCED G2/M CELL CYCLE ARREST

10^6 cells of each cell line were seeded in 3 x 25 cm^2 flasks (F25) in 5 mL of complete medium. 24 h afterwards DEB was added at doses of 0, 0.005, 0.01, 0.025 and 0.05 µg/mL. 48 h after the treatment, cells were trypsinized, PBS washed and resuspended in 200 µL of PBS. 2 mL of ice-cold ethanol 70% was added and cells were placed for 30 min on ice. Ethanol was removed by centrifugation and substituted with 2 mL of Staining solution (40 µg/mL Propidium Iodide, PI, Invitrogen; Pure Link RNasa A 0.1 mg/mL, Invitrogen; PBS 1x). Cell cycle population distribution depending on DNA amount was analyzed by flow cytometry with FACSCalibur (BD Biosciences) as in (Bogliolo et al. 2013). 15,000 events were registered per sample and data was analyzed by FlowJo VX software.

III.5.6 MICRONUCLEI- FRAGILITY TEST

Micronuclei (MN) are small nuclei close to the main nucleus. The origin of MN is due to mal-segregation of whole chromosomes or acentric chromosome fragments which makes them unable to be properly distributed by the mitotic spindle during cell division.

Thus, MN are a sign of genotoxic events and chromosomal instability generated by chromosomal breaks produced either by errors during replication or by ICL agents exposure.

Traditional chromosome aberrations analyses are highly time-consuming and require more technical expertise. Notwithstanding, MN scoring system is one of the most widely used methods to measure genome damage in humans (Fenech et al. 2011). MN assay associated to flow cytometry represents a fast and robust system to obtain cytogenetic damage information (Avlasevich et al. 2006).

Around 3 x10^5 cells from each cell line were seeded in 6-well plates. Twenty four hours later cell cultures were untreated or treated with 0.01 µg/mL of DEB and they were kept in culture enough time for at least one population doubling. Cells were then sequentially stained in order to distinguish MN from apoptotic debris and necrotic chromatin. First of all a staining with Ethidium Monoazyde Bromide (EMA) (0.025 mg/mL) and secondly a staining with Sytox green (0.2 µM). EMA is a dye which covalently binds to chromatin of dying and dead cells after a photo-activation step achieved by keeping cells under a 60 W light bulb (about 30 cm distance) for 20 min. EMA allows to detect dying cells because it just can reach the cells whose membranes are compromised. After the photo-activation period, a wash with cold PBS with 2% FBS was added to remove EMA that was not covalently bound to DNA. After that, a lysis step with 250 µL of lysis solution 1 (0.584 mg/mL NaCl, 1 mg/mL sodium citrate, 0.3 µg/mL IGEPAL, 1 mg/mL RNase A and 0.2 µM Sytox green in deionized water) during 1h at RT was done. Later, a second lysis step was done adding 250 µL of solution lysis 2 (85.6 mg/mL sucrose, 15 mg/mL citric acid and 0.2 µM Sytox green in deionized water) during 30 min at RT. Lysis produces degradation of cytoplasmic membrane that allow penetrance of Sytox green dye that stains nuclei and MN. In this way, this process allowed a differentiation of particles labeled with Sytox green (nuclei and MN of alive cells) or Sytox green and EMA (apoptotic cells). After lysis, samples were stored at 4 ºC until being processed by flow cytometry (up to two days).

Data acquisition was performed by flow cytometry with FACSCalibur; Sytox-associated fluorescence was detected by FL1 channel while EMA-associated fluorescence was detected by FL3 channel. Collected data was analyzed by Flow Jo VX software.

The data of MN presented in this work represents results from five independent experiments each one in duplicate.

III.6- PROTEIN PURIFICATION

III.6.1 TANDEM AFFINITY PURIFICATION

HEK XPF-KO cell line expressing the wt version of XPF with the tandem N-terminal tags SBP and CBP and the HEK XPF-KO cell line expressing an empty vector (EV) tagged were grown until reaching 1 x 10^8 cells of each cell line. Cells expressing TAP-XPF were either non treated or subjected to MMC (1 µM) for 16h or to UVC irradiation (150 J/m^2) and detached after 1h. Cell pellets were processed and purified using InterPlay Mammalian TAP System (Agilent Technologies) according to manufacturer's guidelines except that streptavidin resin was substituted with Streptavidin Magnetic Sepharose beads (GE Healthcare Life Sciences) (40 µl/sample). Calmodulin resin from the last purification step was washed three times in Tris 1M pH 8.5 and 2/3 of the resin volume was sent to mass spectrometry service (PRBB Proteomics- MS facilities) and 1/3 was boiled with Laemmli buffer and loaded in a standard WB gel.

III.6.2 HA-PURIFICATION

HEK XPF-KO cells infected with the XPF-HA were used for XPF protein purification through its C-terminal HA-tag. HEK XPF-KO was used as a control. Two 20-cm culture dishes of HEK XPF-KO were seeded and six 20-cm dishes for HEK XPF-KO +XPF-HA. Out of these six, two dishes were treated with MMC (1.5 µM) during 16h and two with 50 J/m^2 of UVC. UVC treated cells were incubated during 1h at 37ºC before being processed. Cells were trypsinized and lysed with 2 mL of Lysis Buffer (Table XVII) per sample during 15 min at 4ºC. Later, 8 mL of Dilution Buffer (Table XVII) were added before sample sonication (2 x 1 min) and centrifuged at 13,000g during 20 min at 4ºC.

Lysis Buffer	
Final Conc.	Component
50 mM	Tris HCl, pH 7.5
150 mM	KCl
1 mM	EDTA
1%	NP-40
10%	Glycerol
1x	Proteases inhibitor cocktail
	H_2O

Dilution Buffer	
Final Conc.	Component
50 mM	Tris HCl, pH 7.5
150 mM	KCl
1 mM	EDTA
0.1%	Triton X-100
10%	Glycerol
1x	Proteases inhibitor cocktail
	H_2O

Table XVII: Lysis and Dilution Buffers detailed components used for the HA-purification.

Supernatants were filtered with 0.45 µm filters (Millex Syringe Filters) and total protein quantified by Bio-Rad Protein Assay (Biorad). Samples concentrations were adjusted to 10 mg of total protein per tube using 1:5 Lysis:Dilution Buffer. 100 µL of these samples were kept frozen to be used as controls (whole cell extracts (WCE)). Protein purification was performed adding 40 µL of Pierce anti-HA magnetic beads (Thermo Scientific) previously washed in 1:5 Lysis:Dilution buffer. Beads were added to each sample tube and kept rotating overnight at 4ºC. The following day tubes were centrifuged twice at 2,500 g during 5 min at 4ºC, supernatants were discarded and anti-HA magnetic beads were washed ten times in 1:5 buffer before 200 µL of HA Synthetic Peptide (Thermo Fisher) was added. Samples were incubated shaking at 37ºC for 10 min to elute the proteins from the magnetic beads. 10 µL of eluted samples were loaded in a 4-12% agarose gradient WB gel (Mini-PROTEAN Precast gels, Bio-Rad) to check the protein controls. Antibodies used for this WB were: XPF (Mouse Monoclonal Ab-1 (219) Thermo Scientific 1:200) and Tubulin (Mouse, ab7291, Abcam 1:10,000).

III.6.2.1 PROTEIN BAND EXTRACTION FROM SDS GEL

The remaining samples were concentrated by boiling until reducing the volume to around 50 µL and loaded in a 4-12% SDS gel, run at 0.15 Amp for 1:10h. The gel was stained with Coomassie Blue Staining (Thermo Scientific) for around 5h and distained in H_2O overnight. The following day individual protein bands were selected to be cut out from the gel with a scalpel (Figure 21).

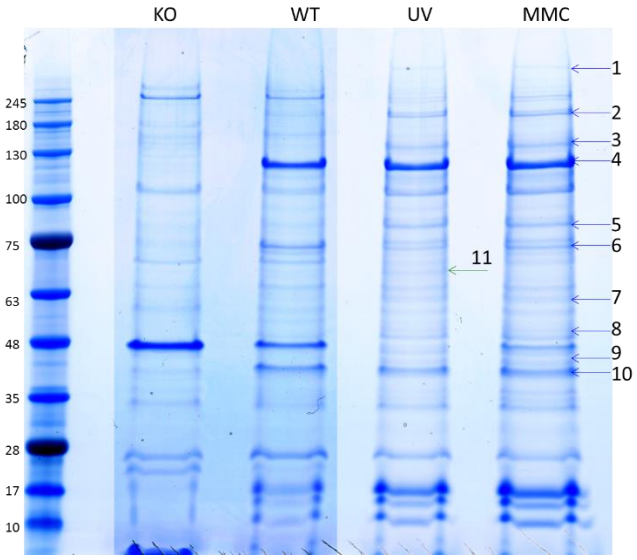

Figure 21: Blue Coomassie SDS gel of XPF-HA purification.

Each individual band was cut in four fragments and dissolved first in 500 µL of Destaining buffer 1 (Table XVIII) during 30 min shaking at 40ºC and secondly in 500 µL of Destaining buffer 2 (Table XVIII).

Destaining buffer 1	
Final Conc	Component
25 mM	Amonium Bicarbonate
50%	Metanol
	H_2O

Destaining buffer 2	
Final Conc	Component
25 mM	Amonium Bicarbonate
50%	Acetonitrile
	H_2O

Table XVIII: Distaining buffers 1 and 2 detailed components used for the protein band extraction of SDS gel.

Then, fragments were washed twice in 500 µL of 25 mM Amonium Bicarbonate during 2 min shaking, the solution was aspirated and 200 µL of Acetonitrile were added during 15 min to remove the water from the gel. Acetonitrile was then removed by a speed vacuum during 10 min. 100 µL of 1:10 Dithiothreitol (DTT) prepared in Amonium Bicarbonate were added to the samples during 1 h shaking at 56ºC. DTT was then removed and samples were washed in 200 µL 25 mM Amonium Bicarbonate shaking at RT during 10 min. Iodoacetomide (IAA) diluted in 25 mM Amonium Bicarbonate was added during 45 min in darkness shaking at 25ºC. After a brief spin, the supernatant was removed and the samples were washed twice in 500 µL for 2 min, then in 200 µL of Acetonitrile for 15 min at RT and dried with the speed vacuum at RT for 15 min. Samples were then digested with 30 µL of Trypsine prepared in 25 mM Amonium Bicarbonate during 10 min. Afterwards, 40 µL of 25 mM Amonium Bicarbonate were added and kept during 16h at 37ºC. Later on, supernatants were transferred to new eppendorfs, 40 µL of 50% Acetonitrile were added and samples were kept in a water bath sonicator for 10 min. The supernatant was removed again and exchanged by 40 µL of 1% Formic Acid during 10 min on the water bath sonicator. These two last steps were repeated and the supernatants were collected. A final water bath sonicator step of 10 min with 70% Acetonitrile was carried and the total supernatant volume was filtered with Centrifugal Filter Units (Millipore) during 1 min at 13,000 g and evaporated until 20 µL of final volume per sample. This volume was finally sent to mass spectrometry service, the ions from the sample were separated according to their mass-to-charge ratio and results were displayed as spectra of the relative abundance of detected ions as a function of the mass-to-charge ratio by specialized softwares.

III.7- STABLE ISOTOPE LABELING WITH AMINO ACIDS IN CELL CULTURE

Stable isotope labeling with aa in cell culture (SILAC) is a technique for *in vivo* incorporation of a label into proteins for mass spectrometry (MS)-based quantitative proteomics (Ong et al. 2002). HEK XPF-KO transduced with XFP-Wt were left untreated or treated with UVC (40J/m^2, 1h recovery time) or MMC (0.5 µg/mL for 21h) treatments in identical culture media except for a 'light' (HEK XPF-KO cells untreated), 'middle' (HEK XPF-

KO + XPF-Wt treated) or 'heavy' (HEK XPF-KO + XPF-Wt untreated) forms of lysine and argnine.

Cells were cultured for 14 days in lysine- and arginine-free DMEM (Thermo Fisher Scientific) containing 10% dialyzed FBS with 200 mg/L L-proline (Sigma). Light media was supplemented with 100 mg/L L-lysine (Thermo Fisher Scientific) and 100 mg/L L-arginine (Thermo Fisher Scientific), middle media was supplemented with 100 mg/L $^{15}N_4$-L-lysine (Thermo Fisher Scientific) and 100 mg/L $^{13}C_6$-L-arginine (Wako Chemicals, Japan), heavy media was supplemented with 100 mg/L $^{13}C_6$,$^{15}N_2$-L-lysine (Wako Chemicals, Japan) and 100 mg/L $^{13}C_6$,$^{15}N_4$L-arginine (Wako Chemicals, Japan).

Cells were lysed in EBC buffer supplemented with protease inhibitor cocktails (Nacalai Tesque, Japan) with brief sonication, and HA-XPF and its interacting proteins were enriched using anti-HA magnetic beads (Thermo Fisher Scientific). Proteins were resolved by SDS-PAGE and in-gel digested with trypsin by standard protocol. Peptide fractions were analyzed on an Easy-nLC1000 coupled to a Q-Exactive instrument (Thermo Fisher Scientific) equipped with a nanoelectrospray source. Peptides were separated on a 50 cm analytical column (75 µm inner diameter) with 2 µm C18 beads (Thermo Fisher Scientific). The column temperature was maintained at 50ºC using an integrated column oven (EASY-Spray, Thermo Fisher Scientific). Each peptide fraction was separated using a 65 min gradient ranging from 0% buffer B (100% ACN and 0.1% formic acid) to 35% buffer B in 60 min and ramped to 95% buffer B in 5 min at a flow rate of 300 nL/min. The washout followed at 95% buffer B for 10 min. Spray voltage was set to 2 kV, s-lens RF level at 50, and heated capillary temperature 320ºC. All experiments were performed in the data-dependent acquisition mode to automatically isolate and fragment top10 multiply-charged precursors (+2, +3 and +4) according to their intensities. Former target ions were dynamically for 15 seconds excluded and all experiments were acquired using positive polarity mode. Full scan resolution was set to 70,000 at m/z 200 and the mass range was set to m/z 380-1500. Full scan ion target value was 3E6 allowing a maximum fill time of 60 ms. Higher-energy collisional dissociation (HCD) fragment scans was acquired with optimal setting for parallel acquisition using 1.6 m/z isolation width and normalized collision energy of 27.

The data were analyzed using SEQUEST in Proteome Discoverer 2.1 (Thermo Fisher Scientific) and searched in the complete human proteome database (Swiss-Prot). The mass tolerances for the precursor and fragment were 10 ppm and 0.02 Da, respectively. Cysteine carbamidomethylation was included as a fixed modification, and N-terminal protein acetylation and methionine oxidation were included as variable modifications. Peptide identification was filtered at a false discovery rate (FDR) < 1%.

This technique provided quantitative information about the interactions stablished by each cell condition based on the mass difference of the different stable-isotope composition. The ratio of peak intensities reflects the relative protein abundance (Figure 22). Abundance ratios were considered reliable over 1.

Figure 22: SILAC experiment with three cell populations labeled. Ratios between samples are calculated comparing the differences in the intensities of the peaks (adapted from (Geiger et al. 2011)).

III.8- COIMMUNOPRECIPITATIONS

In order to confirm protein complexes interactions of XPF and USP11 proteins, endogenous coimmunoprecipitations (CoIP) were performed. 2 x 20 cm Petri dishes were seeded of each cell line. 48h afterwards, cells were trypsinized and lysed using the same buffers as detailed in HA-purification section. After protein quantification and adjustment of the samples to 10 mg in 10 mL, they were incubated overnight with primary antibodies in a final concentration of 1 µg/mL. Antibodies used for the endogenous IP were: XPF (Mouse

Monoclonal Ab-1 (219) Thermo Scientific) and USP11 (Rabbit Monoclonal ab109232, Abcam). The following day, 50 µL of Protein G Magnetic Sepharose beads (GE Healthcare, Life Sciences) were incubated during 3 h rotating at 4ºC with the samples containing the antibodies. After this time antibodies were attached to the beads and these were washed 10 times in 1:5 Dilution buffer as detailed in HA-purification section. Protein complexes were then detached from magnetic beads by boiling them in 40 µL of Laemmli buffer and the eluted proteins were loaded in a MiniProtean Precast gels (Bio-Rad) and standard WB were performed to check CoIP of both proteins.

Besides increasing the amount of XPF-HA tagged in the sample, HA-purifications were also performed to confirm CoIP of USP11 protein following the same protocol.

III.9- *IN VIVO* DOUBLE STRAND BREAKS REPAIR ASSAYS

III.9.1 HOMOLOGOUS RECOMBINATION REPAIR ASSAY

To test the contributive role of XPF and USP11 in HR repair pathway, U2OS carrying the chromosome-integrated reporter DR-GFP (provided by Dr Jasin) were used. This reporter is designed to express the GFP when the HR pathway is activated by the co-expression of the I-SceI endonuclease and GFP fluorescence can be detected and quantified by flow cytometry (Figure 23).

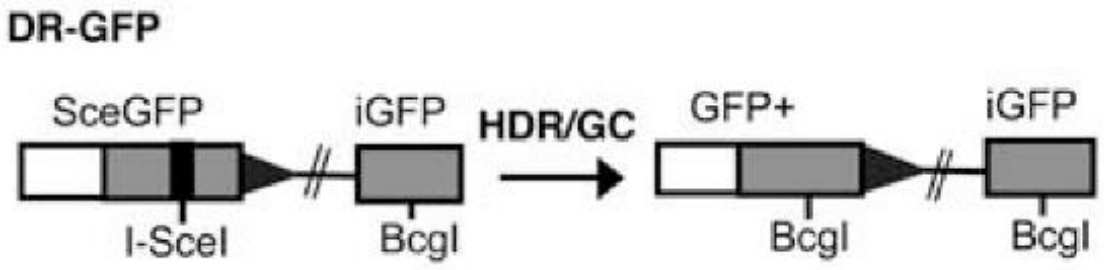

Figure 23: Scheme of the inducible Sce-I reporter system for HR pathway. The reporter contains a GFP gene interrupted by a I-SceI restriction site and a fragment of 5' and 3' truncated of the GFP gene (adapted from (Bennardo et al. 2008)).

siRNA oligos were designed (Sigma) to downregulate XPF and USP11. Negative control was the siRNA of Luciferase and positive control was the siRNA of BRCA2 (Table XIX).

5 x 10^5 U2OS-DR cells were seeded in 6-well plates with 2 mL of DMEM medium. siRNA transfections were performed using Lipofectamine RNAiMAX (Invitrogen) (Table XIX) Transfection Reagent and Opti-MEM (Gibco, Life Technologies) following manufacturer's instructions during two days in a row per duplicate.

siRNA	Sequence	siRNA concentration (nM)	Volume RNAiMAX (µL/well)
Luciferase	5'-CGUACGCGGAAUACUUCGATT-3'	30	7.5
XPF	5'-GCACAAACCUGAAGUUGUA-3'	30	7.5
USP11	5'-CAGAGAUGAAGAAGCGUUA-3'	10	2.5
BRCA2	5'-GGAUUAUACAUAUUUCGCA-3'	10	2.5

Table XIX: siRNA oligo sequences of each gene to target protein downregulations, siRNA concentrations and Lipofectamine RNAiMAX volumes used for the U2OS-DR transfections.

Three different vectors were used to obtain the frequency of transfected cells and the repair efficiency: an EV (CAGGS) as negative control, a GFP expression vector (NZE-GFP) as a positive control and I-Sce endonuclease expression vector (CBAS, kindly provided by Dr Maria Jasin, New York). Cells downregulated with siRNA were transduced with 2.5 µg of one of the three vectors, Polyethylenimine (PEI) (Sigma) and Opti-MEM at a ratio 1:4 DNA/PEI. Two days later cells were analyzed by cell cytometry using the FLH1 channel for the green fluorescence. Data was finally analyzed with FlowJo VX software.

III.9.2 SINGLE STRAND ANNEALING REPAIR ASSAY

U2OS cells used in this assay were carrying the chromosome-integrated reporter SA-GFP to control the SSA induced by the I-SceI endonuclease (Addgene Nº 41594). The reporter was designed to be restored when the SSA repair pathway works (Figure 24); the GFP gene recovers its structure and fluorescence can be detected and quantified by flow cytometry.

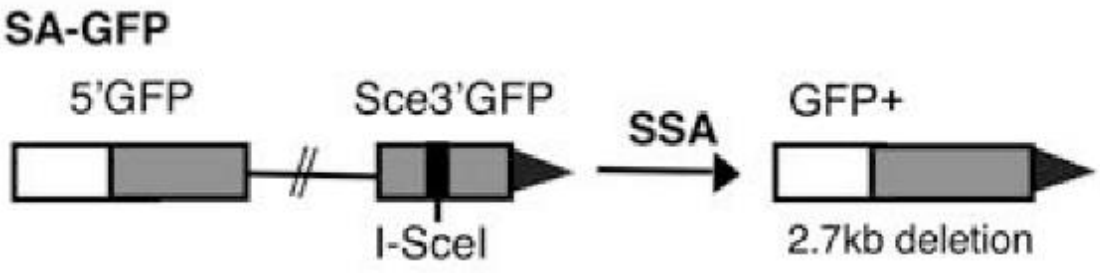

Figure 24: Scheme of the inducible Sce-I reporter system for SSA pathway. The reporter contains a 5' fragment of GFP gene and a 3' fragment of GFP gene with the I-SceI site (adapted from (Bennardo et al. 2008)).

Same siRNA sequences as the ones used in the previous *in vivo* described assay were used to evaluate the role of these proteins in SSA.

All the cells were transduced with 2.5 µg of a vector named pLKO5.sgRNA.EFS.tRFP (Addgene 57823) which produces a red fluorescent protein, and one replicate of the U2OS-SA cells transfected with all the siRNA downregulated genes was, besides, transduced with 2.5 µg of the vector containing the sequence for the I-SceI endonuclease (CBAS). The transfection was performed with PEI (Sigma) and Opti-MEM at a ratio 1:4 DNA/PEI. Two days later cells were analyzed by cell cytometry using the FLH2 channel for the red fluorescence and FLH1 for the green fluorescence. Data was analyzed with FlowJo VX software; double red+green fluorescence values were analyzed for each siRNA transfection transduced either with red or red+SceI vectors (Figure 25); fluorescence values from the red transduced vector were then subtracted from the double transduced red+SceI values and data were represented relative to the negative control (siLuc).

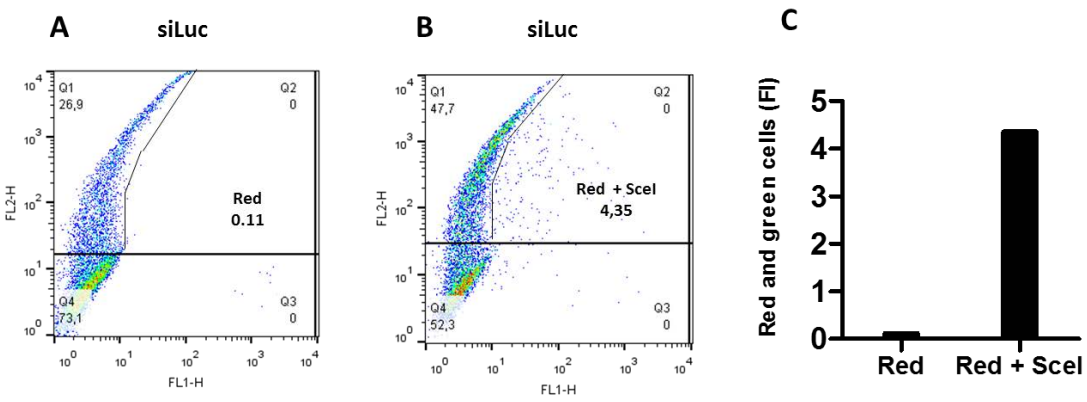

Figure 25: Double fluorescence intensity values in the control (siLuc) sample. For each siRNA transfection, the number of red+green fluorescent cell was analyzed when transducing the cells either with (A) red vector or (B) red+SceI vectors. (C) Fluorescence intensity (FI) in the double transduced sample was almost 40 times higher than in the red vector transduced sample.

Results and Discussion

IV. RESULTS AND DISCUSSION

PROJECT 1

IV.1- ESTABLISHING OF THE HEK 293T TALEN *ERCC4*-KNOCKED OUT AS THE XPF-KO BACKGROUND CELL LINE

The purpose of this project was to analyze the genotype-phenotype correlation of *ERCC4* pathogenic variants. As it is well known, genetic background influences phenotypes and the creation of isogenic cell lines has been a key point of this study. TALEN technology was used to edit the genome of HEK 293T cells. TALEN nucleases were engineered to bind to an *ERCC4* specific sequence to disrupt the gene sequence and generate a human cell line KO for this gene.

Our system consisted of different vectors, a pair of TALEN plasmids (forward and reverse) with the target sequence fused to a FokI nuclease domain and a reporter-based plasmid containing the same *ERCC4* recognition sequence, the red fluorescent protein sequence and an out of frame GFP that could be restored when the DSB was repaired by NHEJ. The fluorescence was visible 48 h post transfection with TALEN and surrogate plasmids. Cells where TALEN proteins were cutting the DNA target site showed red and green fluorescence as showed in figure 26.

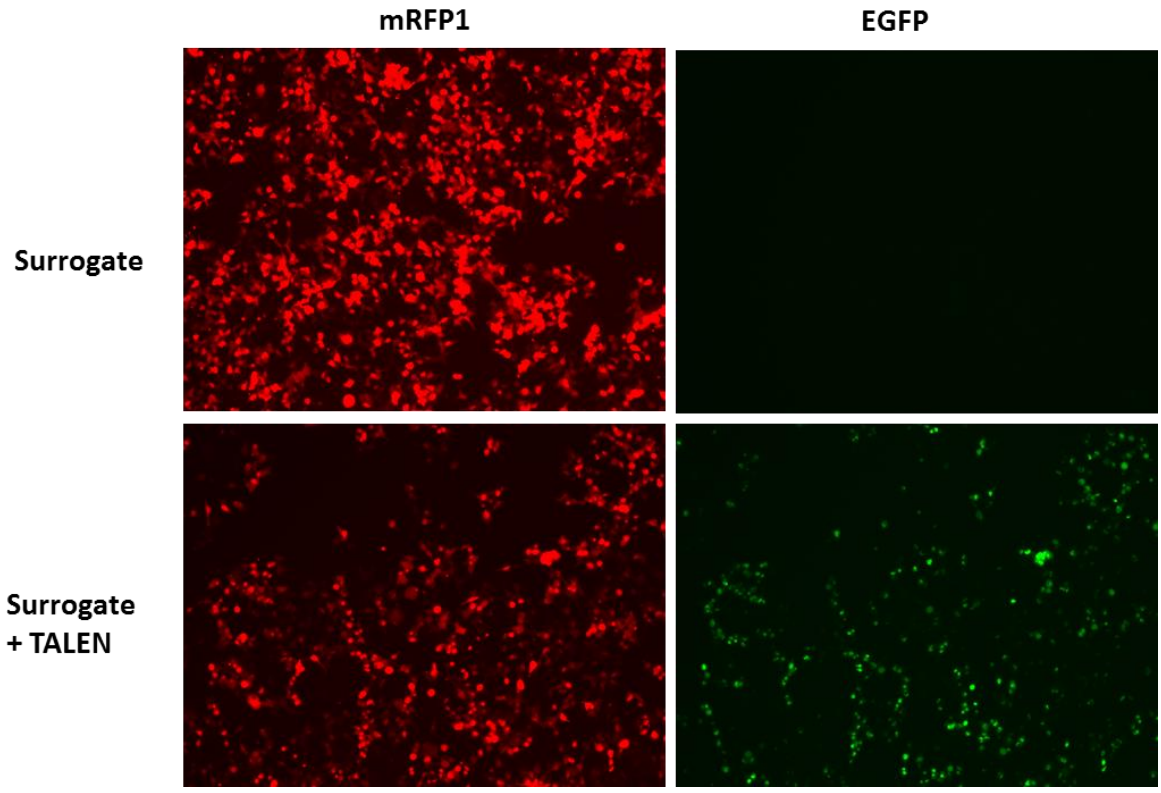

Figure 26: Analysis of TALEN endonuclease activity by fluorescence microscopy. Cell cultures images 48h after transfection with either Surrogate vector or Surrogate + TALEN vectors are shown. Red fluorescence is detected in cells transfected with Surrogate (RFP+) vector; red and green fluorescence is detected in cells transfected with Surrogate + TALEN (RFP+GFP+) vector. No presence of double positive cells was found in cell cultures transfected just with the Surrogate vector.

After cell sorting to select the double fluorescent cells, single cell cloning was performed and, 2-3 weeks later, clones were picked and checked by WB to identify any *ERCC4* KO ones. Three clones showed no XPF band (Figure 27) and clone number 1 was selected to continue the KO validation.

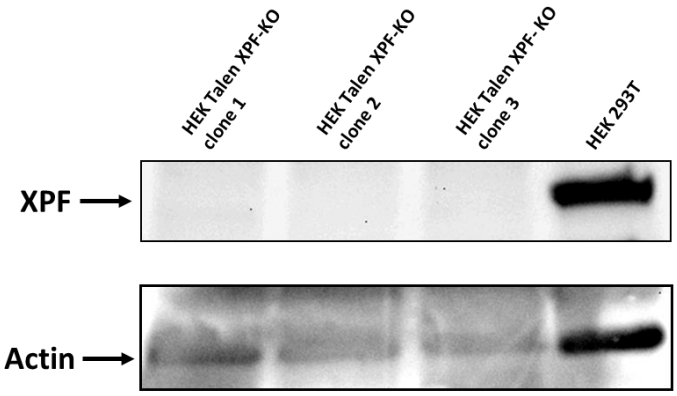

Figure 27: WB analysis of XPF TALEN clones. None of the three clones showed an XPF band meaning that genome edition in order to create a KO was successful. Actin band is shown as a loading control.

Sequencing analysis of genomic DNA from clone 1 revealed that the mutations introduced by the TALEN were two different deletions of 4 and 7 bp respectively: c.281_284del and c.280_286del (Figure 28). Primer walking sequencing of the whole *ERCC4* gene confirmed that the rest of the sequence remained unaltered.

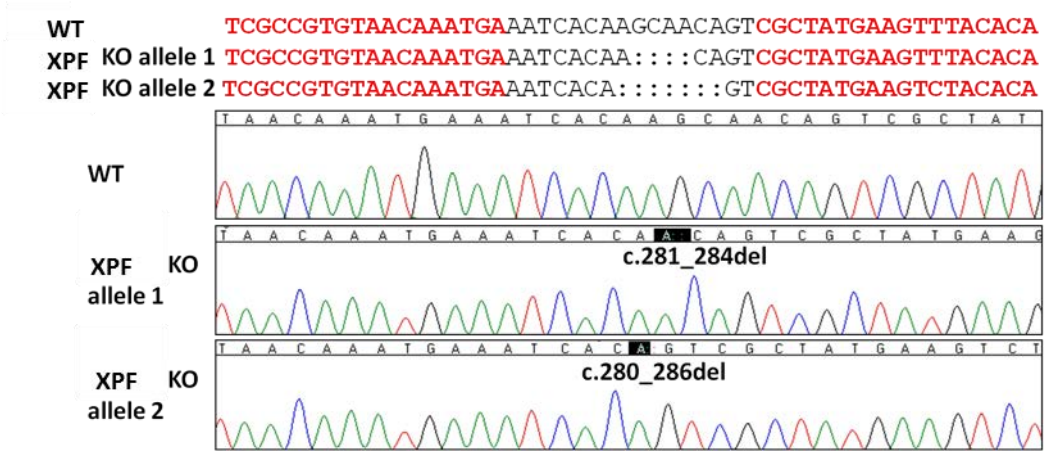

Figure 28: Sequencing reaction chromatograms of heterozygous mutant clones. The KO clone was a compound heterozygote for a 4 bp deletion (c.281_284del) and a 7 bp deletion (c.289_286del) both in exon 2.

The wt cDNA of *ERCC4* modified with SBP and CBP epitopes in N-terminal and HA epitope in C-terminal sites cloned in the pULTRA vector (see materials and methods) was transduced in the HEK XPF-KO cell line (Figure 29). Subsequent, GFP sorting by flow cytometry allowed selection of the infected cells.

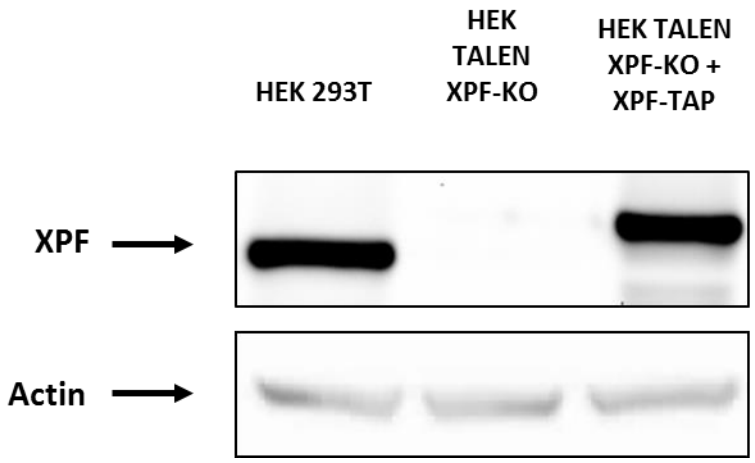

Figure 29: WB validation of the HEK XPF-KO cell line transduced with XPF-tagged viral vectors. XPF band is clearly detectable in HEK 293T and in HEK TALEN XPF-KO + XPF-TAP. The slight difference in the molecular weight from the endogenous XPF of HEK 293T to the exogenous one was due to the TAP and HA epitopes. Actin band is shown as a loading control.

To test whether the exogenous XPF was complementing the cellular phenotype, UVC and DEB sensitivity survival assays of these cell lines were performed. According to expectations, the HEK XPF-KO cell line was hypersensitive to UVC or ICL treatments. HEK XPF-KO was more than 4 times more sensitive to UVC irradiation and more than 10 times to DEB treatment than the control line HEK 293T, however XPF-KO complemented with the XPF-Wt restored the cellular phenotype after both treatments (Figure 30). This genetic complementation evidenced TAP and HA epitopes were not affecting XPF function.

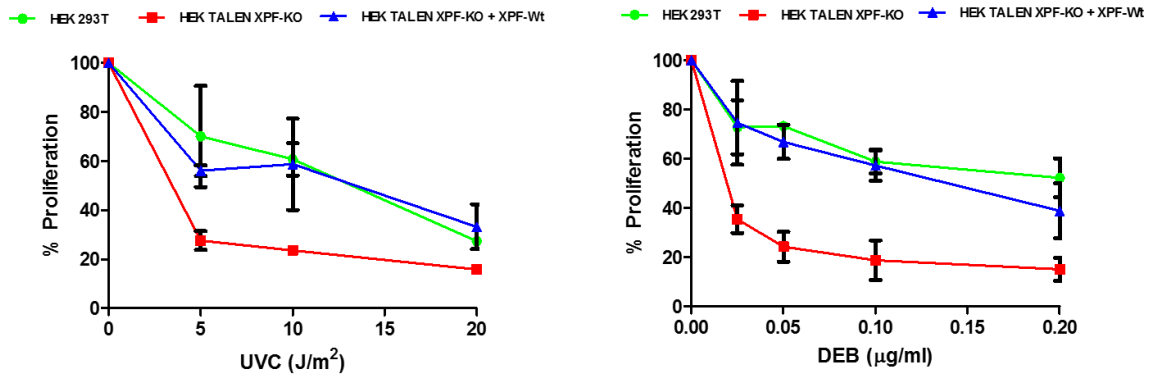

Figure 30: Functional studies of HEK XPF-KO transduced with XPF-Wt compared to positive and negative controls. The proliferation percentage of HEK XPF + XPF-Wt cells was similar to the positive control under UVC irradiation or DEB treatment as exogenous XPF restores the cell phenotype. Graphs represent proliferation percentage media of two independent experiments of two replicates with standard deviation (SD).

Although the phenotype of cells lacking *ERCC4* was previously studied in MEFs (Bogliolo et al. 2013) , this was the first successful attempt to edit a human cell line to achieve an *ERCC4* KO. Previous studies comparing prevalence of *ERCC4* mutation frequency observed in patients with the mutation frequency expected to obtain according to Hardy-Weinberg principle revealed under representations of biallelic combinations of *ERCC4*, indicating that most of biallelic mutations in humans are embryo lethal (Osorio et al. 2013). Actually, all the patients presenting biallelic mutations in XPF retain at least a hypomorfic allele (Bogliolo et al. 2013; Kashiyama et al. 2013). Regarding the similar embryo lethality described in MEFs Xpf-KO, an additional survival including this MEF Xpf-KO cell line was performed to compare the sensitivity to UVC irradiation of the two XPF-KO lines among the different cell models. Consistently, HEK XPF-KO were as sensitive as MEFs Xpf-KO (Figure 31).

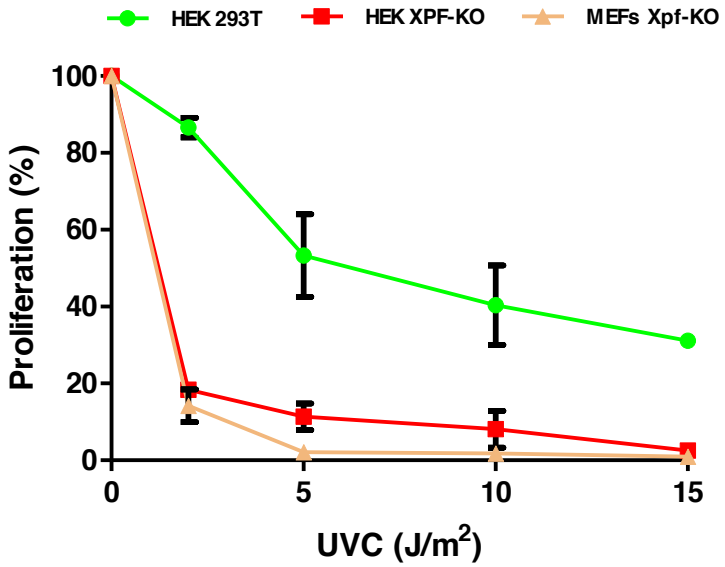

Figure 31: UVC cell survival to compare XPF-KO in different cell lines. The TALEN edited HEK XPF-KO showed levels of UVC sensitivity comparable to MEFs Xpf-KO, previously reported as sensitive. Graph represents proliferation percentage media and SD of two independent experiments of two replicates.

If left unrepaired, chromosome alterations caused by ICL produce a block of the cell cycle in G2/M phase. The HEK XPF-KO phenotype was tested for the percentage of cells stalled in G2/M after being treated with two different doses of DEB. As shown in figure 32, KO cells showed higher amounts of G2/M arrested cells due to the inability of repairing the accumulation of alterations in the chromosomes. The same phenotype was observed in MEFs Xpf-KO (Osorio et al. 2013). Furthermore, analyses of the cell cycle also confirmed that accumulation of cells in G2/M phase of the XPF-KO was restored to the normality after introduction of the XPF-Wt.

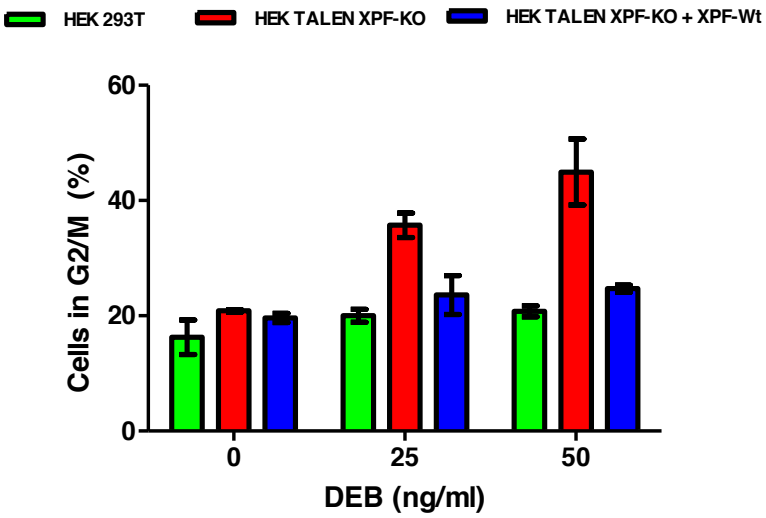

Figure 32: Cell cycle study of HEK XPF-KO cells transduced with exogenous XPF-Wt protein. XPF-KO cells transduced with XPF-Wt reduced their percentage of cells stalled in G2/M phase to similar levels to the HEK 293T. Graph represents the media of two independent experiments with SD.

IV.2- ANALYSES OF DIFFERENT XPF VARIANTS IN AN XPF-KO BACKGROUND

IV.2.1 SELECTION OF THE XPF SINGLE NUCLEOTIDE VARIANTS TO STUDY

Among the several mutations described in patients we selected seven different single nucleotide changes of *ERCC4* that had been associated with a characteristic clinical phenotype (Figure 33).

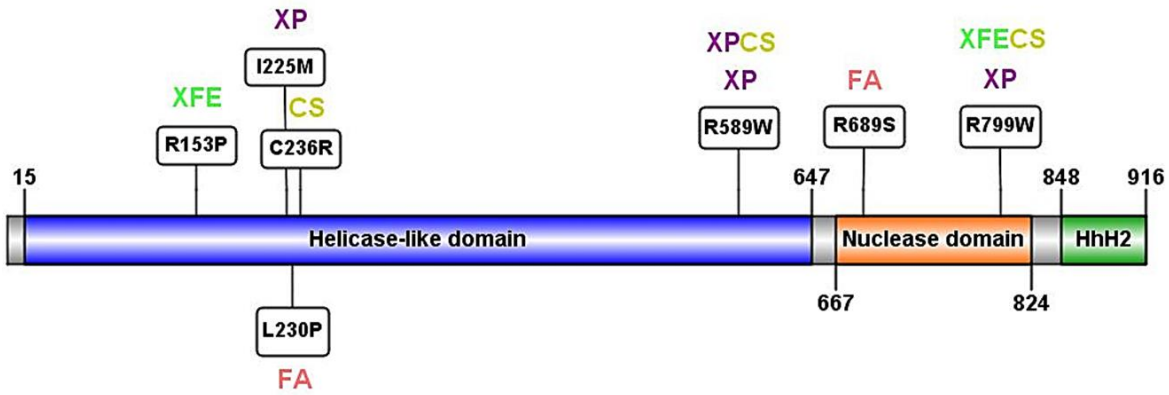

Figure 33: Schematic view of the XPF domains with the selected mutations. Seven single XPF disease-associated variants were selected for the study. Five of them correspond to the helicase-like domain and two of them are located in the nuclease domain. In green, XFE; in purple: XP; in pink, FA; in mustard: CS. The patient XPCSCD had an allele with C236R and the other with R589W. R799W mutation found in homozygosis in XP patients was also found in a cohort of patients with XFE sharing CS features. This figure was created with a protein designing software from (Liu et al. 2015).

The aminoacidic non-conservative substitution of a highly conserved arginine for a proline, R153P, was caused by a nucleotide change (c.458G>C) found in homozygosity in an XFE patient. This aminoacidic change affects the helicase domain, a leucine-rich region involved in the interaction with SLX4 and DNA binding (Klein Douwel et al. 2017). The patient's main feature was the accelerated ageing phenotype and the disease was named as XFE progeroid syndrome (Niedernhofer et al. 2006). Catalytic activity of XPF^{R153P} was almost intact but the mutant was unable to properly locate into the nucleus and remained mislocalized in the cytoplasm due to protein misfolding (Ahmad et al. 2010).

The aminoacidic change I225M caused by a nucleotide substitution (c.653A>G) was found in heterozygosity with another missense mutation (c.1515G>A; G513R) in a patient showing mild XP features (Matsumura et al. 1998). Although I225M is located in the same domain as the R153P, XPF is stable and its interacting ability with SLX4 is not affected (K. Hashimoto et al. 2015). The other missense mutation found in the patient, G513R, is located

C-terminal further in the same domain but it does not lead to complete dysfunction in NER, which explains the mild XP phenotype of XPF^{I225M} (Matsumura et al. 1998).

The aminoacidic change of a highly conserved residue L230P caused by the nucleotide change c.689T>C was found in the paternal allele of an FA patient carrying a 28 bp duplication in exon 11 of the maternal allele (c.2371_2398dup28 [p.Ile800Thrfs*24]). The duplication truncates XPF by missing the HhH_2 domain (Bogliolo et al. 2013). The HhH_2 domain truncated by the duplication is essential for ERCC1 binding while the analyzed mutation affects SLX4 binding (K. Hashimoto et al. 2015).

The aminoacidic change C236R (c.706T>C) was found in heterozygosity in two different patients: a patient with CS disease carried this mutation located in the N-terminal helicase domain and an exon 8 frameshift insertion which generated a premature stop codon (c.1730_1731insA [p.Tyr577*]) in the other allele. A second patient carried c.706T>C mutation in heterozygosity with another missense mutation (c.1765C>T, p.R589W), previously found in XP individuals. This second patient showed a combined syndrome of CS and XP named CSXPCD (Kashiyama et al. 2013). Interestingly, XPF^{C236R} does not affect SLX4 binding despite being in N-terminal region very close to other involved mutations, while XPF^{R589W} severely affects its structure and SLX4 binding ability (K. Hashimoto et al. 2015). R589W change was previously associated with different XP clinical phenotypes: combined with a deletion in exon 3 of the second allele caused severe XP while in heterozygosity with the missenses mutations causing R799W or P379S aminoacidic changes caused mild XP (Ahmad et al. 2010; Kashiyama et al. 2013).

In another FA patient a new *ERCC4* missense mutation was found in exon 11 of one allele (c.2065C>A [p.Arg689Ser]) while the other allele had a 5 bp deletion in exon 8 (c.1484_1488delCTCAA) that leads to a frameshift and a premature stop codon (p.Thr495Asnfs*6) (Bogliolo et al. 2013). This mutation is in the nuclease domain and it affects its excision activity.

The c.2395C>T (R799W) was found in homozygosis in a patient (Sijbers et al. 1998) diagnosed with XP disease but recently was found in heterozygosity with a truncated allele (c.388+1164_792+795del (p.Gly130Aspfs*18)) in a patient from a cohort of patients with

progeria syndromes. The patient showed low RRS levels typical of CS phenotype (Mori et al. 2018). Thus is possible that, regarding also the XP phenotype found in the heterozygote R799W/R589W, a dosage effect of XPF^{R799W} can influence the phenotypical outcomes of the patients.

IV.2.2 EXPRESSION OF THE XPF MUTANT VARIANTS IN AN XPF-KO BACKGROUND

The expression levels of all the mutant XPF proteins (XPF^{R153P}, XPF^{I225M}, XPF^{L230P}, XPF^{C236R}, XPF^{R589W}, XPF^{R689S} and XPF^{R799W}) were assessed by WB (Figure 34).

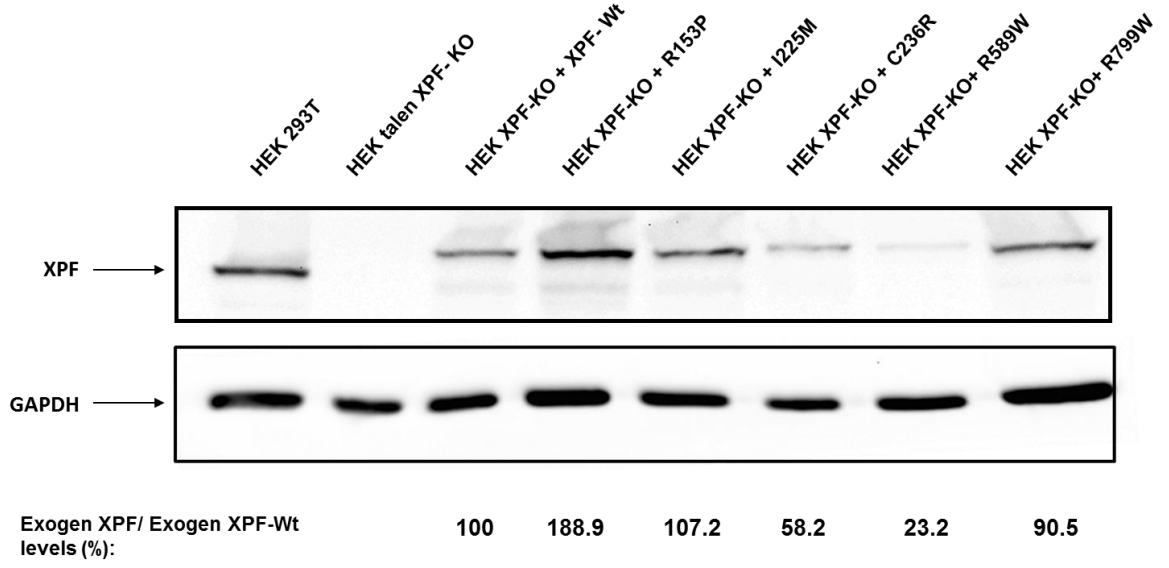

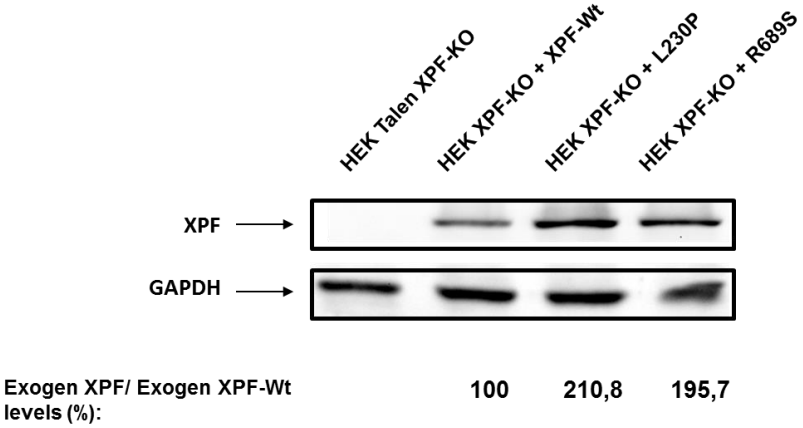

Figure 34: WB levels of each single variant XPF mutant transduced cell line. Levels of XPF proteins are expressed as a percentage relative to the exogenous XPF-Wt. GAPDH is used as a loading control.

All XPF variants were detectable by WB and some of them had levels of expression similar to XPF-Wt (XPF^{I225M} and XPF^{R799W}). XPF^{R153P}, XPF^{L230P} and XPF^{R689S} showed increased levels of protein production compared to the XPF-Wt. This was in contrast to the reduced levels observed in patients (Bogliolo et al. 2013; Mori et al. 2018; Niedernhofer et al. 2006; Sijbers et al. 1998). The increased levels detected in vitro ensure that the cellular phenotype-genotype correlation is not due to a matter of protein quantity, but depends on the single mutation that alters the essential protein in a specific way. XPF^{C236R} and XPF^{R589W}, however, showed decreased levels relative to the Wt-XPF even in vitro, which could further explain the cellular phenotypes of these mutations.

IV.2.3 FUNCTIONAL ANALYSES OF XPF VARIANTS

IV.2.3.1 NER PATHWAY

Several assays were performed to test and compare the behavior of the pathogenic XPF variants after UVC irradiation in an isogenic background: UV sensitivity, UDS and RRS.

First of all we tested the sensitivity of our cell lines to UVC irradiation: figure 35 shows the percentage of surviving cells of each cell line after different doses of UVC radiation.

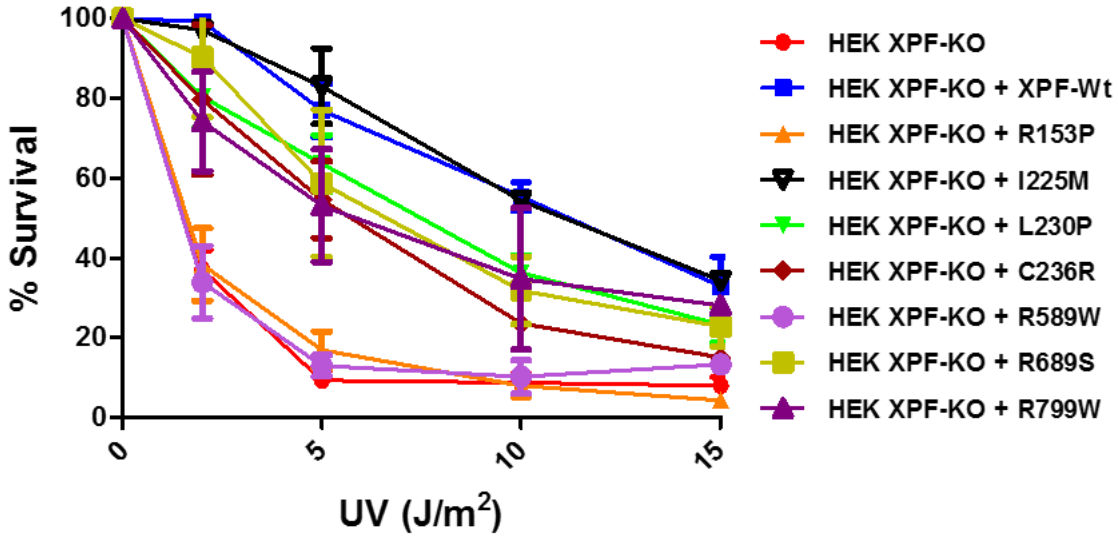

Figure 35: Percentage of surviving cells after increasing doses of UV irradiation. Graph represents the media of at least two independent experiments with two replicates and the standard error of the mean (SEM).

All the variants showed increased levels of sensitivity in comparison with the XPF-Wt with the exception of XPF^{I225M}, that was in contrast with previous studies (Matsumura et al. 1998). Matsumura group found mRNA expression of this variant was similar to Wt fibroblasts but they were unable to detect the mutant protein by WB, suggesting a rapid degradation of the mutant variant. In contrast, our XPF^{I225M} levels were comparable to the Wt as shown in figure 35, which could justify this unexpected resistance. Considering that the clinical phenotype associated to this mutant could be a matter of protein level production that was not corresponding to our XPF^{I225M} protein level, this variant was eliminated from all the successive analyses. For a better understanding, the data has been split into two different graphs, the first one including controls and XPF variants R153P (XFE), L230P (FA) and

R689S (FA); and a second graph with controls and XPF variants C236R (CS), R589W (CS/XP) and R799W (XP and XFE/CS) (Figure 36).

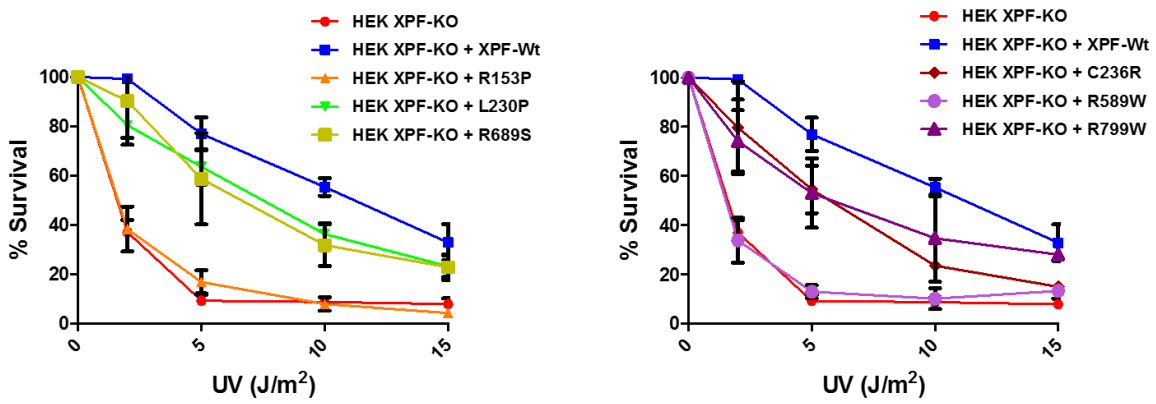

Figure 36: Percentage of surviving cells after increasing doses of UV irradiation. The previous data has been split in two different graphs for a better understanding.

Cells producing XPF^{R153P} and XPF^{R589W} are very sensitive to UV, at similar levels to the XPF-KO. These results are in concordance with the phenotype of the patient in which these mutations were identified, as XPF^{R153P} was found in homozygosis in an XFE progeroid patient that showed skin photosensitivity (Niedernhofer et al. 2006), and XPF^{R589W} was found in XP patients (Gregg et al. 2011) and in an XPCSCD patient providing the mutant allele that confers the XP phenotype (Kashiyama et al. 2013). XPF^{R153P} results for UV sensitivity were essentially identical to the previously reported studies that identified it as 10x more sensitive to UV (Niedernhofer et al. 2006). XP patients main feature is the extreme sensitivity to UV irradiation, although there are different levels of sensitivity from the proteins involved in this disease (Matsumura et al. 1998). Unexpectedly, XPF^{R589W} sensitivity was higher than the previously reported for the XP condition that presented 2-3x more sensitive than XPF-Wt (Gregg et al. 2011), pointing the importance of the residual activity of the second mutant allele Pro379Ser (P379S) in NER. XPF^{R799W} was initially found in homozygosis in an XP patient (Sijbers et al. 1998) but it was recently reclassified as a CS mutant with XFE features when the second allele had an early truncating mutation (Mori et al. 2018). In line with these last results, XPF^{R799W} just showed a mild sensitivity to UVC very similar to the sensitivity of

the Cockayne associated XPF^{C236R} variant. This result also provides an explanation to the mild XP phenotype of the double mutant R589W-R799W (Kashiyama et al. 2013) and indicates that XPF^{R799W} retains the majority of its functions in UVC induced DNA repair. Another hypothesis that could explain the behavior of R799W variant could be a gene dosage effect: in homozygosis it would be associated to mild XP (Sijbers et al. 1998) while in heterozygosis with a null allele it would be associated to atypical XFE disease sharing features of CS (Mori et al. 2018). In heterozygosis with R589W, it would be responsible for the patient's CS features while the R589W would be the cause of the XP phenotype also present in the patient (Fassihi et al. 2016). This last hypothesis highlights the importance of the genetic background of the patients in the modulation of the phenotype.

The two XPF variants found in FA patients, XPF^{L230P} and XPF^{R689S} showed a marked resistance to UVC compared to the defective XPF. These results confirmed previous studies which proved that these two mutations do not seem to completely impair XPF to participate in NER pathway (Bogliolo et al. 2013).

Regarding XPF^{C236R}, previously associated with CS, showed mild UVC sensitivity, in accordance with the low UVC sensitivities of CS patients derived cells (Kashiyama et al. 2013).

To further discern among the XPF variants whose mutation impairs NER pathway, functional analysis to individually evaluate GG-NER and the TC-NER were performed with the whole set of variants. Figure 37 shows UDS assay data representing the ability of each XPF variant cell line to synthesize DNA to repair a damage induced by UVC in the G1 phase of the cell cycle.

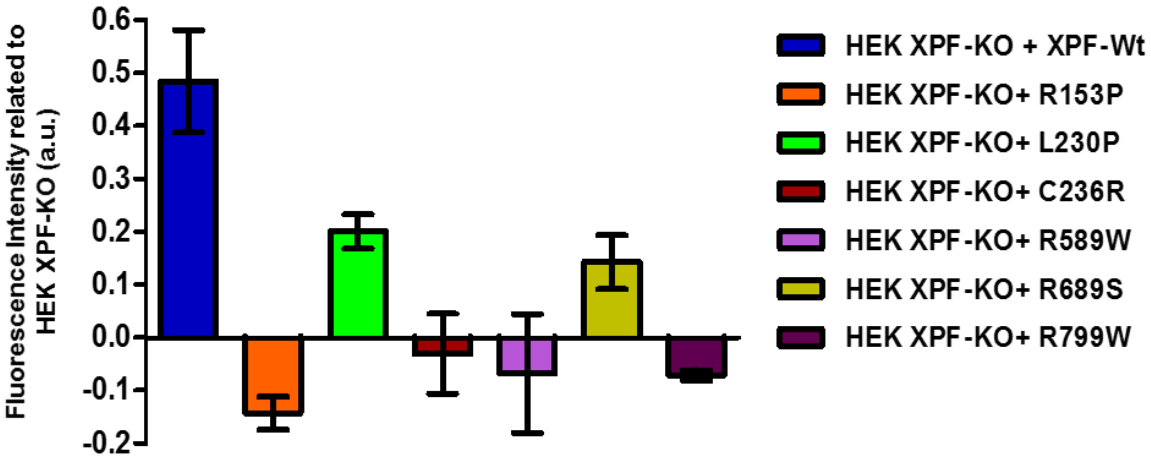

Figure 37: UDS assay of the of XPF mutants set. Fluorescence intensity is represented relative to fluorescence intensity of HEK XPF-KO. Graph represents the media of at least three independent experiments with SD.

These assay results allowed a clear distinction from the XPF mutations that conferred UV sensitivity. Despite all the variants showed a certain grade of impairment in UDS, the two FA associated mutations, XPF^{L230P} and XPF^{R689S} retained around 30-40% of their UDS abilities when compared to the wt-corrected cells. XPF^{R153P} showed the lowest UDS value and the CS and the XP associated mutations, XPF^{C236R}, XPF^{R589W} and XPF^{R799W}, showed UDS levels similar to the XPF-KO. These observations are in line with the UDS levels of the patients-derived cells bearing these mutations (Ahmad et al. 2010; Gregg et al. 2011; Kashiyama et al. 2013; Mori et al. 2018). These results demonstrate that XFE, XP or CS associated mutations impair GG-NER much more then FA related mutations.

The TC-NER subpathway activity of the set of XPF mutants was evaluated by a RRS assay after UV induced damage. The graph from figure 38 represents the ability of each cell line to synthetize RNA after the damage in comparison with the XPF-KO cells.

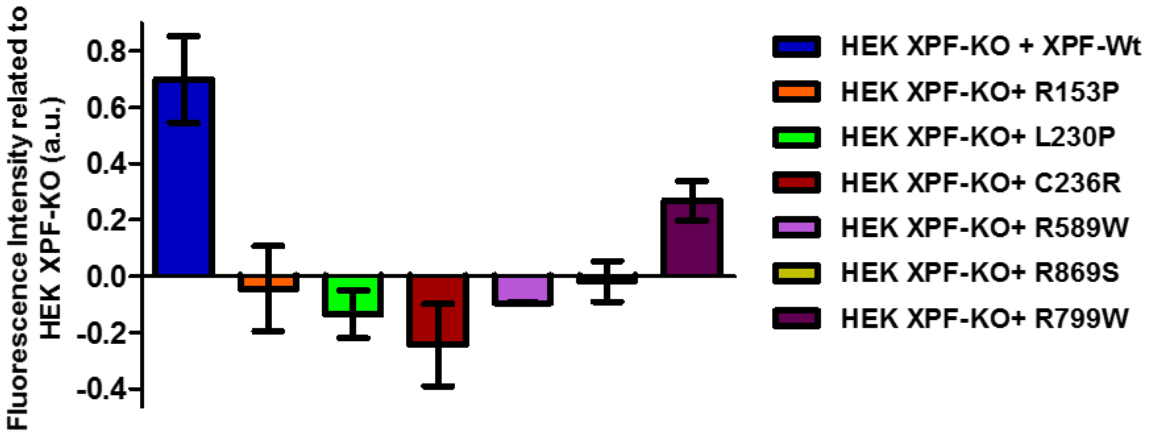

Figure 38: RRS assay of XPF mutants set. Fluorescence intensity is represented relative to fluorescence intensity of HEK XPF-KO. Graph represents the media of at least three independent experiments with SD.

The mutation XPF^{R153P} had low levels of RRS as expected by its inability to reach the nucleus and the mutation associated to CS, XPF^{C236R}, showed the strongest impair in concordance with literature (Kashiyama et al. 2013); notwithstanding XPF^{L230P} and XPF^{R689S} involved in FA, have a high impact in the RRS after UV-induced damage. The XP associated mutation XPF^{R799W} is the only one from the studied variants with a residual ability to synthetize RNA after the damage, which drives to reconsider this assay as a useful tool to discern mutations associated with typical CS pathology rather than XP. Actually, it has been recently put up for debate if RRS levels should be used as a determinant feature for CS classification regarding the phenotype variability of the patients which has driven to the enlargement of diagnosis criteria focusing in their clinical features instead (Wilson et al. 2016). Consequently, with our results, RRS assay would not be able neither to provide conclusive data for pathological XPF variants associated with FA. Interestingly, some of the FA proteins such as BRCA1, FANCD1, FANCD2, FANCA and FANCM have been reported to be involved in resolving RNA-DNA ICLs, which are known as R-loops (Garcia-Rubio et al. 2015; Lafuente-Barquero et al. 2017). These loops are produced when the stalled replication fork forms a hybrid with the transcriptional nascent mRNA. According to the low RRS levels showed by XPF^{L230P} and XPF^{R689S}, one hypothesis could be that XPF was also

one of the FA proteins involved in the removal of these R-loops, therefore XPF mutations could affect its ability to participate in RNA-DNA ICLs repair, resulting in TCR impairment.

IV.2.3.2 ICLR PATHWAY

The repair of the two covalently linked strands of DNA caused by products of the metabolism or external agents is crucial for the survival of cells. The role of XPF as a 5' endonuclease involved in the excision of this damage is largely identified. To test the phenotypical behavior of the XPF variants in the repair of DNA crosslinks, a DEB survival test with increasing doses was performed (Figure 39).

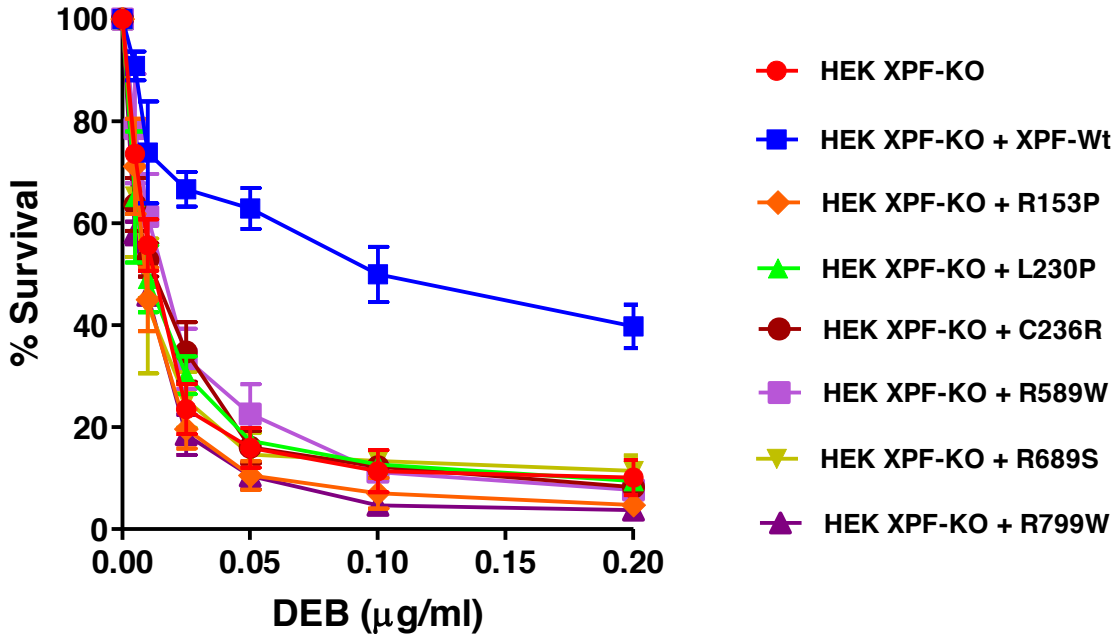

Figure 39: Percentage of surviving cells under increasing doses of DEB. Graph represents the media of at least two independent experiments with two replicates and the SEM.

All the XPF variants cells showed a marked ICL sensitivity, resembling cells lacking XPF. XFE Progeria associated variant XPF^{R153P} was already reported to impair ICL

(Niedernhofer et al. 2006) due to its improper folding and its inability to reach the nucleus. XPF^{R799W} showed a strong sensitivity to DEB, more significant than the around 60% sensitivity to MMC that was considered to classify it as an XFE mutation (Mori et al. 2018). The two FA associated mutants XPF^{L230P} and XPF^{R689S} which were previously reported to impair ICL (Bogliolo et al. 2013) were also very sensitive as the CS associated variant XPF^{C236R} , which was additionally reported to impair ICL (Klein Douwel et al. 2017).

The only XPF variant whose ICLR could be expected to be less affected was XPF^{R589W}, as it has been classified as an XP or XPCSCD variant, but the DEB sensitivity assay did not point towards this hypothesis. One hypothesis to explain this marked DEB sensitivity could be that crosslinks inducers are also responsible for generating DNA mono-adducts, which are repaired by NER (Grant et al. 1998) and therefore XPF mutations affecting NER would be also impairing ICLR. Additionally, it is thought that during TLS in FA pathway, the bypassed mono-adduct is repaired by NER, thereby mutations affecting NER would be also impairing ICLR.

IV.2.3.2.1 ICL- INDUCED G2/M ARREST

The accumulation of chromosome alterations caused by ICL agents exposure is associated with a delay of the cell cycle to come into mitosis phase. A DEB-induced G2/M cell cycle arrest assay was performed to test if the different XPF variants could prevent the cells from being arrested in G2/M phase of the cell cycle due to the DEB-induced chromosome alterations. For a better understanding of the results, data have been plotted in two different graphs sharing the same control cell lines and the same cell lines have been then plotted in two different graphs showing a more accurate view of low DEB doses results (Figure 40).

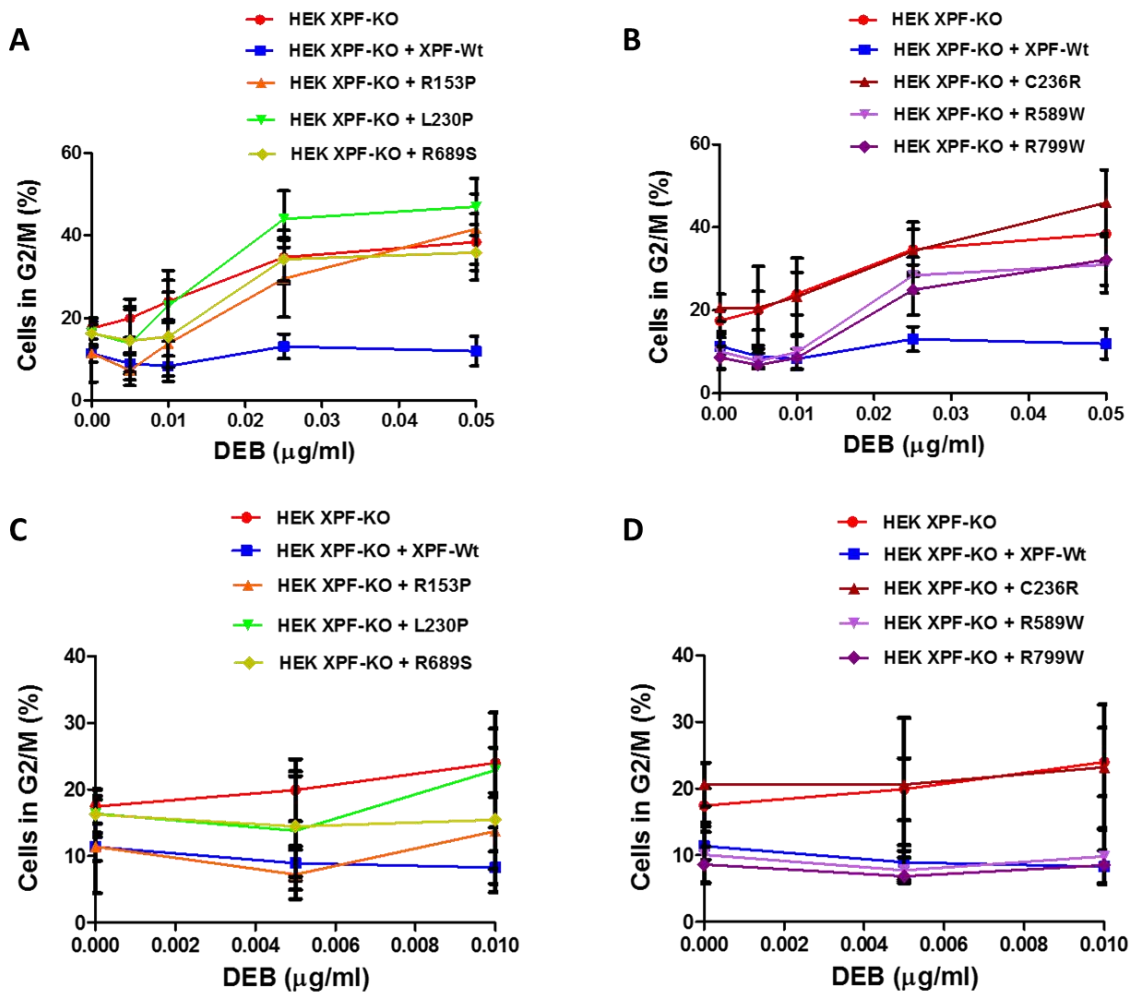

Figure 40: Percentage of cells stalled in G2/M phase after DEB exposition. A and B: Half of the XPF variants are represented in each graph with the positive and negative controls. Each graph represents the media of at least two independent experiments with the SEM. C and D: Plots of low DEB doses are represented here for a better understanding. Each graph represents the media of at least two independent experiments with the SEM.

All the XPF variants showed a higher percentage of G2/M arrested cells than the XPF-Wt. The two mutations associated with FA disease, XPF^{L230P} and XPF^{R689S} followed a similar pattern and, in concordance with previous studies (Osorio et al. 2013) and the DEB survival assay data, display about the same percentage of arrested cells than the negative control. Additionally, progeria associated mutation XPF^{R153P} and CS associated mutation XPF^{C236R}

levels of arrestment were as well very high. This could be easily understood for the XFE mutation but it was less clear for the CS mutation, although the criteria to identify a CS variant covers now a wider range of phenotypes (Wilson et al. 2016) including ICL sensitivity. Our original data show that the G2/M block after ICL treatment could be another useful parameter to be considered in the diagnosis of CS. Regarding the remaining variants, XPF^{R589W} and XPF^{R799W}, showed a very similar phenotype, less severe than the rest of the mutants but still showing large number of arrested cells. Indeed, at low doses of DEB these two cell lines were behaving as the XPF-Wt (Figure 40), which could be explained because R589W is reported to be an XP associated disease, and by hence its main affected DNA repair pathway could be NER instead of ICLR; and R799W, associated to XP and to XFE with CS features, could have a minor impact on ICLR pathway and the cell sensitivity to DEB could be more related (and similar to XPF^{R589W}) to the repair of DEB mono-adducts than to the ICLs.

IV.2.3.2.2 ANALYSIS OF ICL INDUCED CHROMOSOME FRAGILITY

Crosslinker agents produce in ICLR deficient cells chromosome breaks that can be left behind in anaphase and produce MN in the daughter cells. The MN-Fragility test (Avlasevich et al. 2006) provided useful information about the levels of chromosome breaks measured by counting the number of MN. MN formed after treating the set of our XPF variants with DEB is shown in the figure 41.

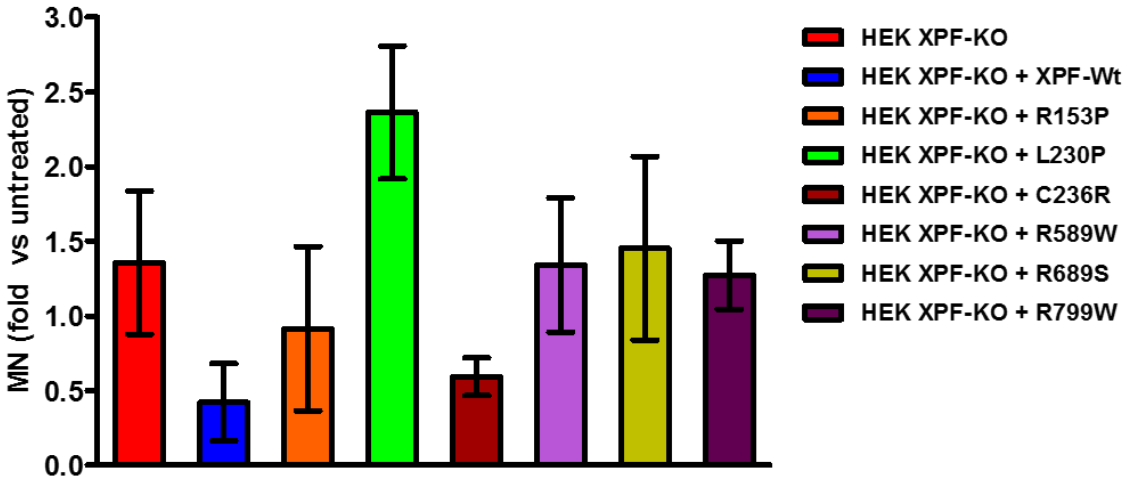

Figure 41: MN test after DEB (0.01 µg/mL) exposure of all XPF variants. Data is represented in fold changed vs untreated cells. Graph represents the media of at least three independent experiments with SD.

XPF^{L230P} (FA) showed the highest number of MN after treatment, in concordance with the chromosome fragility phenotype of the FA patient from which it was identified (Bogliolo et al. 2013). The other FA associated mutation, XPF^{R689S} showed similar levels of MN to the XPF-KO cell line. XPF^{R589W} (XP), and XPF^{R799W} (XP, XFE/CS) variants also showed fragility levels resembling the ones of the XPF-KO cell line. Interestingly, R589W and R799W mutations showed high levels of MN even if the percentages of G2/M arrested cells were moderate, indicating that most of the cells that achieved to reach the mitosis phase accumulated many chromosomal breaks. XPF^{C236R}, CS associated variant, does not show chromosome fragility under DEB exposure, meaning that DEB causes less chromosome alterations probably because more DNA damage is successfully resolved during the prolonged G2/M block (see figure 39) and the percentage of cells reaching telophase do not present so many chromosome breaks. In contrast, the high number of MN found in XPF^{L230P} (and in the other cell lines) suggests that a higher percentage of cells are unable to repair the DNA damage during the G2/M block and that the cells that escape the block carry a heavy burden of breaks. The SD of XPF^{R153P} sample is too large to reach any definitive conclusion.

In the case of R799W and R589W at these doses of DEB the G2/M block is similar to the wt indicating that the G2/M check point in these cells could not be activated. This would explain the increased levels of DNA damage that is not repaired that is found in the daughter cells.

IV.3- OVERVIEW OF THE ANALYZED XPF VARIANTS CELLULAR PHENOTYPES

This has been the first time that the function of several XPF variants associated to distinct clinical phenotypes has been compared in isogenic human cell lines *in vivo*. This enables to analyze if the variability of the phenotypes is correlated with the specific nucleotide changes or it is influenced by other factors such as the genetic background, the ability of the protein to fold properly and reach the nucleus or the possible interactions with other proteins.

At first glance, it is remarkable how the position of the aa substitution along XPF sequence does not define the disease of the patient as it was illustrated in figure 33.

As previously explained, mutation I225M did not show a pathological cellular phenotype and has not been considered in these analyses.

Four variations were confined in the helicase-like domain and two in the nuclease domain but the patients' phenotypes were not determined by these positions. Notwithstanding, none of the mutations were affecting the C-terminal HhH2 domain from which XPF binds to ERCC1 to conform the stable endonuclease heterodimer and mutations in that domain have not been identified in patients to date (McNeil and Melton 2012), since this interaction is essential for XPF functions.

The interaction between XFP and SLX4 is vital for the recruitment of XPF to ICL sites and the activation of the incision. The XPF region involved in SLX4 binding comprises most of the helicase-like domain, from aa 12 to 650. Four of the selected mutations were confined in this section: R153P, L230P, C236R and R589W. Hashimoto and colleagues performed a yeast two-hybrid assay to unravel whether these mutations were preventing SLX4 binding

and found out that R153P, L230P and R589W were abolishing XPF binding ability to SLX4 while C236R was not. Consistently, they also examined if these mutants were disrupting the ERCC1 binding even if their location was not affecting ERCC1 binding site and found that the same three XPF mutations were affecting this interaction, pointing to the magnitude of the aa changes for the viability of XPF (K. Hashimoto et al. 2015). Despite this interpretation relies too heavily in the amount of target proteins obtained by the yeast two-hybrid assay, which is usually poor and could overestimate the significance of the variants, this mapping provides some hints for the phenotype interpretation diminishing the importance of the location of the aa change along the sequence and moreover highlights the importance of further similar studies performed in human cell lines.

In parallel, recent studies have also focused in the impact of generating an XPF-KO human cell line via CRISPR edition and have brought to light the importance of the XPF-ERCC1 heterodimer transference from the cytoplasm to the nucleus (J. Lehmann et al. 2017). Cells lacking XPF retained ERCC1 in the cytoplasm. These studies endorse the previous observations of some XPF mutations phenotypes that were unable to reach the nucleus due to an improper protein folding, such as XPF^{R153P}, XPF^{R799W} (Ahmad et al. 2010) and XPF^{C236R} (K. Hashimoto et al. 2015). In this sense, a more comprehensive study of the heterodimer localization should include all the XPF mutations selected in this project.

Table XX summarizes the cellular phenotype of our variants:

Nucleotide change	XPF mutation	Patient disease	UV sensitivity	UDS	RRS	DEB sensitivity	G2/M	MN
c.458G>C	R153P	XFE						Not conclusive
c.2395C>T	R799W	XP/XFE?/CS?						
c.1765C>T	R589W	XP/ XPCSCD						
c.706T>C	C236R	CS						
c.689T>C	L230P	FA						
c.2065C>A	R689S	FA						

1	2	3	4	5

Table XX: Summary table of the whole set of XPF variants and their cellular phenotypes. For each *ERCC4* nucleotide change, the XPF mutation and the pathology associated found in the patient where it was identified are described. The results of the functional assays performed with cells lacking XPF containing the variants are shown in a red scale from 1 (less affected) to 5 (more affected).

Regarding the analysis of XPF activity in the NER pathway, the UV sensitivity survival provided reliable information to discern mutations more associated to ICLR impairment such as L230P and R689S, which showed marked resistance to UV and considerable levels of UDS. In contrast, XFE associated R153P and XP mutation R589W were clearly disrupting XPF role in NER and ICLR. An interesting finding was the atypical behavior of XPF^{R799W}, who did not show sensitivity to UV. This variant was found in homozygosis in XP patients (Sijbers et al. 1998) and thus a defined phenotype of NER disruption was expected. This variant was also identified in heterozygosis in a patient presenting XFE with CS features thus enforcing the expectations of high levels of UV sensitivity such as the R153P causing XFE. Our results support the hypothesis that the phenotypes associated with XPF mutations are related to other elements of the cellular context like genetic background and/or interacting proteins. The third assay executed to evaluate the role of XPF in NER, the RRS assay, did not contribute significantly to discern among the XPF phenotypes but indicated that the CS associated mutation XPF^{C236R} was the most abruptly affected as expected by its

inability to participate in TCR of NER (Kashiyama et al. 2013). Besides, the unexpected RRS low levels of FA associated XPF variants enable the possibility for the first time of considering XPF as another FA protein involved in the resolving of ICLs in RNA-DNA hybrids (R-loops). R-loops are present in telomeres and contribute to telomere maintenance (Garcia-Rubio et al. 2015; Lafuente-Barquero et al. 2017). XPF plays a role in telomere maintenance; it is known to be involved in the excision of T-loops (Zhu et al. 2003) and it is responsible for telomeres loss when TRF2 is overexpressed (P. Munoz et al. 2005) thus contributing to ageing and genome instability. Although additional studies should be performed to assess the role of XPF in R-loops resolving, RRS assay results points towards its involvement.

A limitation for the NER assays is the cell line used in our studies; HEK 293T are a good human cell line for genome editing and thus were chosen for this study but, on the other hand, are tricky to work with for NER evaluating assays since they weakly adhere to the substrate.

Concerning ICLR analysis, there is a more marked sensitivity in FA associated variants XPF^{L230P} and XPF^{R689S} as reported (Bogliolo et al. 2013) and in the XFE related variants XPF^{R153P}, XPF^{R799W} (Mori et al. 2018; Niedernhofer et al. 2006). Slightly less sensitive are the variants associated with CS features as XPF^{C236R} and XPF^{R589W} (XP).

A very recent study performed by Popp and colleagues classifies for the first time R589W as an FA mutation (Popp et al. 2018). The patient from which it was identified was presented as an FA clinical phenotype, however, bone marrow failure, one of the crucial features to be classified as FA, was absent. Despite the atypical FA clinical phenotype, it was the first FA patient to develop skin photosensitivity. The second allele of *ERCC4* presented a novel splice site mutation (c.793-2A>G) which produced a premature termination of translation (p.Thr265Valfs*13), hence originating a null allele as happened with the previously reported FA XPF variants (Bogliolo et al. 2013). Contrary to Hashimoto group, who found out R589W mutation was abruptly affecting XPF structure and its SLX4 binding (K. Hashimoto et al. 2015) Popp and colleagues detected a residual proportion of XPF^{R589W} escaping from protein misfolding, able to reach the chromatin (Popp et al. 2018)

as happened with the reported FA XPF variants. Interestingly and in concordance to our results this mutant had reduced UVC irradiation resistance, UDS and RRS levels, although contrary to our results, XPF^{R589W} showed higher UVC irradiation resistance levels than XPF^{L230P} (Popp et al. 2018). This combination of findings provides some support for the conceptual premise that there is a link between ICL and NER pathways, reinforce our findings of XP associated variants presenting ICL impairment and endorse the theory that mutations found in specific locations of the sequence should not be associated with discrete DNA repair pathways impairment.

While the G2/M arrest assay evaluates the inability of the cells to reach mitosis due to the chromosome aberrations, the MN-Fragility test focuses in the breaks that chromosomes experience during anaphase and are unable to progress to the daughter cells. For instance, FA associated variants XPF^{L230P} and XPF^{R689S} presented high percentage of G2/M arrested cells and high number of MN, indicating the marked ICLR impairment of these variants, while XPF^{R589W} and XPF^{R799W} showed a mild arrest but a high number of MN, what suggests that in the cells expressing XP associated variants the G2/M checkpoint is not activated by the DNA damage and the cells can relatively easily reach mitosis with a damaged DNA.

The message that stands out from our studies after analyzing a set of XPF variants in a homogenous cellular and genetic background is that despite the cellular functional analyses sometimes provide promising suggestions to understand the genotype, a defined cellular phenotype cannot be correlated to each XPF mutation; functional analysis might help to correlate the genotypes to the cellular phenotypes but definitive statements about the contribution of XPF variants to the phenotype must take in account other factors such as the level of XPF, cell localization, possible interactors that can affect its role in DNA damage repair and the different genetic background of the different patients that could modulate the genotype-phenotype correlations.

PROJECT 2

IV.4- PROTEOMIC STUDY OF XPF INTERACTOME

TAP were performed in order to identify potential XPF interactors that could have a relevant role in DNA repair. The Streptavidin Calmodulin tag placed in the N-terminal site of XPF was used for a double step of XPF purification. HEK XPF-KO cells infected with the tagged XPF or with an EV were grown untreated, treated with MMC or UVC irradiation to obtain protein candidates able to interact with XPF when it is actively participating in ICL or NER pathways. A WB confirming the affinity purification is shown in figure 42.

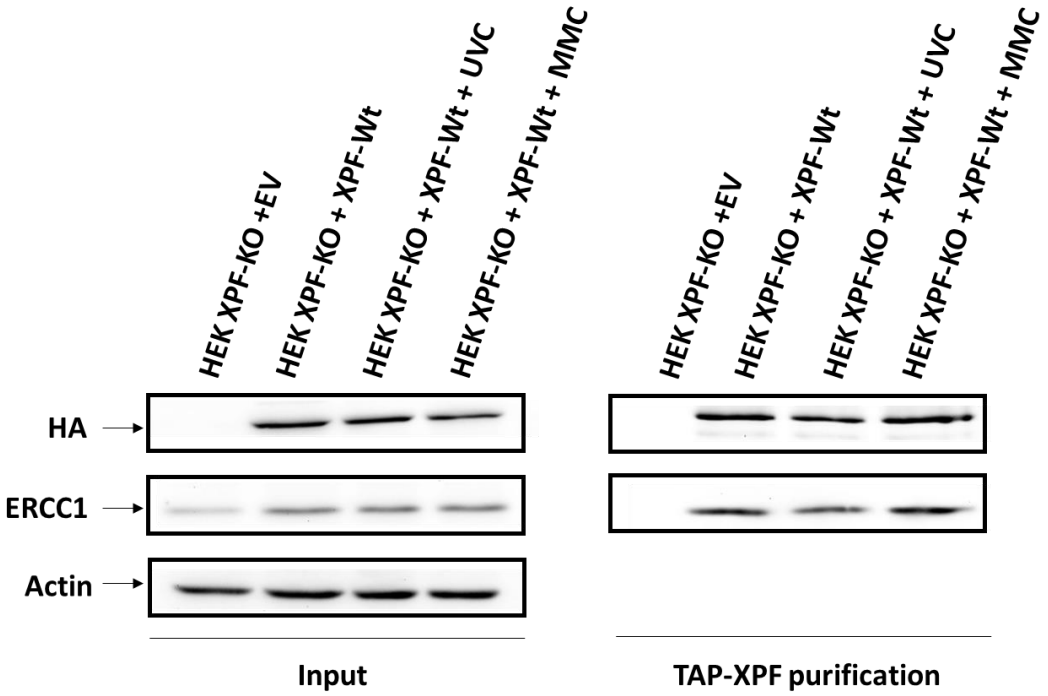

Figure 42: WB validation of the XPF purification through the N-terminal tags. One third of the Streptavidin-Calmodulin XPF purification was tested by WB to confirm XPF presence through HA tag and ERCC1 interaction in transduced HEK XPF-KO under different treatments: UVC (150J/m^2 , detached after 1h) or MMC (1 µM for 16h). Actin was used as a loading control detectable in the input but not in the purification fraction.

Proteins purified through the N-terminal tag under different conditions that were identified by mass spectrometry are shown in the annex (Annex Table I). Some proteins already known to interact with XPF in DNA repair pathways in which XPF takes part appeared, such as ERCC1, SLX4, XPG and XPA but it was not possible to further validate by WB the XPF interaction with new candidates (hnRNPU, ZC3H11A, CCDC81A, PPM1A) found by mass spectrometry, thereby a different proteomic approach based in XPF purification through the C-terminal HA-tag was taken on. This approach consisted in the immunoprecipitation of the HA-tag achieved by a magnetic bead surface coated with anti-HA-antibody and allowed to pool down XPF. The WB confirmation of the XPF-HA purification is shown in figure 43.

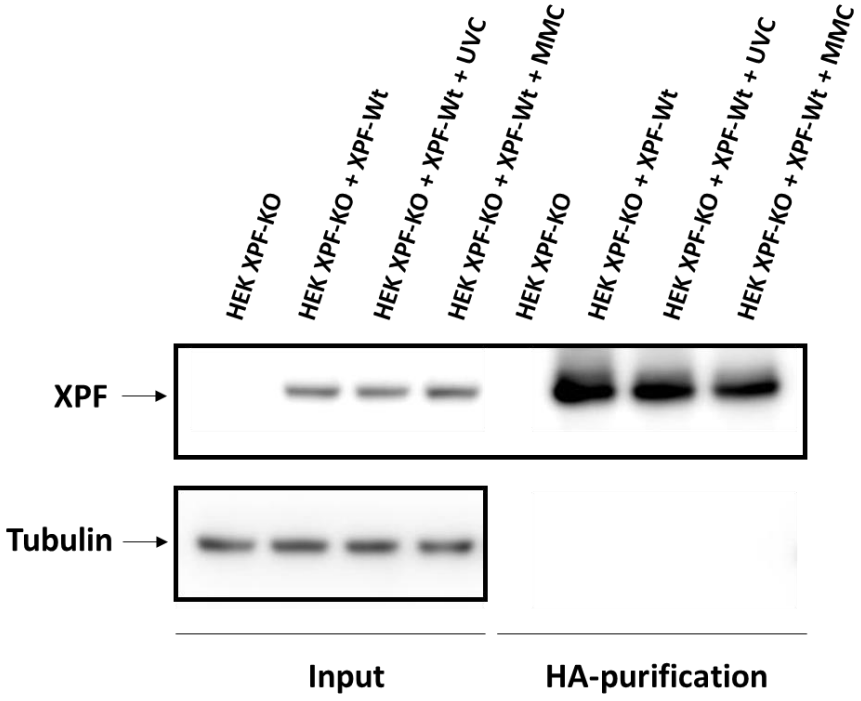

Figure 43: WB validation of the XPF purification through the C-terminal tag. 5% total of purification volume was used to confirm by WB the XPF purification through the HA-tag in transduced HEK XPF-KO under different treatments: UVC (50J/m^2 , detached after 1h) or MMC (1.5 µM for 16h). Tubulin was used as a loading control detectable in the input but not in the purification fraction.

XPF-HA purifications ran in gels and stained with Coomassie Blue Staining to identify and cut single bands from each sample lane were processed by mass spectrometry. A list of protein candidates is shown in annex (Annex Table II).

CoIP to check proteins found by mass spectrometry involved in DNA repair were performed as shown in figure 44.

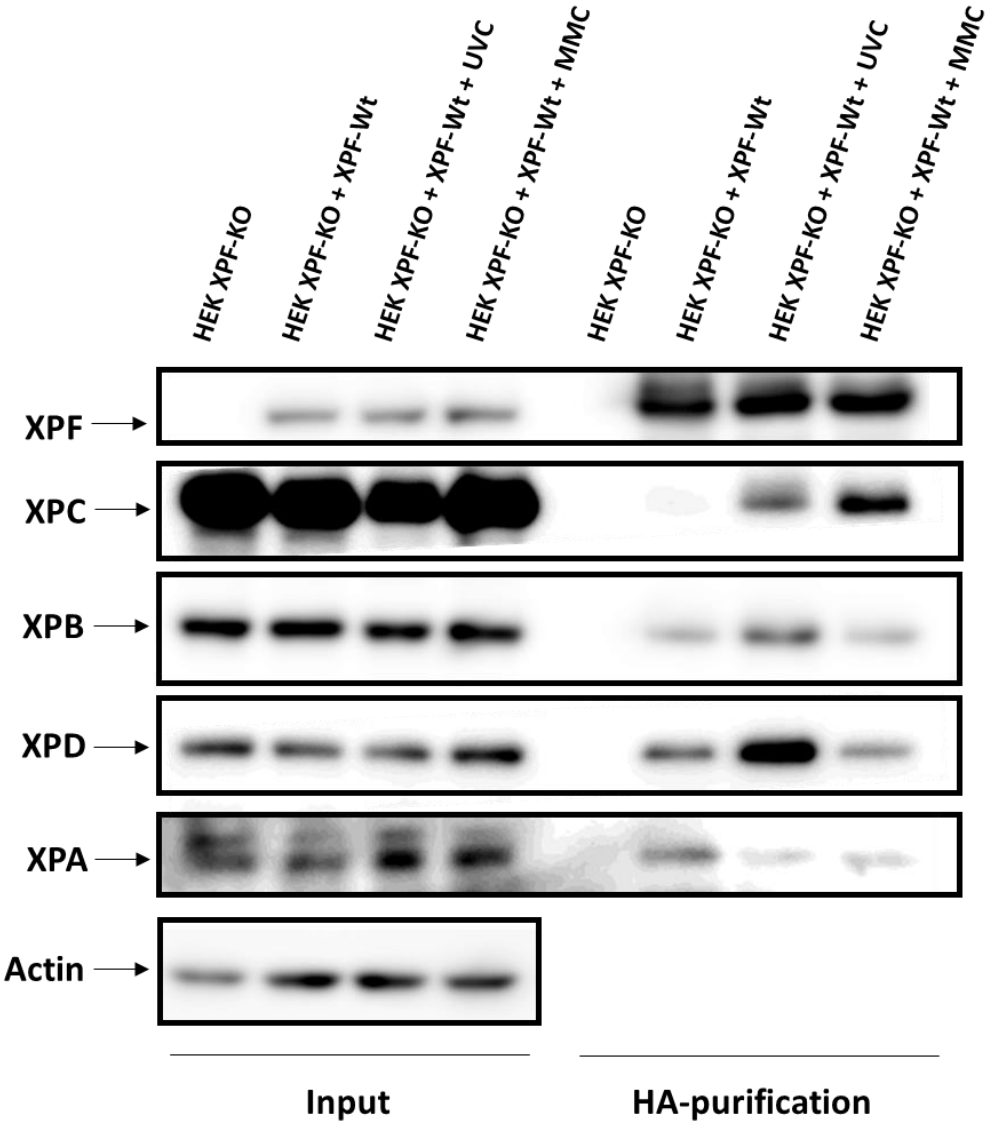

Figure 44: CoIP of XPF and some of the interactors found by mass spectrometry. The detection of XPC, XPB, XPD and XPA confirmed the mass spectrometry results from the HA-XPF purification in the HEK

XPF-KO transduced cell line under different treatments (see figure 43). XPF was used as a precipitation control. XPC interaction seems to be increased under both treatments. XPB and XPD interactions seems to increase under UVC treatment. Actin was used as a loading control detectable in the input but not in the purification fraction.

XPA, XPB, XPC and XPD are proteins involved in NER (Marteijn et al. 2014) and therefore unsurprising to appear as XPF candidate interactors although those interactions could be indirect. XPA is known to interact with XPF-ERCC1 heterodimer through ERCC1 (Su et al. 2012) and XPB, XPC and XPD appear most likely because the indirect cooperation they stablish in NER cascade.

One unanticipated finding was that the mass spectrometry analysis of the two methods of XPF affinity purification (through TAP or HA XPF-tags) did not unravel the same protein candidates. A possible explanation for this apparent inconsistency might be that the different tags by themselves are interacting with specific proteins or covering up possible XPF interactions. Additionally, the UV irradiation dose was not the same for the two purifications; for the TAP-XPF purification the UV dose was 150 J/m^2, which was then reduced to 50 J/m^2 in the HA-XPF purification assay in case the irradiation was too high and some interactions were impaired. Furthermore, mass spectrometry is a highly delicate technique, able to detect many false positive contamination proteins which could also mask real XPF interactors. The fact that the two mass spectrometry batches were performed in different spectrometer services might contribute as well to the variability, although it may strength the validity of the proteins found by both mass spectrometry assays.

Unfortunately, the CoIP performed did not confirm any new interaction of XPF with the candidates (XRCC5/Ku80 and XRCC6/Ku70) found by mass spectrometry of single bands gel digestion. Consequently, another proteomic approach was implemented based on stable isotopes labeling, SILAC (Baple et al. 2014), to get a quantitative and more accurate output of the protein candidates to interact with XPF. HEK XPF-KO transduced with XFP-Wt were cultured under UVC (40J/m^2, detached after 1h) or MMC (0.5 µg/mL for 21h) treatments with different isotopes of lysine and arginine in order to obtain quantitative data of the possible

XPF interactors under different conditions. A list of the mass spectrometry identified proteins is shown in annex (Annex Table III) (Annex Table IV).

Taking into account XPF involvement in DNA repair, we focused on proteins from the obtained data which could have a role in DNA repair and identified USP11 protein as an XPF candidate interactor. *USP11* is located in chromosome X p11.3 and turns into USP11, a deubiquitinase that removes conjugated ubiquitin from target protein and polyubiquitin chains and inhibits proteasome degradation of target proteins (Ideguchi et al. 2002). It participates in DNA repair regulation after DSB (Wiltshire et al. 2010); it is thought to deubiquitilate BRCA2 (Schoenfeld et al. 2004) although this interaction *in vivo* is not totally understood. Besides, USP11 deubiquitilates and stabilizes p53 (Ke et al. 2014) and interacts with other deubiquitylases (DUBs) like USP7, with the transcriptional elongation factors TCEAL1 and TCEAL4 and with the NRF2 regulatory protein KEAP1 (Schoenfeld et al. 2004). All these data support the idea USP11 participates in DNA repair. Recently, it has been reported to interact with XPC (Shah et al. 2017), being this the first time USP11 is seen to take part in NER. Notwithstanding, USP11 is a relatively non studied protein which until now had never been associated with XPF and regarding its reported roles in DSB and NER pathways, it sparks interest in characterizing this potentially relevant XPF interactor in the context of DNA repair.

USP11 showed up to interact constitutively with XPF with a slight tendency to reinforce this interaction under MMC treatment. SILAC assay was able to detect two or three unique peptides of USP11 independently of the conditions, however the parameter which assesses the probability, the Sum PEP Score, was not so high in two out of the three experiments, which might denotes XPF-USP11 interaction is weak or indirect. Concerning these signs, USP11 was considered as a potential candidate whose interaction with XPF should be validated by WB (Figure 45).

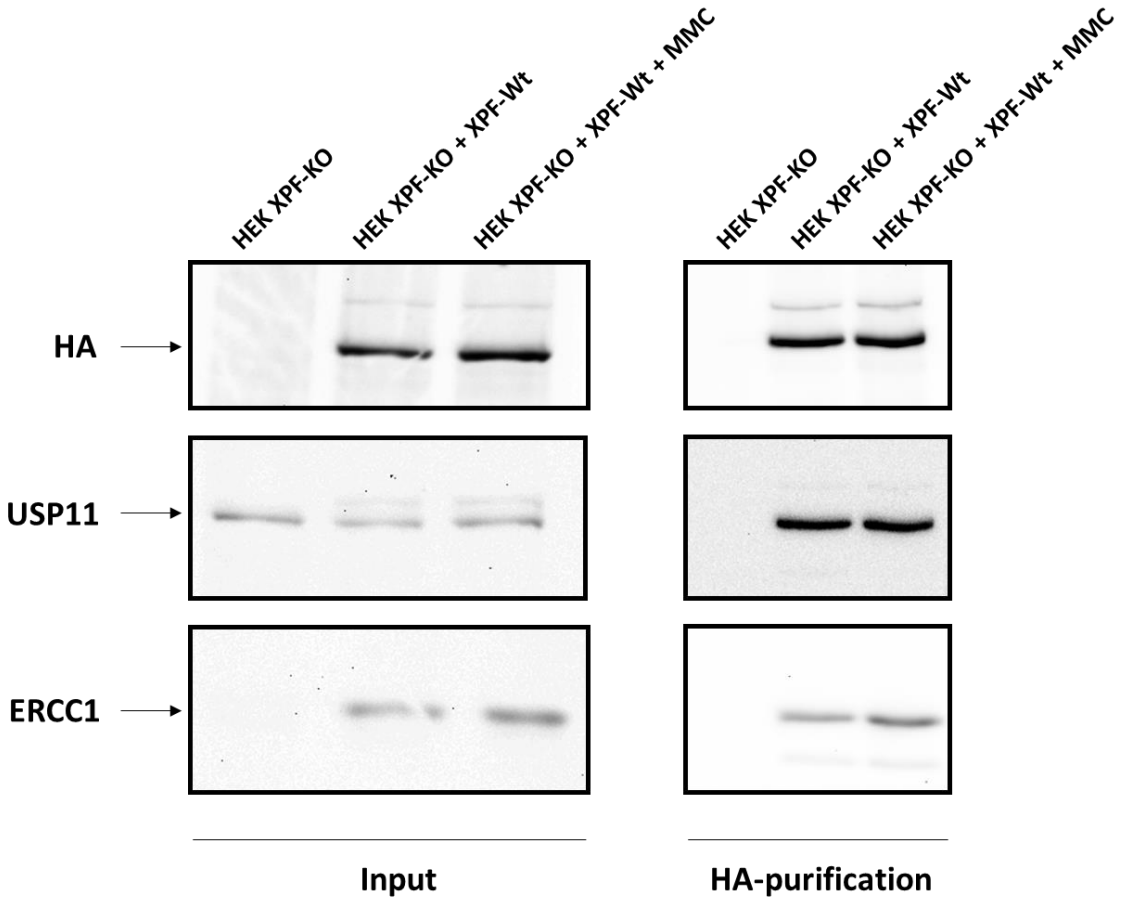

Figure 45: CoIP of USP11 to confirm SILAC results. XPF-HA immunoprecipitation showed a clear USP11 band in HEK XPF-KO + XPF-Wt with and without MMC treatment (1.5 µM for 16h). HA and ERCC1 were used as positive controls.

In order to unravel if USP11-XPF interaction is mediated by the DNA or in contrast, it is a protein-protein interaction, a new CoIP was set adding a DNAse to degrade this potential intermediary. As shown in figure 46, the addition of benzonase to the lysis buffer of the purification did not change USP11 detection, proving in this way that USP11-XPF interaction is not mediated by DNA.

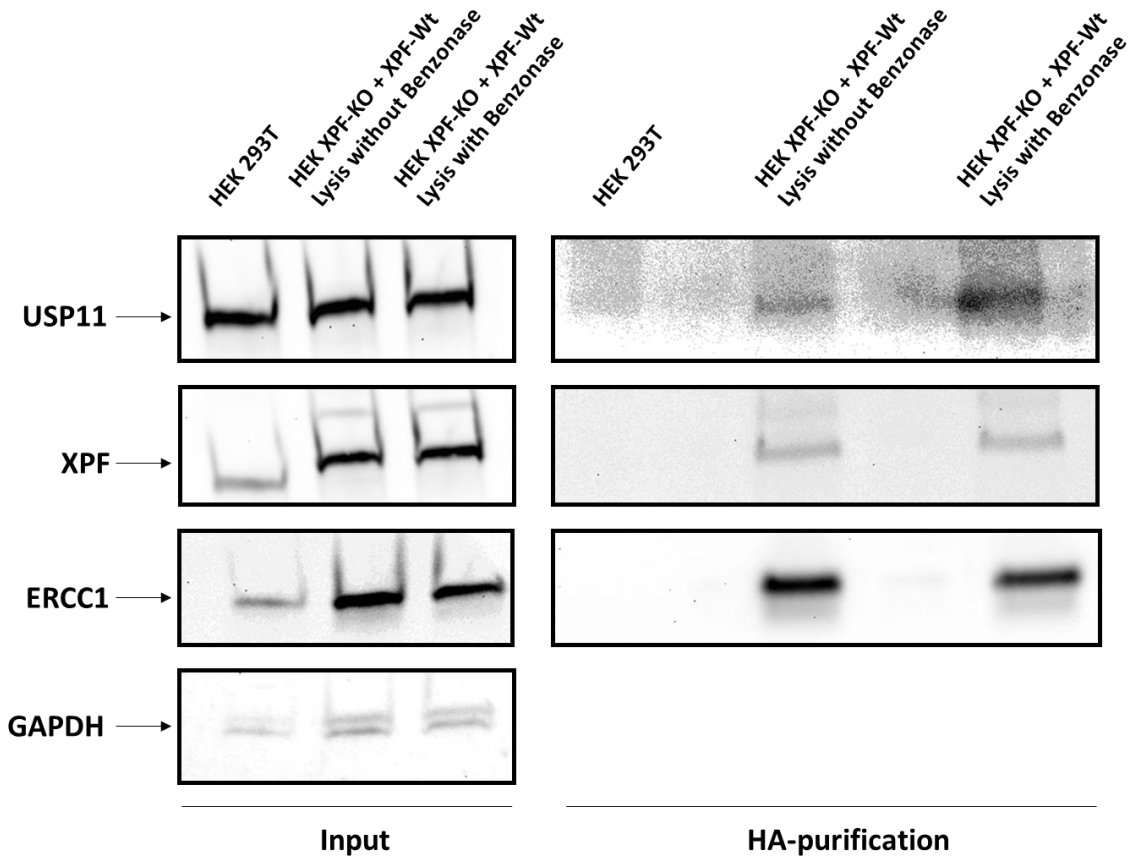

Figure 46: CoIP of USP11 to test the nature of the XPF interaction. HEK XPF-KO+XPF-Wt were treated with a DNAse like benzonase to check if USP11-XPF interaction was mediated by DNA or it was direct. USP11 band is shown independently of benzonase, proving in this way the interaction is DNA independent.

IV.5- GENERATION OF THE HEK *USP11*-KO AND THE DOUBLE KO HEK *XPF/USP11* BY CRISPR TECHNOLOGY

Gene editing CRISPR technology has emerged and improved constantly for the last years. It allows the easily generation of KO, introduction of point mutations, deletions and insertions in specific sites of the genome. It consists of a designed gRNA which leads the nuclease Cas9 to cut in a specific site of the genome that is subsequently repaired in an error prone way that ends up disrupting or modifying the protein reading frame.

CRISPR/Cas9 technique was implemented to obtain a KO of *USP11* in HEK 293T and a double KO HEK *XPF/USP11.* PX458 mammalian expression vector designed to cut exon 2 of *USP11* was used. Infected cells were sorted and divided in 96-well plates to achieve single KO clones of HEK USP11-KO and HEK XPF-KO / USP11-KO that were tested by WB (Figure 47).

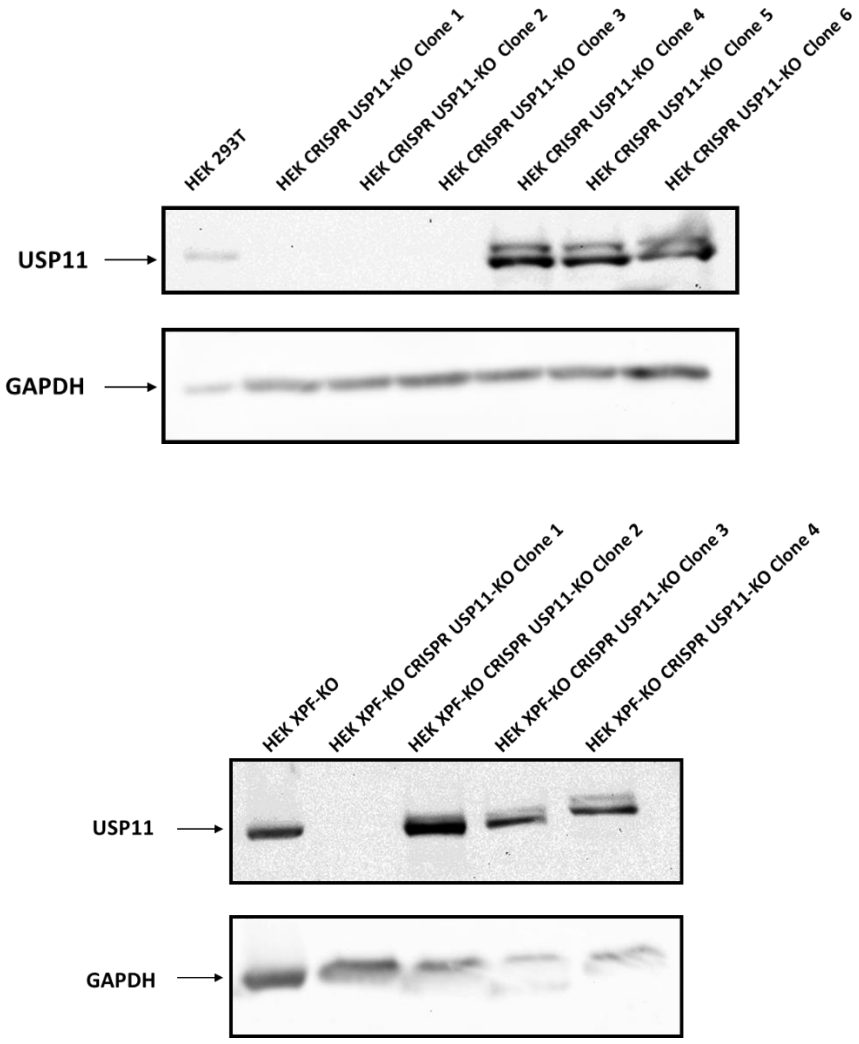

Figure 47: WB analysis of USP11 CRISPR clones in HEK 293T cells (above) and in HEK XPF-KO cells (below). Clones 1 from both WB which did not show USP11 band were selected. GAPDH band is shown as a loading control.

The sequencing analyses of the genomic DNA extracted and amplified by PCR from clone 1 of each cell line revealed that the mutations introduced by the CRISPR were two different single nucleotide insertions, respectively: c.350instT (c.350dup) and c.349insG (c.349dup) (Figure 48).

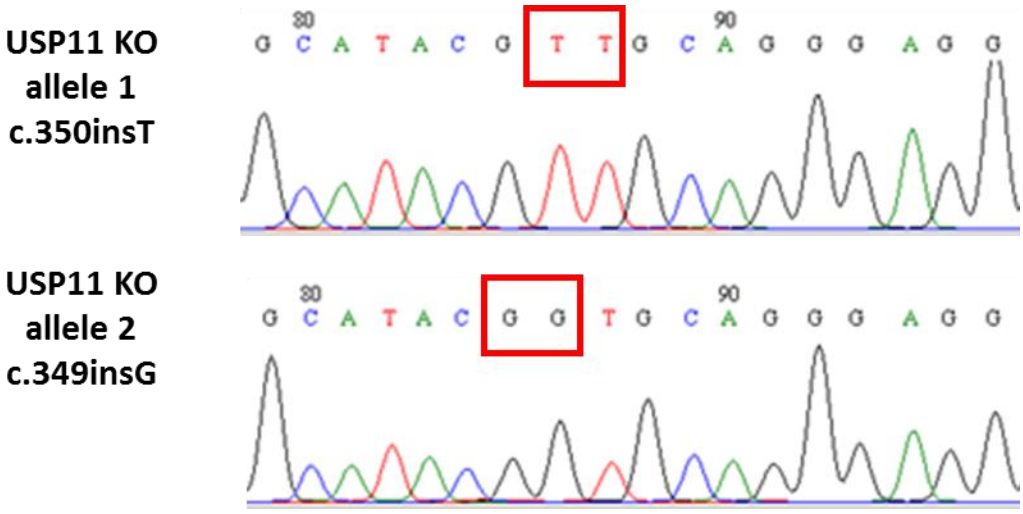

Figure 48: Sequencing reaction chromatograms of heterozygous mutant clones. The USP11-KO clone showed a 1 bp insertion (c.350dup) in one allele and a different 1 bp insertion (c.349dup) in the second allele, both in exon 2.

Functional studies of single and double USP11-KO cells were then performed to test their phenotype under treatments that impair DNA repair pathways where XPF participates. It can be seen from data in figure 49 that HEK USP11-KO cells have a mild reduction of survival after UVC irradiation, however, they were as resistant as the Wt to DEB treatment in terms of percentage of G2/M arrested cells and DEB sensitivity. Double KO XPF/USP11 mostly behaves as the HEK XPF-KO, suggesting that its sensitivity to UVC and DEB treatments, or its inability to reach mitosis is mainly due to the lack of XPF.

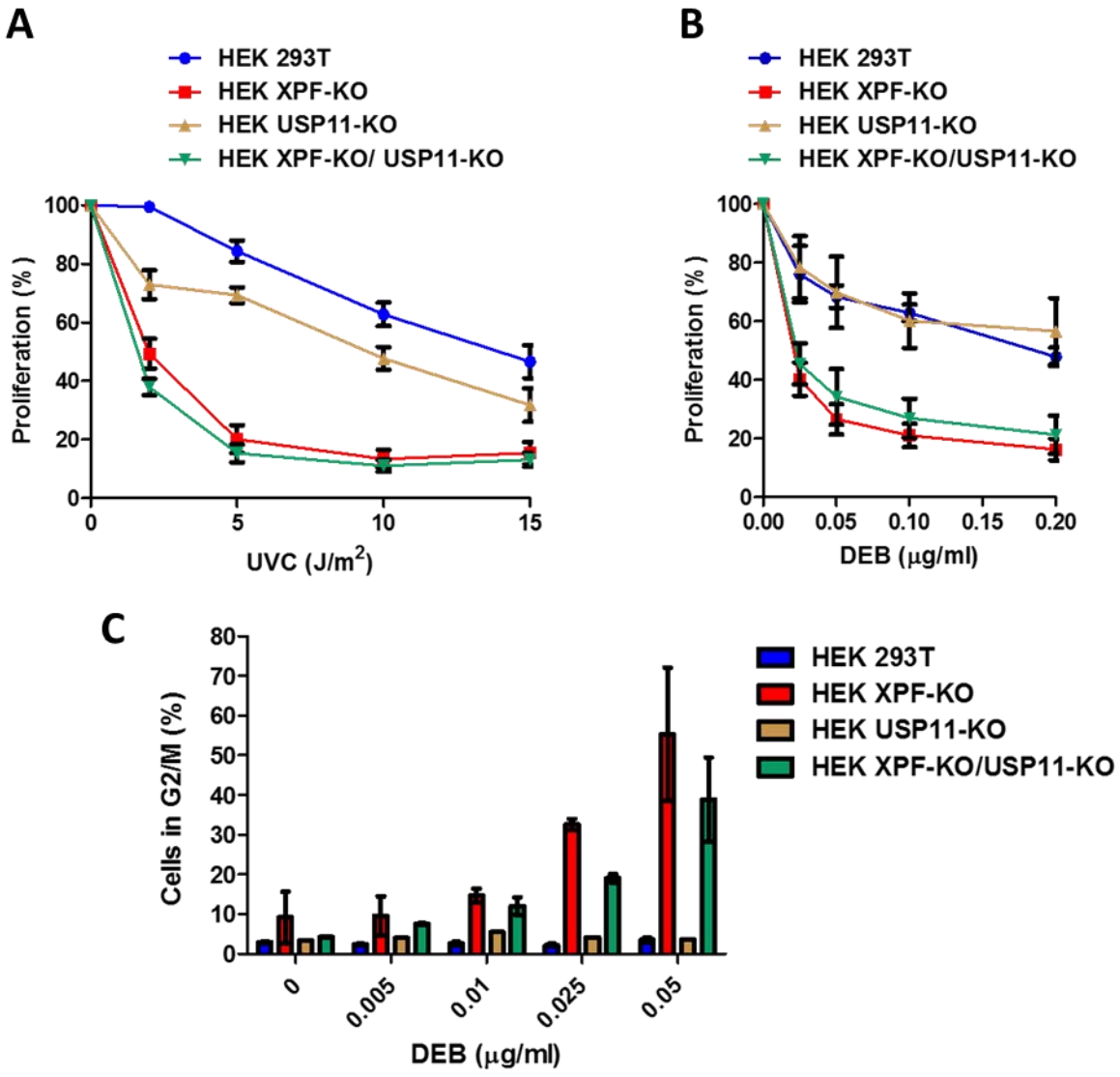

Figure 49: Functional studies of USP11 role in NER and ICLR. UVC cell survival (Figure A) and DEB cell survival (Figure B). The double KO HEK XPF-KO/USP11-KO sensitivity is similar to the HEK XPF-KO levels. USP11 cells showed a slight but consistent sensitivity to UVC. Graphs show proliferation percentage media and SEM of at least three independent experiments of two replicates. Cell cycle study (Figure C) shows the percentage of cells stalled in G2/M phase after DEB exposition. HEK USP11-KO behaves almost as the wild

type HEK 293T and HEK XPF-KO/USP11-KO arrested cells levels are more likely HEK XPF-KO. This graph represents the media of two independent experiments with the SD.

The new generated HEK USP11-KO cell line was used as a control to confirm by an endogenous USP11 immunoprecipitation that XPF-USP11 interaction was not an artifact of HA-tag of XPF (Figure 50). This outcome, together with the rejection of the assumption that USP11 was interacting with XPF throughout the DNA as shown in figure 46, strengthens the confirmation of USP11 as a novel XPF interactor.

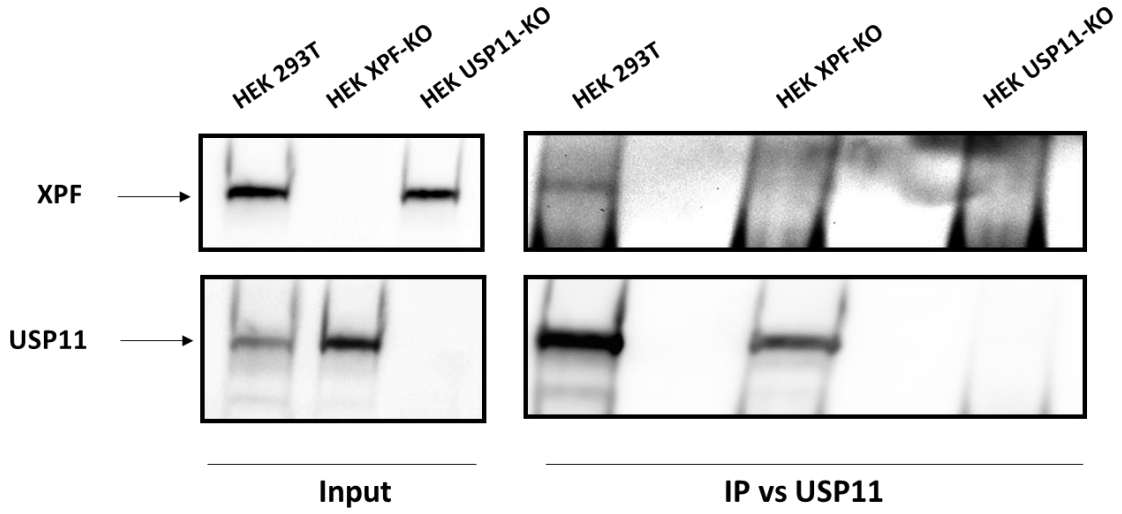

Figure 50: Immunoprecipitation vs USP11. XPF band is shown in the IP of HEK 293T but is absent in the two negative controls. USP11 band is shown in HEK 293T and HEK XPF-KO samples. This endogenous IP vs USP11 confirms the interaction takes place *in vivo* and is not mediated by HA-tag of XPF.

IV.6- ANALYSIS OF XPF AND USP11 ROLES IN *IN VIVO* DOUBLE STRAND BREAKS REPAIR

XPF is known to participate in some DSB repair pathways besides its proved role in NER and ICLR. Considering this new identified XPF-USP11 interaction, we wanted to unravel the role of these two proteins in HR and SSA.

IV.6.1 STUDY OF HOMOLOGOUS RECOMBINATION REPAIR

In order to characterize the role of USP11 in DNA repair by HR, a study using U2OS DR-GFP cell line was performed. This cell line carries a chromosome-integrated reporter to restore a GFP expression cassette by HR when a unique DSB is induced by I-SceI endonuclease expression (Bennardo et al. 2008).

The indicated genes were knockdown by siRNA and depletion efficiency was analyzed by WB (Figure 51). The following figures correspond to one individual assay out of the five HR experiments. *XPF* was downregulated with around 90% of efficiency; *USP11* and *BRCA2* were downregulated with around 100% of efficiency. Figure 52 represents the mean of siRNA transfection efficiency of three WB.

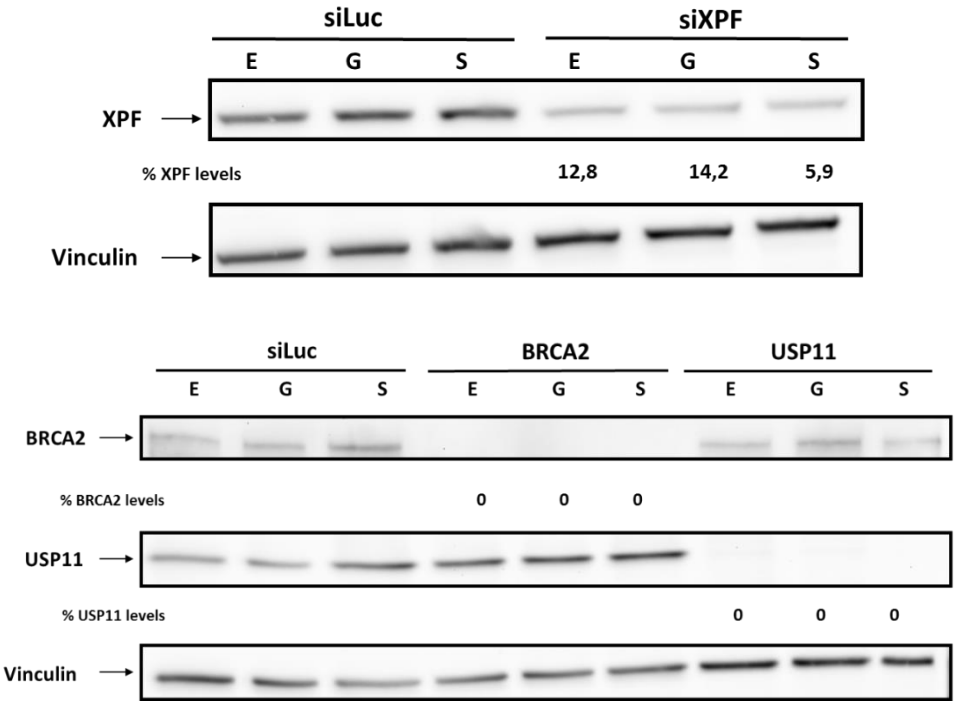

Figure 51: siRNA efficiency in DR-GFP experiments analyzed by WB. Representative WB obtained from a single DR-GFP assay. Percentage of protein level is represented for each downregulated gene respect to siLuc control (considered as a mean of 100%). E= EV; G= GFP vector; S= Sce-I vector. Vinculin was used as a loading control.

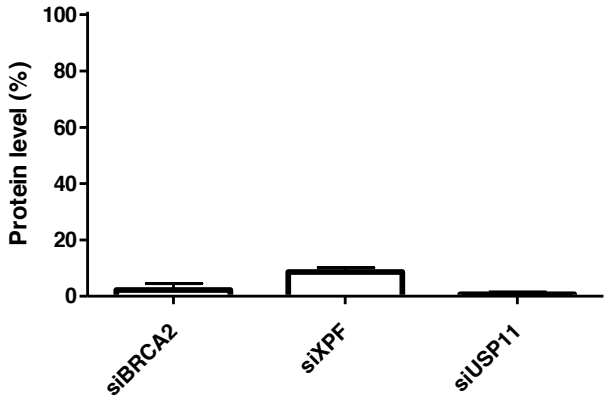

Figure 52: siRNA efficiency in three DR-GFP experiments analyzed by WB. Bars represent the percentage of protein level for each downregulated gene corresponding to the mean of three individual WB data with SEM.

GFP fluorescence was then analyzed by flow cytometry (Figure 53).

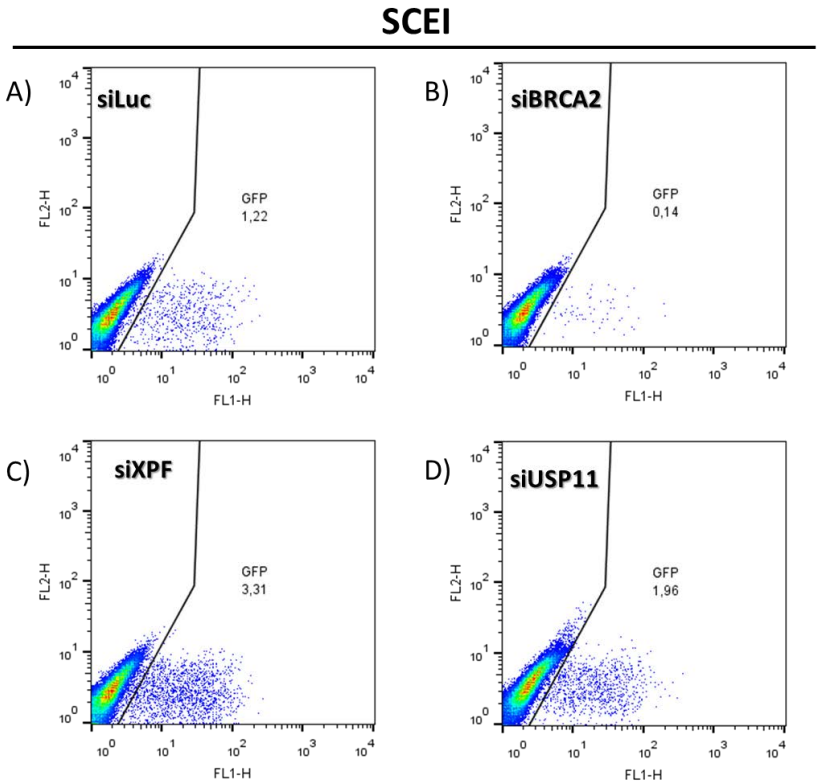

Figure 53: *In vivo* HR pathway in U2OS DR-GFP stable cell line measured by cell cytometry. Following to siRNA and vector transfection, fluorescence of cells was analyzed by cell cytometry. Graphs show the amount

of GFP detected after endonuclease vector (I-SceI) transfection. Samples with EV and GFP vector were used as controls (used to normalize data obtained with I-SceI vector). A) siRNA luciferase (Luc), B) siBRCA2 control, C) siXPF, D) siUSP11.

As can be seen in figure 54, the depletion of XPF or USP11 does not decrease the HR frequency compared to the control siLuc, meaning these two proteins do not play an essential role in HR. In contrast, reduction of BRCA2, our positive control, is clearly impairing HR as expected (Howlett et al. 2002; Michl et al. 2016).

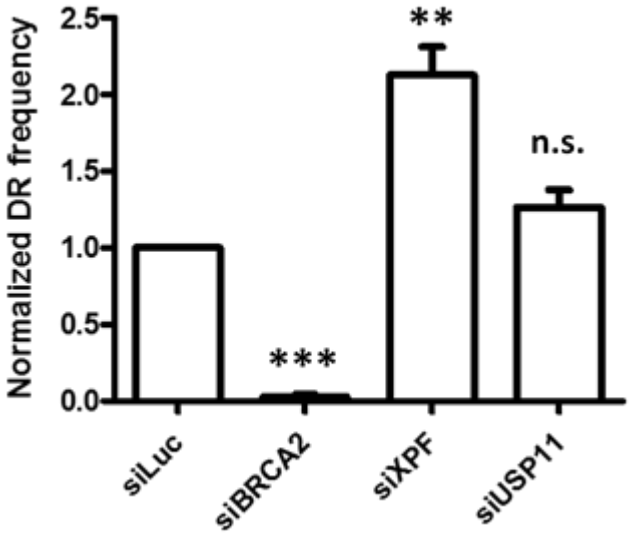

Figure 54: *In vivo* HR pathway in U2OS DR-GFP stable cell line. The flow cytometry analysis of GFP fluorescence is represented for each gene downregulated U2OS DR-GFP cell line. Luc is used as a control and data is normalized respect to it. The mean of five independent experiments is represented with the SEM. Paired t-test is represented, statistical differences were considered when p-valor < 0,005 (n.s.: no significant).

The unambiguous outcome of siXPF HR frequency proves XPF is not essential for HR as it had been previously reported (Ahmad et al. 2008) and HR can take place in absence of XPF (Figure 54). Actually, XPF downregulation increased HR frequency, which turns it as a possible HR negative regulator. DSB repair is crucial for genome stability maintenance and XPF has been reported to participate in MMEJ and SSA, so downregulation of this gene would reduce the backup DSB repair mechanisms, hence increasing the HR of DSB. One possible explanation of XPF as a negative regulator of HR could be that, due to XPF

predisposition to cut bubble structures (Ciccia et al. 2008), it could cut DNA structures formed during HR. These late HR structures excised by XPF would proceed to mitosis containing gaps or breaks which could be then processed by MUS81-EME1, or even by ERCC1, fixing the possible formation of chromosome bridges during anaphase segregation (Naim et al. 2013).

USP11 knockdown does not reduce the HR neither increases it compared to the control (Figure 54), which sets USP11 aside from this DSB repair subpathway.

USP11 has been reported to interact with BRCA2 and PALB2, indeed, it seems to be essential for the formation of the complex BRCA1-PALB2-BRCA2 which is recruited to the DSB site in HR (Orthwein et al. 2015). It deubiquitilates PALB2 so that it can be bound to BRCA1. Orthwein and co-workers saw a reduction of HR when USP11 was downregulated and the subsequent increase of HR when those siUSP11 cells were transfected with a USP11 vector resistant to the siRNA. This is in contrast with our findings: one explanation could be in the levels of USP11 inhibition; while we show complete USP11 inhibition (Figure 52) Orthwein and co-workers have still detectable levels of the band. Despite levels of USP11 inhibition are not shown for that assay they performed an immunoprecipitation vs PALB2 where they also tried to inhibit USP11 but still showed detectable levels of the protein. To unravel if the different inhibition levels are the clue, a complete inhibition should be performed, knocking out *USP11* in this U2OS-DR cells.

Another interesting approach could come from cell cycle. Orthwein and co-workers stated USP11 is cell cycle regulated by proving its loss in G1 after DNA damage was more marked than in S or G2 phases (Orthwein et al. 2015). In this sense, it would be interesting to compare our outcomes with cells synchronized in S phase.

IV.6.2 STUDY OF SINGLE STRAND ANNEALING REPAIR

One of the less characterized repair abilities of XPF-ERCC1 is its role in SSA. Their orthologues in *S. cerevisiae* Rad1-Rad10 have been well understood to participate in MMEJ and SSA. It has been reported that the mammalian heterodimer also participates in DSB

repair by SSA (Ahmad et al. 2008; Chang et al. 2017) but further studies will be needed to elucidate XPF-ERCC1 role in this DNA repair subpathway. Under the assumption that XPF interacts with USP11 and considering there is no report about the role of USP11 in SSA we decided to unravel the role, if any, of USP11 in SSA.

For this purpose, U2OS cells carrying the chromosome-integrated reporter SA-GFP to control the SSA induced by the I-SceI endonuclease were used (Bennardo et al. 2008). Similarly to the DR-GFP system, the GFP sequence is restored by SSA in response to the I-SceI-induced DSB. Additionally in this assay, cells are infected either just with a red fluorescent protein vector (as a control of the efficiency of the transfection), or with a red fluorescent protein vector and I-SceI vector, and both red and green fluorescence are analyzed by cell cytometry.

BRCA2 is known to suppress SSA (Stark et al. 2004), therefore it was used as a control, as its reduction is expected to increase SSA and by consequence GFP fluorescence. Besides individual *XPF*, *USP11* and *BRCA2*, the combinations of two or three genes were also studied.

Genes were knocked-down by siRNA and transfection efficiency was checked by WB (Figure 55) (Figure 56). siXPF downregulated *XPF* more that 80%; *USP11* was downregulated more than 90% and *BRCA2* was downregulated more than 95% in single or combined siRNA downregulations (Figure 57). There was a rather surprising outcome derived from the WB levels of XPF: USP11 downregulation substantially increased XPF levels. This was observed for the individual inhibition of USP11 and the double inhibition USP11/BRCA2. The opposite effect, an increase of USP11 levels when inhibiting XPF, however, was not observed. One hypothesis to explain this situation could be that, USP11 would be directly involved the regulation of XPF-ERCC1 heterodimer levels. Supporting this conjecture, the importance of the ubiquitination of the XPF binding domain of ERCC1, $(HhH)_2$, for the stability of both ERCC1 and XPF proteins has been recently reported (Yang et al. 2017). ERCC1 seems more likely to be altered by ubiquitination than XPF, although the stability of XPF would be also affected by this modification. Additional experiments to

asses ERCC1 ubiquitination in SSA context could uncover the nature of XPF/USP11 epistasis.

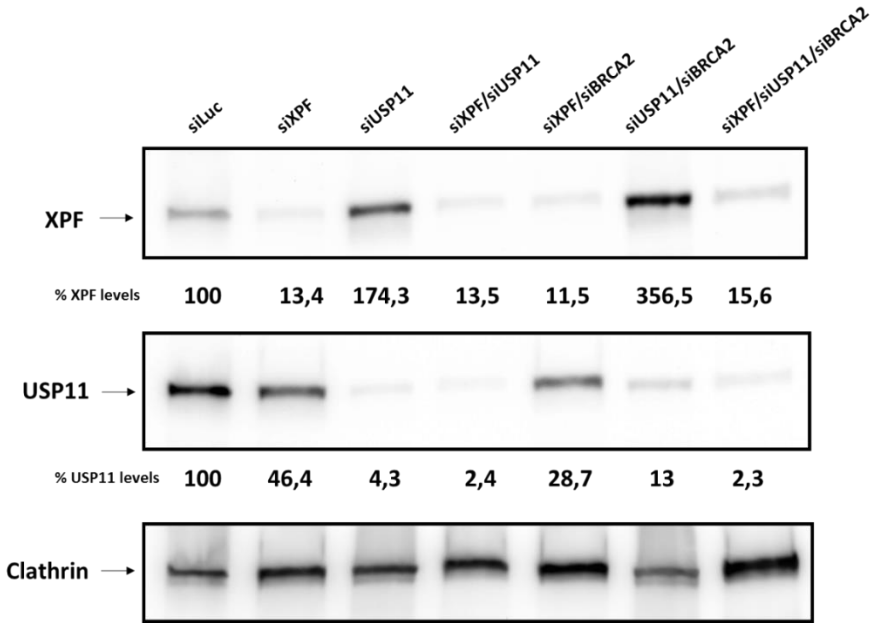

Figure 55: siRNA efficiency in SA-GFP experiments analyzed by WB. Representative WB obtained from a single SA-GFP assay. Percentage of protein level is represented for each downregulated gene, *XPF* or *USP11*, respect to siLuc control. Clathrin was used as a loading control.

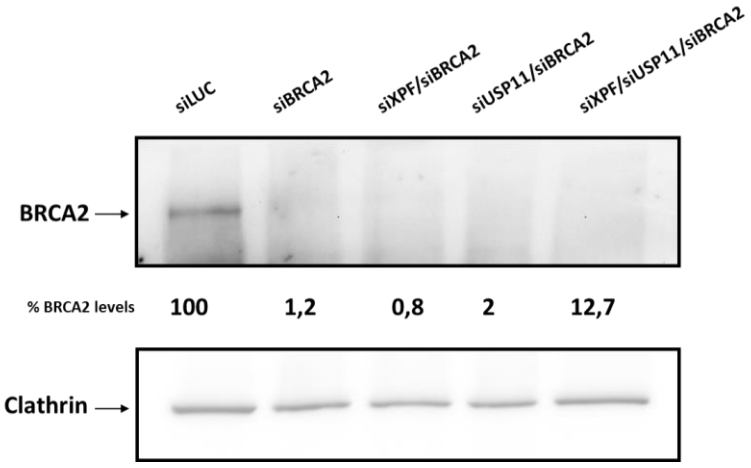

Figure 56: siRNA efficiency in SA-GFP experiments analyzed by WB. Representative WB obtained from a single SA-GFP assay. Percentage of protein level is represented for *BRCA2* downregulated gene, respect to siLuc control. Clathrin was used as a loading control.

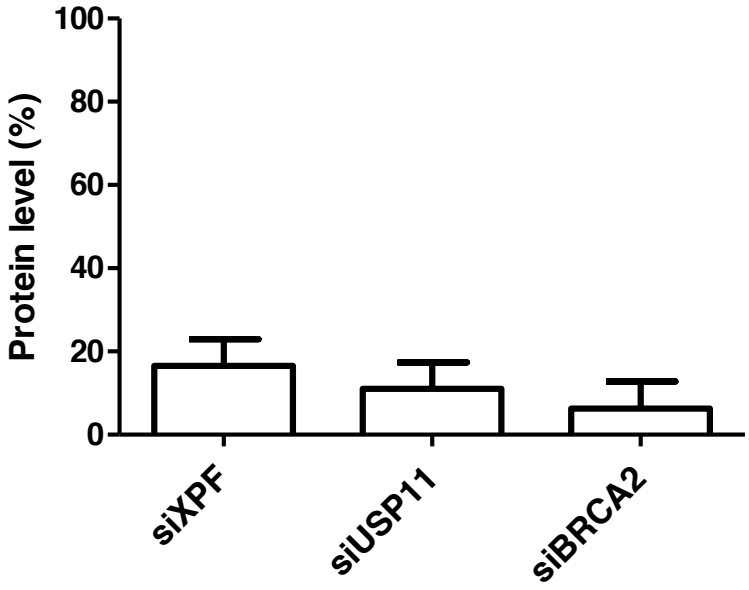

Figure 57: siRNA efficiency in four SA-GFP experiments analyzed by WB. Bars represent the percentage of protein level for each downregulated gene corresponding to the mean of four individual WB data with SD.

The combination of red fluorescence and GFP fluorescence was analyzed by flow cytometry (Figure 58).

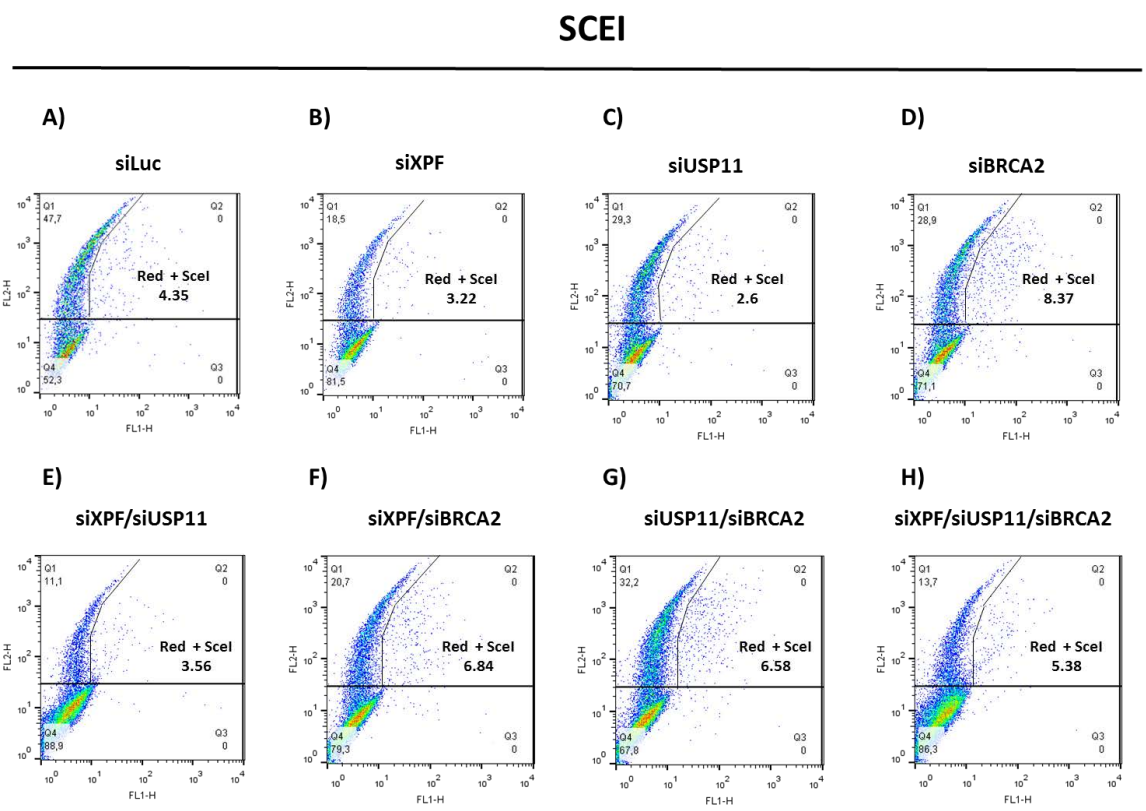

Figure 58: *In vivo* SSA pathway in U2OS SA-GFP stable cell line measured by cell cytometry. Following to siRNA and vector transfection, fluorescence of cells was analyzed by cell cytometry. Graphs show the amount of red fluorescence and GFP detected after red fluorescence vector and endonuclease vector (I-SceI) transfection. All the samples transfected with the same siRNA were infected with red fluorescence protein and half of them were additionally infected with the I-SceI. Red fluorescence was therefore used as a control to normalize data. A) siLuc B) siXPF; C) siUSP11; D) siBRCA2; E) siXPF/siUSP11; F) siXPF/siBRCA2; G) siUSP11/siBRCA2; H) siXPF/siUSP11/siBRCA2.

The results of the SSA fluorescence analysis are set out in figure 59. What stands out in the graph is the remarkable high frequency of SSA when *BRCA2* is downregulated, which confirms its role as a negative regulator of SSA. Comparing the individual knockdown of *XPF* to the siLuc, it results in a drop of SSA frequency about 30%, which confirms a role for XPF in this DSB pathway (Bhargava et al. 2016). Interestingly, *USP11* knockdown drove to similar outcomes, showing a fall of more than 50% respect to the siLuc; which proves for the

first time this protein is involved in SSA. A point of interest arises in the understanding of the downregulation combination of *XPF* and *USP11* at the same time.

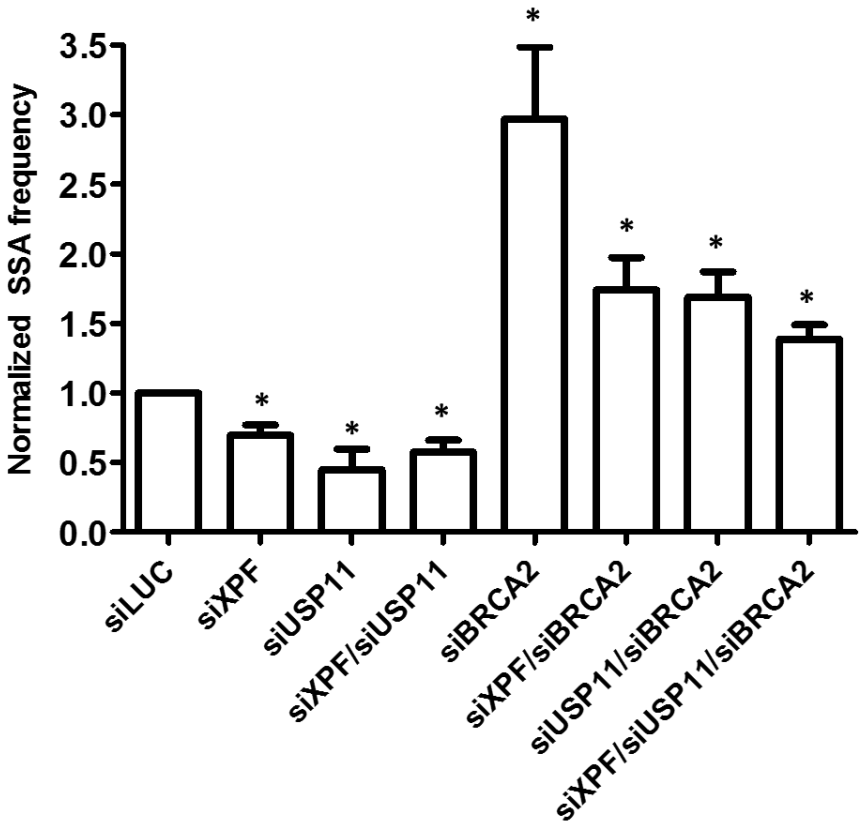

Figure 59: *In vivo* SSA pathway in U2OS SA-GFP stable cell line. The flow cytometry analysis of GFP fluorescence is represented for each gene downregulated U2OS SA-GFP cell line. The mean of four independent experiments is represented with the SEM. Paired t-test is represented, statistical differences were considered when p-valor < 0,005.

As it can be deduced from the figure X, the double knockdown of *XPF* and *USP11* experienced a fall in SSA frequency with values between siXPF and siUSP11 frequency values, pointing out that both proteins might be epistatic in positively regulating SSA. This is the most striking result to emerge from the data, as allows to classify the new XPF interactor USP11 as a protein involved in SSA.

Similar reduction levels are observed with the combination of *BRCA2* downregulation together with *XPF* or *USP11* downregulations, again proving XPF and USP11 have similar roles in SSA. No significant reduction is found in the triple downregulated *BRCA2, XPF* and *USP11* compared to the double BRCA2 knockdowns, pointing again to the epistatic effect of XPF and USP11.

IV.7- UNDERSTANDING THE BIOLOGICAL IMPACT OF XPF-USP11 INTERACTION

Considering USP11 is a deubiquitylase involved in DNA damage response (DDR) (Hendriks et al. 2015) is not inconceivable it could play a role in DNA repair together with XPF both in NER and SSA.

Recent research has suggested USP11 participates in NER regulation by deubiquitilating XPC. XPC acts as a probe checking DNA damage; first, it is polyubiquitinated after UV exposure to enhance its binding to the damage site, secondly it is sumoylated and finally it experiences a second ubiquitination event to be released from the damage site. In order to recover XPC protein and avoid proteasome degradation, USP11 deubiquitylates it, thereby contributing to the NER regulation positively (Shah et al. 2017).

A similar scenario could be envisaged for XPF. Actually, another DUB, USP45 deubiquitylase, has been proved to regulate XPF-ERCC1 activity by deubiquitylating ERCC1. Cells lacking USP45 were hypersensitive to UV irradiation and DNA ICLs and the recruitment of XPF-ERCC1 to the damaged DNA seemed to be regulated by its proper deubiquitination, which would be set out by USP45 (Perez-Oliva et al. 2015). In this case, ERCC1 ubiquitination would control its activity instead of regulating XPF-ERCC1 stability as previously discussed (Yang et al. 2017). In this sense, USP11 outcomes from this research differ from the ones from Perez-Oliva group, as cells lacking USP11 were not hypersensitive to UVC or ICL exposure, but the results stand out for another interesting possibility of participating together with XPF in SSA, which certainly highlights the view that proteins involved in DSB repair are often influenced by a web of inhibitions/activations or by post-

translational modifications rather than individually taking part in the pathways (Surralles et al. 2004).

A study of potential USP11 de-ubiquitinating sites should be performed, although not just focusing in XPF-ERCC1 heterodimer; assuming its epistasis, USP11 could deubiquitylate other proteins associated to SSA repair, regulating in that way their participation in DSB repair pathways. This would not be against the idea of the physical interaction between XPF-ERCC1 and USP11, which has been widely proved in this study, but gives a hint of the possibilities of USP11 to be deubiquitinating other surrounding proteins maybe by taking advantage of the interaction with XPF heterodimer and travelling recruited to it or, in contrast, making USP11 unable to proper deubiquitylate target proteins since the union to XPF-ERCC1 could avoid USP11 deubiquitinating ability.

Actually, some target proteins of USP11 involved in DSB repair have already been reported, such as PALB2 (Orthwein et al. 2015) and BRCA2 (Schoenfeld et al. 2004), whose reduction increases the frequency of SSA (Stark et al. 2004). Additionally, these genes are considered FBOC genes (Bogliolo and Surralles 2015), which could spur the study of other target proteins of USP11 which could be involved in cancer.

This study has provided a deeper insight into the molecular biology of XPF in DSB repair. The identification of USP11 as an XPF interactor lays the groundwork for future research into characterizing this interaction and points towards the study of post-translational modifications in SSA DNA repair context.

Conclusions

V. CONCLUSIONS

1. Functional analyses reveal that the position of the amino acid substitution along XPF sequence by itself does not clearly define which DNA repair pathway is impaired and therefore neither determines the patient's clinical phenotype. Such outcomes imply that other factors must be taken in account including the levels of XPF, cell localization and possible interactors that can affect its role in DNA damage repair.

2. XPF variants identified in patients with FA are able to retain mild NER activity, while XPF variants identified in patients with other diseases present both ICL and UV sensitivities. This could be due to intrastrand lesions that also require XPF to be repaired .

3. Cells with FA associated variants hardly reach mitosis and, the ones that do, experience chromosome breaks; on the contrary, cells from XP and CS associated variants can relatively easily reach mitosis with damaged DNA.

4. USP11 is a deubiquitinase involved in DNA repair that emerges as a novel XPF interactor. XPF-USP11 interaction is DNA damage-independent and is not mediated by DNA.

5. *ERCC4* and *USP11* are epistatic genes involved in SSA. USP11 does not participate in other DNA repair pathways such as ICL and HR but could have a minor role in NER that requires further investigation.

6. XPF plays a role in both HR and SSA pathways by positively regulating SSA and negatively regulating HR.

Bibliography

VI. BIBLIOGRAPHY

Abdullah, U. B., et al. (2017), 'RPA activates the XPF-ERCC1 endonuclease to initiate processing of DNA interstrand crosslinks', *EMBO J,* 36 (14), 2047-60.

Ahmad, A., et al. (2008), 'ERCC1-XPF endonuclease facilitates DNA double-strand break repair', *Mol Cell Biol,* 28 (16), 5082-92.

Ahmad, A., et al. (2010), 'Mislocalization of XPF-ERCC1 nuclease contributes to reduced DNA repair in XP-F patients', *PLoS Genet,* 6 (3), e1000871.

Andreassen, P. R. and Ren, K. (2009), 'Fanconi anemia proteins, DNA interstrand crosslink repair pathways, and cancer therapy', *Curr Cancer Drug Targets,* 9 (1), 101-17.

Avlasevich, S. L., et al. (2006), 'In vitro micronucleus scoring by flow cytometry: differential staining of micronuclei versus apoptotic and necrotic chromatin enhances assay reliability', *Environ Mol Mutagen,* 47 (1), 56-66.

Baple, E. L., et al. (2014), 'Hypomorphic PCNA mutation underlies a human DNA repair disorder', *J Clin Invest,* 124 (7), 3137-46.

Barve, A., Ghaskadbi, S., and Ghaskadbi, S. (2013), 'Conservation of the nucleotide excision repair pathway: characterization of hydra Xeroderma Pigmentosum group F homolog', *PLoS One,* 8 (4), e61062.

Bennardo, N., et al. (2008), 'Alternative-NHEJ is a mechanistically distinct pathway of mammalian chromosome break repair', *PLoS Genet,* 4 (6), e1000110.

Bessho, T., et al. (1997), 'Reconstitution of human excision nuclease with recombinant XPF-ERCC1 complex', *J Biol Chem,* 272 (6), 3833-7.

Bhargava, R., Onyango, D. O., and Stark, J. M. (2016), 'Regulation of Single-Strand Annealing and its Role in Genome Maintenance', *Trends Genet,* 32 (9), 566-75.

Bluteau, D., et al. (2017), 'Biallelic inactivation of REV7 is associated with Fanconi anemia', *J Clin Invest,* 127 (3), 1117.

Bogliolo, M. and Surralles, J. (2015), 'Fanconi anemia: a model disease for studies on human genetics and advanced therapeutics', *Curr Opin Genet Dev,* 33, 32-40.

Bogliolo, M., et al. (2017), 'Biallelic truncating FANCM mutations cause early-onset cancer but not Fanconi anemia', *Genet Med*.

Bogliolo, M., et al. (2007), 'Histone H2AX and Fanconi anemia FANCD2 function in the same pathway to maintain chromosome stability', *EMBO J,* 26 (5), 1340-51.

Bogliolo, M., et al. (2013), 'Mutations in ERCC4, encoding the DNA-repair endonuclease XPF, cause Fanconi anemia', *Am J Hum Genet,* 92 (5), 800-6.

Boisvert, R. A. and Howlett, N. G. (2014), 'The Fanconi anemia ID2 complex: dueling saxes at the crossroads', *Cell Cycle,* 13 (19), 2999-3015.

Brookman, K. W., et al. (1996), 'ERCC4 (XPF) encodes a human nucleotide excision repair protein with eukaryotic recombination homologs', *Mol Cell Biol,* 16 (11), 6553-62.

Carre, G., et al. (2017), 'Xeroderma pigmentosum complementation group F: A rare cause of cerebellar ataxia with chorea', *J Neurol Sci,* 376, 198-201.

Catucci, I., et al. (2017), 'Individuals with FANCM biallelic mutations do not develop Fanconi anemia, but show risk for breast cancer, chemotherapy toxicity and may display chromosome fragility', *Genet Med*.

Ceccaldi, R., et al. (2015), 'Homologous-recombination-deficient tumours are dependent on Poltheta-mediated repair', *Nature,* 518 (7538), 258-62.

Ciccia, A., McDonald, N., and West, S. C. (2008), 'Structural and functional relationships of the XPF/MUS81 family of proteins', *Annu Rev Biochem,* 77, 259-87.

Cohn, M. A., et al. (2009), 'UAF1 is a subunit of multiple deubiquitinating enzyme complexes', *J Biol Chem,* 284 (8), 5343-51.

Cong, L., et al. (2013), 'Multiplex genome engineering using CRISPR/Cas systems', *Science,* 339 (6121), 819-23.

Crossan, G. P. and Patel, K. J. (2012), 'The Fanconi anaemia pathway orchestrates incisions at sites of crosslinked DNA', *J Pathol,* 226 (2), 326-37.

Crossan, G. P., et al. (2011), 'Disruption of mouse Slx4, a regulator of structure-specific nucleases, phenocopies Fanconi anemia', *Nat Genet,* 43 (2), 147-52.

Croteau, D. L., Peng, Y., and Van Houten, B. (2008), 'DNA repair gets physical: mapping an XPA-binding site on ERCC1', *DNA Repair (Amst),* 7 (5), 819-26.

Chang, H. H. Y., et al. (2017), 'Non-homologous DNA end joining and alternative pathways to double-strand break repair', *Nat Rev Mol Cell Biol,* 18 (8), 495-506.

Chu, G. and Chang, E. (1988), 'Xeroderma pigmentosum group E cells lack a nuclear factor that binds to damaged DNA', *Science,* 242 (4878), 564-7.

Damia, G., et al. (1996), 'Sensitivity of CHO mutant cell lines with specific defects in nucleotide excision repair to different anti-cancer agents', *Int J Cancer,* 66 (6), 779-83.

Das, D., et al. (2017), 'Single-stranded DNA Binding by the Helix-Hairpin-Helix Domain of XPF Protein Contributes to the Substrate Specificity of the ERCC1-XPF Protein Complex', *J Biol Chem,* 292 (7), 2842-53.

de Laat, W. L., et al. (1998), 'Mapping of interaction domains between human repair proteins ERCC1 and XPF', *Nucleic Acids Res,* 26 (18), 4146-52.

Dronkert, M. L. and Kanaar, R. (2001), 'Repair of DNA interstrand cross-links', *Mutat Res,* 486 (4), 217-47.

Enoiu, M., Jiricny, J., and Scharer, O. D. (2012), 'Repair of cisplatin-induced DNA interstrand crosslinks by a replication-independent pathway involving transcription-coupled repair and translesion synthesis', *Nucleic Acids Res,* 40 (18), 8953-64.

Fassihi, H., et al. (2016), 'Deep phenotyping of 89 xeroderma pigmentosum patients reveals unexpected heterogeneity dependent on the precise molecular defect', *Proc Natl Acad Sci U S A,* 113 (9), E1236-45.

Feeney, L., et al. (2017), 'RPA-Mediated Recruitment of the E3 Ligase RFWD3 Is Vital for Interstrand Crosslink Repair and Human Health', *Mol Cell,* 66 (5), 610-21 e4.

Fenech, M., et al. (2011), 'The HUMN and HUMNxL international collaboration projects on human micronucleus assays in lymphocytes and buccal cells--past, present and future', *Mutagenesis,* 26 (1), 239-45.

Fousteri, M., et al. (2006), 'Cockayne syndrome A and B proteins differentially regulate recruitment of chromatin remodeling and repair factors to stalled RNA polymerase II in vivo', *Mol Cell,* 23 (4), 471-82.

Garcia-Rubio, M. L., et al. (2015), 'The Fanconi Anemia Pathway Protects Genome Integrity from R-loops', *PLoS Genet,* 11 (11), e1005674.

Geiger, T., et al. (2011), 'Use of stable isotope labeling by amino acids in cell culture as a spike-in standard in quantitative proteomics', *Nat Protoc,* 6 (2), 147-57.

Grant, D. F., Bessho, T., and Reardon, J. T. (1998), 'Nucleotide excision repair of melphalan monoadducts', *Cancer Res,* 58 (22), 5196-200.

Gregg, S. Q., Robinson, A. R., and Niedernhofer, L. J. (2011), 'Physiological consequences of defects in ERCC1-XPF DNA repair endonuclease', *DNA Repair (Amst),* 10 (7), 781-91.

Gueiderikh, A., Rosselli, F., and Neto, J. B. C. (2017), 'A never-ending story: the steadily growing family of the FA and FA-like genes', *Genet Mol Biol,* 40 (2), 398-407.

Guervilly, J. H., et al. (2015), 'The SLX4 complex is a SUMO E3 ligase that impacts on replication stress outcome and genome stability', *Mol Cell,* 57 (1), 123-37.

Hashimoto, K., et al. (2015), 'Physical interaction between SLX4 (FANCP) and XPF (FANCQ) proteins and biological consequences of interaction-defective missense mutations', *DNA Repair (Amst),* 35, 48-54.

Hashimoto, S., Anai, H., and Hanada, K. (2016), 'Mechanisms of interstrand DNA crosslink repair and human disorders', *Genes Environ,* 38, 9.

He, C., et al. (2017), 'Two novel mutations in ERCC6 cause Cockayne syndrome B in a Chinese family', *Mol Med Rep,* 15 (6), 3957-62.

Hendriks, I. A., et al. (2015), 'Ubiquitin-specific Protease 11 (USP11) Deubiquitinates Hybrid Small Ubiquitin-like Modifier (SUMO)-Ubiquitin Chains to Counteract RING Finger Protein 4 (RNF4)', *J Biol Chem,* 290 (25), 15526-37.

Hodskinson, M. R., et al. (2014), 'Mouse SLX4 is a tumor suppressor that stimulates the activity of the nuclease XPF-ERCC1 in DNA crosslink repair', *Mol Cell,* 54 (3), 472-84.

Hoeijmakers, J. H. (2009), 'DNA damage, aging, and cancer', *N Engl J Med,* 361 (15), 1475-85.

Howlett, N. G., et al. (2002), 'Biallelic inactivation of BRCA2 in Fanconi anemia', *Science,* 297 (5581), 606-9.

Huertas, P. and Jackson, S. P. (2009), 'Human CtIP mediates cell cycle control of DNA end resection and double strand break repair', *J Biol Chem,* 284 (14), 9558-65.

Hutton, R. D., et al. (2010), 'PCNA and XPF cooperate to distort DNA substrates', *Nucleic Acids Res,* 38 (5), 1664-75.

Ideguchi, H., et al. (2002), 'Structural and functional characterization of the USP11 deubiquitinating enzyme, which interacts with the RanGTP-associated protein RanBPM', *Biochem J,* 367 (Pt 1), 87-95.

Imoto, K., et al. (2013), 'Ancient origin of a Japanese xeroderma pigmentosum founder mutation', *J Dermatol Sci,* 69 (2), 175-6.

Inano, S., et al. (2017), 'RFWD3-Mediated Ubiquitination Promotes Timely Removal of Both RPA and RAD51 from DNA Damage Sites to Facilitate Homologous Recombination', *Mol Cell,* 66 (5), 622-34 e8.

Iyama, T., et al. (2015), 'CSB interacts with SNM1A and promotes DNA interstrand crosslink processing', *Nucleic Acids Res,* 43 (1), 247-58.

Jia, N., et al. (2015), 'A rapid, comprehensive system for assaying DNA repair activity and cytotoxic effects of DNA-damaging reagents', *Nat Protoc,* 10 (1), 12-24.

Kashiyama, K., et al. (2013), 'Malfunction of nuclease ERCC1-XPF results in diverse clinical manifestations and causes Cockayne syndrome, xeroderma pigmentosum, and Fanconi anemia', *Am J Hum Genet,* 92 (5), 807-19.

Katsuki, Y. and Takata, M. (2016), 'Defects in homologous recombination repair behind the human diseases: FA and HBOC', *Endocr Relat Cancer,* 23 (10), T19-37.

Ke, J. Y., et al. (2014), 'USP11 regulates p53 stability by deubiquitinating p53', *J Zhejiang Univ Sci B,* 15 (12), 1032-8.

Kiiski, J. I., et al. (2014), 'Exome sequencing identifies FANCM as a susceptibility gene for triple-negative breast cancer', *Proc Natl Acad Sci U S A,* 111 (42), 15172-7.

Kim, J. M., et al. (2009), 'Inactivation of murine Usp1 results in genomic instability and a Fanconi anemia phenotype', *Dev Cell,* 16 (2), 314-20.

Kim, Y. (2014), 'Nuclease delivery: versatile functions of SLX4/FANCP in genome maintenance', *Mol Cells,* 37 (8), 569-74.

Kim, Y., et al. (2013), 'Regulation of multiple DNA repair pathways by the Fanconi anemia protein SLX4', *Blood,* 121 (1), 54-63.

Kleijer, W. J., et al. (2008), 'Incidence of DNA repair deficiency disorders in western Europe: Xeroderma pigmentosum, Cockayne syndrome and trichothiodystrophy', *DNA Repair (Amst),* 7 (5), 744-50.

Klein Douwel, D., et al. (2017), 'Recruitment and positioning determine the specific role of the XPF-ERCC1 endonuclease in interstrand crosslink repair', *EMBO J,* 36 (14), 2034-46.

Klein Douwel, D., et al. (2014), 'XPF-ERCC1 acts in Unhooking DNA interstrand crosslinks in cooperation with FANCD2 and FANCP/SLX4', *Mol Cell,* 54 (3), 460-71.

Knies, K., et al. (2017), 'Biallelic mutations in the ubiquitin ligase RFWD3 cause Fanconi anemia', *J Clin Invest,* 127 (8), 3013-27.

Knipscheer, P., et al. (2009), 'The Fanconi anemia pathway promotes replication-dependent DNA interstrand cross-link repair', *Science,* 326 (5960), 1698-701.

Kuraoka, I., et al. (2008), 'Isolation of XAB2 complex involved in pre-mRNA splicing, transcription, and transcription-coupled repair', *J Biol Chem,* 283 (2), 940-50.

Lachaud, C., et al. (2016), 'Ubiquitinated Fancd2 recruits Fan1 to stalled replication forks to prevent genome instability', *Science,* 351 (6275), 846-9.

Lachaud, C., et al. (2014), 'Distinct functional roles for the two SLX4 ubiquitin-binding UBZ domains mutated in Fanconi anemia', *J Cell Sci,* 127 (Pt 13), 2811-7.

Lafuente-Barquero, J., et al. (2017), 'The Smc5/6 complex regulates the yeast Mph1 helicase at RNA-DNA hybrid-mediated DNA damage', *PLoS Genet,* 13 (12), e1007136.

Lehmann, A. R. (2011), 'DNA polymerases and repair synthesis in NER in human cells', *DNA Repair (Amst),* 10 (7), 730-3.

Lehmann, A. R., McGibbon, D., and Stefanini, M. (2011), 'Xeroderma pigmentosum', *Orphanet J Rare Dis,* 6, 70.

Lehmann, J., et al. (2017), 'XPF knockout via CRISPR/Cas9 reveals that ERCC1 is retained in the cytoplasm without its heterodimer partner XPF', *Cell Mol Life Sci,* 74 (11), 2081-94.

Liang, C. C., et al. (2016), 'The FANCD2-FANCI complex is recruited to DNA interstrand crosslinks before monoubiquitination of FANCD2', *Nat Commun,* 7, 12124.

Liang, Q., et al. (2014), 'A selective USP1-UAF1 inhibitor links deubiquitination to DNA damage responses', *Nat Chem Biol,* 10 (4), 298-304.

Liu, W., et al. (2015), 'IBS: an illustrator for the presentation and visualization of biological sequences', *Bioinformatics,* 31 (20), 3359-61.

Lopez-Otin, C., et al. (2013), 'The hallmarks of aging', *Cell,* 153 (6), 1194-217.

Manandhar, M., Boulware, K. S., and Wood, R. D. (2015), 'The ERCC1 and ERCC4 (XPF) genes and gene products', *Gene,* 569 (2), 153-61.

Marteijn, J. A., et al. (2014), 'Understanding nucleotide excision repair and its roles in cancer and ageing', *Nat Rev Mol Cell Biol,* 15 (7), 465-81.

Mason, J. M. and Sekiguchi, J. M. (2011), 'Snm1B/Apollo functions in the Fanconi anemia pathway in response to DNA interstrand crosslinks', *Hum Mol Genet,* 20 (13), 2549-59.

Mastro, T. L. and Forsburg, S. L. (2014), 'Increased meiotic crossovers and reduced genome stability in absence of Schizosaccharomyces pombe Rad16 (XPF)', *Genetics,* 198 (4), 1457-72.

Mathew, C. G. (2006), 'Fanconi anaemia genes and susceptibility to cancer', *Oncogene,* 25 (43), 5875-84.

Matsumura, Y., et al. (1998), 'Characterization of molecular defects in xeroderma pigmentosum group F in relation to its clinically mild symptoms', *Hum Mol Genet,* 7 (6), 969-74.

Matsunaga, T., et al. (1996), 'Replication protein A confers structure-specific endonuclease activities to the XPF-ERCC1 and XPG subunits of human DNA repair excision nuclease', *J Biol Chem,* 271 (19), 11047-50.

McNeil, E. M. and Melton, D. W. (2012), 'DNA repair endonuclease ERCC1-XPF as a novel therapeutic target to overcome chemoresistance in cancer therapy', *Nucleic Acids Res,* 40 (20), 9990-10004.

McHugh, P. J., Spanswick, V. J., and Hartley, J. A. (2001), 'Repair of DNA interstrand crosslinks: molecular mechanisms and clinical relevance', *Lancet Oncol,* 2 (8), 483-90.

Michl, J., Zimmer, J., and Tarsounas, M. (2016), 'Interplay between Fanconi anemia and homologous recombination pathways in genome integrity', *EMBO J,* 35 (9), 909-23.

Miura, T., et al. (2012), 'Homologous recombination via synthesis-dependent strand annealing in yeast requires the Irc20 and Srs2 DNA helicases', *Genetics,* 191 (1), 65-78.

Mori, T., et al. (2018), 'ERCC4 variants identified in a cohort of patients with segmental progeroid syndromes', *Hum Mutat,* 39 (2), 255-65.

Muniandy, P. A., et al. (2010), 'DNA interstrand crosslink repair in mammalian cells: step by step', *Crit Rev Biochem Mol Biol,* 45 (1), 23-49.

Munoz, I. M., et al. (2009), 'Coordination of structure-specific nucleases by human SLX4/BTBD12 is required for DNA repair', *Mol Cell,* 35 (1), 116-27.

Munoz, P., et al. (2005), 'XPF nuclease-dependent telomere loss and increased DNA damage in mice overexpressing TRF2 result in premature aging and cancer', *Nat Genet,* 37 (10), 1063-71.

Naim, V., et al. (2013), 'ERCC1 and MUS81-EME1 promote sister chromatid separation by processing late replication intermediates at common fragile sites during mitosis', *Nat Cell Biol,* 15 (8), 1008-15.

Natale, V. and Raquer, H. (2017), 'Xeroderma pigmentosum-Cockayne syndrome complex', *Orphanet J Rare Dis,* 12 (1), 65.

Niedernhofer, L. J., et al. (2006), 'A new progeroid syndrome reveals that genotoxic stress suppresses the somatotroph axis', *Nature,* 444 (7122), 1038-43.

Nijman, S. M., et al. (2005), 'The deubiquitinating enzyme USP1 regulates the Fanconi anemia pathway', *Mol Cell,* 17 (3), 331-9.

O'Donnell, L. and Durocher, D. (2010), 'DNA repair has a new FAN1 club', *Mol Cell,* 39 (2), 167-9.

Ong, S. E., et al. (2002), 'Stable isotope labeling by amino acids in cell culture, SILAC, as a simple and accurate approach to expression proteomics', *Mol Cell Proteomics,* 1 (5), 376-86.

Orthwein, A., et al. (2015), 'A mechanism for the suppression of homologous recombination in G1 cells', *Nature,* 528 (7582), 422-6.

Osorio, A., et al. (2013), 'Evaluation of rare variants in the new fanconi anemia gene ERCC4 (FANCQ) as familial breast/ovarian cancer susceptibility alleles', *Hum Mutat,* 34 (12), 1615-8.

Park, J. Y., et al. (2016), 'Complementation of hypersensitivity to DNA interstrand crosslinking agents demonstrates that XRCC2 is a Fanconi anaemia gene', *J Med Genet,* 53 (10), 672-80.

Perez-Oliva, A. B., et al. (2015), 'USP45 deubiquitylase controls ERCC1-XPF endonuclease-mediated DNA damage responses', *EMBO J,* 34 (3), 326-43.

Peterlongo, P., et al. (2015), 'FANCM c.5791C>T nonsense mutation (rs144567652) induces exon skipping, affects DNA repair activity and is a familial breast cancer risk factor', *Hum Mol Genet,* 24 (18), 5345-55.

Popp, I., et al. (2018), 'Fanconi anemia with sun-sensitivity caused by a Xeroderma pigmentosum-associated missense mutation in XPF', *BMC Med Genet,* 19 (1), 7.

Prakash, S. and Prakash, L. (2000), 'Nucleotide excision repair in yeast', *Mutat Res,* 451 (1-2), 13-24.

Ran, F. A., et al. (2013), 'Genome engineering using the CRISPR-Cas9 system', *Nat Protoc,* 8 (11), 2281-308.

Raschle, M., et al. (2008), 'Mechanism of replication-coupled DNA interstrand crosslink repair', *Cell,* 134 (6), 969-80.

Rouillon, C. and White, M. F. (2011), 'The evolution and mechanisms of nucleotide excision repair proteins', *Res Microbiol,* 162 (1), 19-26.

Roy, U. and Scharer, O. D. (2016), 'Involvement of translesion synthesis DNA polymerases in DNA interstrand crosslink repair', *DNA Repair (Amst),* 44, 33-41.

Saito, T. T., et al. (2012), 'SLX-1 is required for maintaining genomic integrity and promoting meiotic noncrossovers in the Caenorhabditis elegans germline', *PLoS Genet,* 8 (8), e1002888.

Sarkar, J., et al. (2015), 'SLX4 contributes to telomere preservation and regulated processing of telomeric joint molecule intermediates', *Nucleic Acids Res,* 43 (12), 5912-23.

Sawyer, S. L., et al. (2015), 'Biallelic mutations in BRCA1 cause a new Fanconi anemia subtype', *Cancer Discov,* 5 (2), 135-42.

Scharer, O. D. (2017), 'ERCC1-XPF endonuclease-positioned to cut', *EMBO J*.

Schoenfeld, A. R., et al. (2004), 'BRCA2 is ubiquitinated in vivo and interacts with USP11, a deubiquitinating enzyme that exhibits prosurvival function in the cellular response to DNA damage', *Mol Cell Biol,* 24 (17), 7444-55.

Segui, N., et al. (2015), 'Germline Mutations in FAN1 Cause Hereditary Colorectal Cancer by Impairing DNA Repair', *Gastroenterology,* 149 (3), 563-6.

Sfeir, A. and Symington, L. S. (2015), 'Microhomology-Mediated End Joining: A Back-up Survival Mechanism or Dedicated Pathway?', *Trends Biochem Sci,* 40 (11), 701-14.

Shah, P., et al. (2017), 'Regulation of XPC deubiquitination by USP11 in repair of UV-induced DNA damage', *Oncotarget,* 8 (57), 96522-35.

Sigurdsson, S., Dirac-Svejstrup, A. B., and Svejstrup, J. Q. (2010), 'Evidence that transcript cleavage is essential for RNA polymerase II transcription and cell viability', *Mol Cell,* 38 (2), 202-10.

Sijbers, A. M., et al. (1998), 'Homozygous R788W point mutation in the XPF gene of a patient with xeroderma pigmentosum and late-onset neurologic disease', *J Invest Dermatol,* 110 (5), 832-6.

Sijbers, A. M., et al. (1996), 'Xeroderma pigmentosum group F caused by a defect in a structure-specific DNA repair endonuclease', *Cell,* 86 (5), 811-22.

Singh, T. R., et al. (2009), 'Impaired FANCD2 monoubiquitination and hypersensitivity to camptothecin uniquely characterize Fanconi anemia complementation group M', *Blood,* 114 (1), 174-80.

Sinha, S., et al. (2016), 'Risky business: Microhomology-mediated end joining', *Mutat Res,* 788, 17-24.

Somyajit, K., Subramanya, S., and Nagaraju, G. (2012), 'Distinct roles of FANCO/RAD51C protein in DNA damage signaling and repair: implications for Fanconi anemia and breast cancer susceptibility', *J Biol Chem,* 287 (5), 3366-80.

Stark, J. M., et al. (2004), 'Genetic steps of mammalian homologous repair with distinct mutagenic consequences', *Mol Cell Biol,* 24 (21), 9305-16.

Su, Y., et al. (2012), 'Multiple DNA binding domains mediate the function of the ERCC1-XPF protein in nucleotide excision repair', *J Biol Chem,* 287 (26), 21846-55.

Sugasawa, K., et al. (1998), 'Xeroderma pigmentosum group C protein complex is the initiator of global genome nucleotide excision repair', *Mol Cell,* 2 (2), 223-32.

Surralles, J., et al. (2004), 'Molecular cross-talk among chromosome fragility syndromes', *Genes Dev,* 18 (12), 1359-70.

Taylor, M. R. G., et al. (2015), 'Rad51 Paralogs Remodel Pre-synaptic Rad51 Filaments to Stimulate Homologous Recombination', *Cell,* 162 (2), 271-86.

Tian, M., et al. (2004), 'Growth retardation, early death, and DNA repair defects in mice deficient for the nucleotide excision repair enzyme XPF', *Mol Cell Biol,* 24 (3), 1200-5.

Tomida, J., et al. (2015), 'REV7 is essential for DNA damage tolerance via two REV3L binding sites in mammalian DNA polymerase zeta', *Nucleic Acids Res,* 43 (2), 1000-11.

Tripsianes, K., et al. (2005), 'The structure of the human ERCC1/XPF interaction domains reveals a complementary role for the two proteins in nucleotide excision repair', *Structure,* 13 (12), 1849-58.

Trujillo, J. P., et al. (2012), 'On the role of FAN1 in Fanconi anemia', *Blood,* 120 (1), 86-9.

Tsodikov, O. V., et al. (2005), 'Crystal structure and DNA binding functions of ERCC1, a subunit of the DNA structure-specific endonuclease XPF-ERCC1', *Proc Natl Acad Sci U S A,* 102 (32), 11236-41.

Tsodikov, O. V., et al. (2007), 'Structural basis for the recruitment of ERCC1-XPF to nucleotide excision repair complexes by XPA', *EMBO J,* 26 (22), 4768-76.

van Twest, S., et al. (2017), 'Mechanism of Ubiquitination and Deubiquitination in the Fanconi Anemia Pathway', *Mol Cell,* 65 (2), 247-59.

Vermeij, W. P., Hoeijmakers, J. H., and Pothof, J. (2014), 'Aging: not all DNA damage is equal', *Curr Opin Genet Dev,* 26, 124-30.

Volker, M., et al. (2001), 'Sequential assembly of the nucleotide excision repair factors in vivo', *Mol Cell,* 8 (1), 213-24.

Wang, A. T., et al. (2011), 'Human SNM1A and XPF-ERCC1 collaborate to initiate DNA interstrand cross-link repair', *Genes Dev,* 25 (17), 1859-70.

Wang, B., et al. (2007), 'Abraxas and RAP80 form a BRCA1 protein complex required for the DNA damage response', *Science,* 316 (5828), 1194-8.

West, S. C., et al. (2015), 'Resolution of Recombination Intermediates: Mechanisms and Regulation', *Cold Spring Harb Symp Quant Biol,* 80, 103-9.

Wilson, B. T., et al. (2016), 'The Cockayne Syndrome Natural History (CoSyNH) study: clinical findings in 102 individuals and recommendations for care', *Genet Med,* 18 (5), 483-93.

Wiltshire, T. D., et al. (2010), 'Sensitivity to poly(ADP-ribose) polymerase (PARP) inhibition identifies ubiquitin-specific peptidase 11 (USP11) as a regulator of DNA double-strand break repair', *J Biol Chem,* 285 (19), 14565-71.

Williams, H. L., Gottesman, M. E., and Gautier, J. (2013), 'The differences between ICL repair during and outside of S phase', *Trends Biochem Sci,* 38 (8), 386-93.

Wyatt, H. D., et al. (2017), 'The SMX DNA Repair Tri-nuclease', *Mol Cell,* 65 (5), 848-60 e11.

Yagi, T., et al. (1998), 'Complete restoration of normal DNA repair characteristics in group F xeroderma pigmentosum cells by over-expression of transfected XPF cDNA', *Carcinogenesis,* 19 (1), 55-60.

Yang, L., Ritchie, A. M., and Melton, D. W. (2017), 'Disruption of DNA repair in cancer cells by ubiquitination of a destabilising dimerization domain of nucleotide excision repair protein ERCC1', *Oncotarget,* 8 (33), 55246-64.

Zhang, J. and Walter, J. C. (2014), 'Mechanism and regulation of incisions during DNA interstrand cross-link repair', *DNA Repair (Amst),* 19, 135-42.

Zhang, X., et al. (2012), 'Mutations in UVSSA cause UV-sensitive syndrome and destabilize ERCC6 in transcription-coupled DNA repair', *Nat Genet,* 44 (5), 593-7.

Zhao, X., et al. (2017), 'Cell cycle-dependent control of homologous recombination', *Acta Biochim Biophys Sin (Shanghai)*, 1-14.

Zhu, X. D., et al. (2003), 'ERCC1/XPF removes the 3' overhang from uncapped telomeres and represses formation of telomeric DNA-containing double minute chromosomes', *Mol Cell,* 12 (6), 1489-98.

Annex

			Control			WT				
			MMJS_01	MMJS_05	MMJS_09	MMJS_02	MMJS_06	MMJS_10	Control	WT
Accession	Description	Σ# PSMs	A2: Area	B2: Area	C2: Area	D2: Area	E2: Area	F2: Area	COUNTS	COUNTS
P07992	DNA excision repair protein ERCC-1 OS=Homo sapiens GN=ERCC1 PE=1 SV=1 - [ERCC1_HUMAN]	44				1,729E8	1,064E8	3,324E8	0	3
Q92889	DNA repair endonuclease XPF OS=Homo sapiens GN=ERCC4 PE=1 SV=3 - [XPF_HUMAN]	117				2,537E8	1,571E8	4,117E8	0	3
P22090	40S ribosomal protein S4, Y isoform 1 OS=Homo sapiens GN=RPS4Y1 PE=1 SV=2 - [RS4Y1_HUMAN]	7				3,893E6	2,673E6	2,380E7	0	3
P46782	40S ribosomal protein S5 OS=Homo sapiens GN=RPS5 PE=1 SV=4 - [RS5_HUMAN]	4					1,585E6	9,882E6	0	2
P62263	40S ribosomal protein S14 OS=Homo sapiens GN=RPS14 PE=1 SV=3 - [RS14_HUMAN]	2					3,648E6	4,551E6	0	2
P84098	60S ribosomal protein L19 OS=Homo sapiens GN=RPL19 PE=1 SV=1 - [RL19_HUMAN]	2				2,089E6	2,379E6		0	2
P62280	40S ribosomal protein S11 OS=Homo sapiens GN=RPS11 PE=1 SV=3 - [RS11_HUMAN]	2				1,281E6	3,855E6		0	2
P61247	40S ribosomal protein S3a OS=Homo sapiens GN=RPS3A PE=1 SV=2 - [RS3A_HUMAN]	2					1,315E7	2,058E7	0	2
P11142	Heat shock cognate 71 kDa protein OS=Homo sapiens GN=HSPA8 PE=1 SV=1 - [HSP7C_HUMAN]	4				4,199E6	4,368E6	2,928E6	0	3
O75152	Zinc finger CCCH domain-containing protein 11A OS=Homo sapiens GN=ZC3H11A PE=1 SV=3 - [ZC11A_HUMAN]	2					2,281E5	3,475E5	0	2
P36578	60S ribosomal protein L4 OS=Homo sapiens GN=RPL4 PE=1 SV=5 - [RL4_HUMAN]	2					3,671E6	3,522E6	0	2
Q00839	Heterogeneous nuclear ribonucleoprotein U OS=Homo sapiens GN=HNRNPU PE=1 SV=6 - [HNRPU_HUMAN]	2					5,227E6	3,908E6	0	2
Q8IY92	Structure-specific endonuclease subunit SLX4 OS=Homo sapiens GN=SLX4 PE=1 SV=3 - [SLX4_HUMAN]	3					2,479E6	6,354E6	0	2
Q9H1R3	Myosin light chain kinase 2, skeletal/cardiac muscle OS=Homo sapiens GN=MYLK2 PE=1 SV=3 - [MYLK2_HUMAN]	2				1,466E7		2,643E7	0	2
P21333	Filamin-A OS=Homo sapiens GN=FLNA PE=1 SV=4 - [FLNA_HUMAN]	2					1,002E8	1,951E5	0	2
P98198	Probable phospholipid-transporting ATPase ID OS=Homo sapiens GN=ATP8B2 PE=2 SV=2 - [AT8B2_HUMAN]	2					1,866E7	5,789E7	0	2

			Control			WT + UV				
			MMJS_01	MMJS_05	MMJS_09	MMJS_03	MMJS_07	MMJS_11	Control	WT_UV
Accession	Description	Σ# PSMs	A2: Area	B2: Area	C2: Area	D2: Area	E2: Area	F2: Area	COUNTS	COUNTS
Q92889	DNA repair endonuclease XPF OS=Homo sapiens GN=ERCC4 PE=1 SV=3 - [XPF_HUMAN]	147				4,315E8	5,509E8	3,951E8	0	3
P07992	DNA excision repair protein ERCC-1 OS=Homo sapiens GN=ERCC1 PE=1 SV=1 - [ERCC1_HUMAN]	58				3,315E8	4,984E8	3,328E8	0	3
P28715	DNA repair protein complementing XP-G cells OS=Homo sapiens GN=ERCC5 PE=1 SV=3 - [ERCC5_HUMAN]	8				1,965E6	1,135E7		0	2
P62701	40S ribosomal protein S4, X isoform OS=Homo sapiens GN=RPS4X PE=1 SV=2 - [RS4X_HUMAN]	14				1,070E7	1,177E7	1,289E7	0	3
Q00839	Heterogeneous nuclear ribonucleoprotein U OS=Homo sapiens GN=HNRNPU PE=1 SV=6 - [HNRPU_HUMAN]	7				1,934E6	1,928E7	5,071E6	0	3
P0CW22	40S ribosomal protein S17-like OS=Homo sapiens GN=RPS17L PE=2 SV=1 - [RS17L_HUMAN]	9				4,070E7	4,136E7	3,558E7	0	3
P61247	40S ribosomal protein S3a OS=Homo sapiens GN=RPS3A PE=1 SV=2 - [RS3A_HUMAN]	5					2,499E7	1,582E7	0	2
P46783	40S ribosomal protein S10 OS=Homo sapiens GN=RPS10 PE=1 SV=1 - [RS10_HUMAN]	7					1,009E7	1,171E7	0	2
P15880	40S ribosomal protein S2 OS=Homo sapiens GN=RPS2 PE=1 SV=2 - [RS2_HUMAN]	5				1,249E7	1,885E7	1,513E7	0	3
Q8IY92	Structure-specific endonuclease subunit SLX4 OS=Homo sapiens GN=SLX4 PE=1 SV=3 - [SLX4_HUMAN]	5				1,951E6	6,336E6	4,696E6	0	3
P27635	60S ribosomal protein L10 OS=Homo sapiens GN=RPL10 PE=1 SV=4 - [RL10_HUMAN]	3				7,522E6	1,312E7		0	2
P36578	60S ribosomal protein L4 OS=Homo sapiens GN=RPL4 PE=1 SV=5 - [RL4_HUMAN]	4				3,284E6	4,739E6	3,700E6	0	3
P11142	Heat shock cognate 71 kDa protein OS=Homo sapiens GN=HSPA8 PE=1 SV=1 - [HSP7C_HUMAN]	7				9,205E6	9,211E6	2,947E6	0	3
Q02878	60S ribosomal protein L6 OS=Homo sapiens GN=RPL6 PE=1 SV=3 - [RL6_HUMAN]	3				1,803E6	2,788E6		0	2
P62851	40S ribosomal protein S25 OS=Homo sapiens GN=RPS25 PE=1 SV=1 - [RS25_HUMAN]	4				5,834E5	2,770E7	7,636E5	0	3
P84098	60S ribosomal protein L19 OS=Homo sapiens GN=RPL19 PE=1 SV=1 - [RL19_HUMAN]	3				5,632E6	5,045E6		0	2
P49411	Elongation factor Tu, mitochondrial OS=Homo sapiens GN=TUFM PE=1 SV=2 - [EFTU_HUMAN]	5				9,372E5	3,568E6	3,114E5	0	3
P46782	40S ribosomal protein S5 OS=Homo sapiens GN=RPS5 PE=1 SV=4 - [RS5_HUMAN]	3				4,975E6		1,162E7	0	2

Q08J23	tRNA (cytosine(34)-C(5))-methyltransferase OS=Homo sapiens GN=NSUN2 PE=1 SV=2 - [NSUN2_HUMAN]	4				1,021E6	1,217E6		0	2
P62249	40S ribosomal protein S16 OS=Homo sapiens GN=RPS16 PE=1 SV=2 - [RS16_HUMAN]	2					2,393E7	1,328E7	0	2
P61254	60S ribosomal protein L26 OS=Homo sapiens GN=RPL26 PE=1 SV=1 - [RL26_HUMAN]	3					6,980E6	3,566E6	0	2
P09651	Heterogeneous nuclear ribonucleoprotein A1 OS=Homo sapiens GN=HNRNPA1 PE=1 SV=5 - [ROA1_HUMAN]	2				5,022E5	3,483E5		0	2
P83881	60S ribosomal protein L36a OS=Homo sapiens GN=RPL36A PE=1 SV=2 - [RL36A_HUMAN]	2				2,109E6		1,542E6	0	2
P12004	Proliferating cell nuclear antigen OS=Homo sapiens GN=PCNA PE=1 SV=1 - [PCNA_HUMAN]	2				2,012E6	2,881E6		0	2
Q04637	Eukaryotic translation initiation factor 4 gamma 1 OS=Homo sapiens GN=EIF4G1 PE=1 SV=4 - [IF4G1_HUMAN]	2				1,115E6	5,542E5		0	2
P62750	60S ribosomal protein L23a OS=Homo sapiens GN=RPL23A PE=1 SV=1 - [RL23A_HUMAN]	2				1,485E6	2,941E6		0	2
P50402	Emerin OS=Homo sapiens GN=EMD PE=1 SV=1 - [EMD_HUMAN]	3				8,070E5	4,876E5	2,784E5	0	3
P30153	Serine/threonine-protein phosphatase 2A 65 kDa regulatory subunit A alpha isoform OS=Homo sapiens GN=PPP2R1A PE=1 SV=4 - [2AAA_HUMAN]	2				1,003E6	6,167E5		0	2
P62263	40S ribosomal protein S14 OS=Homo sapiens GN=RPS14 PE=1 SV=3 - [RS14_HUMAN]	3				8,509E6	8,947E6	3,640E6	0	3
P67809	Nuclease-sensitive element-binding protein 1 OS=Homo sapiens GN=YBX1 PE=1 SV=3 - [YBOX1_HUMAN]	2				7,346E5	9,559E5		0	2
P42677	40S ribosomal protein S27 OS=Homo sapiens GN=RPS27 PE=1 SV=3 - [RS27_HUMAN]	2				4,567E6	6,884E6		0	2
P62910	60S ribosomal protein L32 OS=Homo sapiens GN=RPL32 PE=1 SV=2 - [RL32_HUMAN]	3				1,752E6	3,238E6	2,216E6	0	3
Q9UNF1	Melanoma-associated antigen D2 OS=Homo sapiens GN=MAGED2 PE=1 SV=2 - [MAGD2_HUMAN]	3				7,165E5	7,848E5	2,134E5	0	3
Q9Y5J1	U3 small nucleolar RNA-associated protein 18 homolog OS=Homo sapiens GN=UTP18 PE=1 SV=3 - [UTP18_HUMAN]	2				2,718E6		4,786E6	0	2
O75152	Zinc finger CCCH domain-containing protein 11A OS=Homo sapiens GN=ZC3H11A PE=1 SV=3 - [ZC11A_HUMAN]	3				6,005E5	5,476E5	3,293E5	0	3
P23025	DNA repair protein complementing XP-A cells OS=Homo sapiens GN=XPA PE=1 SV=1 - [XPA_HUMAN]	3				5,317E6	4,451E7		0	2
Q8WWK9	Cytoskeleton-associated protein 2 OS=Homo sapiens GN=CKAP2 PE=1 SV=1 - [CKAP2_HUMAN]	2					3,597E5	3,692E5	0	2

			Control			MMC				
			MMJS_01	MMJS_05	MMJS_09	MMJS_04	MMJS_08	MMJS_12	Control	WT_UV
Accession	Description	Σ# PSMs	A2: Area	B2: Area	C2: Area	D2: Area	E2: Area	F2: Area	COUNTS	COUNTS
Q92889	DNA repair endonuclease XPF OS=Homo sapiens GN=ERCC4 PE=1 SV=3 - [XPF_HUMAN]	104				1,994E8	7,553E7	4,130E8	0	3
P07992	DNA excision repair protein ERCC-1 OS=Homo sapiens GN=ERCC1 PE=1 SV=1 - [ERCC1_HUMAN]	38				1,630E8	5,050E7	2,996E8	0	3
Q6UWP8	Suprabasin OS=Homo sapiens GN=SBSN PE=2 SV=2 - [SBSN_HUMAN]	2				2,634E5		2,536E5	0	2
P36578	60S ribosomal protein L4 OS=Homo sapiens GN=RPL4 PE=1 SV=5 - [RL4_HUMAN]	3				1,228E6	1,808E6	3,566E6	0	3
P35813	Protein phosphatase 1A OS=Homo sapiens GN=PPM1A PE=1 SV=1 - [PPM1A_HUMAN]	3				2,941E7	6,363E7	4,977E7	0	3
Q00839	Heterogeneous nuclear ribonucleoprotein U OS=Homo sapiens GN=HNRNPU PE=1 SV=6 - [HNRPU_HUMAN]	3				2,618E6	2,267E6	2,208E6	0	3
Q9H1R3	Myosin light chain kinase 2, skeletal/cardiac muscle OS=Homo sapiens GN=MYLK2 PE=1 SV=3 - [MYLK2_HUMAN]	2				1,869E7		2,015E7	0	2
Q6ZN84	Coiled-coil domain-containing protein 81 OS=Homo sapiens GN=CCDC81 PE=2 SV=2 - [CCD81_HUMAN]	2				1,991E8	2,485E8		0	2

Annex Table I: Mass spectrometry data from XPF-TAP purification. Interactors of XPF purificated samples without treatment, with UVC irradiation (150J/m^2 1h of recovery) or MMC treatment (1.5 µM, 16h) per triplicate are shown here in respect to the control (XPF-KO). PSMs: total number of identified peptide spectra matched for the protein.

	Protein FDR Confidence	Accession	Description	Exp. q-value	Sum PEP Score	Coverage	# Peptides	# PSMs	# Unique Peptides	# Protein Groups	# AAs	MW [kDa]	calc. pI	Score Sequest HT	# Peptides Sequest HT
B1	High	P49454	Centromere protein F [OS=Homo sapiens]	0	3,04047	1,3084112	3	4	3	1	3210	367,537	5,07	3,65088141	3
	Medium	Q9UQ35	serine/arginine repetitive matrix protein 2 [OS=Homo sapiens]	0,01613	1,23225	0,4723837	1	1	1	1	2752	299,438	12,06	1,79620183	1
	Medium	Q14676	Mediator of DNA damage checkpoint protein 1 [OS=Homo sapiens]	0,01613	2,56698	1,4839636	3	3	3	1	2089	226,529	5,47	0	3
	Medium	Q8TDI0	Chromodomain-helicase-DNA-binding protein 5 [OS=Homo sapiens]	0,01613	0,97757	0,6653019	1	1	1	1	1954	222,909	6,15	0	1

	Protein FDR Confidence	Accession	Description	Exp. q-value	Sum PEP Score	Coverage	# Peptides	# PSMs	# Unique Peptides	# Protein Groups	# AAs	MW [kDa]	calc. pI	Score Sequest HT	# Peptides Sequest HT
B2	High	Q14676	Mediator of DNA damage checkpoint protein 1 [OS=Homo sapiens]	0	52,3107	14,600287	18	43	18	1	2089	226,529	5,47	67,8228009	18
	High	A6NHR9-1	structural maintenance of chromosomes flexible hinge domain-containing	0	60,4648	15,112219	26	55	26	1	2005	226,231	7,3	69,6142339	26
	Medium	Q14690	Protein RRP5 homolog [OS=Homo sapiens]	0,02924	1,43321	0,5344735	1	3	1	1	1871	208,57	8,87	0	1
	High	Q8WWQ0	PH-interacting protein [OS=Homo sapiens]	0	2,60642	0,7138935	1	2	1	1	1821	206,56	8,85	0	1
	High	Q8IY92	Structure-specific endonuclease subunit SLX4 [OS=Homo sapiens]	0	8,67743	3,217012	5	11	5	1	1834	199,889	6,06	11,9492532	5
	High	O14646	Chromodomain-helicase-DNA-binding protein 1 [OS=Homo sapiens]	0	20,0259	5,497076	9	18	9	1	1710	196,567	7,14	20,7677811	9
	High	P51532-1	Transcription activator BRG1 [OS=Homo sapiens]	0	12,5927	4,1894353	6	11	6	1	1647	184,53	7,88	5,92011726	6
	High	Q02880	DNA topoisomerase 2-beta [OS=Homo sapiens]	0	270,988	46,125461	65	357	51	1	1626	183,152	8	703,432699	65
	High	Q8NI27-1	THO complex subunit 2 [OS=Homo sapiens]	0	41,5965	13,370998	19	49	19	1	1593	182,659	8,44	56,8713735	19
	High	P11388-4	Isoform 4 of DNA topoisomerase 2-alpha [OS=Homo sapiens]	0	331,182	46,401985	78	535	64	1	1612	182,567	8,63	1038,95821	78
	High	Q9NRL2	Bromodomain adjacent to zinc finger domain protein 1A [OS=Homo sapie	0	69,7098	22,622108	29	70	29	1	1556	178,592	6,6	59,9467206	29
	High	O60306	Intron-binding protein aquarius [OS=Homo sapiens]	0	11,8733	4,3771044	7	9	7	1	1485	171,186	6,37	1,61474156	7
	High	Q9UIG0	Tyrosine-protein kinase BAZ1B [OS=Homo sapiens]	0	14,0301	5,9339177	8	12	8	1	1483	170,796	8,48	3,98667264	8
	High	P39880-3	Isoform 3 of Homeobox protein cut-like 1 [OS=Homo sapiens]	0	5,33713	2,176781	3	3	3	1	1516	165,587	5,86	1,81653965	3
	High	Q9ULI0	ATPase family AAA domain-containing protein 2B [OS=Homo sapiens]	0	7,48184	2,7434842	4	7	1	1	1458	164,811	6,8	8,00571334	4
	High	Q9NTI5	Sister chromatid cohesion protein PDS5 homolog B [OS=Homo sapiens]	0	12,9433	6,219765	7	11	7	1	1447	164,563	8,47	8,11630535	7
	High	Q96T23	remodeling and spacing factor 1 [OS=Homo sapiens]	0	22,9626	11,936155	12	21	12	1	1441	163,72	5,01	12,5643468	12
	High	Q6PL18-1	ATPase family AAA domain-containing protein 2 [OS=Homo sapiens]	0	12,9099	4,676259	6	10	3	1	1390	158,456	6,32	13,860622	6
	High	Q7Z3K3-1	Pogo transposable element with ZNF domain [OS=Homo sapiens]	0	10,6252	4,822695	6	7	6	1	1410	155,245	7,4	5,38452554	6
	High	Q9P2E9-1	Ribosome-binding protein 1 [OS=Homo sapiens]	0	41,4923	15,531915	18	35	18	1	1410	152,381	8,6	25,3741769	18
	High	Q9UKV3-1	Apoptotic chromatin condensation inducer in the nucleus [OS=Homo sapi	0	273,671	41,983594	45	359	2	1	1341	151,771	6,43	808,990564	45
	High	Q9UKV3-5	Isoform 4 of Apoptotic chromatin condensation inducer in the nucleus [O	0	264,112	41,415663	45	358	2	1	1328	150,467	6,43	780,37653	45
	High	Q9BQG0-2	Isoform 2 of Myb-binding protein 1A [OS=Homo sapiens]	0	2,49976	0,7507508	1	2	1	1	1332	149,274	9,28	0	1
	High	P28715-1	DNA repair protein complementing XP-G cells [OS=Homo sapiens]	0	9,02981	4,0472175	4	7	4	1	1186	133,027	5,22	3,68164706	4

	Protein FDR Confidence	Accession	Description	Exp. q-value	Sum PEP Score	Coverage	# Peptides	# PSMs	# Unique Peptides	# Protein Groups	# AAs	MW [kDa]	calc. pI	Score Sequest HT	# Peptides Sequest HT
B3	High	Q9UKV3-1	Apoptotic chromatin condensation inducer in the nucleus [OS=Homo sapi	0	11,2331	4,1014169	6	9	6	1	1341	151,771	6,43	6,36114132	6
	High	O75533-1	splicing factor 3B subunit 1 [OS=Homo sapiens]	0	6,02079	2,3006135	3	5	3	1	1304	145,738	7,09	3,58734798	3
	High	Q13045-1	protein flightless-1 homolog [OS=Homo sapiens]	0	7,95636	2,3640662	3	5	3	1	1269	144,659	6,05	5,3245815	3
	High	Q08211	Atp-dependent rna helicase a [OS=Homo sapiens]	0	209,245	41,968504	50	237	50	1	1270	140,869	6,84	421,519841	50
	Medium	P54098	DNA polymerase subunit gamma-1 [OS=Homo sapiens]	0,02985	1,20377	0,8878128	1	2	1	1	1239	139,473	6,9	0	1
	High	Q14562	ATP-dependent RNA helicase dhx8 [OS=Homo sapiens]	0	19,8116	8,2786885	8	11	8	1	1220	139,227	8,32	13,1515679	8
	High	Q7L2E3-2	Isoform 2 of Putative ATP-dependent RNA helicase DHX30 [OS=Homo sapi	0	17,9869	9,2471358	10	15	10	1	1222	136,03	8,6	7,858495	10
	High	Q9Y2K7	Lysine-specific demethylase 2A [OS=Homo sapiens]	0	35,1578	14,457831	15	32	15	1	1162	132,708	7,58	31,1919024	15
	Medium	Q9UNY4-1	transcription termination factor 2 [OS=Homo sapiens]	0,02985	1,12819	1,0327022	1	1	1	1	1162	129,508	8,37	0	1
	High	P35251-1	Replication factor C subunit 1 [OS=Homo sapiens]	0	5,5051	3,2229965	3	4	3	1	1148	128,175	9,36	0	3

	High	Q69YQ0-1	Cytospin-A [OS=Homo sapiens]	0	19,2347	10,026858	10	18	10	1	1117	124,525	5,72	13,4054443	10
	High	Q9H2P0	Activity-dependent neuroprotector homeobox protein [OS=Homo sapiens	0	4,9846	1,9056261	2	3	2	1	1102	123,485	7,34	1,74325895	2
	High	P28370-1	Probable global transcription activator SNF2L1 [OS=Homo sapiens]	0	29,1232	14,516129	16	26	9	1	1054	122,527	8,09	23,9319128	16

	Protein FDR Confidence	Accession	Description	Exp. q-value	Sum PEP Score	Coverage	# Peptides	# PSMs	# Unique Peptides	# Protein Groups	# AAs	MW [kDa]	calc. pI	Score Sequest HT	# Peptides Sequest HT
B4	High	Q16531	DNA damage-binding protein 1 [OS=Homo sapiens]	0	1,656	0,6140351	1	1	1	1	1140	126,887	5,26	0	1
	High	Q9Y5B9	FACT complex subunit SPT16 [OS=Homo sapiens]	0	236,278	56,35148	53	224	53	1	1047	119,838	5,66	421,827204	53
	High	P42285	Superkiller viralicidic activity 2-like 2 [OS=Homo sapiens]	0	13,0166	7,0057582	6	9	6	1	1042	117,729	6,52	5,31437433	6
	High	Q9H0A0	N-acetyltransferase 10 [OS=Homo sapiens]	0	41,6117	20,487805	18	43	18	1	1025	115,657	8,27	35,1092795	18
	High	Q14527	Helicase-like transcription factor [OS=Homo sapiens]	0	17,9357	7,4331021	7	15	7	1	1009	113,857	8,6	11,3782876	7
	High	P09874	Poly [ADP-ribose] polymerase 1 [OS=Homo sapiens]	0	918,825	79,092702	101	1894	101	1	1014	113,012	8,88	5095,15786	101
	High	P49916-1	DNA ligase 3 [OS=Homo sapiens]	0	6,574	4,2616452	4	4	4	1	1009	112,835	9,01	1,73698843	4
	High	Q8N5C6	S1 RNA-binding domain-containing protein 1 [OS=Homo sapiens]	0	5,33347	2,9145729	3	3	3	1	995	111,705	8,72	4,23382056	3
	High	O75400	pre-mRNA-processing factor 40 homolog A [OS=Homo sapiens]	0	1,80355	0,9404389	1	1	1	1	957	108,737	7,56	0	1
	High	Q9Y2W1	Thyroid hormone receptor-associated protein 3 [OS=Homo sapiens]	0	2,09887	1,2565445	1	1	1	1	955	108,601	10,15	0	1
	Medium	Q96T37-1	Putative RNA-binding protein 15 [OS=Homo sapiens]	0,01875	1,31885	1,9447288	1	1	1	1	977	107,124	10,08	0	1
	High	Q9NYF8-1	Bcl-2-associated transcription factor 1 [OS=Homo sapiens]	0	9,44791	3,9130435	4	13	4	1	920	106,059	9,98	5,59469521	4
	High	Q01831	DNA repair protein complementing XP-C cells [OS=Homo sapiens]	0	1,91222	0,7446809	1	1	1	1	940	105,887	8,9	1,74018943	1
	High	Q9Y5B6	PAX3- and PAX7-binding protein 1 [OS=Homo sapiens]	0	1,52871	1,1995638	1	2	1	1	917	104,739	5,68	0	1
	High	Q92889	DNA repair endonuclease XPF [OS=Homo sapiens]	0	561,256	69,432314	68	1005	68	1	916	104,42	6,93	2501,60384	68

	Protein FDR Confidence	Accession	Description	Exp. q-value	Sum PEP Score	Coverage	# Peptides	# PSMs	# Unique Peptides	# Protein Groups	# AAs	MW [kDa]	calc. pI	Score Sequest HT	# Peptides Sequest HT
B5	High	Q99459	Cell division cycle 5-like protein [OS=Homo sapiens]	0	2,79891	2,1197007	2	2	2	1	802	92,194	8,18	0	2
	High	P11387	DNA topoisomerase 1 [OS=Homo sapiens]	0	62,2559	30,980392	22	74	22	1	765	90,669	9,31	74,3361579	22
	High	P19447	TFIIH basal transcription factor complex helicase XPB subunit [OS=Homo s	0	2,40935	2,8132992	2	2	2	1	782	89,221	7,23	0	2
	High	P18074-1	Tfiih basal transcription factor complex helicase xpd subunit [OS=Homo sa	0	77,3474	45,789474	26	73	26	1	760	86,854	7,15	97,8966215	26
	High	P13010	X-ray repair cross-complementing protein 5 [OS=Homo sapiens]	0	222,706	65,437158	41	231	41	1	732	82,652	5,81	504,726853	41
	High	Q92499	ATP-dependent RNA helicase DDX1 [OS=Homo sapiens]	0	9,10576	7,972973	5	6	5	1	740	82,38	7,23	1,96563959	5
	High	P49959-3	Isoform 3 of Double-strand break repair protein MRE11A [OS=Homo sapie	0	4,69188	2,6722925	2	2	2	1	711	81,02	6,15	0	2
	High	Q13330-1	Metastasis-associated protein MTA1 [OS=Homo sapiens]	0	16,3639	9,3706294	6	11	6	1	715	80,735	9,26	13,4378451	6
	High	Q92841	Probable ATP-dependent RNA helicase DDX17 [OS=Homo sapiens]	0	77,1622	37,722908	23	82	22	1	729	80,222	8,27	110,649328	23
	High	O00571	ATP-dependent RNA helicase DDX3X [OS=Homo sapiens]	0	3,41329	3,4743202	2	3	1	1	662	73,198	7,18	1,6029582	2
	High	Q06787	fragile X mental retardation protein 1 [OS=Homo sapiens]	0	3,11035	3,3227848	2	4	1	1	632	71,131	7,42	1,849424	2
	Medium	P12956	X-ray repair cross-complementing protein 6 [OS=Homo sapiens]	0,02849	1,25088	1,6420361	1	2	1	1	609	69,799	6,64	0	1
	High	P51114-1	Fragile X mental retardation syndrome-related protein 1 [OS=Homo sapie	0	3,38758	4,1867955	2	4	1	1	621	69,678	6,15	1,849424	2
	High	P18887	DNA repair protein XRCC1 [OS=Homo sapiens]	0	120,491	40,442338	22	152	22	1	633	69,434	6,39	318,499228	22

	Protein FDR Confidence	Accession	Description	Exp. q-value	Sum PEP Score	Coverage	# Peptides	# PSMs	# Unique Peptides	# Protein Groups	# AAs	MW [kDa]	calc. pI	Score Sequest HT	# Peptides Sequest HT
	Medium	O94776	Metastasis-associated protein MTA2 [OS=Homo sapiens]	0,02457	1,68173	1,497006	1	1	1	1	668	74,976	9,66	0	1
	High	P12956	X-ray repair cross-complementing protein 6 [OS=Homo sapiens]	0	293,384	66,502463	43	290	43	1	609	69,799	6,64	604,855505	43
	High	P51114-1	Fragile X mental retardation syndrome-related protein 1 [OS=Homo sapie	0	23,0774	13,204509	8	18	7	1	621	69,678	6,15	14,782655	8

	High	P18887	DNA repair protein XRCC1 [OS=Homo sapiens]	0	10,4819	6,6350711	5	9	5	1	633	69,434	6,39	4,35622644	5
	High	P17844	probable ATP-dependent RNA helicase DDX5 [OS=Homo sapiens]	0	54,984	26,384365	15	59	8	1	614	69,105	8,92	98,3988343	15
B6	High	Q06787-9	Isoform 9 of Fragile X mental retardation protein 1 [OS=Homo sapiens]	0	56,2177	25,859247	13	42	1	1	611	68,924	7,42	60,3885313	13
	High	Q9NUW8	tyrosyl-DNA phosphodiesterase 1 [OS=Homo sapiens]	0	13,9941	12,5	6	9	6	1	608	68,377	7,65	11,6622963	6
	High	P27694	Replication protein A 70 kDa DNA-binding subunit [OS=Homo sapiens]	0	7,25115	5,6818182	3	3	3	1	616	68,095	7,21	4,03435028	3
	High	Q06787-2	Isoform 1 of Fragile X mental retardation protein 1 [OS=Homo sapiens]	0	57,1791	27,609428	13	44	1	1	594	66,93	7,23	58,2799848	13
	Medium	Q96JB3-1	hypermethylated in cancer 2 protein [OS=Homo sapiens]	0,02338	1,99913	1,6260163	1	2	1	1	615	66,114	6,38	4,49058175	1
	High	Q86UE4	protein LYRIC [OS=Homo sapiens]	0	39,0493	17,697595	8	18	8	1	582	63,799	9,32	20,924956	8

	Protein FDR Confidence	Accession	Description	Exp. q-value	Sum PEP Score	Coverage	# Peptides	# PSMs	# Unique Peptides	# Protein Groups	# AAs	MW [kDa]	calc. pI	Score Sequest HT	# Peptides Sequest HT
	High	Q96T60	Bifunctional polynucleotide phosphatase/kinase [OS=Homo sapiens]	0	29,0737	19,769674	9	25	9	1	521	57,04	8,46	26,468871	9
	High	Q9UMS4	Pre-mRNA-processing factor 19 [OS=Homo sapiens]	0	57,0677	44,642857	15	76	15	1	504	55,146	6,61	102,408488	15
B7	High	Q53EL6-1	Programmed cell death protein 4 [OS=Homo sapiens]	0	4,36609	5,9701493	2	2	2	1	469	51,703	5,21	1,77377677	2
	High	P54727	UV excision repair protein RAD23 homolog B [OS=Homo sapiens]	0	3,37334	4,400978	2	3	2	1	409	43,145	4,84	0	2
	High	P35659-1	Protein DEK [OS=Homo sapiens]	0	4,39982	5,0666667	2	7	2	1	375	42,648	8,56	5,44552088	2

	Protein FDR Confidence	Accession	Description	Exp. q-value	Sum PEP Score	Coverage	# Peptides	# PSMs	# Unique Peptides	# Protein Groups	# AAs	MW [kDa]	calc. pI	Score Sequest HT	# Peptides Sequest HT
	High	P18754-2	Isoform 2 of Regulator of chromosome condensation [OS=Homo sapiens]	0	100,901	44,026549	14	72	14	1	452	48,115	8,16	136,571179	14
	High	Q5VYV7	protein SLX4IP [OS=Homo sapiens]	0	5,71772	7,1078431	2	3	2	1	408	45,524	9,42	2,58791447	2
B8	High	P31689-1	DnaJ homolog subfamily A member 1 [OS=Homo sapiens]	0	4,27253	9,5717884	2	2	2	1	397	44,839	7,08	0	2
	High	P35659-1	Protein DEK [OS=Homo sapiens]	0,00521	1,26376	2,6666667	1	1	1	1	375	42,648	8,56	0	1
	High	Q8IWS0-1	PHD finger protein 6 [OS=Homo sapiens]	0	12,9506	24,931507	7	14	7	1	365	41,264	8,68	11,8915551	7
	High	P07992-3	Isoform 3 of DNA excision repair protein ERCC-1 [OS=Homo sapiens]	0	13,5667	17,027864	5	17	5	1	323	35,541	8,82	22,9325138	5

	Protein FDR Confidence	Accession	Description	Exp. q-value	Sum PEP Score	Coverage	# Peptides	# PSMs	# Unique Peptides	# Protein Groups	# AAs	MW [kDa]	calc. pI	Score Sequest HT	# Peptides Sequest HT
	High	Q13888-1	General transcription factor IIH subunit 2 [OS=Homo sapiens]	0	13,0229	12,658228	5	12	5	1	395	44,39	6,76	15,955723	5
	High	Q7Z2E3-1	Aprataxin [OS=Homo sapiens]	0	18,6507	23,876404	6	22	6	1	356	40,714	9,17	33,1994686	6
	High	P40938	replication factor C subunit 3 [OS=Homo sapiens]	0	26,118	32,303371	8	17	8	1	356	40,53	8,34	12,86112	8
	High	P35249	replication factor C subunit 4 [OS=Homo sapiens]	0	17,1125	22,865014	7	19	7	1	363	39,657	8,02	24,9743071	7
B9	High	Q9NWY4	UPF0609 protein C4orf27 [OS=Homo sapiens]	0	2,95832	7,2254335	2	4	2	1	346	39,411	6,8	0	2
	High	P35250-1	Replication factor C subunit 2 [OS=Homo sapiens]	0	33,0394	38,135593	11	31	11	1	354	39,132	6,44	48,434146	11
	High	P40937-1	Replication factor C subunit 5 [OS=Homo sapiens]	0	5,56723	9,7058824	3	5	3	1	340	38,472	7,2	3,63496196	3
	High	P06746	DNA polymerase beta [OS=Homo sapiens]	0	56,6169	53,432836	18	58	18	1	335	38,154	8,95	96,6008033	18
	High	P07992-3	Isoform 3 of DNA excision repair protein ERCC-1 [OS=Homo sapiens]	0	46,1709	37,4613	10	55	10	1	323	35,541	8,82	107,632045	10

	Protein FDR Confidence	Accession	Description	Exp. q-value	Sum PEP Score	Coverage	# Peptides	# PSMs	# Unique Peptides	# Protein Groups	# AAs	MW [kDa]	calc. pI	Score Sequest HT	# Peptides Sequest HT
	High	P40938	replication factor C subunit 3 [OS=Homo sapiens]	0	6,52059	9,8314607	3	4	3	1	356	40,53	8,34	1,71456885	3
	High	P35249	replication factor C subunit 4 [OS=Homo sapiens]	0	46,314	47,107438	14	37	14	1	363	39,657	8,02	52,1136779	14

B10	High	P35250-1	Replication factor C subunit 2 [OS=Homo sapiens]	0	2,54741	8,4745763	2	3	2	1	354	39,132	6,44	0	2
	High	P40937-1	Replication factor C subunit 5 [OS=Homo sapiens]	0	28,3904	41,764706	12	25	12	1	340	38,472	7,2	24,0994389	12
	High	P06746	DNA polymerase beta [OS=Homo sapiens]	0	14,5683	26,268657	7	15	7	1	335	38,154	8,95	5,78062606	7
	High	P07992-1	DNA excision repair protein ERCC-1 [OS=Homo sapiens]	0	196,393	83,164983	26	282	26	1	297	32,542	6,25	644,410699	26
	High	P23025	DNA repair protein complementing XP-A cells [OS=Homo sapiens]	0	32,036	26,373626	5	18	5	1	273	31,348	6,73	38,937887	5

	Protein FDR Confidence	Accession	Description	Exp. q-value	Sum PEP Score	Coverage	# Peptides	# PSMs	# Unique Peptides	# Protein Groups	# AAs	MW [kDa]	calc. pI	Score Sequest HT	# Peptides Sequest HT
B11	High	P18887	DNA repair protein XRCC1 [OS=Homo sapiens]	0,00559	1,11323	1,5797788	1	2	1	1	633	69,434	6,39	1,78366733	1
	High	P27694	Replication protein A 70 kDa DNA-binding subunit [OS=Homo sapiens]	0	5,44427	7,7922078	4	5	4	1	616	68,095	7,21	6,93868244	4
	High	Q9UGN5-1	Poly [ADP-ribose] polymerase 2 [OS=Homo sapiens]	0	5,76665	5,8319039	3	4	3	1	583	66,164	8,88	1,97141039	3
	High	Q96JB3-1	hypermethylated in cancer 2 protein [OS=Homo sapiens]	0	1,7073	1,6260163	1	2	1	1	615	66,114	6,38	2,33989549	1
	High	P32780	General transcription factor IIH subunit 1 [OS=Homo sapiens]	0	44,0655	40,875912	16	43	16	1	548	61,993	8,66	77,8674933	16
	High	Q13112	Chromatin assembly factor 1 subunit B [OS=Homo sapiens]	0	3,13674	3,9355993	2	2	2	1	559	61,454	7,5	0	2
	High	Q96NY9	crossover junction endonuclease MUS81 [OS=Homo sapiens]	0,00559	0,81192	1,0889292	1	1	1	1	551	61,135	9,73	0	1

	Protein FDR Confidence	Accession	Description	Exp. q-value	Sum PEP Score	Coverage	# Peptides	# PSMs	# Unique Peptides	# Protein Groups	# AAs	MW [kDa]	calc. pI	Score Sequest HT	# Peptides Sequest HT
B12		P29375-1	Lysine-specific demethylase 5A [OS=Homo sapiens]	0	0,59172	1	1	1	1	1690	191,97	6,49	0	1	
		Q92623	Tetratricopeptide repeat protein 9A [OS=Homo sapiens]	0	4,05405	1	1	1	1	222	24,364	8,98	0	1	
		Q12912-1	Lymphoid-restricted membrane protein [OS=Homo sapiens]	0	1,44144	1	4	1	1	555	62,083	5,85	0	1	
		P19237	Troponin I, slow skeletal muscle [OS=Homo sapiens]	0	4,27807	1	3	1	1	187	21,679	9,58	6,1745	1	
		Q9NVE4	Coiled-coil domain-containing protein 87 [OS=Homo sapiens]	0	0,8245	1	1	1	1	849	96,342	8,59	0	1	

Annex Table II: Mass spectrometry data from XPF-HA purification from individual bands of SDS gel. Interactors of XPF purificated samples with UV irradiation (50J/m^2; 1h of recovery) (Band 11; B11) or under MMC treatment (1.5 µM, 16h) (the rest of bands except B12) are shown here. (B12 came from a gel fragment without protein band, negative control). Proteins identified in each single band are ordered according to the MW expected from the SDS gel band size. Q-value: minimal false discovery rate at which the identification is considered correct. Posterior Error Probability (PEP) score: probability that the observed peptide spectrum matches (PSM) is incorrect. Coverage: percentage of the protein sequence covered by identified peptides (confident coverage threshold >1). Peptides: total number of distinct peptide sequences identified in the protein group. Unique peptides: The number of peptide sequences that are unique to a protein group. Protein Groups: number of proteins displayed in the Protein Group Members view. Sequest-HT: Algorithm to identify collections of tandem mass spectra to peptide sequences that have been generated from databases of protein sequences.

Protein FDR Confidence	Accession	Description	Sum PEP Score	Coverage	# Peptides	# PSMs	# Unique Peptides	# AAs	MW [kDa]	Gene ID	Abundance Ratio (log2): (Medium) / (Light)	Abundance Ratio (log2): (Heavy) / (Light)	Abundance Ratio (log2): (Medium) / (Heavy)	# Razor Peptides
High	O95816	BAG family molecular chaperone regulator 2 [OS=Homo sapiens]	6,85250485	11,3744076	2	2	2	211	23,757	BAG2	10,82	11,37	-0,55	0
High	Q562R1	Beta-actin-like protein 2 [OS=Homo sapiens]	133,465686	17,8191489	8	55	1	376	41,976	ACTBL2	11,17	11,17	0	0
High	P23025	DNA repair protein complementing XP-A cells [OS=Homo sapiens]	5,55021315	7,69230769	1	1	1	273	31,348	XPA	8,08	9,72	-1,64	0
Low	Q92552-2	Isoform 2 of 28S ribosomal protein S27, mitochondrial [OS=Homo sapiens]	1,95506845	2,57009346	1	1	1	428	49,119	MRPS27	8,72	8,87	-0,15	0
Medium	O75165	DnaJ homolog subfamily C member 13 [OS=Homo sapiens]	2,98399909	0,49041462	1	2	1	2243	254,252	DNAJC13	8,22	8,24	-0,02	0
High	P07992-1	DNA excision repair protein ERCC-1 [OS=Homo sapiens]	369,829473	62,6262626	25	140	25	297	32,542	ERCC1	4,67	4,79	-0,12	0
High	Q709F0-1	acyl-CoA dehydrogenase family member 11 [OS=Homo sapiens]	94,1642326	26,4102564	18	29	18	780	87,228	ACAD11	4,18	4,54	-0,37	0
High	P49759-3	Isoform 3 of Dual specificity protein kinase CLK1 [OS=Homo sapiens]	109,692773	37,0722433	17	34	15	526	61,718	CLK1	-1,47	4,31	-5,78	2
High	Q8IY92	Structure-specific endonuclease subunit SLX4 [OS=Homo sapiens]	643,363168	53,653217	91	252	90	1834	199,889	SLX4	4,13	4,29	-0,17	2
High	Q92889	DNA repair endonuclease XPF [OS=Homo sapiens]	1100,2576	75,3275109	84	842	84	916	104,42	ERCC4	4,24	4,27	-0,02	0
High	Q96CN7	Isochorismatase domain-containing protein 1 [OS=Homo sapiens]	19,9897381	22,4832215	4	5	4	298	32,216	ISOC1	3,2	4,14	-0,94	0
Medium	Q7Z2W4	zinc finger CCCH-type antiviral protein 1 [OS=Homo sapiens]	4,51681823	2,2172949	2	2	2	902	101,367	ZC3HAV1	0,85	4,03	-3,17	0
High	Q9H1R3	Myosin light chain kinase 2, skeletal/cardiac muscle [OS=Homo sapiens]	22,7916376	1,84563758	2	21	2	596	64,644	MYLK2	3,56	3,78	-0,22	0
Low	Q9BPX3	Condensin complex subunit 3 [OS=Homo sapiens]	0,97183558	0,98522167	1	1	1	1015	114,262	NCAPG	-1,41	3,66	-5,07	0
High	P19338	Nucleolin [OS=Homo sapiens]	59,6385982	21,2676056	14	17	14	710	76,568	NCL	1,72	3,01	-1,29	0
Low	Q14956	Transmembrane glycoprotein NMB [OS=Homo sapiens]	1,09658441	3,14685315	1	1	1	572	63,882	GPNMB	2,19	2,79	-0,6	0
High	Q96HS1-1	Serine/threonine-protein phosphatase Pgam5, mitochondrial [OS=Homo sapier	99,7088792	59,1695502	14	26	14	289	31,985	PGAM5	2,84	2,44	0,41	0
High	O43390-2	Isoform 2 of Heterogeneous nuclear ribonucleoprotein R [OS=Homo sapiens]	11,5906465	6,91823899	4	6	4	636	71,17	HNRNPR	-0,24	2,36	-2,6	0
Medium	Q5RI15-2	Isoform 2 of Cytochrome c oxidase protein 20 homolog [OS=Homo sapiens]	4,29174911	10,7692308	1	1	1	130	14,659	COX20	2,33	2,36	-0,03	0
High	Q6P5R6	60S ribosomal protein L22-like 1 [OS=Homo sapiens]	85,4034051	64,7540984	8	47	7	122	14,598	RPL22L1	2,41	2,31	0,11	1
High	O60934	Nibrin [OS=Homo sapiens]	5,75272142	3,05039788	3	3	3	754	84,906	NBN	1,41	2,06	-0,65	0
High	O15460-1	Prolyl 4-hydroxylase subunit alpha-2 [OS=Homo sapiens]	6,50951015	3,73831776	2	2	2	535	60,864	P4HA2	1,53	2,04	-0,51	0
High	P18077	60S ribosomal protein L35a [OS=Homo sapiens]	15,3926509	40	6	9	6	110	12,53	RPL35A	1,18	1,92	-0,74	0
High	P05387	60S acidic ribosomal protein P2 [OS=Homo sapiens]	23,3201849	33,9130435	3	7	3	115	11,658	RPLP2	1,54	1,91	-0,37	0
High	Q14690	Protein RRP5 homolog [OS=Homo sapiens]	4,76667781	1,65686799	3	3	3	1871	208,57	PDCD11	0,96	1,91	-0,95	0
High	Q02878	60S ribosomal protein L6 [OS=Homo sapiens]	102,204729	48,6111111	15	29	15	288	32,708	RPL6	1,02	1,82	-0,8	0
High	Q96EY4	translation machinery-associated protein 16 [OS=Homo sapiens]	70,7767715	46,3054187	11	22	11	203	23,849	TMA16	0,4	1,79	-1,39	0
High	P49327	Fatty acid synthase [OS=Homo sapiens]	226,111601	26,3639984	55	76	54	2511	273,254	FASN	0,14	1,78	-1,64	2
High	O43824	Putative GTP-binding protein 6 [OS=Homo sapiens]	22,0331504	12,0155039	6	7	6	516	56,848	GTPBP6	1,72	1,75	-0,03	0
High	Q06787	fragile X mental retardation protein 1 [OS=Homo sapiens]	28,3418144	9,49367089	5	9	1	632	71,131	FMR1	1,3	1,74	-0,43	4
High	P36578	60S ribosomal protein L4 [OS=Homo sapiens]	41,3524971	21,5456674	9	20	9	427	47,667	RPL4	0,93	1,72	-0,78	0
High	O76021	Ribosomal L1 domain-containing protein 1 [OS=Homo sapiens]	7,85722872	6,32653061	2	2	2	490	54,939	RSL1D1	0,83	1,68	-0,84	0
High	P49959-3	Isoform 3 of Double-strand break repair protein MRE11A [OS=Homo sapiens]	9,67931699	7,87623066	4	4	4	711	81,02	MRE11A	0,67	1,66	-1	0
Low	Q9H1X3	dnaJ homolog subfamily C member 25 [OS=Homo sapiens]	1,053646	2,22222222	1	1	1	360	42,377	DNAJC25	1,52	1,66	-0,14	0
Low	Q93009	Ubiquitin carboxyl-terminal hydrolase 7 [OS=Homo sapiens]	1,90692869	0,81669691	1	1	1	1102	128,22	USP7	-0,02	1,65	-1,67	0
High	Q04637-9	Isoform 9 of Eukaryotic translation initiation factor 4 gamma 1 [OS=Homo sapie	7,05004987	3,54919054	3	3	3	1606	176,128		-1,46	1,64	-3,1	0
Low	O60437	periplakin [OS=Homo sapiens]	1,08375667	0,45558087	1	1	1	1756	204,623	PPL	-4,33	1,63	-5,96	0
High	P61313-1	60S ribosomal protein L15 [OS=Homo sapiens]	30,3092459	22,5490196	4	9	4	204	24,131	RPL15	0,83	1,61	-0,77	0
High	P04075-2	Isoform 2 of Fructose-bisphosphate aldolase A [OS=Homo sapiens]	12,4608942	10,5263158	4	4	4	418	45,232	ALDOA	-0,33	1,59	-1,92	0
Medium	P05455	Lupus La protein [OS=Homo sapiens]	3,50473326	3,43137255	1	1	1	408	46,808	SSB	0,37	1,56	-1,19	0
High	Q9BRG2	SH2 domain-containing protein 3A [OS=Homo sapiens]	7,08464757	5,38194444	4	4	4	576	63,054	SH2D3A	1,6	1,54	0,07	0
Medium	P52294	Importin subunit alpha-5 [OS=Homo sapiens]	4,39328285	3,1598513	2	2	2	538	60,184	KPNA1	1,28	1,52	-0,24	0
High	Q13015	protein AF1q [OS=Homo sapiens]	4,73897517	17,7777778	1	1	1	90	10,055	MLLT11	0,29	1,5	-1,21	0
Medium	Q9HCE1	Putative helicase MOV-10 [OS=Homo sapiens]	3,97676788	2,29312064	2	2	2	1003	113,599	MOV10	0,54	1,49	-0,95	0
Medium	O60832-1	H/ACA ribonucleoprotein complex subunit 4 [OS=Homo sapiens]	3,14736602	3,69649805	2	2	2	514	57,638	DKC1	0,82	1,49	-0,67	0
High	Q8IZL8	Proline-, glutamic acid- and leucine-rich protein 1 [OS=Homo sapiens]	5,03523952	1,85840708	2	3	2	1130	119,624	PELP1	-0,58	1,47	-2,06	0
High	P05386	60S acidic ribosomal protein P1 [OS=Homo sapiens]	4,99097426	14,0350877	1	2	1	114	11,507	RPLP1	0,84	1,47	-0,62	0
Medium	Q9H2U1	ATP-dependent RNA helicase DHX36 [OS=Homo sapiens]	3,79492681	1,98412698	2	2	2	1008	114,688	DHX36	0,25	1,44	-1,18	0
High	P07237	Protein disulfide-isomerase [OS=Homo sapiens]	23,8758236	11,023622	5	7	5	508	57,081	P4HB	1,99	1,43	0,55	0
High	P12277	Creatine kinase B-type [OS=Homo sapiens]	28,9101846	21,7847769	6	8	6	381	42,617	CKB	-1,9	1,41	-3,31	0
High	P53396-1	ATP-citrate synthase [OS=Homo sapiens]	83,1565296	22,3433243	19	28	19	1101	120,762	ACLY	-0,7	1,39	-2,09	0
High	P50914	60S ribosomal protein L14 [OS=Homo sapiens]	24,378671	15,8139535	3	7	3	215	23,417	RPL14	0,9	1,38	-0,47	0
High	A1L0T0	Acetolactate synthase-like protein [OS=Homo sapiens]	6,16887451	4,2721519	2	2	2	632	67,825	ILVBL	1,37	1,38	0	0
High	P05388	60S acidic ribosomal protein P0 [OS=Homo sapiens]	33,0680237	24,6056782	7	11	7	317	34,252	RPLP0	0,58	1,27	-0,69	0
Medium	P40429	60S ribosomal protein L13a [OS=Homo sapiens]	3,08338731	7,8817734	2	2	2	203	23,562	RPL13A	0,7	1,27	-0,57	0
Low	O75600-2	Isoform 2 of 2-amino-3-ketobutyrate coenzyme A ligase, mitochondrial [OS=Ho	1,86201327	2,24719101	1	1	1	445	47,944	GCAT	1,08	1,27	-0,2	0
Low	Q14241	Transcription elongation factor B polypeptide 3 [OS=Homo sapiens]	2,21246868	0,87719298	1	1	1	798	89,853	TCEB3	0,63	1,26	-0,63	0
Medium	P51784	Ubiquitin carboxyl-terminal hydrolase 11 [OS=Homo sapiens]	4,61891399	2,18068536	2	2	2	963	109,747	USP11	0,96	1,25	-0,28	0
Medium	Q9H583	HEAT repeat-containing protein 1 [OS=Homo sapiens]	3,6471774	1,07276119	2	2	2	2144	242,215	HEATR1	-0,04	1,25	-1,29	0
High	Q00839	Heterogeneous nuclear ribonucleoprotein U [OS=Homo sapiens]	108,997008	21,3333333	19	34	18	825	90,528	HNRNPU	0,11	1,23	-1,12	1
High	P25205-2	Isoform 2 of DNA replication licensing factor MCM3 [OS=Homo sapiens]	26,8692348	7,97186401	6	10	6	853	95,848	MCM3	0,2	1,22	-1,02	0

Medium	O95985	DNA topoisomerase 3-beta-1 [OS=Homo sapiens]	3,98000686	1,85614849	2	2	2	862	96,599	TOP3B	1,02	1,21	-0,19	0
High	P62424	60S ribosomal protein L7a [OS=Homo sapiens]	78,4262425	41,7293233	11	25	11	266	29,977	RPL7A	0,38	1,19	-0,81	0
High	Q92878-2	Isoform 2 of DNA repair protein RAD50 [OS=Homo sapiens]	53,1891611	16,0091047	21	26	21	1318	154,491		0,66	1,19	-0,53	0
High	P18124	60S ribosomal protein L7 [OS=Homo sapiens]	46,602609	39,516129	8	17	8	248	29,207	RPL7	0,49	1,19	-0,7	0
High	Q07020	60S ribosomal protein L18 [OS=Homo sapiens]	48,7779873	36,1702128	6	11	6	188	21,621	RPL18	0,48	1,17	-0,69	0
High	O75616-1	GTPase Era, mitochondrial [OS=Homo sapiens]	10,7406698	6,63615561	2	4	2	437	48,319	ERAL1	1,58	1,15	0,43	0
High	Q9Y6N1	Cytochrome c oxidase assembly protein COX11, mitochondrial [OS=Homo sapie	10,3175539	12,3188406	2	3	2	276	31,41	COX11	1,28	1,15	0,12	0
High	P02786	Transferrin receptor protein 1 [OS=Homo sapiens]	47,6267254	14,2105263	9	16	9	760	84,818	TFRC	1,01	1,12	-0,11	0
High	P06737-1	Glycogen phosphorylase, liver form [OS=Homo sapiens]	50,5342359	15,7024793	12	16	12	847	97,087	PYGL	-0,97	1,11	-2,07	0
Medium	Q99832	T-complex protein 1 subunit eta [OS=Homo sapiens]	4,34288829	2,946593	2	2	2	543	59,329	CCT7	-0,38	1,11	-1,49	0
High	Q08211	Atp-dependent rna helicase a [OS=Homo sapiens]	82,6229654	14,4094488	15	26	15	1270	140,869	DHX9	-0,49	1,1	-1,59	0
Low	Q13907-2	Isoform 2 of Isopentenyl-diphosphate Delta-isomerase 1 [OS=Homo sapiens]	2,10857406	3,16901408	1	1	1	284	32,465	IDI1	0,79	1,1	-0,31	0
High	Q9NUL7	Probable ATP-dependent RNA helicase DDX28 [OS=Homo sapiens]	89,9438566	42,4074074	19	32	19	540	59,545	DDX28	1,28	1,09	0,19	0
High	Q7L2E3-2	Isoform 2 of Putative ATP-dependent RNA helicase DHX30 [OS=Homo sapiens]	11,0935433	2,37315876	3	5	3	1222	136,03	DHX30	0,47	1,09	-0,62	0
High	Q9NR30-1	Nucleolar RNA helicase 2 [OS=Homo sapiens]	63,0303361	19,412516	14	24	11	783	87,29	DDX21	0,47	1,08	-0,62	0
High	Q02543	60S ribosomal protein L18a [OS=Homo sapiens]	11,2915939	26,1363636	5	5	5	176	20,749	RPL18A	0,63	1,07	-0,44	0
Medium	P98175-1	RNA-binding protein 10 [OS=Homo sapiens]	2,55783391	0,75268817	1	1	1	930	103,469	RBM10	-0,08	1,07	-1,14	0
Low	Q8TDN6	Ribosome biogenesis protein BRX1 homolog [OS=Homo sapiens]	2,22076437	1,98300283	1	1	1	353	41,375	BRIX1	0,11	1,05	-0,94	0
Low	A4D1E9-1	GTP-binding protein 10 [OS=Homo sapiens]	1,76776648	2,3255814	1	1	1	387	42,906	GTPBP10	0,89	1,05	-0,16	0
High	Q9NYF8-1	Bcl-2-associated transcription factor 1 [OS=Homo sapiens]	133,332621	33,9130435	28	51	26	920	106,059	BCLAF1	0,78	1,04	-0,26	2
High	P53680	AP-2 complex subunit sigma [OS=Homo sapiens]	6,54311266	10,5633803	2	3	2	142	17,007	AP2S1	0,83	1,04	-0,21	0
Low	Q15717-2	Isoform 2 of ELAV-like protein 1 [OS=Homo sapiens]	1,58703573	2,54957507	1	1	1	353	38,972	ELAVL1	0	1,03	-1,03	0
High	P22102-1	trifunctional purine biosynthetic protein adenosine-3 [OS=Homo sapiens]	13,6824871	6,03960396	6	7	6	1010	107,699	GART	-0,86	1,02	-1,88	0
High	Q08170	Serine/arginine-rich splicing factor 4 [OS=Homo sapiens]	6,90898988	5,66801619	3	4	3	494	56,645	SRSF4	0,18	1,02	-0,84	0
High	Q53HL2	Borealin [OS=Homo sapiens]	5,5438945	6,78571429	2	2	2	280	31,304	CDCA8	-0,47	1,02	-1,49	0
High	Q9H0D6-1	5'-3' exoribonuclease 2 [OS=Homo sapiens]	5,58731186	2,52631579	2	2	2	950	108,513	XRN2	0,47	1	-0,53	0
High	P39023	60S ribosomal protein L3 [OS=Homo sapiens]	87,4042255	39,7022333	15	26	15	403	46,08	RPL3	0,53	0,97	-0,44	0
High	P55795	heterogeneous nuclear ribonucleoprotein H2 [OS=Homo sapiens]	30,3362148	23,3853007	8	10	2	449	49,232	HNRNPH2	0,44	0,97	-0,53	0
High	P06744-2	Isoform 2 of Glucose-6-phosphate isomerase [OS=Homo sapiens]	24,2820297	11,0720562	6	8	6	569	64,284	GPI	-2,04	0,97	-3,01	0
High	P22087	rRNA 2'-O-methyltransferase fibrillarin [OS=Homo sapiens]	12,8098375	14,3302181	3	3	3	321	33,763	FBL	0,64	0,97	-0,32	0
High	Q8IWC1	MAP7 domain-containing protein 3 [OS=Homo sapiens]	57,7526684	16,7808219	13	20	13	876	98,368	MAP7D3	1,03	0,95	0,08	0
High	P13639	Elongation factor 2 [OS=Homo sapiens]	73,1288812	20,979021	15	24	14	858	95,277	EEF2	0,31	0,94	-0,63	0
High	Q92900	Regulator of nonsense transcripts 1 [OS=Homo sapiens]	54,7320061	18,5119575	19	21	19	1129	124,267	UPF1	0,02	0,94	-0,92	0
High	P56270-2	Isoform 2 of Myc-associated zinc finger protein [OS=Homo sapiens]	27,5303771	13,3874239	6	9	6	493	51,04	MAZ	0,79	0,94	-0,15	0
High	O75676	Ribosomal protein S6 kinase alpha-4 [OS=Homo sapiens]	24,9978941	10,1036269	8	10	8	772	85,552	RPS6KA4	1,45	0,94	0,52	0
High	Q8WWC4	Uncharacterized protein C2orf47, mitochondrial [OS=Homo sapiens]	10,8446663	4,81099656	1	2	1	291	32,524	C2orf47	0,98	0,94	0,04	0
High	P12532-2	Isoform 2 of Creatine kinase U-type, mitochondrial [OS=Homo sapiens]	5,99906545	7,8125	2	2	2	448	50,389	KMT1A; CKMT	-1,62	0,94	-2,56	0
High	Q96AY2-2	Isoform 2 of Crossover junction endonuclease EME1 [OS=Homo sapiens]	18,9419538	9,77701544	6	9	6	583	64,738	EME1	1	0,92	0,08	0
High	Q8IUF8	Bifunctional lysine-specific demethylase and histidyl-hydroxylase MINA [OS=Ho	55,9831016	28,8172043	12	17	12	465	52,767	MINA	0,49	0,91	-0,42	0
Low	P23526-1	Adenosylhomocysteinase [OS=Homo sapiens]	1,21183163	1,62037037	1	1	1	432	47,685	AHCY	-8,38	0,91	-9,29	0
High	Q13085-4	Isoform 4 of Acetyl-CoA carboxylase 1 [OS=Homo sapiens]	5,20645921	1,5107008	3	3	3	2383	269,827	ACACA	0,31	0,9	-0,59	0
High	P50402	Emerin [OS=Homo sapiens]	49,0795043	34,2519685	8	13	8	254	28,976	EMD	1,05	0,88	0,17	0
High	Q7L0Y3	Mitochondrial ribonuclease P protein 1 [OS=Homo sapiens]	30,5471088	24,8138958	8	10	8	403	47,317	TRMT10C	1,05	0,88	0,16	0
High	P46777	60S ribosomal protein L5 [OS=Homo sapiens]	38,9390321	29,6296296	8	13	8	297	34,341	RPL5	-0,25	0,87	-1,12	0
High	P38159-1	RNA-binding motif protein, X chromosome [OS=Homo sapiens]	37,0054949	16,3682864	6	13	6	391	42,306	RBMX	0,21	0,87	-0,65	0
High	P33992	DNA replication licensing factor mcm5 [OS=Homo sapiens]	29,7237159	12,8065395	8	11	8	734	82,233	MCM5	0,56	0,87	-0,31	0
High	P57678	Gem-associated protein 4 [OS=Homo sapiens]	6,36507932	1,79584121	2	3	2	1058	119,96	GEMIN4	0,54	0,87	-0,33	0
High	P0DMV8	heat shock 70 kDa protein 1A [OS=Homo sapiens]	371,935961	53,1981279	37	113	31	641	70,009	SPA1B; HSPA1	0,86	0,86	0,01	0
High	P11940-1	Polyadenylate-binding protein 1 [OS=Homo sapiens]	120,759939	32,3899371	18	34	18	636	70,626	PABPC1	0,3	0,86	-0,57	0
High	O14654	insulin receptor substrate 4 [OS=Homo sapiens]	212,672866	31,9809069	34	103	34	1257	133,685	IRS4	0,98	0,85	0,13	0
Low	O14979-1	Heterogeneous nuclear ribonucleoprotein D-like [OS=Homo sapiens]	1,84043281	1,9047619	1	2	1	420	46,409	HNRNPDL; HNRI	-0,25	0,85	-1,1	0
High	P62906	60S ribosomal protein L10A [OS=Homo sapiens]	26,4217161	27,1889401	6	11	6	217	24,816	RPL10A	0,46	0,84	-0,38	0
High	Q9BXS5-2	Isoform 2 of AP-1 complex subunit mu-1 [OS=Homo sapiens]	10,2764377	6,89655172	4	5	4	435	49,809	AP1M1	0,51	0,84	-0,32	0
High	P52272	Heterogeneous nuclear ribonucleoprotein M [OS=Homo sapiens]	136,702608	39,3150685	27	60	27	730	77,464	HNRNPM	0,36	0,82	-0,46	0
High	Q92947-1	Glutaryl-CoA dehydrogenase, mitochondrial [OS=Homo sapiens]	7,20032097	4,33789954	2	2	2	438	48,096	GCDH	0,57	0,82	-0,25	0
High	P46940	Ras GTPase-activating-like protein IQGAP1 [OS=Homo sapiens]	14,0226222	3,43995172	5	7	5	1657	189,134	IQGAP1	-0,7	0,81	-1,51	0
Medium	Q92797-1	Symplekin [OS=Homo sapiens]	2,88839019	1,25588697	2	2	2	1274	141,059	SYMPK	-0,58	0,8	-1,39	0
High	Q96NY9	crossover junction endonuclease MUS81 [OS=Homo sapiens]	41,6275074	18,5117967	9	13	9	551	61,135	MUS81	0,71	0,79	-0,08	0
High	P84090	Enhancer of rudimentary homolog [OS=Homo sapiens]	32,8473623	36,5384615	4	12	4	104	12,251	ERH	0,51	0,79	-0,29	0
High	Q14566	DNA replication licensing factor MCM6 [OS=Homo sapiens]	31,9595037	11,6930572	10	12	10	821	92,831	MCM6	0,03	0,79	-0,76	0
High	Q3ZCQ8-2	Isoform 2 of Mitochondrial import inner membrane translocase subunit TIM50	30,9981278	10,9649123	5	9	5	456	50,433	TIMM50	0,28	0,78	-0,5	0
Low	P50570-1	Dynamin-2 [OS=Homo sapiens]	1,90239567	2,18390805	1	1	1	870	98,003	DNM2	-0,29	0,78	-1,07	0
High	P21333	Filamin-A [OS=Homo sapiens]	7,49681062	2,15338119	4	4	4	2647	280,564	FLNA	-0,49	0,77	-1,26	0
Low	P62714	serine/threonine-protein phosphatase 2A catalytic subunit beta isoform [OS=Ho	1,9722428	2,58899676	1	1	1	309	35,552	PPP2CB	-0,05	0,75	-0,8	0

Medium	Q13459-1	Unconventional myosin-IXb [OS=Homo sapiens]	4,43064023	1,85442745	3	3	3	2157	243,249	MYO9B	0,61	0,74	-0,12	0
Medium	O75419-3	Isoform 3 of Cell division control protein 45 homolog [OS=Homo sapiens]	3,96657624	1,83946488	1	1	1	598	68,724	CDC45	0,39	0,74	-0,35	0
High	Q96EY1-1	DnaJ homolog subfamily A member 3, mitochondrial [OS=Homo sapiens]	59,0078841	25,8333333	11	16	11	480	52,456	DNAJA3	0,98	0,72	0,26	0
High	Q96MU7-1	YTH domain-containing protein 1 [OS=Homo sapiens]	31,2702196	13,6176066	10	14	10	727	84,649	YTHDC1	-0,08	0,72	-0,81	0
High	P50395-1	Rab GDP dissociation inhibitor beta [OS=Homo sapiens]	8,65867616	8,53932584	3	3	3	445	50,631	GDI2	-1,61	0,71	-2,32	0
High	O75691	Small subunit processome component 20 homolog [OS=Homo sapiens]	8,35540881	1,04129264	2	4	2	2785	318,182	UTP20	0,9	0,71	0,19	0
High	O14949	Cytochrome b-c1 complex subunit 8 [OS=Homo sapiens]	29,063213	35,3658537	4	8	4	82	9,9	UQCRQ	0,9	0,7	0,2	0
High	P28288	ATP-binding cassette sub-family D member 3 [OS=Homo sapiens]	7,09154458	2,8831563	2	4	2	659	75,428	ABCD3	0,62	0,7	-0,08	0
High	O00148	ATP-dependent RNA helicase DDX39A [OS=Homo sapiens]	29,4948252	13,5831382	6	12	6	427	49,098	DDX39A	0,58	0,69	-0,11	0
High	P06748	Nucleophosmin [OS=Homo sapiens]	16,296628	19,7278912	5	7	5	294	32,555	NPM1	-0,3	0,69	-0,99	0
High	Q9P0J6	39S ribosomal protein L36, mitochondrial [OS=Homo sapiens]	5,36073646	13,592233	2	4	2	103	11,777	MRPL36	0,08	0,69	-0,61	0
Low	Q14157-5	Isoform 5 of Ubiquitin-associated protein 2-like [OS=Homo sapiens]	1,85108901	0,81521739	1	1	1	1104	116,569	UBAP2L	-1,23	0,69	-1,91	0
High	P17844	probable ATP-dependent RNA helicase DDX5 [OS=Homo sapiens]	69,2435524	23,7785016	15	24	10	614	69,105	DDX5	0,19	0,68	-0,49	0
High	O00567	Nucleolar protein 56 [OS=Homo sapiens]	11,4611035	6,22895623	3	4	3	594	66,009	NOP56	0,7	0,68	0,02	0
Low	Q9UM00-1	Transmembrane and coiled-coil domain-containing protein 1 [OS=Homo sapien	1,14819149	4,25531915	1	1	1	188	21,161	TMCO1	0,48	0,68	-0,2	0
High	P20020	Plasma membrane calcium-transporting ATPase 1 [OS=Homo sapiens]	13,0283904	4,45151033	4	5	4	1258	138,668	ATP2B1	-0,25	0,67	-0,92	0
High	Q15233	Non-POU domain-containing octamer-binding protein [OS=Homo sapiens]	6,93734064	6,7940552	3	3	2	471	54,197	NONO	-0,29	0,67	-0,96	1
Medium	Q13620	Cullin-4B [OS=Homo sapiens]	4,23202126	2,08105148	2	3	2	913	103,916	CUL4B	-0,85	0,67	-1,53	0
Medium	P78371-1	T-complex protein 1 subunit beta [OS=Homo sapiens]	3,08181234	2,80373832	1	1	1	535	57,452	CCT2	-0,54	0,66	-1,19	0
Low	Q6KCM7-3	Isoform 3 of Calcium-binding mitochondrial carrier protein SCaMC-2 [OS=Homo	1,05222329	1,55339806	1	1	1	515	56,846	SLC25A25	0,18	0,66	-0,49	0
High	P25398	40S ribosomal protein S12 [OS=Homo sapiens]	14,7963532	12,8787879	2	6	2	132	14,505	RPS12	-0,2	0,65	-0,85	0
High	Q09161	Nuclear cap-binding protein subunit 1 [OS=Homo sapiens]	18,3601143	6,83544304	5	6	5	790	91,781	NCBP1	-0,19	0,64	-0,82	0
High	P68431	Histone H3.1 [OS=Homo sapiens]	16,4936742	47,7941176	5	11	5	136	15,394	T1H3H; HIST1	-0,03	0,64	-0,67	0
Medium	Q9Y312	Protein AAR2 homolog [OS=Homo sapiens]	2,32239305	1,82291667	1	1	1	384	43,444	AAR2	-0,24	0,64	-0,89	0
High	P07900-2	Isoform 2 of Heat shock protein HSP 90-alpha [OS=Homo sapiens]	235,821952	42,0374707	34	68	19	854	98,099	HSP90AA1	-0,87	0,63	-1,49	16
Low	Q9Y483	Metal-response element-binding transcription factor 2 [OS=Homo sapiens]	2,24078557	1,68634064	1	1	1	593	67,063	MTF2	0,56	0,63	-0,07	0
High	P41252	isoleucine--tRNA ligase, cytoplasmic [OS=Homo sapiens]	47,4870102	8,00316957	10	23	10	1262	144,406	IARS	-0,24	0,62	-0,85	0
High	P67809	Nuclease-sensitive element-binding protein 1 [OS=Homo sapiens]	10,0952	14,1975309	4	4	4	324	35,903	YBX1	0,12	0,62	-0,51	0
High	Q8NDV7	Trinucleotide repeat-containing gene 6A protein [OS=Homo sapiens]	14,2993901	4,68909276	7	8	7	1962	210,169	TNRC6A	0,75	0,61	0,15	0
High	P49593	Protein phosphatase 1F [OS=Homo sapiens]	31,9034703	21,5859031	7	9	7	454	49,8	PPM1F	0,7	0,59	0,11	0
Medium	Q8IXM3	39S ribosomal protein L41, mitochondrial [OS=Homo sapiens]	4,4295089	5,10948905	1	2	1	137	15,373	MRPL41	0,65	0,59	0,06	0
High	P30050-1	60S ribosomal protein L12 [OS=Homo sapiens]	16,7216576	42,4242424	5	6	5	165	17,808	RPL12	0,18	0,58	-0,4	0
High	P04843	Dolichyl-diphosphooligosaccharide--protein glycosyltransferase subunit 1 [OS=H	7,98014377	2,96540362	2	3	2	607	68,527	RPN1	-0,36	0,58	-0,94	0
High	Q9GZS1-1	DNA-directed RNA polymerase I subunit RPA49 [OS=Homo sapiens]	6,6670128	6,02910603	3	3	3	481	53,928	POLR1E	1,47	0,58	0,89	0
Medium	Q9Y3T9	Nucleolar complex protein 2 homolog [OS=Homo sapiens]	3,88243468	1,20160214	1	2	1	749	84,866	NOC2L	0	0,58	-0,58	0
High	P07814	Bifunctional glutamate/proline--tRNA ligase [OS=Homo sapiens]	72,7000529	14,9470899	20	33	20	1512	170,483	EPRS	-0,35	0,57	-0,91	0
High	P09651-1	Heterogeneous nuclear ribonucleoprotein A1 [OS=Homo sapiens]	21,6208456	15,0537634	4	5	4	372	38,723	HNRNPA1	-1,9	0,57	-2,47	0
High	Q96TA2-1	ATP-dependent zinc metalloprotease YME1L1 [OS=Homo sapiens]	5,247169	2,45795602	2	3	2	773	86,401	YME1L1	0,42	0,57	-0,16	0
High	Q15149-1	plectin [OS=Homo sapiens]	138,396471	8,73185312	37	54	37	4684	531,466	PLEC	0,23	0,56	-0,33	0
High	Q9UNX3	60S ribosomal protein L26-like 1 [OS=Homo sapiens]	67,542463	51,7241379	11	34	3	145	17,246	RPL26L1	0,62	0,56	0,06	0
Medium	Q15386-1	Ubiquitin-protein ligase E3C [OS=Homo sapiens]	4,61078263	2,21606648	3	3	3	1083	123,844	UBE3C	0,49	0,56	-0,07	0
Medium	Q9UI26-2	Isoform 2 of Importin-11 [OS=Homo sapiens]	4,28029914	0,98522167	1	2	1	1015	116,932	IPO11	-0,32	0,56	-0,89	0
High	P63010-2	Isoform 2 of AP-2 complex subunit beta [OS=Homo sapiens]	54,8479133	20,1892744	19	26	19	951	105,625	AP2B1	0,2	0,55	-0,35	0
High	P53007	Tricarboxylate transport protein, mitochondrial [OS=Homo sapiens]	108,070017	34,7266881	10	41	10	311	33,991	SLC25A1	0,69	0,54	0,16	0
High	Q9BVI4	Nucleolar complex protein 4 homolog [OS=Homo sapiens]	15,7158574	10,6589147	4	6	4	516	58,431	NOC4L	0,88	0,54	0,34	0
High	P04181-1	Ornithine aminotransferase, mitochondrial [OS=Homo sapiens]	32,1325605	17,7676538	6	10	6	439	48,504	OAT	0,91	0,53	0,38	0
High	P05141	ADP/ATP translocase 2 [OS=Homo sapiens]	485,712102	61,7449664	26	245	9	298	32,831	SLC25A5	0,63	0,52	0,1	37
High	Q14204	Cytoplasmic dynein 1 heavy chain 1 [OS=Homo sapiens]	411,506234	27,2707706	106	156	106	4646	532,072	DYNC1H1	-0,25	0,52	-0,77	0
High	P62805	histone H4 [OS=Homo sapiens]	134,716346	58,2524272	10	50	10	103	11,36	6T1H4H; HIST	-0,07	0,52	-0,59	0
High	P42704	Leucine-rich PPR motif-containing protein, mitochondrial [OS=Homo sapiens]	82,0336161	18,4361549	25	37	25	1394	157,805	LRPPRC	0,03	0,52	-0,48	0
High	Q96JP5-1	E3 ubiquitin-protein ligase ZFP91 [OS=Homo sapiens]	65,3287312	24,5614035	14	25	14	570	63,406	ZFP91	0,62	0,52	0,11	0
High	Q12906-7	Isoform 7 of Interleukin enhancer-binding factor 3 [OS=Homo sapiens]	64,022626	17,5946548	14	21	14	898	95,748	ILF3	-0,56	0,52	-1,08	0
High	O00743-3	Isoform 3 of Serine/threonine-protein phosphatase 6 catalytic subunit [OS=Hon	14,8199964	6,14035088	2	4	2	342	38,921	PPP6C	0,51	0,52	-0,01	0
High	Q8WVM0	Dimethyladenosine transferase 1, mitochondrial [OS=Homo sapiens]	125,967786	42,7745665	13	33	13	346	39,518	TFB1M	0,7	0,51	0,19	0
High	Q9P2J5	Leucine--tRNA ligase, cytoplasmic [OS=Homo sapiens]	9,75366439	2,12585034	3	4	3	1176	134,379	LARS	-0,88	0,51	-1,39	0
High	Q9Y2W1	Thyroid hormone receptor-associated protein 3 [OS=Homo sapiens]	119,821558	30,8900524	23	42	21	955	108,601	THRAP3	0,3	0,5	-0,2	0
Medium	Q9UN86	Ras GTPase-activating protein-binding protein 2 [OS=Homo sapiens]	4,60907301	2,69709544	1	2	1	482	54,088	G3BP2	0,07	0,5	-0,42	0
High	P04350	Tubulin beta-4A chain [OS=Homo sapiens]	710,744432	82,4324324	27	351	4	444	49,554	TUBB4A	0,5	0,48	0,01	2
High	P11142-1	Heat shock cognate 71 kDa protein [OS=Homo sapiens]	509,349529	60,9907121	39	167	31	646	70,854	HSPA8	0,22	0,48	-0,26	13
High	P60891	ribose-phosphate pyrophosphokinase 1 [OS=Homo sapiens]	75,3384937	35,5345912	9	21	9	318	34,812	PRPS1	0,37	0,48	-0,11	0
High	P26639-2	Isoform 2 of Threonine--tRNA ligase, cytoplasmic [OS=Homo sapiens]	9,63448943	4,4973545	3	4	3	756	86,806	TARS	-1,48	0,48	-1,96	0
High	P33991	DNA replication licensing factor MCM4 [OS=Homo sapiens]	91,6360134	23,986095	16	25	16	863	96,498	MCM4	0,01	0,47	-0,46	0
High	O95347-1	structural maintenance of chromosomes protein 2 [OS=Homo sapiens]	56,9692243	16,2071846	16	22	16	1197	135,572	SMC2	0,15	0,47	-0,32	0
High	P61978-2	Isoform 2 of Heterogeneous nuclear ribonucleoprotein K [OS=Homo sapiens]	31,5770267	23,9224138	9	10	9	464	50,996	HNRNPK	-0,97	0,47	-1,43	0

High	P17812	CTP synthase 1 [OS=Homo sapiens]	65,8080667	20,4737733	11	19	11	591	66,648	CTPS1	0,27	0,46	-0,19	0
High	Q9H6H4-1	Receptor expression-enhancing protein 4 [OS=Homo sapiens]	22,6655918	16,7315175	3	7	3	257	29,376	REEP4	0,72	0,46	0,26	0
High	P55884-2	Isoform 2 of Eukaryotic translation initiation factor 3 subunit B [OS=Homo sapie	10,0821844	3,66552119	2	3	2	873	98,967		-1,12	0,46	-1,58	0
High	P08559-4	Isoform 4 of Pyruvate dehydrogenase E1 component subunit alpha, somatic for	6,74920218	6,54205607	3	3	3	428	47,549	PDHA1	0,07	0,46	-0,39	0
High	Q9BQE3	Tubulin alpha-1C chain [OS=Homo sapiens]	581,614935	68,8195991	28	247	2	449	49,863	TUBA1C	0,41	0,45	-0,04	3
High	Q9UJK0	Ribosome biogenesis protein TSR3 homolog [OS=Homo sapiens]	87,7345881	45,8333333	11	25	11	312	33,575	TSR3	0,85	0,45	0,4	0
High	P00338-3	Isoform 3 of L-lactate dehydrogenase A chain [OS=Homo sapiens]	44,6551869	29,3628809	9	13	8	361	39,812	LDHA	-1,49	0,45	-1,95	1
High	Q96P70	Importin-9 [OS=Homo sapiens]	27,5111096	8,3573487	9	12	9	1041	115,889	IPO9	-0,13	0,45	-0,58	0
Low	O94822-3	Isoform 3 of E3 ubiquitin-protein ligase listerin [OS=Homo sapiens]	1,0345631	0,71743929	1	1	1	1812	205,046	LTN1	0,23	0,45	-0,23	0
High	Q92841	Probable ATP-dependent RNA helicase DDX17 [OS=Homo sapiens]	84,8348018	25,3772291	16	33	11	729	80,222	DDX17	0,06	0,44	-0,39	6
High	P43243	Matrin-3 [OS=Homo sapiens]	52,4504746	23,7308146	13	18	13	847	94,565	MATR3	-0,14	0,44	-0,58	0
High	O94906-1	Pre-mRNA-processing factor 6 [OS=Homo sapiens]	35,1497802	13,4962806	11	13	11	941	106,858	PRPF6	-0,78	0,44	-1,22	0
High	Q6R327-3	Isoform 3 of Rapamycin-insensitive companion of mTOR [OS=Homo sapiens]	9,72759399	1,6743649	2	3	2	1732	194,888	RICTOR	2	0,44	1,57	0
High	P35998	26S protease regulatory subunit 7 [OS=Homo sapiens]	4,74193098	5,08083141	2	2	2	433	48,603	PSMC2	-0,4	0,44	-0,84	0
High	Q9NQ29	putative RNA-binding protein Luc7-like 1 [OS=Homo sapiens]	422,486496	47,1698113	26	198	18	371	43,701	LUC7L	0,54	0,43	0,11	0
High	P06899	Histone H2B type 1-J [OS=Homo sapiens]	137,994765	57,9365079	9	58	2	126	13,896	HIST1H2BJ	0,06	0,43	-0,36	0
High	P04637	Cellular tumor antigen p53 [OS=Homo sapiens]	56,8627829	28,4987277	10	14	10	393	43,625	TP53	-0,23	0,43	-0,66	0
High	O75683	Surfeit locus protein 6 [OS=Homo sapiens]	15,8096652	12,1883657	5	6	5	361	41,426	SURF6	-0,83	0,43	-1,26	0
High	Q9NZ01-1	Very-long-chain enoyl-CoA reductase [OS=Homo sapiens]	12,3669352	7,14285714	2	4	2	308	36,011	TECR	0,62	0,43	0,2	0
Low	Q13045-1	protein flightless-1 homolog [OS=Homo sapiens]	1,11221397	0,55161545	1	1	1	1269	144,659	FLII	-0,51	0,43	-0,94	0
High	P11586	C-1-tetrahydrofolate synthase, cytoplasmic [OS=Homo sapiens]	98,9925701	29,5187166	23	34	23	935	101,495	MTHFD1	-0,77	0,42	-1,19	0
High	O95782	AP-2 complex subunit alpha-1 [OS=Homo sapiens]	54,6050431	14,7389969	14	19	9	977	107,478	AP2A1	0,46	0,42	0,04	5
High	Q96CW1	AP-2 complex subunit mu [OS=Homo sapiens]	14,5115814	9,1954023	5	7	5	435	49,623	AP2M1	0,39	0,42	-0,03	0
High	O00425	Insulin-like growth factor 2 mRNA-binding protein 3 [OS=Homo sapiens]	12,4339133	6,7357513	4	5	1	579	63,666	IGF2BP3	-0,56	0,41	-0,97	0
High	Q13595-1	Transformer-2 protein homolog alpha [OS=Homo sapiens]	12,2864123	8,15602837	2	3	2	282	32,669	TRA2A	-0,51	0,41	-0,92	0
High	P51553-1	isocitrate dehydrogenase [NAD] subunit gamma, mitochondrial [OS=Homo sapi	8,82556394	5,8524173	2	3	2	393	42,767	IDH3G	0,15	0,41	-0,26	0
Low	Q9Y2A7-2	Isoform 2 of Nck-associated protein 1 [OS=Homo sapiens]	1,21781413	1,2345679	1	1	1	1134	129,433	NCKAP1	-1,48	0,41	-1,9	0
High	P49458	Signal recognition particle 9 kDa protein [OS=Homo sapiens]	26,632907	43,0232558	4	8	4	86	10,105	SRP9; SRP9P1	0,28	0,4	-0,12	0
High	O60884	DnaJ homolog subfamily A member 2 [OS=Homo sapiens]	19,1206483	8,73786408	3	7	3	412	45,717	DNAJA2	0,9	0,4	0,49	0
High	Q9BUJ2-1	Heterogeneous nuclear ribonucleoprotein U-like protein 1 [OS=Homo sapiens]	16,6011478	6,42523364	5	6	4	856	95,679	HNRNPUL1	-0,09	0,4	-0,49	0
High	Q14697-2	Isoform 2 of Neutral alpha-glucosidase AB [OS=Homo sapiens]	52,3278306	16,4596273	14	20	14	966	109,369	GANAB	-0,75	0,39	-1,14	0
High	P40939	Trifunctional enzyme subunit alpha, mitochondrial [OS=Homo sapiens]	37,1488177	12,9750983	9	11	9	763	82,947	HADHA	-0,49	0,39	-0,88	0
High	P62937	peptidyl-prolyl cis-trans isomerase A [OS=Homo sapiens]	23,1816634	32,7272727	4	8	4	165	18,001	PPIA	-2,13	0,39	-2,52	0
High	P31943	Heterogeneous nuclear ribonucleoprotein H [OS=Homo sapiens]	65,2501612	34,298441	11	18	4	449	49,198	HNRNPH1	-0,36	0,38	-0,74	8
High	P0C0S5	Histone H2A.Z [OS=Homo sapiens]	27,7682082	31,25	3	17	2	128	13,545	H2AFZ	0,1	0,38	-0,28	0
High	P57088	Transmembrane protein 33 [OS=Homo sapiens]	11,6222835	8,50202429	2	3	2	247	27,96	TMEM33	-0,12	0,38	-0,5	0
High	Q96D09	G-protein coupled receptor-associated sorting protein 2 [OS=Homo sapiens]	6,86761294	5,01193317	3	4	3	838	93,715	2; ARMCX5-G	0,05	0,38	-0,33	0
High	Q4KWH8-1	1-phosphatidylinositol 4,5-bisphosphate phosphodiesterase eta-1 [OS=Homo sa	14,7399278	4,78440638	7	9	7	1693	189,104	PLCH1	0,86	0,37	0,49	0
Medium	Q96GA3	protein LTV1 homolog [OS=Homo sapiens]	3,93465876	4	2	3	2	475	54,821	LTV1	0,4	0,37	0,03	0
High	P62995	transformer-2 protein homolog beta [OS=Homo sapiens]	17,8804254	18,75	5	7	5	288	33,646	TRA2B	0,1	0,36	-0,26	0
High	P26599-3	Isoform 3 of Polypyrimidine tract-binding protein 1 [OS=Homo sapiens]	6,90983917	5,02692998	2	3	2	557	59,596	PTBP1	-0,64	0,36	-1	0
High	Q00610-1	Clathrin heavy chain 1 [OS=Homo sapiens]	141,376152	25,0149254	35	48	35	1675	191,493	CLTC	-1,8	0,35	-2,16	0
High	Q7L3S4	Zinc finger protein 771 [OS=Homo sapiens]	120,734285	54,5741325	16	37	16	317	35,679	ZNF771	0,59	0,35	0,24	0
High	Q9BTC0	Death-inducer obliterator 1 [OS=Homo sapiens]	68,2259411	10,9821429	20	30	20	2240	243,723	DIDO1	-0,3	0,35	-0,65	0
High	P62826	GTP-binding nuclear protein RAN [OS=Homo sapiens]	31,2353856	19,9074074	4	10	4	216	24,408	RAN	-0,51	0,35	-0,86	0
High	Q8TEX9-2	Isoform 2 of Importin-4 [OS=Homo sapiens]	16,7647043	6,00184672	5	8	5	1083	118,826		-0,02	0,35	-0,37	0
Medium	Q07666	KH domain-containing, RNA-binding, signal transduction-associated protein 1 [(	4,70311552	3,16027088	1	1	1	443	48,197	KHDRBS1	-0,16	0,35	-0,51	0
Medium	Q15003	Condensin complex subunit 2 [OS=Homo sapiens]	2,804931	1,75438596	1	1	1	741	82,511	NCAPH	0,39	0,35	0,04	0
Low	P27694	Replication protein A 70 kDa DNA-binding subunit [OS=Homo sapiens]	2,08102657	2,5974026	1	1	1	616	68,095	RPA1	2,11	0,35	1,76	0
High	Q9NTJ3-1	Structural maintenance of chromosomes protein 4 [OS=Homo sapiens]	58,9267891	15,6832298	18	24	18	1288	147,091	SMC4	0,15	0,34	-0,19	0
High	Q8NI27-1	THO complex subunit 2 [OS=Homo sapiens]	19,2861286	4,45699937	8	11	8	1593	182,659	THOC2	-0,36	0,34	-0,7	0
High	Q15070-1	Mitochondrial inner membrane protein OXA1L [OS=Homo sapiens]	9,65033729	2,75862069	1	3	1	435	48,516	OXA1L	0,48	0,34	0,13	0
High	O00411	DNA-directed RNA polymerase, mitochondrial [OS=Homo sapiens]	7,40508261	2,68292683	3	3	3	1230	138,532	POLRMT	-0,03	0,34	-0,37	0
High	Q5SW79-1	Centrosomal protein of 170 kDa [OS=Homo sapiens]	6,7064532	1,51515152	2	4	2	1584	175,187	CEP170	0,22	0,34	-0,12	0
High	P40227-1	T-complex protein 1 subunit zeta [OS=Homo sapiens]	13,1626273	12,4293785	5	9	5	531	57,988	CCT6A	-0,54	0,33	-0,87	0
High	P63167	Dynein light chain 1, cytoplasmic [OS=Homo sapiens]	33,0885794	39,3258427	4	7	1	89	10,359	DYNLL1	-0,29	0,32	-0,61	0
High	Q7KZF4	staphylococcal nuclease domain-containing protein 1 [OS=Homo sapiens]	14,6724764	8,35164835	6	8	6	910	101,934	SND1	-1,26	0,32	-1,58	0
High	P46087-4	Isoform 4 of Probable 28S rRNA (cytosine(4447)-C(5))-methyltransferase [OS=H	11,309058	5,68047337	4	4	4	845	92,803	NOP2	0,07	0,32	-0,25	0
High	Q99460	26S proteasome non-ATPase regulatory subunit 1 [OS=Homo sapiens]	9,51226258	3,98740818	3	3	3	953	105,769	PSMD1	-1,44	0,32	-1,77	0
Medium	P82933	28S ribosomal protein S9, mitochondrial [OS=Homo sapiens]	3,78038457	4,7979798	2	2	2	396	45,806	MRPS9	0,53	0,32	0,21	0
Low	O00487	26S proteasome non-ATPase regulatory subunit 14 [OS=Homo sapiens]	1,18349356	2,25806452	1	1	1	310	34,555	PSMD14	-0,7	0,32	-1,02	0
High	P22695	Cytochrome b-c1 complex subunit 2, mitochondrial [OS=Homo sapiens]	213,932023	43,9293598	17	60	17	453	48,413	UQCRC2	0,68	0,31	0,36	0
High	P13010	X-ray repair cross-complementing protein 5 [OS=Homo sapiens]	22,1491202	11,4754098	8	9	8	732	82,652	XRCC5	-0,19	0,31	-0,49	0
High	Q9BQ83-1	Structure-specific endonuclease subunit SLX1 [OS=Homo sapiens]	19,1436987	18,1818182	4	5	4	275	30,751	SLX1B; SLX1A	10,68	0,31	10,37	0

High	P28715-1	DNA repair protein complementing XP-G cells [OS=Homo sapiens]	18,1256284	7,92580101	7	7	7	1186	133,027	ERCC5	9,51	0,31	9,2	0
High	P63220	40S ribosomal protein S21 [OS=Homo sapiens]	14,4428081	24,0963855	3	5	3	83	9,106	RPS21	0,35	0,31	0,04	0
High	P18074-1	Tfiih basal transcription factor complex helicase xpd subunit [OS=Homo sapiens	8,56561353	5,65789474	4	4	4	760	86,854	ERCC2	11,76	0,31	11,45	0
High	Q15758-1	Neutral amino acid transporter B(0) [OS=Homo sapiens]	7,57975141	4,99075786	2	2	2	541	56,562	SLC1A5	0,38	0,31	0,07	0
High	Q9BPW8	Protein NipSnap homolog 1 [OS=Homo sapiens]	7,46593999	11,2676056	2	3	2	284	33,289	NIPSNAP1	11,49	0,31	11,18	0
High	Q13155	aminoacyl tRNA synthase complex-interacting multifunctional protein 2 [OS=Ho	7,42540602	2,8125	1	2	1	320	35,326	AIMP2	-0,16	0,31	-0,46	0
Medium	Q01844-5	Isoform 5 of RNA-binding protein EWS [OS=Homo sapiens]	4,58864927	5,74886536	2	2	2	661	68,923	EWSR1	-1,36	0,31	-1,67	0
Medium	Q9NZ56	Formin-2 [OS=Homo sapiens]	3,44867201	0,92915215	1	1	1	1722	179,993	FMN2	12,59	0,31	12,27	0
Low	O75477	erlin-1 [OS=Homo sapiens]	1,71783122	2,02312139	1	1	1	346	38,901	ERLIN1	11,31	0,31	11	0
Low	Q7Z2T5-1	TRMT1-like protein [OS=Homo sapiens]	1,67019548	1,09140518	1	1	1	733	81,695	TRMT1L	0,03	0,31	-0,28	0
High	P21127-2	Isoform SV1 of Cyclin-dependent kinase 11B [OS=Homo sapiens]	228,406249	45,7800512	40	85	40	782	91,276	CDK11B	-0,72	0,3	-1,02	0
High	P16403	Histone H1.2 [OS=Homo sapiens]	155,134886	30,9859155	12	58	2	213	21,352	HIST1H1C	0,27	0,3	-0,03	0
High	P11387	DNA topoisomerase 1 [OS=Homo sapiens]	49,6176493	16,0784314	11	20	11	765	90,669	TOP1	-0,35	0,3	-0,65	0
Medium	Q8N0V3-1	Putative ribosome-binding factor A, mitochondrial [OS=Homo sapiens]	4,20653986	7,28862974	2	2	2	343	38,335	RBFA	0,56	0,3	0,26	0
Low	O75494-1	Serine/arginine-rich splicing factor 10 [OS=Homo sapiens]	1,45754805	4,96183206	1	1	1	262	31,282	10; LOC10099	-0,18	0,3	-0,48	0
High	P08238	Heat shock protein HSP 90-beta [OS=Homo sapiens]	213,172398	49,1712707	34	65	17	724	83,212	HSP90AB1	-1,09	0,29	-1,38	2
High	P39019	40S ribosomal protein S19 [OS=Homo sapiens]	52,5103314	57,9310345	9	19	9	145	16,051	RPS19	-0,04	0,28	-0,33	0
High	P07195	L-lactate dehydrogenase B chain [OS=Homo sapiens]	60,8995539	29,6407186	8	15	7	334	36,615	LDHB	-1,58	0,27	-1,85	0
High	O75147	Obscurin-like protein 1 [OS=Homo sapiens]	53,1553534	8,33333333	13	18	13	1896	206,817	OBSL1	0,33	0,27	0,06	0
High	Q93008-3	Probable ubiquitin carboxyl-terminal hydrolase FAF-X [OS=Homo sapiens]	10,4444573	1,75097276	4	4	4	2570	292,094	USP9X	-0,31	0,27	-0,58	0
Low	P49750-4	Isoform 4 of YLP motif-containing protein 1 [OS=Homo sapiens]	1,33714777	0,4193849	1	1	1	2146	241,495	YLPM1	-7,76	0,27	-8,03	0
High	P06733-1	alpha-enolase [OS=Homo sapiens]	195,468706	61,5207373	22	74	22	434	47,139	ENO1	-0,28	0,26	-0,54	0
High	P42677	40S ribosomal protein S27 [OS=Homo sapiens]	124,575195	41,6666667	6	37	3	84	9,455	RPS27	0,38	0,26	0,13	6
High	Q12905	Interleukin enhancer-binding factor 2 [OS=Homo sapiens]	23,8989616	13,3333333	5	7	5	390	43,035	ILF2	-0,72	0,26	-0,98	0
Medium	Q9UKE5-1	Traf2 and NCK-interacting protein kinase [OS=Homo sapiens]	2,36032579	1,02941176	2	2	2	1360	154,848	TNIK	0,55	0,26	0,29	0
High	P38646	Stress-70 protein, mitochondrial [OS=Homo sapiens]	230,731237	43,2989691	33	66	32	679	73,635	HSPA9	0,21	0,25	-0,04	0
High	P61513	60S ribosomal protein L37a [OS=Homo sapiens]	101,56569	59,7826087	7	39	7	92	10,268	RPL37A	0,21	0,25	-0,03	0
High	Q9HCB6	Spondin-1 [OS=Homo sapiens]	23,8337319	11,771995	8	10	8	807	90,914	SPON1	0,47	0,25	0,22	0
High	P62273-2	Isoform 2 of 40S ribosomal protein S29 [OS=Homo sapiens]	13,6165669	20,8955224	2	12	2	67	8,082	RPS29	0,26	0,25	0,01	0
High	O14735	CDP-diacylglycerol--inositol 3-phosphatidyltransferase [OS=Homo sapiens]	11,3432692	6,10328638	1	3	1	213	23,523	CDIPT	0,2	0,25	-0,06	0
High	P33993-1	DNA replication licensing factor MCM7 [OS=Homo sapiens]	273,51774	54,9374131	32	96	32	719	81,257	MCM7	0,28	0,24	0,04	0
High	P08670	Vimentin [OS=Homo sapiens]	97,4459132	54,5064378	25	31	24	466	53,619	VIM	-1,04	0,24	-1,28	0
High	P63244	Guanine nucleotide-binding protein subunit beta-2-like 1 [OS=Homo sapiens]	96,5711932	48,8958991	14	25	14	317	35,055	GNB2L1; RACK	-0,18	0,24	-0,42	0
High	O95831-1	Apoptosis-inducing factor 1, mitochondrial [OS=Homo sapiens]	69,0894727	27,0799347	14	24	14	613	66,859	AIFM1	0,11	0,24	-0,13	0
High	Q96T37-1	Putative RNA-binding protein 15 [OS=Homo sapiens]	31,9715381	10,0307062	8	11	8	977	107,124	RBM15	-0,12	0,24	-0,36	0
High	Q9NX20	39S ribosomal protein L16, mitochondrial [OS=Homo sapiens]	19,7175095	11,1553785	2	5	2	251	28,431	MRPL16	0,01	0,24	-0,23	0
High	P39656	Dolichyl-diphosphooligosaccharide--protein glycosyltransferase 48 kDa subunit	17,7708371	6,79824561	3	6	3	456	50,769	DDOST	-0,11	0,24	-0,35	0
High	Q58EX7	Puratrophin-1 [OS=Homo sapiens]	18,0057681	2,93870697	4	7	3	1191	130,72	PLEKHG4	-0,47	0,23	-0,7	1
High	Q53EL6-1	Programmed cell death protein 4 [OS=Homo sapiens]	16,6639925	5,54371002	2	5	2	469	51,703	PDCD4	0,39	0,23	0,16	0
High	Q92499	ATP-dependent RNA helicase DDX1 [OS=Homo sapiens]	16,1549105	12,1621622	6	7	6	740	82,38	DDX1	-0,02	0,23	-0,25	0
High	P15880	40S ribosomal protein S2 [OS=Homo sapiens]	224,033265	56,996587	18	80	18	293	31,305	RPS2	0,04	0,22	-0,18	0
High	P38919	Eukaryotic initiation factor 4A-III [OS=Homo sapiens]	38,0416254	22,1411192	8	16	6	411	46,841	EIF4A3	-0,65	0,22	-0,87	2
High	Q9Y3U8	60S ribosomal protein L36 [OS=Homo sapiens]	34,9425342	30,4761905	4	20	4	105	12,246	RPL36	0,04	0,22	-0,18	0
High	Q9NZI8	Insulin-like growth factor 2 mRNA-binding protein 1 [OS=Homo sapiens]	21,5563802	10,745234	6	7	3	577	63,441	IGF2BP1	-0,58	0,22	-0,8	3
High	P22626	heterogeneous nuclear ribonucleoproteins A2/B1 [OS=Homo sapiens]	19,6928298	13,8810198	5	7	5	353	37,407	HNRNPA2B1	-1,44	0,22	-1,67	0
High	Q5H9R7-5	Isoform 5 of Serine/threonine-protein phosphatase 6 regulatory subunit 3 [OS=	13,3962014	3,29920364	3	5	3	879	98,423	PPP6R3	0,17	0,22	-0,05	0
High	Q86VP6-1	cullin-associated nedd8-dissociated protein 1 [OS=Homo sapiens]	97,7389241	22,3577236	24	35	23	1230	136,289	CAND1	-0,78	0,21	-0,99	0
High	P32969	60S ribosomal protein L9 [OS=Homo sapiens]	77,4642314	25,5208333	4	20	4	192	21,85	RPL9	0,01	0,21	-0,19	0
High	P49368-1	T-complex protein 1 subunit gamma [OS=Homo sapiens]	52,6208938	20,3669725	11	19	11	545	60,495	CCT3	-0,02	0,21	-0,23	0
High	P52597	Heterogeneous nuclear ribonucleoprotein F [OS=Homo sapiens]	31,7973683	28,4337349	8	14	6	415	45,643	HNRNPF	-0,12	0,21	-0,33	0
High	P30876	DNA-directed RNA polymerase II subunit RPB2 [OS=Homo sapiens]	16,9875402	5,36626917	6	7	6	1174	133,811	POLR2B	0,42	0,21	0,21	0
Medium	Q8N5N7	39S ribosomal protein L50, mitochondrial [OS=Homo sapiens]	4,05173378	9,49367089	1	1	1	158	18,313	MRPL50	0,97	0,21	0,76	0
Low	P08574	Cytochrome c1, heme protein, mitochondrial [OS=Homo sapiens]	1,41128022	2,15384615	1	1	1	325	35,399	CYC1	0,37	0,21	0,15	0
High	P27708	CAD protein [OS=Homo sapiens]	384,055207	31,1011236	58	122	58	2225	242,829	CAD	-0,17	0,2	-0,37	0
High	P53621-2	Isoform 2 of Coatomer subunit alpha [OS=Homo sapiens]	102,807609	18,0859692	20	31	20	1233	139,235	COPA	-0,11	0,2	-0,31	0
High	P37108	Signal recognition particle 14 kDa protein [OS=Homo sapiens]	59,1449498	36,0294118	5	17	5	136	14,561	SRP14	0,31	0,2	0,11	0
High	Q15366-2	Isoform 2 of Poly(rC)-binding protein 2 [OS=Homo sapiens]	53,7269251	27,8688525	9	21	4	366	38,627	PCBP2	-0,93	0,2	-1,13	0
High	Q5SRE5	Nucleoporin NUP188 homolog [OS=Homo sapiens]	9,22732557	1,88679245	4	5	4	1749	195,917	NUP188	-0,22	0,2	-0,42	0
Medium	Q9Y6D6	Brefeldin A-inhibited guanine nucleotide-exchange protein 1 [OS=Homo sapiens	4,22694481	0,75716604	2	3	2	1849	208,634	ARFGEF1	0,03	0,2	-0,16	0
Medium	Q9NPL8	Complex I assembly factor TIMMDC1, mitochondrial [OS=Homo sapiens]	2,84740592	3,15789474	1	1	1	285	32,158	TIMMDC1	0,31	0,2	0,11	0
High	Q9BYG3	MKI67 FHA domain-interacting nucleolar phosphoprotein [OS=Homo sapiens]	234,508825	62,116041	19	52	19	293	34,201	MKI67IP; NIFK	0,6	0,19	0,41	0
High	P17987	T-complex protein 1 subunit alpha [OS=Homo sapiens]	180,796683	59,352518	25	47	25	556	60,306	TCP1	0,04	0,19	-0,15	0
High	P06493	Cyclin-dependent kinase 1 [OS=Homo sapiens]	44,4991901	43,7710438	11	16	10	297	34,074	CDK1	0,21	0,19	0,02	0
High	P55084	Trifunctional enzyme subunit beta, mitochondrial [OS=Homo sapiens]	17,8853126	9,07172996	4	6	4	474	51,262	HADHB	-0,17	0,19	-0,36	0

High	Q7Z6Z7	E3 ubiquitin-protein ligase HUWE1 [OS=Homo sapiens]	5,96823398	0,86877	3	3	3	4374	481,589	HUWE1	-1,44	0,19	-1,63	0
High	Q9HDC5	junctophilin-1 [OS=Homo sapiens]	48,9181275	16,4901664	10	21	10	661	71,642	JPH1	0,61	0,18	0,44	0
High	O15235	28S ribosomal protein S12, mitochondrial [OS=Homo sapiens]	46,0383807	44,9275362	6	25	6	138	15,163	MRPS12	0,29	0,18	0,11	0
High	P61927	60S ribosomal protein L37 [OS=Homo sapiens]	27,7161047	37,1134021	7	43	7	97	11,071	RPL37	0,01	0,18	-0,17	0
High	Q9BRX2	Protein pelota homolog [OS=Homo sapiens]	27,6033797	12,2077922	4	7	4	385	43,332	PELO	0,44	0,18	0,27	0
High	Q8IXB1-1	DnaJ homolog subfamily C member 10 [OS=Homo sapiens]	11,4203451	3,65699874	3	5	3	793	91,021	DNAJC10	0,39	0,18	0,21	0
High	Q8IXI1	Mitochondrial Rho GTPase 2 [OS=Homo sapiens]	8,29722164	2,75080906	2	3	2	618	68,075	RHOT2	-0,21	0,18	-0,4	0
Medium	Q9P0J0-2	Isoform 2 of NADH dehydrogenase [ubiquinone] 1 alpha subcomplex subunit 13	2,59998036	6,30630631	1	1	1	222	24,866		0,28	0,18	0,1	0
High	Q6UN15-3	Isoform 3 of Pre-mRNA 3'-end-processing factor FIP1 [OS=Homo sapiens]	409,978028	53,6538462	29	154	1	520	58,341	FIP1L1	0,33	0,17	0,16	0
High	P23396-1	40S ribosomal protein S3 [OS=Homo sapiens]	376,078244	81,8930041	27	161	27	243	26,671	RPS3	0,15	0,17	-0,02	0
High	P62266	40S ribosomal protein S23 [OS=Homo sapiens]	308,656194	72,027972	18	442	18	143	15,798	RPS23	0,11	0,17	-0,07	0
High	P22314	Ubiquitin-like modifier-activating enzyme 1 [OS=Homo sapiens]	112,677626	25,8034026	21	35	21	1058	117,774	UBA1	-2,47	0,17	-2,64	0
High	Q9UG63-2	Isoform 2 of ATP-binding cassette sub-family F member 2 [OS=Homo sapiens]	93,0703672	23,9747634	15	26	15	634	72,397	ABCF2	0,43	0,17	0,26	0
High	Q96C36	Pyrroline-5-carboxylate reductase 2 [OS=Homo sapiens]	52,4612817	16,25	4	11	3	320	33,616	PYCR2	0,29	0,17	0,13	0
High	P22061-2	Isoform 2 of Protein-L-isoaspartate(D-aspartate) O-methyltransferase [OS=Hom	9,39341792	10,5263158	2	4	2	228	24,664	PCMT1	0,17	0,17	0	0
Medium	P47897	glutamine--tRNA ligase [OS=Homo sapiens]	3,28304242	3,09677419	2	2	2	775	87,743	QARS	-0,7	0,17	-0,88	0
Medium	A6ZKI3	protein FAM127A [OS=Homo sapiens]	2,59192971	6,19469027	1	1	1	113	13,163	FAM127A	-0,25	0,17	-0,42	0
Low	Q16650	T-box brain protein 1 [OS=Homo sapiens]	1,25758912	1,75953079	1	1	1	682	74,007	TBR1	-0,02	0,17	-0,19	0
High	O60762	Dolichol-phosphate mannosyltransferase subunit 1 [OS=Homo sapiens]	42,8954581	25,7692308	5	12	5	260	29,616	DPM1	0,35	0,16	0,2	0
High	O15027-5	Isoform 5 of Protein transport protein Sec16A [OS=Homo sapiens]	24,5116763	5,81553839	9	12	9	2201	235,607		-0,09	0,16	-0,25	0
High	P62318	small nuclear ribonucleoprotein sm d3 [OS=Homo sapiens]	12,8966055	31,7460317	3	6	3	126	13,907	SNRPD3	-0,32	0,16	-0,47	0
High	P00846	ATP synthase subunit A [OS=Homo sapiens]	4,73960463	4,42477876	1	2	1	226	24,801	ATP6	-0,36	0,16	-0,53	0
Medium	Q96F07	Cytoplasmic FMR1-interacting protein 2 [OS=Homo sapiens]	3,18963305	0,93896714	1	1	1	1278	148,302	CYFIP2	-1,32	0,16	-1,48	0
Low	Q9Y5V0	Zinc finger protein 706 [OS=Homo sapiens]	1,18336106	14,4736842	1	1	1	76	8,492	ZNF706	0,25	0,16	0,09	0
High	P62269	40S ribosomal protein S18 [OS=Homo sapiens]	317,720305	63,8157895	24	283	24	152	17,708	RPS18	0,31	0,15	0,17	0
High	O00571	ATP-dependent RNA helicase DDX3X [OS=Homo sapiens]	305,088109	54,6827795	32	101	32	662	73,198	DDX3X	0,38	0,15	0,23	0
High	Q14739	Lamin-B receptor [OS=Homo sapiens]	63,3255368	17,5609756	10	21	10	615	70,658	LBR	0,2	0,15	0,05	0
High	P50991	T-complex protein 1 subunit delta [OS=Homo sapiens]	34,6123547	13,9146568	7	11	7	539	57,888	CCT4	-0,09	0,15	-0,25	0
High	P13674-2	Isoform 2 of Prolyl 4-hydroxylase subunit alpha-1 [OS=Homo sapiens]	34,4502465	18,5393258	8	9	8	534	60,929	P4HA1	0,9	0,15	0,75	0
High	Q9H6F5	Coiled-coil domain-containing protein 86 [OS=Homo sapiens]	13,4800511	16,9444444	4	5	4	360	40,211	CCDC86	0,51	0,15	0,36	0
High	Q8IWS0-1	PHD finger protein 6 [OS=Homo sapiens]	210,311968	55,3424658	19	97	6	365	41,264	PHF6	0,2	0,14	0,06	22
High	P07910-1	Heterogeneous nuclear ribonucleoproteins C1/C2 [OS=Homo sapiens]	106,843055	36,2745098	14	28	14	306	33,65	HNRNPC	-0,84	0,14	-0,98	0
High	P62899	60S ribosomal protein L31 [OS=Homo sapiens]	99,3194423	57,6	10	55	10	125	14,454	RPL31	0,06	0,14	-0,09	0
Medium	Q15645	Pachytene checkpoint protein 2 homolog [OS=Homo sapiens]	4,59049056	4,62962963	2	2	2	432	48,52	TRIP13	-0,11	0,14	-0,25	0
Medium	A5YKK6	CCR4-NOT transcription complex subunit 1 [OS=Homo sapiens]	4,38205283	0,84175084	2	3	2	2376	266,768	CNOT1	-0,73	0,14	-0,88	0
Low	Q9H0U3	Magnesium transporter protein 1 [OS=Homo sapiens]	2,15658033	2,68656716	1	1	1	335	38,011	MAGT1	-0,07	0,14	-0,22	0
Low	P59894	Doublecortin domain-containing protein 1 [OS=Homo sapiens]	1,65915945	1,97740113	1	1	1	354	39,834	DCDC1	0,16	0,14	0,02	0
High	P26373-1	60S ribosomal protein L13 [OS=Homo sapiens]	200,828523	55,450237	17	92	17	211	24,247	RPL13	0,01	0,13	-0,12	0
High	P31689-1	DnaJ homolog subfamily A member 1 [OS=Homo sapiens]	73,1135989	30,9823678	10	28	10	397	44,839	DNAJA1	0,37	0,13	0,24	0
High	P10412	Histone H1.4 [OS=Homo sapiens]	141,051392	30,1369863	12	56	2	219	21,852	HIST1H1E	0,21	0,12	0,09	14
High	P46778	60S ribosomal protein L21 [OS=Homo sapiens]	68,9934094	50,625	8	22	8	160	18,553	RPL21	0,12	0,12	0	0
High	P43246-1	DNA mismatch repair protein MSH2 [OS=Homo sapiens]	23,959652	6,63811563	6	10	6	934	104,677	MSH2	0,13	0,12	0,01	0
High	Q9NSE4	Isoleucine--tRNA ligase, mitochondrial [OS=Homo sapiens]	15,3653786	7,60869565	6	6	6	1012	113,719	IARS2	-0,42	0,12	-0,54	0
High	P04844-1	Dolichyl-diphosphooligosaccharide--protein glycosyltransferase subunit 2 [OS=H	9,69973069	5,70522979	2	2	2	631	69,241	RPN2	0,13	0,12	0	0
High	Q9Y4W6	AFG3-like protein 2 [OS=Homo sapiens]	8,07888628	3,76411543	3	3	3	797	88,528	AFG3L2	0,11	0,12	-0,01	0
High	Q14684	Ribosomal RNA processing protein 1 homolog B [OS=Homo sapiens]	6,44506295	5,67282322	3	3	3	758	84,375	RRP1B	-0,34	0,12	-0,46	0
High	P62249	40S ribosomal protein S16 [OS=Homo sapiens]	242,362634	75,3424658	18	142	18	146	16,435	RPS16	0,19	0,11	0,08	0
High	P09874	Poly [ADP-ribose] polymerase 1 [OS=Homo sapiens]	72,0148884	22,2879684	18	27	18	1014	113,012	PARP1	-0,54	0,11	-0,65	0
High	P46779	60S ribosomal protein L28 [OS=Homo sapiens]	47,8387584	45,9854015	10	27	10	137	15,738	RPL28	0,11	0,11	0	0
High	P78316	Nucleolar protein 14 [OS=Homo sapiens]	38,7356982	12,6021004	8	13	8	857	97,607	NOP14	0	0,11	-0,11	0
High	P10809	60 kDa heat shock protein, mitochondrial [OS=Homo sapiens]	36,2886473	17,9755672	9	10	9	573	61,016	HSPD1	-0,33	0,11	-0,44	0
High	Q14839-2	Isoform 2 of Chromodomain-helicase-DNA-binding protein 4 [OS=Homo sapiens	32,5065063	5,6185567	9	12	9	1940	220,709	CHD4	-0,17	0,11	-0,28	0
High	Q9Y6A4	Cilia- and flagella-associated protein 20 [OS=Homo sapiens]	23,4732414	27,9792746	5	8	5	193	22,76	6orf80; CFAP	0,53	0,11	0,42	0
High	P51610-4	Isoform 4 of Host cell factor 1 [OS=Homo sapiens]	9,99435226	1,49110149	3	4	3	2079	213,272	HCFC1	-1,95	0,11	-2,06	0
Medium	Q9Y4R8	telomere length regulation protein TEL2 homolog [OS=Homo sapiens]	3,70257982	2,15053763	2	3	2	837	91,689	TELO2	0,14	0,11	0,03	0
Medium	Q9UHB9	Signal recognition particle subunit SRP68 [OS=Homo sapiens]	3,15242734	2,07336523	1	1	1	627	70,686	SRP68	-0,7	0,11	-0,82	0
Medium	Q09666-1	Neuroblast differentiation-associated protein AHNAK [OS=Homo sapiens]	2,91793307	1,68081494	1	2	1	5890	628,699	AHNAK	-2,87	0,11	-2,98	0
Medium	Q8N3U4-2	Isoform 2 of Cohesin subunit SA-2 [OS=Homo sapiens]	2,50390101	1,02523659	1	1	1	1268	145,658	STAG2	-0,63	0,11	-0,74	0
High	P68371	Tubulin beta-4B chain [OS=Homo sapiens]	925,949084	83,1460674	31	441	1	445	49,799	TUBB4B	0,09	0,1	-0,02	85
High	P62979	Ubiquitin-40S ribosomal protein S27a [OS=Homo sapiens]	284,409998	58,3333333	13	134	11	156	17,953	RPS27A	-0,04	0,1	-0,14	3
High	P62913	60S ribosomal protein L11 [OS=Homo sapiens]	146,818096	65,7303371	13	67	13	178	20,24	RPL11	0,11	0,1	0,01	0
High	Q5QNW6-2	Isoform 2 of Histone H2B type 2-F [OS=Homo sapiens]	148,497379	54,4776119	9	61	2	134	14,832	HIST2H2BF	-0,14	0,09	-0,23	19
High	Q92616	translational activator GCN1 [OS=Homo sapiens]	90,8958214	13,1037065	28	37	28	2671	292,572	GCN1L1; GCN	-0,33	0,09	-0,43	0
High	P29372	DNA-3-methyladenine glycosylase [OS=Homo sapiens]	84,763927	48,6577181	11	21	11	298	32,848	MPG	0,1	0,09	0,01	0

High	Q16891	MICOS complex subunit Mic60 [OS=Homo sapiens]	49,2336534	17,8100264	13	18	13	758	83,626	IMMT	-0,03	0,09	-0,12	0
High	O14776-1	Transcription elongation regulator 1 [OS=Homo sapiens]	44,2655366	9,74499089	11	18	11	1098	123,823	TCERG1	-0,14	0,09	-0,23	0
High	P19367-3	Isoform 3 of Hexokinase-1 [OS=Homo sapiens]	28,097739	7,70901194	7	11	7	921	102,672	HK1	-0,87	0,09	-0,95	0
High	Q9H7H0-3	Isoform 3 of Methyltransferase-like protein 17, mitochondrial [OS=Homo sapier	27,6626637	17,1548117	6	9	6	478	53,017	METTL17	0,1	0,09	0	0
High	Q5T200-1	Zinc finger CCCH domain-containing protein 13 [OS=Homo sapiens]	9,32780788	1,49880096	2	3	2	1668	196,519	ZC3H13	-0,38	0,09	-0,46	0
Medium	O95168-1	NADH dehydrogenase [ubiquinone] 1 beta subcomplex subunit 4 [OS=Homo sa	3,85277183	10,0775194	1	2	1	129	15,199	NDUFB4	-0,4	0,09	-0,49	0
High	Q8N1F7-1	Nuclear pore complex protein Nup93 [OS=Homo sapiens]	155,049555	44,4444444	30	50	30	819	93,43	NUP93	0,01	0,08	-0,07	0
High	Q9Y285	Phenylalanine--tRNA ligase alpha subunit [OS=Homo sapiens]	73,4261591	23,4251969	11	25	11	508	57,528	FARSA	0,22	0,08	0,15	0
High	P46783	40S ribosomal protein S10 [OS=Homo sapiens]	33,7742512	40	5	11	5	165	18,886	RPS10	-0,08	0,08	-0,16	0
High	P31040	Succinate dehydrogenase [ubiquinone] flavoprotein subunit, mitochondrial [OS	15,8977539	3,76506024	2	4	2	664	72,645	SDHA	-0,91	0,08	-0,99	0
High	Q07955-1	Serine/arginine-rich splicing factor 1 [OS=Homo sapiens]	6,87424786	7,66129032	2	3	2	248	27,728	SRSF1	-0,07	0,08	-0,15	0
High	P62857	40S ribosomal protein S28 [OS=Homo sapiens]	114,440347	57,9710145	7	49	7	69	7,836	RPS28	0,22	0,07	0,15	0
High	P62917	60S ribosomal protein L8 [OS=Homo sapiens]	114,180018	63,8132296	14	41	14	257	28,007	RPL8	-0,48	0,07	-0,55	0
High	P83731	60S ribosomal protein L24 [OS=Homo sapiens]	104,750705	42,6751592	11	61	11	157	17,768	RPL24	0,04	0,07	-0,03	0
High	P14625	Endoplasmin [OS=Homo sapiens]	42,4273988	10,9589041	11	13	9	803	92,411	HSP90B1	-1,27	0,07	-1,34	0
High	Q9Y678	Coatomer subunit gamma-1 [OS=Homo sapiens]	10,5929006	4,91990847	3	3	3	874	97,655	COPG1	-0,31	0,07	-0,38	0
High	O75306-1	NADH dehydrogenase [ubiquinone] iron-sulfur protein 2, mitochondrial [OS=Hc	6,46905912	3,45572354	2	3	2	463	52,512	NDUFS2	0,06	0,07	0	0
High	P49411	elongation factor Tu, mitochondrial [OS=Homo sapiens]	422,348415	68,3628319	27	150	27	452	49,51	TUFM	0	0,06	-0,06	0
High	P62244	40S ribosomal protein S15a [OS=Homo sapiens]	231,724544	81,5384615	15	104	15	130	14,83	RPS15A	-0,05	0,06	-0,11	0
High	O15269	serine palmitoyltransferase 1 [OS=Homo sapiens]	7,30319321	4,86257928	3	5	3	473	52,71	SPTLC1	0,54	0,06	0,48	0
Medium	P55769	NHP2-like protein 1 [OS=Homo sapiens]	2,586365	9,375	1	1	1	128	14,165	NHP2L1; SNU1	-0,15	0,06	-0,21	0
High	Q8WUQ7-2	Isoform 2 of Cactin [OS=Homo sapiens]	382,740797	40,3208556	42	114	42	935	107,871		0,68	0,05	0,63	0
High	Q69YN4	protein virilizer homolog [OS=Homo sapiens]	7,46947176	3,75275938	5	5	5	1812	201,898	KIAA1429	-0,64	0,05	-0,69	0
High	Q9HAV4	exportin-5 [OS=Homo sapiens]	6,97451921	2,65780731	3	4	3	1204	136,222	XPO5	-0,55	0,05	-0,61	0
High	Q8IY17-4	Isoform 4 of Neuropathy target esterase [OS=Homo sapiens]	4,77990803	1,45454545	1	2	1	1375	150,859	PNPLA6	0,96	0,05	0,91	0
Medium	P48729-1	Casein kinase I isoform alpha [OS=Homo sapiens]	2,88107425	2,96735905	1	1	1	337	38,89	CSNK1A1	0,21	0,05	0,15	0
High	P42766	60S ribosomal protein L35 [OS=Homo sapiens]	227,640769	42,2764228	12	139	12	123	14,543	RPL35	0,12	0,04	0,08	0
High	P62280	40S ribosomal protein S11 [OS=Homo sapiens]	193,259336	56,9620253	17	73	17	158	18,419	RPS11	0,01	0,04	-0,03	0
High	O94761	ATP-dependent DNA helicase Q4 [OS=Homo sapiens]	51,0714502	15,1490066	13	19	13	1208	132,993	RECQL4	0,26	0,04	0,22	0
High	Q9NRA0-5	Isoform 5 of Sphingosine kinase 2 [OS=Homo sapiens]	34,0813181	8,40998686	5	9	5	761	80,154	SPHK2	0,18	0,04	0,14	0
High	O75367-1	Core histone macro-H2A.1 [OS=Homo sapiens]	21,433573	16,6666667	5	7	3	372	39,592	H2AFY	-0,33	0,04	-0,37	2
High	Q8WUM0	Nuclear pore complex protein Nup133 [OS=Homo sapiens]	5,52014526	3,11418685	3	3	3	1156	128,898	NUP133	0,97	0,04	0,93	0
Medium	P27695	DNA-(apurinic or apyrimidinic site) lyase [OS=Homo sapiens]	3,0714723	2,83018868	1	2	1	318	35,532	APEX1	-1,61	0,04	-1,65	0
High	P62829	60S ribosomal protein L23 [OS=Homo sapiens]	487,879021	77,1428571	17	379	17	140	14,856	RPL23	0,15	0,03	0,13	0
High	Q9HCM4-2	Isoform 2 of Band 4.1-like protein 5 [OS=Homo sapiens]	423,750486	74,0594059	32	173	6	505	57,849	EPB41L5	0,64	0,03	0,61	0
High	P27635	60S ribosomal protein L10 [OS=Homo sapiens]	393,733406	63,5514019	18	242	18	214	24,588	RPL10	0,06	0,03	0,02	0
High	P62847-4	Isoform 4 of 40S ribosomal protein S24 [OS=Homo sapiens]	226,98215	16,6089965	6	78	6	289	32,41	RPS24	0,05	0,03	0,02	0
High	Q13263	Transcription intermediary factor 1-beta [OS=Homo sapiens]	59,5099119	19,8802395	15	22	15	835	88,493	TRIM28	-0,77	0,03	-0,8	0
High	Q15428	splicing factor 3a subunit 2 [OS=Homo sapiens]	12,9133633	3,01724138	1	3	1	464	49,224	SF3A2	-0,42	0,03	-0,46	0
High	P35613	Basigin [OS=Homo sapiens]	9,96551648	6,23376623	2	3	2	385	42,174	BSG	-0,04	0,03	-0,07	0
High	P62081	40S ribosomal protein S7 [OS=Homo sapiens]	212,882488	71,6494845	18	89	18	194	22,113	RPS7	0,1	0,02	0,08	0
High	P62277	40S ribosomal protein S13 [OS=Homo sapiens]	200,792255	50,3311258	12	84	12	151	17,212	RPS13	-0,02	0,02	-0,04	0
High	P62861	40S ribosomal protein S30 [OS=Homo sapiens]	59,8340912	33,8983051	5	52	5	59	6,644	FAU	0,04	0,02	0,02	0
High	P60842	Eukaryotic initiation factor 4A-I [OS=Homo sapiens]	33,7551252	15,270936	6	16	4	406	46,125	EIF4A1	-0,74	0,02	-0,76	0
High	O43143	Pre-mRNA-splicing factor ATP-dependent RNA helicase DHX15 [OS=Homo sapie	202,790699	44,0251572	31	68	30	795	90,875	DHX15	-0,36	0,01	-0,37	0
High	Q5T280	putative methyltransferase C9orf114 [OS=Homo sapiens]	192,406411	51,5957447	19	70	19	376	41,982	C9orf114	0,6	0,01	0,59	0
High	P46781	40S ribosomal protein S9 [OS=Homo sapiens]	191,565858	62,8865979	21	107	21	194	22,578	RPS9	0,02	0,01	0,01	0
High	Q15393-1	Splicing factor 3B subunit 3 [OS=Homo sapiens]	146,268112	26,5406738	25	40	25	1217	135,492	SF3B3	-0,57	0,01	-0,57	0
High	Q8IY37	Probable ATP-dependent RNA helicase DHX37 [OS=Homo sapiens]	42,3648134	12,6188418	13	17	13	1157	129,464	DHX37	0,07	0,01	0,05	0
Low	O95394-4	Isoform 3 of Phosphoacetylglucosamine mutase [OS=Homo sapiens]	1,65345144	1,57894737	1	1	1	570	62,902	PGM3	-0,54	0,01	-0,54	0
High	P61247	40S ribosomal protein S3a [OS=Homo sapiens]	459,231344	70,8333333	28	180	28	264	29,926	RPS3A	0,02	0	0,02	0
High	P68366	Tubulin alpha-4A chain [OS=Homo sapiens]	427,842433	53,125	22	174	4	448	49,892	TUBA4A	-0,22	0	-0,22	0
High	P55060-1	Exportin-2 [OS=Homo sapiens]	85,0827423	25,7466529	21	30	21	971	110,346	CSE1L	-1,1	0	-1,1	0
High	Q96L34-1	Map/microtubule affinity-regulating kinase 4 [OS=Homo sapiens]	71,6072932	31,7819149	19	26	17	752	82,468	MARK4	0,13	0	0,13	0
High	O14880	Microsomal glutathione S-transferase 3 [OS=Homo sapiens]	46,601784	32,8947368	4	13	4	152	16,506	MGST3	-0,12	0	-0,12	0
High	Q9UQE7	Structural maintenance of chromosomes protein 3 [OS=Homo sapiens]	35,235628	9,77814297	11	16	11	1217	141,454	SMC3	-0,22	0	-0,22	0
High	Q16718	NADH dehydrogenase [ubiquinone] 1 alpha subcomplex subunit 5 [OS=Homo sa	6,75117745	7,75862069	1	3	1	116	13,45	NDUFA5	-0,12	0	-0,12	0
Low	Q14137	Ribosome biogenesis protein BOP1 [OS=Homo sapiens]	2,01597417	4,28954424	2	2	2	746	83,577	BOP1	0	0	0	0
Low	Q7Z3U7-1	Protein MON2 homolog [OS=Homo sapiens]	1,34678749	0,58241118	1	1	1	1717	190,237	MON2	-0,34	0	-0,34	0
High	P08708	40S ribosomal protein S17 [OS=Homo sapiens]	327,37403	73,3333333	16	109	16	135	15,54	RPS17; RPS17	0,03	-0,01	0,04	0
High	P83881	60S ribosomal protein L36a [OS=Homo sapiens]	170,830434	48,1132075	13	81	4	106	12,433	RPL36A	0,07	-0,01	0,08	16
High	P11498	pyruvate carboxylase, mitochondrial [OS=Homo sapiens]	9,22038567	3,65025467	3	3	3	1178	129,551	PC	-0,05	-0,01	-0,04	0
High	P62701	40S ribosomal protein S4, X isoform [OS=Homo sapiens]	489,085896	75,2851711	28	250	28	263	29,579	RPS4X	-0,05	-0,02	-0,03	0
High	P62851	40S ribosomal protein S25 [OS=Homo sapiens]	96,6725104	52	10	81	10	125	13,734	RPS25	0,02	-0,02	0,04	0

High	P20700	Lamin-B1 [OS=Homo sapiens]	62,8090822	26,7918089	14	24	11	586	66,368	LMNB1	-0,46	-0,02	-0,44	1
High	P30837	Aldehyde dehydrogenase X, mitochondrial [OS=Homo sapiens]	58,0311947	22,0502901	11	16	9	517	57,17	ALDH1B1	-0,17	-0,02	-0,15	2
High	P61006	Ras-related protein Rab-8A [OS=Homo sapiens]	13,8440926	9,17874396	2	4	2	207	23,653	RAB8A	-0,24	-0,02	-0,23	0
Low	P10745	Retinol-binding protein 3 [OS=Homo sapiens]	1,51927462	0,56134723	1	1	1	1247	135,278	RBP3	0,03	-0,02	0,05	0
High	P0C0S8	histone H2A type 1 [OS=Homo sapiens]	145,05545	41,5384615	8	65	4	130	14,083	M; HIST1H2AI;	-0,19	-0,03	-0,15	9
High	Q14232	Translation initiation factor eIF-2B subunit alpha [OS=Homo sapiens]	42,3441892	27,8688525	7	13	7	305	33,691	EIF2B1	0,1	-0,03	0,14	0
High	P52701	DNA mismatch repair protein MSH6 [OS=Homo sapiens]	17,7564335	5,66176471	7	10	7	1360	152,689	MSH6	-0,06	-0,03	-0,03	0
High	Q9P035	Very-long-chain (3R)-3-hydroxyacyl-CoA dehydratase 3 [OS=Homo sapiens]	14,5533332	9,94475138	3	5	3	362	43,132	TPLAD1; HACD	-0,54	-0,03	-0,51	0
High	P51571	translocon-associated protein subunit delta [OS=Homo sapiens]	11,483404	28,9017341	4	4	4	173	18,987	SSR4	0,73	-0,03	0,76	0
High	Q9Y277-2	Isoform 2 of Voltage-dependent anion-selective channel protein 3 [OS=Homo sa	5,61692743	6,33802817	2	2	2	284	30,77	VDAC3	-0,37	-0,03	-0,34	0
High	P78527	DNA-dependent protein kinase catalytic subunit [OS=Homo sapiens]	1063,16165	45,3246124	187	364	187	4128	468,788	PRKDC	-0,53	-0,04	-0,49	0
High	P05023	Sodium/potassium-transporting ATPase subunit alpha-1 [OS=Homo sapiens]	212,019335	34,3108504	28	55	28	1023	112,824	ATP1A1	-0,24	-0,04	-0,2	0
High	P63173	60s ribosomal protein l38 [OS=Homo sapiens]	147,312909	57,1428571	8	67	8	70	8,213	RPL38	0,11	-0,04	0,14	0
High	P60866-2	Isoform 2 of 40S ribosomal protein S20 [OS=Homo sapiens]	99,8523293	36,6197183	7	43	7	142	15,995	RPS20	0,1	-0,04	0,14	0
High	P61254	60S ribosomal protein L26 [OS=Homo sapiens]	97,4225938	51,7241379	12	44	4	145	17,248	RPL26	0,01	-0,04	0,05	9
High	O60264	SWI/SNF-related matrix-associated actin-dependent regulator of chromatin sub	32,9211224	11,3117871	11	14	11	1052	121,828	SMARCA5	-0,5	-0,04	-0,46	0
High	Q9BXP5	serrate RNA effector molecule homolog [OS=Homo sapiens]	9,98014123	4,33789954	4	5	3	876	100,604	SRRT	-0,3	-0,04	-0,26	0
High	O95433	activator of 90 kDa heat shock protein ATPase homolog 1 [OS=Homo sapiens]	8,60649433	10,9467456	4	5	4	338	38,25	AHSA1	-0,96	-0,04	-0,93	0
High	Q9NRP0-2	Isoform 2 of Oligosaccharyltransferase complex subunit OSTC [OS=Homo sapier	7,91917474	7,01754386	1	2	1	171	19,158	OSTC	-0,36	-0,04	-0,32	0
Low	P51532-1	Transcription activator BRG1 [OS=Homo sapiens]	1,84375381	0,85003036	1	1	1	1647	184,53	SMARCA4	-1,24	-0,04	-1,21	0
High	Q10570	Cleavage and polyadenylation specificity factor subunit 1 [OS=Homo sapiens]	665,503145	58,1427581	71	303	71	1443	160,782	CPSF1	0,22	-0,05	0,27	0
High	Q9UQ35	serine/arginine repetitive matrix protein 2 [OS=Homo sapiens]	328,17988	27,2165698	56	141	56	2752	299,438	SRRM2	-0,01	-0,05	0,04	0
High	Q9BQG0-2	Isoform 2 of Myb-binding protein 1A [OS=Homo sapiens]	28,8533827	7,95795796	11	15	11	1332	149,274	MYBBP1A	-0,53	-0,05	-0,48	0
High	Q96A33-1	Coiled-coil domain-containing protein 47 [OS=Homo sapiens]	15,7809946	11,8012422	4	5	4	483	55,838	CCDC47	-0,02	-0,05	0,03	0
High	P18621-3	Isoform 3 of 60S ribosomal protein L17 [OS=Homo sapiens]	475,473928	53,9473684	19	351	19	228	26,356	PL17-C18ORF3	-0,02	-0,06	0,03	0
High	P46782	40S ribosomal protein S5 [OS=Homo sapiens]	278,628357	57,3529412	16	143	16	204	22,862	RPS5	0,08	-0,06	0,14	0
High	P46776	60S ribosomal protein L27a [OS=Homo sapiens]	118,867126	42,5675676	8	55	8	148	16,551	RPL27A	0,07	-0,06	0,12	0
High	Q8IWX8	Calcium homeostasis endoplasmic reticulum protein [OS=Homo sapiens]	87,2989452	14,8471616	11	23	11	916	103,637	CHERP	-0,43	-0,06	-0,37	0
High	Q92621	Nuclear pore complex protein Nup205 [OS=Homo sapiens]	65,6068653	11,2823062	21	27	21	2012	227,776	NUP205	-0,2	-0,06	-0,14	0
High	Q9Y2X3	Nucleolar protein 58 [OS=Homo sapiens]	17,1620414	12,2873346	5	5	5	529	59,541	NOP58	0,26	-0,06	0,32	0
High	Q6PKG0-1	La-related protein 1 [OS=Homo sapiens]	6,2681144	2,55474453	3	3	3	1096	123,434	LARP1	-0,2	-0,06	-0,14	0
Low	Q9H3U1	Protein unc-45 homolog A [OS=Homo sapiens]	1,21282301	0,95338983	1	1	1	944	103,011	UNC45A	0,1	-0,06	0,16	0
High	P56134	ATP synthase subunit f, mitochondrial [OS=Homo sapiens]	28,3098247	25,5319149	2	8	2	94	10,911	ATP5J2	0,05	-0,07	0,12	0
Medium	Q6P4A7-1	Sideroflexin-4 [OS=Homo sapiens]	4,19392536	7,12166172	2	2	2	337	37,974	SFXN4	-0,14	-0,07	-0,07	0
High	Q71U36	tubulin alpha-1A chain [OS=Homo sapiens]	573,685576	73,1707317	29	236	2	451	50,104	TUBA1A	-0,1	-0,08	-0,02	48
High	O75964	ATP synthase subunit g, mitochondrial [OS=Homo sapiens]	59,9613605	46,6019417	4	11	4	103	11,421	ATP5L	-0,15	-0,08	-0,07	0
High	P49792	E3 SUMO-protein ligase RanBP2 [OS=Homo sapiens]	36,7097046	5,64516129	12	20	12	3224	357,974	RANBP2	-0,44	-0,08	-0,36	0
High	Q9H2S9	Zinc finger protein Eos [OS=Homo sapiens]	15,7913962	5,98290598	3	4	3	585	64,065	IKZF4	-0,36	-0,08	-0,29	0
High	P43307	Translocon-associated protein subunit alpha [OS=Homo sapiens]	10,1932122	6,64335664	2	4	2	286	32,215	SSR1	-0,06	-0,08	0,02	0
High	Q8NF37	Lysophosphatidylcholine acyltransferase 1 [OS=Homo sapiens]	9,1543903	6,3670412	2	3	2	534	59,113	LPCAT1	0,4	-0,08	0,48	0
Medium	Q9GZT3-1	SRA stem-loop-interacting RNA-binding protein, mitochondrial [OS=Homo sapie	3,1079054	9,17431193	1	1	1	109	12,341	SLIRP	0,14	-0,08	0,21	0
High	P62987	Ubiquitin-60S ribosomal protein L40 [OS=Homo sapiens]	42,0019126	34,375	4	21	2	128	14,719	UBA52	-0,13	-0,09	-0,05	0
High	Q9BX10	GTP-binding protein 2 [OS=Homo sapiens]	15,0952725	3,32225914	2	4	2	602	65,727	GTPBP2	-0,38	-0,09	-0,3	0
Medium	Q9BZL6	Serine/threonine-protein kinase D2 [OS=Homo sapiens]	3,56290396	2,0501139	2	2	2	878	96,689	PRKD2	-0,03	-0,09	0,05	0
High	P56192	Methionine--tRNA ligase, cytoplasmic [OS=Homo sapiens]	131,977544	38,6666667	27	43	27	900	101,052	MARS	-0,4	-0,1	-0,29	0
High	Q9H5V9-1	UPF0428 protein CXorf56 [OS=Homo sapiens]	41,0047235	38,2882883	7	17	7	222	25,608	CXorf56	0,62	-0,1	0,71	0
High	P35241-5	Isoform 5 of Radixin [OS=Homo sapiens]	10,3753187	4,63576159	3	4	3	604	71,005	RDX	-0,56	-0,1	-0,46	0
High	Q9NSI2-1	protein FAM207A [OS=Homo sapiens]	7,72545331	5,2173913	1	3	1	230	25,441	FAM207A	0,86	-0,1	0,96	0
High	Q13509	tubulin beta-3 chain [OS=Homo sapiens]	511,920025	36,2222222	18	242	1	450	50,4	TUBB3	-0,18	-0,11	-0,06	2
High	P62241	40S ribosomal protein S8 [OS=Homo sapiens]	441,487307	65,8653846	22	180	22	208	24,19	RPS8	-0,12	-0,11	-0,01	0
High	O75533-1	splicing factor 3B subunit 1 [OS=Homo sapiens]	176,488509	27,4539877	30	63	30	1304	145,738	SF3B1	-0,55	-0,11	-0,44	0
High	Q9NTI5	Sister chromatid cohesion protein PDS5 homolog B [OS=Homo sapiens]	17,8638762	4,35383552	5	7	5	1447	164,563	PDS5B	-0,48	-0,11	-0,37	0
High	P0C7P4	Putative cytochrome b-c1 complex subunit Rieske-like protein 1 [OS=Homo sap	7,8262561	12,3674912	2	4	1	283	30,796	UQCRFS1P1	0,57	-0,11	0,68	1
Medium	Q9ULD4	Bromodomain and PHD finger-containing protein 3 [OS=Homo sapiens]	3,09956787	0,58091286	1	2	1	1205	135,66	BRPF3	0,71	-0,11	0,82	0
High	P29597	Non-receptor tyrosine-protein kinase TYK2 [OS=Homo sapiens]	46,1271976	9,09856782	9	16	9	1187	133,565	TYK2	0,15	-0,12	0,27	0
High	Q5SSJ5-1	Heterochromatin protein 1-binding protein 3 [OS=Homo sapiens]	17,7037468	9,5840868	5	7	5	553	61,169	HP1BP3	-0,07	-0,12	0,05	0
High	P35232	Prohibitin [OS=Homo sapiens]	9,4324493	7,72058824	2	3	2	272	29,786	PHB	-1,79	-0,12	-1,68	0
Medium	Q7RTV0	PHD finger-like domain-containing protein 5A [OS=Homo sapiens]	3,93716124	19,0909091	2	2	2	110	12,397	PHF5A	-0,1	-0,12	0,02	0
Low	Q6PJI9-1	WD repeat-containing protein 59 [OS=Homo sapiens]	1,55098468	1,43737166	1	1	1	974	109,724	WDR59	0,38	-0,12	0,5	0
High	P20719	Homeobox protein Hox-A5 [OS=Homo sapiens]	39,8121191	26,6666667	6	12	5	270	29,327	HOXA5	-0,44	-0,13	-0,31	1
High	Q92973-1	transportin-1 [OS=Homo sapiens]	13,8593566	6,01336303	5	6	5	898	102,289	TNPO1	-0,89	-0,13	-0,76	0
High	Q12872-2	Isoform 2 of Splicing factor, suppressor of white-apricot homolog [OS=Homo sa	8,24273293	3,38983051	3	3	3	1003	109,945	SFSWAP	-0,29	-0,13	-0,16	0
High	O43837-1	isocitrate dehydrogenase [NAD] subunit beta, mitochondrial [OS=Homo sapiens	5,5618637	2,85714286	1	2	1	385	42,157	IDH3B	0,03	-0,13	0,16	0
High	Q5JTH9-1	RRP12-like protein [OS=Homo sapiens]	274,349973	38,5505012	43	129	42	1297	143,611	RRP12	0,22	-0,14	0,36	2

High	Q9P2N5	RNA-binding protein 27 [OS=Homo sapiens]	119,542771	21,8867925	21	35	20	1060	118,645	RBM27	-0,2	-0,14	-0,06	0
High	P84098	60S ribosomal protein L19 [OS=Homo sapiens]	107,824897	34,6938776	12	48	12	196	23,451	RPL19	-0,17	-0,14	-0,04	0
High	Q13009	T-lymphoma invasion and metastasis-inducing protein 1 [OS=Homo sapiens]	57,7319812	15,4619736	20	23	20	1591	177,398	TIAM1	0,11	-0,14	0,24	0
High	Q9Y4W2	Ribosomal biogenesis protein LAS1L [OS=Homo sapiens]	33,3302278	19,7547684	11	13	11	734	83,013	LAS1L	-0,21	-0,14	-0,07	0
High	P61204	ADP-ribosylation factor 3 [OS=Homo sapiens]	29,8400792	30,9392265	4	7	2	181	20,588	ARF3	1,77	-0,14	1,92	0
High	P36542-1	ATP synthase subunit gamma, mitochondrial [OS=Homo sapiens]	204,156016	52,0134228	14	65	14	298	32,975	ATP5C1	0,03	-0,15	0,17	0
High	P62263	40S ribosomal protein S14 [OS=Homo sapiens]	188,902267	41,7218543	9	59	9	151	16,263	RPS14	0,08	-0,15	0,23	0
High	Q5C9Z4	nucleolar MIF4G domain-containing protein 1 [OS=Homo sapiens]	120,094109	23,1395349	19	35	19	860	96,198	NOM1	0,24	-0,15	0,38	0
High	P46734-3	Isoform 2 of Dual specificity mitogen-activated protein kinase kinase 3 [OS=Hon	50,3336292	35,2272727	12	21	12	352	39,914		0,09	-0,15	0,24	0
High	P49207	60S ribosomal protein L34 [OS=Homo sapiens]	43,2084763	38,4615385	8	26	8	117	13,284	RPL34	-0,23	-0,15	-0,08	0
High	P62891	60S ribosomal protein L39 [OS=Homo sapiens]	34,2117355	25,4901961	3	67	3	51	6,403	PL39; RPL39P	-0,09	-0,15	0,07	0
High	Q9BRX9	WD repeat domain-containing protein 83 [OS=Homo sapiens]	19,0760429	14,2857143	5	6	5	315	34,321	WDR83	-0,7	-0,15	-0,56	0
High	Q9ULX6	A-kinase anchor protein 8-like [OS=Homo sapiens]	6,51216232	4,48916409	3	3	3	646	71,604	AKAP8L	-0,18	-0,15	-0,04	0
Medium	P35658-5	Isoform 5 of Nuclear pore complex protein Nup214 [OS=Homo sapiens]	2,90308999	0,62111801	1	1	1	2093	215,269	NUP214	-0,83	-0,15	-0,69	0
High	P62888	60S ribosomal protein L30 [OS=Homo sapiens]	93,4056582	66,0869565	7	33	7	115	12,776	RPL30	-0,32	-0,16	-0,16	0
High	P28340	DNA polymerase delta catalytic subunit [OS=Homo sapiens]	32,917106	12,6467931	13	15	12	1107	123,553	POLD1	-0,22	-0,16	-0,06	0
High	P55072	Transitional endoplasmic reticulum ATPase [OS=Homo sapiens]	10,8363175	4,21836228	3	4	3	806	89,266	VCP	-2,47	-0,16	-2,31	0
High	Q6PGP7	Tetratricopeptide repeat protein 37 [OS=Homo sapiens]	5,77171368	1,91815857	3	4	3	1564	175,375	TTC37	-0,7	-0,16	-0,54	0
Low	O60341-2	Isoform 2 of Lysine-specific histone demethylase 1A [OS=Homo sapiens]	2,15895353	0,68493151	1	1	1	876	95,096	KDM1A	-0,79	-0,16	-0,63	0
High	P62753	40S RIBOSOMAL PROTEIN S6 [OS=Homo sapiens]	646,985723	57,0281124	29	308	29	249	28,663	RPS6	-0,07	-0,17	0,11	0
High	Q14498-2	Isoform 2 of RNA-binding protein 39 [OS=Homo sapiens]	531,795074	57,6335878	26	238	23	524	58,62	RBM39	0,02	-0,17	0,2	6
High	P62841	40S ribosomal protein S15 [OS=Homo sapiens]	448,307495	67,5862069	7	127	7	145	17,029	RPS15	-0,27	-0,17	-0,1	0
High	Q9C0J8	pre-mRNA 3' end processing protein WDR33 [OS=Homo sapiens]	390,190579	47,6047904	56	160	56	1336	145,799	WDR33	0,08	-0,17	0,25	0
High	P12236	ADP/ATP translocase 3 [OS=Homo sapiens]	361,24692	63,4228188	22	180	3	298	32,845	SLC25A6	-0,14	-0,17	0,03	6
High	Q15459	splicing factor 3A subunit 1 [OS=Homo sapiens]	28,0986207	12,2320303	8	10	8	793	88,831	SF3A1	-0,66	-0,17	-0,49	0
High	P61353	60S ribosomal protein L27 [OS=Homo sapiens]	24,4089129	30,8823529	4	9	4	136	15,788	RPL27	-0,23	-0,17	-0,06	0
High	Q9NRZ9	Lymphoid-specific helicase [OS=Homo sapiens]	21,3382957	7,99522673	6	9	6	838	97,012	HELLS	-0,04	-0,17	0,13	0
High	Q9HCS7	Pre-mRNA-splicing factor SYF1 [OS=Homo sapiens]	18,4221143	8,30409357	6	6	6	855	99,946	XAB2	0,15	-0,17	0,32	0
High	Q9HC62	Sentrin-specific protease 2 [OS=Homo sapiens]	17,8764831	8,14940577	4	5	4	589	67,812	SENP2	-0,42	-0,17	-0,25	0
Medium	P00492	Hypoxanthine-guanine phosphoribosyltransferase [OS=Homo sapiens]	3,04973253	4,58715596	1	1	1	218	24,564	HPRT1	-0,47	-0,17	-0,31	0
Medium	P23258	tubulin gamma-1 chain [OS=Homo sapiens]	2,78129963	3,99113082	2	2	2	451	51,138	TUBG1	0,78	-0,17	0,96	0
Low	Q8N823-1	Zinc finger protein 611 [OS=Homo sapiens]	1,60730305	1,13475177	1	2	1	705	81,397	ZNF611	-0,12	-0,17	0,05	0
High	Q9Y3Z3	deoxynucleoside triphosphate triphosphohydrolase SAMHD1 [OS=Homo sapien	64,1385239	21,884984	13	24	13	626	72,155	SAMHD1	-0,03	-0,18	0,14	0
High	P49755	Transmembrane emp24 domain-containing protein 10 [OS=Homo sapiens]	33,6059667	13,6986301	3	7	3	219	24,96	TMED10	-0,11	-0,18	0,07	0
High	P62304	small nuclear ribonucleoprotein E [OS=Homo sapiens]	11,2453015	11,9565217	1	4	1	92	10,797	SNRPE	-0,26	-0,18	-0,07	0
High	O15371	Eukaryotic translation initiation factor 3 subunit D [OS=Homo sapiens]	6,1434135	3,83211679	2	3	2	548	63,932	EIF3D	-0,83	-0,18	-0,65	0
High	P78549	Endonuclease III-like protein 1 [OS=Homo sapiens]	9,95284287	14,4230769	4	4	4	312	34,368	NTHL1	-0,27	-0,19	-0,07	0
High	Q96DI7-2	Isoform 2 of U5 small nuclear ribonucleoprotein 40 kDa protein [OS=Homo sapi	6,33731506	6,35696822	2	2	2	409	44,488	SNRNP40	-0,41	-0,19	-0,22	0
High	Q13573	SNW domain-containing protein 1 [OS=Homo sapiens]	6,19027104	3,91791045	2	2	2	536	61,456	SNW1	-0,24	-0,19	-0,05	0
Medium	Q96IX5	Up-regulated during skeletal muscle growth protein 5 [OS=Homo sapiens]	3,57381417	17,2413793	1	1	1	58	6,453	USMG5	-0,21	-0,19	-0,02	0
High	Q7Z6E9	E3 ubiquitin-protein ligase RBBP6 [OS=Homo sapiens]	358,626137	36,1049107	62	170	62	1792	201,442	RBBP6	-0,81	-0,2	-0,61	0
High	P62750	60S ribosomal protein L23a [OS=Homo sapiens]	209,056546	48,0769231	12	64	12	156	17,684	RPL23A	-0,09	-0,2	0,11	0
High	Q9BQ67	Glutamate-rich WD repeat-containing protein 1 [OS=Homo sapiens]	7,50416949	7,62331839	3	3	3	446	49,388	GRWD1	-0,02	-0,2	0,17	0
Low	Q9Y4A5	Transformation/transcription domain-associated protein [OS=Homo sapiens]	1,94500414	0,23322104	1	1	1	3859	437,318	TRRAP	-0,54	-0,2	-0,34	0
High	O43592	Exportin-T [OS=Homo sapiens]	141,817427	25,2598753	20	40	20	962	109,893	XPOT	-0,15	-0,21	0,07	0
High	P12004	proliferating cell nuclear antigen [OS=Homo sapiens]	89,8909954	65,5172414	15	30	15	261	28,75	PCNA	-0,31	-0,21	-0,1	0
High	P32322-3	Isoform 3 of Pyrroline-5-carboxylate reductase 1, mitochondrial [OS=Homo sapi	36,5618575	18,4971098	5	10	4	346	35,958	PYCR1	0,08	-0,21	0,29	1
High	P52292	Importin subunit alpha-1 [OS=Homo sapiens]	11,7078716	4,15879017	2	4	2	529	57,826	KPNA2	-0,56	-0,21	-0,34	0
High	P56385	ATP synthase subunit e, mitochondrial [OS=Homo sapiens]	10,5821937	34,7826087	2	3	2	69	7,928	ATP5I	0,14	-0,21	0,35	0
High	O60547-1	GDP-mannose 4,6 dehydratase [OS=Homo sapiens]	8,27088019	15,3225806	5	5	5	372	41,923	GMDS	-0,39	-0,21	-0,18	0
High	P55209	Nucleosome assembly protein 1-like 1 [OS=Homo sapiens]	7,75280897	2,81329923	1	2	1	391	45,346	NAP1L1	-0,71	-0,21	-0,5	0
High	Q8TB37-1	Iron-sulfur protein NUBPL [OS=Homo sapiens]	7,63204543	7,8369906	2	2	2	319	34,061	NUBPL	0,08	-0,21	0,28	0
Low	Q9P013	spliceosome-associated protein CWC15 homolog [OS=Homo sapiens]	2,10980261	4,80349345	1	1	1	229	26,608	CWC15	1,3	-0,21	1,52	0
Low	P60468	protein transport protein Sec61 subunit beta [OS=Homo sapiens]	2,02026957	11,4583333	1	1	1	96	9,968	SEC61B	-0,23	-0,21	-0,02	0
Low	Q9NVU7	Protein SDA1 homolog [OS=Homo sapiens]	1,48932097	0,87336245	1	1	1	687	79,82	SDAD1	0,33	-0,21	0,54	0
High	Q9BRR8	G patch domain-containing protein 1 [OS=Homo sapiens]	133,281515	26,6380236	19	36	19	931	103,282	GPATCH1	-0,81	-0,22	-0,59	0
High	Q9NVI7	ATPase family AAA domain-containing protein 3A [OS=Homo sapiens]	32,3602705	12,6182965	8	12	8	634	71,325	ATAD3A	-0,22	-0,22	0	0
High	Q9Y388	RNA-binding motif protein, X-linked 2 [OS=Homo sapiens]	19,1984032	10,2484472	3	5	3	322	37,313	RBMX2	0,34	-0,22	0,56	0
High	Q9UHR5-1	SAP30-binding protein [OS=Homo sapiens]	13,3812551	11,3636364	3	3	3	308	33,85	SAP30BP	-0,42	-0,22	-0,2	0
High	Q5T3I0-3	Isoform 3 of G patch domain-containing protein 4 [OS=Homo sapiens]	11,111341	5,54323725	3	5	3	451	50,897	GPATCH4	-0,2	-0,22	0,01	0
High	Q6NUK1	Calcium-binding mitochondrial carrier protein SCaMC-1 [OS=Homo sapiens]	5,24939833	4,19287212	2	3	2	477	53,32	SLC25A24	-0,32	-0,22	-0,1	0
High	Q9P2I0	Cleavage and polyadenylation specificity factor subunit 2 [OS=Homo sapiens]	427,005538	66,8797954	44	109	44	782	88,431	CPSF2	0,19	-0,23	0,42	0
High	Q6P2Q9	Pre-mRNA-processing-splicing factor 8 [OS=Homo sapiens]	310,220259	34,0042827	67	110	67	2335	273,427	PRPF8	-0,3	-0,23	-0,07	0
High	Q9BXF6	Rab11 family-interacting protein 5 [OS=Homo sapiens]	238,187218	58,0398162	29	72	29	653	70,372	RAB11FIP5	0,03	-0,23	0,26	0

High	Q4KMP7	TBC1 domain family member 10B [OS=Homo sapiens]	178,677476	36,2623762	24	54	24	808	87,145	TBC1D10B	-0,16	-0,23	0,07	0
High	P55786	puromycin-sensitive aminopeptidase [OS=Homo sapiens]	136,118007	31,5560392	24	42	24	919	103,211	NPEPPS	-0,44	-0,23	-0,22	0
High	Q13724-1	Mannosyl-oligosaccharide glucosidase [OS=Homo sapiens]	119,110916	31,5412186	20	35	20	837	91,861	MOGS	0,07	-0,23	0,3	0
High	Q9NWK9	Box C/D snoRNA protein 1 [OS=Homo sapiens]	19,8754015	12,1276596	5	6	5	470	53,884	ZNHIT6	-0,02	-0,23	0,21	0
High	Q8TED0	U3 small nucleolar RNA-associated protein 15 homolog [OS=Homo sapiens]	10,8161371	7,72200772	4	5	4	518	58,379	UTP15	-0,19	-0,23	0,04	0
High	Q9Y305-4	Isoform 4 of Acyl-coenzyme A thioesterase 9, mitochondrial [OS=Homo sapiens	5,83854005	4,24107143	2	3	2	448	50,818	ACOT9	-0,26	-0,23	-0,03	0
High	Q6P1X5	Transcription initiation factor TFIID subunit 2 [OS=Homo sapiens]	769,268011	57,4645538	68	250	68	1199	136,883	TAF2	-0,53	-0,24	-0,29	0
High	Q9Y383	Putative RNA-binding protein Luc7-like 2 [OS=Homo sapiens]	700,190355	62,5	40	463	32	392	46,486	LUC7L2	-0,11	-0,24	0,13	19
High	Q9H329-2	Isoform 2 of Band 4.1-like protein 4B [OS=Homo sapiens]	190,789918	43,8223938	20	67	18	518	58,529	EPB41L4B	0,25	-0,24	0,49	0
High	Q00325-2	Isoform B of Phosphate carrier protein, mitochondrial [OS=Homo sapiens]	162,79495	47,3684211	18	76	18	361	39,933	SLC25A3	-0,21	-0,24	0,03	0
High	Q9NVP1	ATP-dependent RNA helicase DDX18 [OS=Homo sapiens]	101,452214	29,2537313	15	37	15	670	75,359	DDX18	0,22	-0,24	0,45	0
High	Q14974	Importin subunit beta-1 [OS=Homo sapiens]	51,0637032	14,4977169	11	17	11	876	97,108	KPNB1	-1,23	-0,24	-0,99	0
High	Q8WWY3	U4/U6 small nuclear ribonucleoprotein Prp31 [OS=Homo sapiens]	7,20166663	8,01603206	3	3	3	499	55,421	PRPF31	-0,51	-0,24	-0,27	0
High	Q9NWV8	BRISC and BRCA1-A complex member 1 [OS=Homo sapiens]	6,80760345	6,07902736	2	2	2	329	36,537	BABAM1	0,43	-0,24	0,68	0
Low	Q7Z7F7-2	Isoform 2 of 39S ribosomal protein L55, mitochondrial [OS=Homo sapiens]	1,13990167	4,87804878	1	1	1	164	18,891	MRPL55	-0,27	-0,24	-0,03	0
High	O75643-1	U5 small nuclear ribonucleoprotein 200 kDa helicase [OS=Homo sapiens]	390,229913	41,4325843	67	118	67	2136	244,353	SNRNP200	-0,18	-0,25	0,07	0
High	Q9UII4	E3 ISG15--protein ligase HERC5 [OS=Homo sapiens]	349,503507	47,65625	42	92	42	1024	116,777	HERC5	-0,11	-0,25	0,14	0
High	Q14683	structural maintenance of chromosomes protein 1a [OS=Homo sapiens]	117,087594	23,0332522	26	48	26	1233	143,144	SMC1A	-0,28	-0,25	-0,03	0
High	Q9H8M2-5	Bromodomain-containing protein 9 [OS=Homo sapiens]	104,472246	27,3031826	13	30	13	597	66,958	BRD9	-0,41	-0,25	-0,16	0
High	Q9UGY1	Nucleolar protein 12 [OS=Homo sapiens]	50,8979685	46,0093897	7	17	7	213	24,648	NOL12	-0,4	-0,25	-0,15	0
High	O60306	Intron-binding protein aquarius [OS=Homo sapiens]	48,6311451	11,3131313	13	20	12	1485	171,186	AQR	0,34	-0,25	0,59	0
High	Q9NX58	Cell growth-regulating nucleolar protein [OS=Homo sapiens]	18,9874841	18,9973615	6	8	6	379	43,588	LYAR	-0,28	-0,25	-0,04	0
High	P46977	Dolichyl-diphosphooligosaccharide--protein glycosyltransferase subunit STT3A [	9,7833673	3,68794326	3	4	3	705	80,477	STT3A	-0,92	-0,25	-0,67	0
High	Q9ULX3	RNA-binding protein NOB1 [OS=Homo sapiens]	5,09520193	2,42718447	1	2	1	412	46,646	NOB1	0,28	-0,25	0,52	0
High	P12235	ADP/ATP translocase 1 [OS=Homo sapiens]	373,231795	68,1208054	22	167	4	298	33,043	SLC25A4	-0,22	-0,26	0,04	0
High	Q13200	26S proteasome non-ATPase regulatory subunit 2 [OS=Homo sapiens]	73,6239213	13,6563877	9	18	9	908	100,136	PSMD2	-0,6	-0,26	-0,35	0
High	A0FGR8-6	Isoform 6 of Extended synaptotagmin-2 [OS=Homo sapiens]	21,5584186	9,12951168	6	8	6	942	104,643		0,79	-0,26	1,05	0
High	Q5VTL8	Pre-mRNA-splicing factor 38B [OS=Homo sapiens]	15,5256977	7,69230769	5	9	5	546	64,429	PRPF38B	0	-0,26	0,26	0
High	O14617-5	Isoform 5 of AP-3 complex subunit delta-1 [OS=Homo sapiens]	6,24635261	1,97530864	2	2	2	1215	136,565	AP3D1	-0,38	-0,26	-0,12	0
Medium	P45954	Short/branched chain specific acyl-CoA dehydrogenase, mitochondrial [OS=Hor	2,43663759	1,85185185	1	1	1	432	47,455	ACADSB	-0,22	-0,26	0,04	0
Low	Q6ZW31-1	Rho GTPase-activating protein SYDE1 [OS=Homo sapiens]	1,5079384	1,63265306	1	1	1	735	79,743	SYDE1	0,12	-0,26	0,37	0
High	Q969Q0	60S ribosomal protein L36a-like [OS=Homo sapiens]	143,334135	44,3396226	10	72	1	106	12,461	RPL36AL	-0,08	-0,27	0,19	0
High	Q16531	DNA damage-binding protein 1 [OS=Homo sapiens]	93,4904837	25,1754386	22	34	22	1140	126,887	DDB1	-0,17	-0,27	0,11	0
High	Q8N6R0-5	Methyltransferase-like protein 13 [OS=Homo sapiens]	34,4520372	10,0143062	7	12	7	699	78,718	METTL13	0,1	-0,27	0,38	0
High	P53597	Succinyl-CoA ligase [ADP/GDP-forming] subunit alpha, mitochondrial [OS=Homo	17,8239568	12,1387283	3	6	3	346	36,227	SUCLG1	-0,22	-0,27	0,05	0
High	Q8IWA0	WD repeat-containing protein 75 [OS=Homo sapiens]	7,38863221	4,09638554	3	4	3	830	94,438	WDR75	0,49	-0,27	0,76	0
High	Q01081	Splicing factor U2AF 35 kDa subunit [OS=Homo sapiens]	217,891217	51,25	13	83	13	240	27,854	OC102724594	-0,16	-0,28	0,13	0
High	P62910	60S ribosomal protein L32 [OS=Homo sapiens]	65,1406165	39,2592593	7	16	7	135	15,85	RPL32	-0,13	-0,28	0,15	0
High	Q9Y5B9	FACT complex subunit SPT16 [OS=Homo sapiens]	9,4066584	4,48901624	3	5	3	1047	119,838	SUPT16H	-1,06	-0,28	-0,78	0
High	Q9Y3B4	Splicing factor 3B subunit 6 [OS=Homo sapiens]	5,30519151	26,4	3	4	3	125	14,576	5F3B14; SF3B	-1,38	-0,28	-1,1	0
High	P68104	Elongation factor 1-alpha 1 [OS=Homo sapiens]	192,457137	52,8138528	19	84	19	462	50,109	EEF1A1	-0,81	-0,29	-0,52	0
High	Q15365	Poly(RC)-binding protein 1 [OS=Homo sapiens]	115,147953	67,4157303	16	35	11	356	37,474	PCBP1	-0,49	-0,29	-0,19	8
High	P53618	Coatomer subunit beta [OS=Homo sapiens]	64,7895193	14,9003148	11	21	11	953	107,074	COPB1	-0,73	-0,29	-0,43	0
High	P53985	Monocarboxylate transporter 1 [OS=Homo sapiens]	41,6189008	17,4	7	17	7	500	53,909	SLC16A1	-0,41	-0,29	-0,12	0
High	P61619	Protein transport protein Sec61 subunit alpha isoform 1 [OS=Homo sapiens]	32,9898583	16,3865546	5	9	5	476	52,231	SEC61A1	-0,38	-0,29	-0,09	0
High	P48651	phosphatidylserine synthase 1 [OS=Homo sapiens]	13,1435429	5,70824524	2	8	2	473	55,491	PTDSS1	0,35	-0,29	0,65	0
High	P40938	replication factor C subunit 3 [OS=Homo sapiens]	11,1502894	8,98876404	2	2	2	356	40,53	RFC3	-0,12	-0,29	0,17	0
High	Q9UL03	Integrator complex subunit 6 [OS=Homo sapiens]	7,02109331	2,93122886	3	4	3	887	100,326	INTS6	0,12	-0,29	0,41	0
High	Q8WTT2	Nucleolar complex protein 3 homolog [OS=Homo sapiens]	201,762809	43	32	61	32	800	92,49	NOC3L	-0,19	-0,3	0,1	0
High	Q9UGN5-1	Poly [ADP-ribose] polymerase 2 [OS=Homo sapiens]	189,997391	44,2538593	25	54	25	583	66,164	PARP2	0,21	-0,3	0,51	0
High	Q99623	Prohibitin-2 [OS=Homo sapiens]	32,6386419	27,4247492	8	10	8	299	33,276	PHB2	-1,86	-0,3	-1,56	0
Medium	Q7Z736	Pleckstrin homology domain-containing family H member 3 [OS=Homo sapiens]	3,78015361	1,51324086	1	1	1	793	85,264	PLEKHH3	-0,03	-0,3	0,27	0
Low	Q9BZL1	ubiquitin-like protein 5 [OS=Homo sapiens]	2,14819149	12,3287671	1	1	1	73	8,541	UBL5	-0,41	-0,3	-0,12	0
High	O95232-1	Luc7-like protein 3 [OS=Homo sapiens]	445,811232	62,7314815	37	287	37	432	51,435	LUC7L3	-0,16	-0,31	0,14	0
High	Q9NXF1	Testis-expressed sequence 10 protein [OS=Homo sapiens]	172,319532	36,7061356	28	53	28	929	105,608	TEX10	-0,56	-0,31	-0,24	0
High	Q14244	Ensconsin [OS=Homo sapiens]	90,4327392	25,3671562	20	37	19	749	84,002	MAP7	-0,02	-0,31	0,28	1
High	P06576	ATP synthase subunit beta, mitochondrial [OS=Homo sapiens]	84,623284	34,4045369	12	17	12	529	56,525	ATP5B	-0,27	-0,31	0,04	0
High	O00483	Cytochrome c oxidase subunit NDUFA4 [OS=Homo sapiens]	26,9792509	45,6790123	5	10	5	81	9,364	NDUFA4	-0,1	-0,31	0,21	0
High	Q16629	serine/arginine-rich splicing factor 7 [OS=Homo sapiens]	23,1583319	27,3109244	5	11	5	238	27,35	SRSF7	0,3	-0,31	0,61	0
High	Q99805	Transmembrane 9 superfamily member 2 [OS=Homo sapiens]	16,6293592	4,37405732	3	7	3	663	75,725	TM9SF2	0,01	-0,31	0,31	0
High	O94788-1	retinal dehydrogenase 2 [OS=Homo sapiens]	5,89073902	3,08880309	3	3	1	518	56,688	ALDH1A2	-0,33	-0,31	-0,02	0
High	Q9UKV8	Protein argonaute-2 [OS=Homo sapiens]	268,491408	57,9743888	38	79	38	859	97,146	AGO2; EIF2C2	-0,33	-0,32	0	0
High	Q15029	116 kDa U5 small nuclear ribonucleoprotein component [OS=Homo sapiens]	155,263681	37,5514403	27	44	26	972	109,366	EFTUD2	-0,24	-0,32	0,08	1
High	Q9NRC8	NAD-dependent protein deacetylase sirtuin-7 [OS=Homo sapiens]	83,5911391	33,5	10	19	10	400	44,87	SIRT7	0,2	-0,32	0,51	0

High	Q9NP97	Dynein light chain roadblock-type 1 [OS=Homo sapiens]	29,3533413	33,3333333	3	7	3	96	10,915	DYNLRB1	-0,13	-0,32	0,18	0
High	P02545	Prelamin-A/C [OS=Homo sapiens]	12,5597783	6,62650602	4	6	3	664	74,095	LMNA	-0,86	-0,32	-0,54	0
High	Q9P2Y4	Zinc finger protein 219 [OS=Homo sapiens]	10,0131002	8,44875346	4	4	4	722	76,83	ZNF219	-1,58	-0,32	-1,26	0
High	Q15369-1	Transcription elongation factor B polypeptide 1 [OS=Homo sapiens]	8,37543013	30,3571429	3	4	3	112	12,465	TCEB1	-0,31	-0,32	0,01	0
Low	A6NHR9-1	structural maintenance of chromosomes flexible hinge domain-containing prote	1,33086915	0,49875312	1	1	1	2005	226,231	SMCHD1	-2,15	-0,32	-1,83	0
High	P27448-5	MAP/microtubule affinity-regulating kinase 3 [OS=Homo sapiens]	200,16928	44,6215139	31	61	23	753	84,436	MARK3	-0,01	-0,33	0,32	6
High	P82914	28S ribosomal protein S15, mitochondrial [OS=Homo sapiens]	13,1439335	13,618677	4	5	4	257	29,823	MRPS15	2,29	-0,33	2,62	0
High	Q9Y5A9-1	YTH domain-containing family protein 2 [OS=Homo sapiens]	13,0293582	6,7357513	4	5	4	579	62,296	YTHDF2	-0,2	-0,33	0,13	0
High	Q8IVT5-1	kinase suppressor of Ras 1 [OS=Homo sapiens]	5,50057412	2,60021668	2	2	2	923	102,096	KSR1	0,03	-0,33	0,36	0
High	Q7L4I2-1	Arginine/serine-rich coiled-coil protein 2 [OS=Homo sapiens]	5,34581078	5,76036866	3	5	3	434	50,529	RSRC2	-0,38	-0,33	-0,05	0
Medium	Q5VYK3	Proteasome-associated protein ECM29 homolog [OS=Homo sapiens]	4,24842857	1,62601626	3	3	3	1845	204,16	KIAA0368	-0,9	-0,33	-0,57	0
High	P62854	40S ribosomal protein S26 [OS=Homo sapiens]	170,58864	52,173913	7	116	7	115	13,007	C101929876;	-0,22	-0,34	0,12	0
High	P26641-2	Isoform 2 of Elongation factor 1-gamma [OS=Homo sapiens]	124,755646	50,3080082	20	44	20	487	56,114	EEF1G	-1,16	-0,34	-0,82	0
High	O43175	D-3-phosphoglycerate dehydrogenase [OS=Homo sapiens]	107,403916	42,2138837	16	35	16	533	56,614	PHGDH	-0,6	-0,34	-0,25	0
High	P14406	Cytochrome c oxidase subunit 7A2, mitochondrial [OS=Homo sapiens]	7,40214747	15,6626506	1	2	1	83	9,39	COX7A2	-0,24	-0,34	0,1	0
Medium	Q9NU22	Midasin [OS=Homo sapiens]	3,17608859	0,37526805	2	2	2	5596	632,42	MDN1	-0,18	-0,34	0,16	0
High	P26368	Splicing factor U2AF 65 kDa subunit [OS=Homo sapiens]	441,097293	64,2105263	25	152	25	475	53,467	U2AF2	-0,19	-0,35	0,17	0
High	P25705-1	ATP synthase subunit alpha, mitochondrial [OS=Homo sapiens]	292,65724	59,3128391	27	73	27	553	59,714	ATP5A1	-0,29	-0,35	0,06	0
High	Q9NYV4-1	Cyclin-dependent kinase 12 [OS=Homo sapiens]	91,2547468	19,6644295	23	40	18	1490	164,054	CDK12	-0,31	-0,35	0,03	5
High	Q9NWT8	Aurora kinase A-interacting protein [OS=Homo sapiens]	27,7450546	10,0502513	3	9	3	199	22,34	AURKAIP1	-0,23	-0,35	0,11	0
High	Q03701	CCAAT/enhancer-binding protein zeta [OS=Homo sapiens]	11,2188959	3,98481973	4	5	4	1054	120,898	CEBPZ	0,01	-0,35	0,36	0
High	Q5JVF3-4	Isoform 4 of PCI domain-containing protein 2 [OS=Homo sapiens]	6,65700841	6,18101545	2	2	2	453	52,066	PCID2	-0,55	-0,35	-0,21	0
High	Q99459	Cell division cycle 5-like protein [OS=Homo sapiens]	155,878328	46,1346633	26	43	26	802	92,194	CDC5L	-0,24	-0,36	0,12	0
High	O14980	Exportin-1 [OS=Homo sapiens]	117,624636	27,3576097	24	40	24	1071	123,306	XPO1	-0,84	-0,36	-0,48	0
High	Q9BRT6	Protein LLP homolog [OS=Homo sapiens]	105,043339	44,9612403	6	26	6	129	15,215	LLPH	-0,44	-0,36	-0,08	0
High	P08865	40S ribosomal protein SA [OS=Homo sapiens]	87,7374086	48,1355932	10	22	10	295	32,833	RPSA	-0,23	-0,36	0,13	0
High	Q8N2M8	CLK4-associating serine/arginine rich protein [OS=Homo sapiens]	36,8895205	17,5074184	7	17	7	674	77,115	CLASRP	0,4	-0,36	0,76	0
High	Q9H5Z1	Probable ATP-dependent RNA helicase DHX35 [OS=Homo sapiens]	24,9012914	13,5135135	7	8	7	703	78,86	DHX35	-0,94	-0,36	-0,58	0
High	O95299-2	Isoform 2 of NADH dehydrogenase [ubiquinone] 1 alpha subcomplex subunit 10	9,26031036	6,06060606	3	4	3	429	48,532	NDUFA10	0,12	-0,36	0,48	0
High	P05198	Eukaryotic translation initiation factor 2 subunit 1 [OS=Homo sapiens]	6,63048039	9,84126984	3	3	3	315	36,089	EIF2S1	-0,82	-0,36	-0,46	0
High	Q9UHX1-2	Isoform 2 of Poly(U)-binding-splicing factor PUF60 [OS=Homo sapiens]	256,262206	63,2841328	27	66	27	542	58,135	PUF60	-0,19	-0,37	0,18	0
High	Q13435	Splicing factor 3b subunit 2 [OS=Homo sapiens]	70,7915471	20,1117318	16	23	16	895	100,165	SF3B2	-0,98	-0,37	-0,61	0
High	P48047	ATP synthase subunit O, mitochondrial [OS=Homo sapiens]	51,3162719	48,3568075	8	13	8	213	23,263	ATP5O	-0,23	-0,37	0,14	0
High	Q05519	serine/arginine-rich splicing factor 11 [OS=Homo sapiens]	29,8027691	12,3966942	4	13	4	484	53,51	SRSF11	-0,22	-0,37	0,15	0
High	Q14980-1	nuclear mitotic apparatus protein 1 [OS=Homo sapiens]	29,7308964	6,00472813	10	12	10	2115	238,115	NUMA1	-0,59	-0,37	-0,22	0
High	O75251	NADH dehydrogenase [ubiquinone] iron-sulfur protein 7, mitochondrial [OS=Ho	7,70295519	4,22535211	1	2	1	213	23,548	NDUFS7	-0,09	-0,37	0,28	0
High	P19474	E3 ubiquitin-protein ligase TRIM21 [OS=Homo sapiens]	496,934635	66,9473684	42	175	42	475	54,135	TRIM21	-0,32	-0,38	0,06	0
High	O95639	Cleavage and polyadenylation specificity factor subunit 4 [OS=Homo sapiens]	201,239255	61,33829	14	60	14	269	30,235	CPSF4	-0,07	-0,38	0,31	0
High	Q9UKM9-1	RNA-binding protein Raly [OS=Homo sapiens]	7,38485789	8,49673203	3	3	3	306	32,444	RALY	-1,74	-0,38	-1,36	0
Medium	O00422	Histone deacetylase complex subunit SAP18 [OS=Homo sapiens]	2,40352898	4,5751634	1	2	1	153	17,55	SAP18	-0,71	-0,38	-0,33	0
Low	O94874-1	E3 UFM1-protein ligase 1 [OS=Homo sapiens]	1,74569367	1,25944584	1	1	1	794	89,54	UFL1	-1,48	-0,38	-1,1	0
High	Q6UN15-1	Pre-mRNA 3'-end-processing factor FIP1 [OS=Homo sapiens]	482,065198	59,7643098	34	174	6	594	66,487	FIP1L1	-0,12	-0,39	0,28	43
High	P62306	Small nuclear ribonucleoprotein F [OS=Homo sapiens]	22,2586144	24,4186047	2	7	2	86	9,719	SNRPF	-0,07	-0,39	0,32	0
High	P12956	X-ray repair cross-complementing protein 6 [OS=Homo sapiens]	17,0064399	7,8817734	4	5	4	609	69,799	XRCC6	-0,54	-0,39	-0,15	0
High	Q9Y3C1	nucleolar protein 16 [OS=Homo sapiens]	146,598229	60,6741573	13	36	13	178	21,175	NOP16	0,17	-0,4	0,57	0
High	Q53H12	Acylglycerol kinase, mitochondrial [OS=Homo sapiens]	39,8469582	28,6729858	9	15	9	422	47,107	AGK	-0,35	-0,4	0,05	0
High	P40937-1	Replication factor C subunit 5 [OS=Homo sapiens]	18,7833108	16,4705882	5	6	5	340	38,472	RFC5	-0,35	-0,4	0,06	0
High	Q5XKP0	MICOS complex subunit MIC13 [OS=Homo sapiens]	8,64121076	28,8135593	3	3	3	118	13,079	C19orf70	-0,15	-0,4	0,25	0
Medium	P35606	Coatomer subunit beta' [OS=Homo sapiens]	4,54913958	1,98675497	2	3	2	906	102,422	COPB2	-0,49	-0,4	-0,09	0
Low	O43681	ATPase ASNA1 [OS=Homo sapiens]	1,06940751	2,01149425	1	1	1	348	38,767	ASNA1	-0,6	-0,4	-0,2	0
High	O00139-2	Isoform 2 of Kinesin-like protein KIF2A [OS=Homo sapiens]	43,0259034	18,1818182	10	13	10	660	74,996	KIF2A	-0,24	-0,41	0,17	0
High	O43663-1	Protein regulator of cytokinesis 1 [OS=Homo sapiens]	15,2298899	5,16129032	4	8	3	620	71,562	PRC1	-0,35	-0,41	0,06	0
Medium	Q96S44	TP53-regulating kinase [OS=Homo sapiens]	3,22381541	6,71936759	2	2	2	253	28,143	TP53RK	-0,4	-0,41	0,01	0
High	Q9UKF6	Cleavage and polyadenylation specificity factor subunit 3 [OS=Homo sapiens]	80,82251	19,4444444	11	21	11	684	77,436	CPSF3	0,09	-0,42	0,51	0
High	Q9UBB9-1	Tuftelin-interacting protein 11 [OS=Homo sapiens]	57,3921874	22,7001195	16	20	16	837	96,758	TFIP11	0,6	-0,42	1,02	0
High	O00488	Zinc finger protein 593 [OS=Homo sapiens]	19,0754954	17,1641791	2	4	2	134	15,19	ZNF593	-0,15	-0,42	0,28	0
High	P07737	profilin-1 [OS=Homo sapiens]	15,9422627	37,1428571	4	8	4	140	15,045	PFN1	-10,37	-0,42	-9,94	0
High	Q149N8	E3 ubiquitin-protein ligase SHPRH [OS=Homo sapiens]	9,01220886	2,7332145	4	4	4	1683	192,957	SHPRH	-0,74	-0,42	-0,32	0
High	P07437	tubulin beta chain [OS=Homo sapiens]	915,210706	83,3333333	31	430	5	444	49,639	TUBB	-0,37	-0,43	0,06	5
High	Q9BZI7-1	Regulator of nonsense transcripts 3B [OS=Homo sapiens]	130,662532	38,9233954	20	41	20	483	57,727	UPF3B	-0,13	-0,43	0,3	0
High	O43290	U4/U6.U5 tri-snRNP-associated protein 1 [OS=Homo sapiens]	96,3730233	28,875	16	24	16	800	90,2	SART1	-0,92	-0,43	-0,49	0
High	P78347	General transcription factor II-I [OS=Homo sapiens]	77,7468891	21,743487	19	30	19	998	112,346	GTF2I	-0,8	-0,43	-0,37	0
High	Q9Y5B6	PAX3- and PAX7-binding protein 1 [OS=Homo sapiens]	58,3897935	20,7197383	15	17	15	917	104,739	6CFC1; PAXBP	0,45	-0,43	0,88	0
High	Q86Y39-1	NADH dehydrogenase [ubiquinone] 1 alpha subcomplex subunit 11 [OS=Homo	56,8735568	57,4468085	5	13	5	141	14,843	NDUFA11	-0,28	-0,43	0,15	0

High	Q9UKV3-1	Apoptotic chromatin condensation inducer in the nucleus [OS=Homo sapiens]	35,4104819	8,12826249	9	12	9	1341	151,771	ACIN1	-0,7	-0,43	-0,27	0
High	Q96FJ2	Dynein light chain 2, cytoplasmic [OS=Homo sapiens]	34,0392244	39,3258427	5	9	2	89	10,343	DYNLL2	-0,52	-0,43	-0,09	3
High	Q53GQ0	Very-long-chain 3-oxoacyl-CoA reductase [OS=Homo sapiens]	31,1698382	18,5897436	4	9	4	312	34,302	HSD17B12	-0,11	-0,43	0,33	0
High	O14545	TRAF-type zinc finger domain-containing protein 1 [OS=Homo sapiens]	21,8979701	8,24742268	4	7	4	582	64,8	TRAFD1	0,26	-0,43	0,69	0
High	Q63HN8-4	Isoform 2 of E3 ubiquitin-protein ligase RNF213 [OS=Homo sapiens]	11,8567257	0,91324201	4	6	4	5256	596,106	RNF213	-0,65	-0,43	-0,22	0
High	Q96K58-2	Isoform 2 of Zinc finger protein 668 [OS=Homo sapiens]	9,31586597	10,7476636	4	4	4	642	70,46		-0,26	-0,43	0,17	0
High	O00566	U3 small nucleolar ribonucleoprotein protein Mpp10 [OS=Homo sapiens]	25,15691	8,95741557	4	7	4	681	78,816	MPHOSPH10	-0,26	-0,44	0,18	0
High	Q8WVS4	WD repeat-containing protein 60 [OS=Homo sapiens]	23,3041549	6,56660413	6	8	6	1066	122,496	WDR60	-0,19	-0,44	0,26	0
High	P61163	Alpha-centractin [OS=Homo sapiens]	6,97267817	7,18085106	3	3	3	376	42,587	ACTR1A	-0,8	-0,44	-0,37	0
High	O95470	sphingosine-1-phosphate lyase 1 [OS=Homo sapiens]	4,99127075	4,57746479	2	2	2	568	63,483	SGPL1	-0,62	-0,44	-0,18	0
High	P60709	Actin, cytoplasmic 1 [OS=Homo sapiens]	511,915087	77,3333333	25	165	11	375	41,71	ACTB	-0,5	-0,45	-0,05	32
High	Q16630-2	Isoform 2 of Cleavage and polyadenylation specificity factor subunit 6 [OS=Hom	217,018869	32,9931973	19	64	19	588	63,432	CPSF6	-0,51	-0,45	-0,07	0
High	Q9H9J4-1	Ubiquitin carboxyl-terminal hydrolase 42 [OS=Homo sapiens]	55,2961514	13,7462236	14	19	14	1324	145,302	USP42	-0,5	-0,45	-0,05	0
High	Q14004-1	Cyclin-dependent kinase 13 [OS=Homo sapiens]	39,1010993	8,53174603	10	16	5	1512	164,823	CDK13	-0,28	-0,45	0,17	0
High	Q9UBS4	DnaJ homolog subfamily B member 11 [OS=Homo sapiens]	4,74537036	2,23463687	1	3	1	358	40,489	DNAJB11	-0,99	-0,45	-0,53	0
High	P25490	Transcriptional repressor protein YY1 [OS=Homo sapiens]	36,5988982	21,7391304	9	14	9	414	44,685	YY1	-0,4	-0,46	0,06	0
High	O43660-1	Pleiotropic regulator 1 [OS=Homo sapiens]	23,1910149	12,6459144	5	6	5	514	57,158	PLRG1	0,1	-0,46	0,56	0
Medium	O43159	ribosomal rna-processing protein 8 [OS=Homo sapiens]	2,84496777	4,16666667	1	1	1	456	50,683	RRP8	0,06	-0,46	0,52	0
High	P68032	Actin, alpha cardiac muscle 1 [OS=Homo sapiens]	238,953912	40,3183024	16	103	3	377	41,992	ACTC1	-0,55	-0,47	-0,08	0
High	O75746	Calcium-binding mitochondrial carrier protein Aralar1 [OS=Homo sapiens]	42,2086702	14,0117994	9	14	4	678	74,715	SLC25A12	0,15	-0,47	0,61	0
High	P47914	60S ribosomal protein L29 [OS=Homo sapiens]	36,6689549	20,754717	3	20	3	159	17,741	RPL29	-0,32	-0,47	0,16	0
High	Q7L014	probable ATP-dependent RNA helicase DDX46 [OS=Homo sapiens]	366,4211	45,2958293	46	134	46	1031	117,29	DDX46	-0,44	-0,48	0,04	0
High	Q07157	Tight junction protein ZO-1 [OS=Homo sapiens]	100,963203	20,7093822	25	35	25	1748	195,34	TJP1	-0,92	-0,48	-0,44	0
High	P42695	condensin-2 complex subunit D3 [OS=Homo sapiens]	24,0867083	7,61014686	8	11	8	1498	168,783	NCAPD3	-0,17	-0,48	0,31	0
High	Q14558-2	Isoform 2 of Phosphoribosyl pyrophosphate synthase-associated protein 1 [OS=	7,77651461	7,79220779	2	4	2	385	42,44	PRPSAP1	-0,39	-0,48	0,1	0
Medium	P48444	Coatomer subunit delta [OS=Homo sapiens]	2,52607531	2,54403131	1	1	1	511	57,174	ARCN1	-1,14	-0,48	-0,66	0
High	O00541-1	Pescadillo homolog [OS=Homo sapiens]	143,010138	38,4353741	20	44	20	588	67,96	PES1	-0,35	-0,49	0,14	0
High	O60783	28S ribosomal protein S14, mitochondrial [OS=Homo sapiens]	30,0187914	21,875	2	6	2	128	15,129	MRPS14	0,04	-0,49	0,53	0
Medium	P10599-1	thioredoxin [OS=Homo sapiens]	4,39545148	8,57142857	1	2	1	105	11,73	TXN	-0,61	-0,49	-0,12	0
Medium	Q92610	Zinc finger protein 592 [OS=Homo sapiens]	3,26647687	1,89423836	2	2	2	1267	137,441	ZNF592	-0,34	-0,49	0,15	0
Medium	A3KMH1	von Willebrand factor A domain-containing protein 8 [OS=Homo sapiens]	3,01686592	1,04986877	2	2	2	1905	214,689	VWA8	0,15	-0,49	0,65	0
Medium	Q9UEG4	zinc finger protein 629 [OS=Homo sapiens]	3,68511864	2,41657077	2	2	2	869	96,559	ZNF629	-0,54	-0,5	-0,04	0
Medium	Q9Y6M4-2	Isoform 2 of Casein kinase I isoform gamma-3 [OS=Homo sapiens]	2,4285241	1,75824176	1	2	1	455	52,344	CSNK1G3	-0,03	-0,5	0,47	0
High	Q9BZF3-5	Isoform 5 of Oxysterol-binding protein-related protein 6 [OS=Homo sapiens]	255,344397	55,0573514	41	74	1	959	108,89	OSBPL6	-0,72	-0,51	-0,22	39
High	Q9UNQ2	Probable dimethyladenosine transferase [OS=Homo sapiens]	144,181397	68,6900958	21	44	21	313	35,214	DIMT1	-0,37	-0,51	0,14	0
High	Q71UM5	40S ribosomal protein S27-like [OS=Homo sapiens]	87,4280294	41,6666667	6	29	3	84	9,471	RPS27L	-0,32	-0,51	0,19	0
High	Q9H936	Mitochondrial glutamate carrier 1 [OS=Homo sapiens]	48,6937206	43,3436533	10	14	10	323	34,448	SLC25A22	-0,15	-0,51	0,36	0
High	P62316	Small nuclear ribonucleoprotein Sm D2 [OS=Homo sapiens]	15,1861058	33,0508475	3	6	3	118	13,518	SNRPD2	-0,75	-0,51	-0,23	0
High	P56945-6	Isoform 6 of Breast cancer anti-estrogen resistance protein 1 [OS=Homo sapien	495,414049	66,5938865	46	161	46	916	97,817	BCAR1	-0,25	-0,52	0,27	0
High	Q8TAA9	vang-like protein 1 [OS=Homo sapiens]	5,37861597	3,05343511	1	1	1	524	59,937	VANGL1	-0,74	-0,52	-0,22	0
High	P56182	Ribosomal RNA processing protein 1 homolog A [OS=Homo sapiens]	64,7183224	29,0672451	15	21	15	461	52,807	RRP1	0,01	-0,53	0,54	0
High	P18085	ADP-ribosylation factor 4 [OS=Homo sapiens]	27,3535644	26,6666667	4	8	2	180	20,498	ARF4	-0,64	-0,53	-0,11	1
Medium	O14734	Acyl-coenzyme A thioesterase 8 [OS=Homo sapiens]	2,41634789	2,82131661	1	1	1	319	35,891	ACOT8	-0,74	-0,53	-0,22	0
High	Q86VM9	Zinc finger CCCH domain-containing protein 18 [OS=Homo sapiens]	12,4968416	5,35152151	5	5	5	953	106,315	ZC3H18	-0,34	-0,54	0,21	0
Low	Q9H9P8-1	L-2-hydroxyglutarate dehydrogenase, mitochondrial [OS=Homo sapiens]	1,8247782	2,59179266	1	1	1	463	50,284	L2HGDH	-0,58	-0,54	-0,04	0
High	Q2TAK8-3	Isoform 3 of PWWP domain-containing protein MUM1 [OS=Homo sapiens]	16,6965586	7,11354309	4	6	4	731	80,649		0,19	-0,55	0,74	0
High	Q9H7N4	Splicing factor, arginine/serine-rich 19 [OS=Homo sapiens]	7,23260793	1,44817073	2	3	1	1312	139,186	SCAF1	-0,88	-0,55	-0,32	0
High	O43809	Cleavage and polyadenylation specificity factor subunit 5 [OS=Homo sapiens]	116,272624	58,1497797	10	28	10	227	26,211	NUDT21	-0,65	-0,56	-0,1	0
High	Q8N684-3	Isoform 3 of Cleavage and polyadenylation specificity factor subunit 7 [OS=Hom	76,492166	31,9066148	14	24	14	514	56,341	CPSF7	-0,47	-0,56	0,09	0
High	Q96QV6	Histone H2A type 1-A [OS=Homo sapiens]	55,4790174	40,4580153	5	32	1	131	14,225	HIST1H2AA	-0,07	-0,56	0,49	0
High	P51116	Fragile X mental retardation syndrome-related protein 2 [OS=Homo sapiens]	31,1383026	14,7102526	6	8	5	673	74,178	FXR2	-0,53	-0,56	0,02	1
High	P23458	Tyrosine-protein kinase JAK1 [OS=Homo sapiens]	12,3717304	5,19930676	5	6	5	1154	133,191	JAK1	-0,29	-0,56	0,27	0
High	Q9UL54-1	Serine/threonine-protein kinase TAO2 [OS=Homo sapiens]	7,08689918	3,07692308	4	4	4	1235	138,166	TAOK2	0,34	-0,56	0,9	0
Medium	Q9H3G5	Probable serine carboxypeptidase CPVL [OS=Homo sapiens]	2,47716469	2,10084034	1	1	1	476	54,129	CPVL	-1,03	-0,56	-0,46	0
High	Q92522	Histone H1x [OS=Homo sapiens]	47,6860576	36,1502347	9	17	9	213	22,474	H1FX	-0,65	-0,57	-0,08	0
High	E9PRG8	Uncharacterized protein C11orf98 [OS=Homo sapiens]	32,2835939	23,7704918	4	9	3	122	13,79	02288414; C1	-0,29	-0,57	0,27	0
High	Q86VI3	Ras GTPase-activating-like protein IQGAP3 [OS=Homo sapiens]	31,2649028	7,54138565	10	12	10	1631	184,584	IQGAP3	-0,59	-0,57	-0,03	0
High	P21953	2-oxoisovalerate dehydrogenase subunit beta, mitochondrial [OS=Homo sapien	6,61334676	11,7346939	3	3	3	392	43,095	BCKDHB	-2,56	-0,57	-1,98	0
High	O75400	pre-mRNA-processing factor 40 homolog A [OS=Homo sapiens]	329,870915	38,3490073	36	114	36	957	108,737	PRPF40A	-0,66	-0,58	-0,08	0
High	Q9UMS4	Pre-mRNA-processing factor 19 [OS=Homo sapiens]	95,2623801	30,7539683	11	23	11	504	55,146	PRPF19	-0,21	-0,58	0,37	0
High	Q14257-2	Isoform 2 of Reticulocalbin-2 [OS=Homo sapiens]	24,3039391	18,5074627	4	5	4	335	39,115	RCN2	-0,21	-0,58	0,38	0
High	P48643	T-complex protein 1 subunit epsilon [OS=Homo sapiens]	21,1737905	8,87245841	4	7	4	541	59,633	CCT5	-0,47	-0,58	0,12	0
High	Q6P087	RNA pseudouridylate synthase domain-containing protein 3 [OS=Homo sapiens	14,6059261	15,0997151	5	6	5	351	38,437	RPUSD3	-0,39	-0,58	0,19	0
High	O95696-2	Isoform 2 of Bromodomain-containing protein 1 [OS=Homo sapiens]	6,92290548	1,51387721	2	2	2	1189	133,159	RD1; LOC908	-0,59	-0,58	-0,01	0

High	P16615	Sarcoplasmic/endoplasmic reticulum calcium ATPase 2 [OS=Homo sapiens]	150,952573	29,9424184	27	46	27	1042	114,683	ATP2A2	-0,56	-0,59	0,04	0
High	Q9BSD7	Cancer-related nucleoside-triphosphatase [OS=Homo sapiens]	23,1398209	30,5263158	4	6	4	190	20,7	NTPCR	-0,48	-0,59	0,11	0
High	P17858-1	ATP-dependent 6-phosphofructokinase, liver type [OS=Homo sapiens]	13,5669429	6,41025641	3	7	3	780	84,964	PFKL	-1,15	-0,59	-0,56	0
High	Q9P2R7	Succinyl-CoA ligase [ADP-forming] subunit beta, mitochondrial [OS=Homo sapie	10,6260823	7,99136069	4	5	4	463	50,285	SUCLA2	-0,48	-0,59	0,12	0
High	Q08J23	tRNA (Cytosine(34)-C(5))-methyltransferase [OS=Homo sapiens]	183,245952	55,9322034	29	56	29	767	86,416	NSUN2	-0,66	-0,6	-0,06	0
High	Q13523	Serine/threonine-protein kinase PRP4 homolog [OS=Homo sapiens]	76,6408812	16,4846077	16	33	16	1007	116,916	PRPF4B	-0,85	-0,6	-0,26	0
High	Q12923-4	Isoform 4 of Tyrosine-protein phosphatase non-receptor type 13 [OS=Homo sa	24,6624907	6,70682731	12	15	12	2490	277,335	PTPN13	-0,47	-0,6	0,13	0
High	Q5SY16	Polynucleotide 5'-hydroxyl-kinase NOL9 [OS=Homo sapiens]	18,2149799	5,6980057	3	7	3	702	79,272	NOL9	-0,5	-0,6	0,1	0
High	P41091	eukaryotic translation initiation factor 2 subunit 3 [OS=Homo sapiens]	11,7315085	8,68644068	4	5	4	472	51,077	EIF2S3	-0,9	-0,6	-0,31	0
High	P52907	F-actin-capping protein subunit alpha-1 [OS=Homo sapiens]	11,432402	8,74125874	2	4	2	286	32,902	CAPZA1	-0,75	-0,6	-0,15	0
High	Q9P258	Protein RCC2 [OS=Homo sapiens]	30,9767214	17,816092	9	10	9	522	56,049	RCC2	-0,66	-0,61	-0,06	0
Medium	Q86XI2-2	Isoform 2 of Condensin-2 complex subunit G2 [OS=Homo sapiens]	2,79353706	1,55709343	2	2	2	1156	132,111	NCAPG2	-0,96	-0,61	-0,35	0
Low	P78346-2	Isoform 2 of Ribonuclease P protein subunit p30 [OS=Homo sapiens]	2,09307265	1,86335404	1	1	1	322	35,542	RPP30	-0,38	-0,61	0,23	0
High	Q9H0A0	N-acetyltransferase 10 [OS=Homo sapiens]	505,534323	65,9512195	65	151	64	1025	115,657	NAT10	-0,46	-0,62	0,16	1
High	Q9Y2J2	Band 4.1-like protein 3 [OS=Homo sapiens]	79,1399711	16,375345	16	24	15	1087	120,603	EPB41L3	-0,99	-0,62	-0,37	1
High	Q9H307	Pinin [OS=Homo sapiens]	50,919574	15,7601116	11	18	11	717	81,565	PNN	-1,32	-0,62	-0,71	0
High	P61964	WD repeat-containing protein 5 [OS=Homo sapiens]	24,2293454	20,6586826	4	6	4	334	36,565	WDR5	-0,64	-0,62	-0,02	0
High	Q8N1G4	Leucine-rich repeat-containing protein 47 [OS=Homo sapiens]	8,54003848	1,88679245	1	2	1	583	63,434	LRRC47	-0,26	-0,62	0,36	0
High	P63172	Dynein light chain Tctex-type 1 [OS=Homo sapiens]	7,38502501	23,0088496	2	3	2	113	12,444	DYNLT1	-0,23	-0,62	0,39	0
High	Q9BYT3-1	Serine/threonine-protein kinase 33 [OS=Homo sapiens]	91,1409464	33,07393	17	27	17	514	57,794	STK33	-0,46	-0,63	0,17	0
High	O15344-1	E3 ubiquitin-protein ligase Midline-1 [OS=Homo sapiens]	37,380239	14,3928036	9	12	9	667	75,203	MID1	-0,56	-0,63	0,07	0
High	Q9BQC6	Ribosomal protein 63, mitochondrial [OS=Homo sapiens]	7,9597541	12,745098	1	2	1	102	12,259	MRP63; MRPL5	-0,03	-0,63	0,6	0
High	P35268	60S ribosomal protein L22 [OS=Homo sapiens]	59,4156055	58,59375	6	24	5	128	14,778	RPL22	-0,61	-0,64	0,04	0
High	Q9P031	Thyroid transcription factor 1-associated protein 26 [OS=Homo sapiens]	53,4816773	33,1950207	7	16	7	241	28,652	CCDC59	-0,44	-0,64	0,2	0
High	P19447	TFIIH basal transcription factor complex helicase XPB subunit [OS=Homo sapien	36,7031342	14,0664962	9	13	9	782	89,221	ERCC3	0,91	-0,64	1,55	0
High	P84103	Serine/arginine-rich splicing factor 3 [OS=Homo sapiens]	24,0111965	30,4878049	4	9	4	164	19,318	SRSF3	-1,18	-0,64	-0,54	0
High	Q96CS3	FAS-associated factor 2 [OS=Homo sapiens]	5,48036455	3,37078652	2	3	2	445	52,591	FAF2	-0,36	-0,64	0,29	0
High	Q9UBX3-2	Isoform 2 of Mitochondrial dicarboxylate carrier [OS=Homo sapiens]	33,941594	32,7702703	8	15	8	296	32,125	SLC25A10	-0,4	-0,65	0,26	0
High	Q9H9B4	Sideroflexin-1 [OS=Homo sapiens]	30,0422322	25,4658385	7	11	7	322	35,596	SFXN1	-0,92	-0,65	-0,28	0
High	P17509	Homeobox protein Hox-B6 [OS=Homo sapiens]	12,7925099	8,92857143	2	4	1	224	25,416	HOXB6	-0,14	-0,65	0,51	0
High	Q6P5Z2	Serine/threonine-protein kinase N3 [OS=Homo sapiens]	6,09553278	0,78740157	1	3	1	889	99,358	PKN3	-0,05	-0,65	0,6	0
High	Q12986	Transcriptional repressor NF-X1 [OS=Homo sapiens]	62,9283875	17,3214286	14	20	14	1120	124,312	NFX1	-0,43	-0,66	0,22	0
High	Q9HC21	Mitochondrial thiamine pyrophosphate carrier [OS=Homo sapiens]	9,91015584	8,75	3	5	3	320	35,488	SLC25A19	-0,56	-0,66	0,1	0
High	P11177	Pyruvate dehydrogenase E1 component subunit beta, mitochondrial [OS=Homo	36,8624554	25,6267409	8	15	8	359	39,208	PDHB	-0,7	-0,67	-0,03	0
High	P51570-2	Isoform 2 of Galactokinase [OS=Homo sapiens]	30,0149725	14,4549763	5	9	5	422	45,329	GALK1	-0,77	-0,67	-0,1	0
High	Q86WJ1-1	Chromodomain-helicase-DNA-binding protein 1-like [OS=Homo sapiens]	16,9477069	8,80713489	6	7	6	897	100,921	CHD1L	-0,42	-0,67	0,25	0
High	P46821	microtubule-associated protein 1B [OS=Homo sapiens]	8,40318859	0,97244733	2	3	2	2468	270,468	MAP1B	-0,46	-0,67	0,22	0
Medium	Q9HA47-4	Isoform 4 of Uridine-cytidine kinase 1 [OS=Homo sapiens]	2,8680607	2,83687943	1	1	1	282	32,254	UCK1	-1,14	-0,67	-0,47	0
High	Q96T76-8	Isoform 5 of MMS19 nucleotide excision repair protein homolog [OS=Homo sap	16,7044958	6,75547098	5	6	5	1051	115,631		-2,09	-0,68	-1,41	0
High	Q9BU76-1	Multiple myeloma tumor-associated protein 2 [OS=Homo sapiens]	575,311229	70,7224335	34	289	34	263	29,394	C1orf35	-0,78	-0,69	-0,09	0
High	Q15542	Transcription initiation factor TFIID subunit 5 [OS=Homo sapiens]	19,8518335	9,5	6	9	6	800	86,776	TAF5	-1,21	-0,69	-0,52	0
Medium	Q9NZJ7	Mitochondrial carrier homolog 1 [OS=Homo sapiens]	3,07237304	3,0848329	1	1	1	389	41,517	MTCH1	-0,55	-0,69	0,14	0
Medium	P57740	Nuclear pore complex protein Nup107 [OS=Homo sapiens]	2,62063718	2,7027027	2	2	2	925	106,307	NUP107	-1,23	-0,69	-0,54	0
High	Q9UI30	Multifunctional methyltransferase subunit TRM112-like protein [OS=Homo sapi	22,9689778	32	3	5	3	125	14,19	TRMT112	-0,87	-0,7	-0,17	0
High	Q9P015	39S ribosomal protein L15, mitochondrial [OS=Homo sapiens]	19,9072287	21,9594595	5	5	5	296	33,399	MRPL15	-0,55	-0,7	0,16	0
Medium	Q5JWF2-1	Guanine nucleotide-binding protein G(S) subunit alpha isoforms XLas [OS=Hom	3,21084251	1,06075217	1	1	1	1037	110,956	GNAS	-3,02	-0,7	-2,31	0
High	P49756-1	RNA-binding protein 25 [OS=Homo sapiens]	380,50486	48,1613286	48	125	48	843	100,124	RBM25	-0,73	-0,71	-0,02	0
High	Q9UJS0-2	Isoform 2 of Calcium-binding mitochondrial carrier protein Aralar2 [OS=Homo s	101,661851	36,3905325	16	25	11	676	74,257	SLC25A13	-0,54	-0,71	0,18	5
High	Q14680	Maternal embryonic leucine zipper kinase [OS=Homo sapiens]	13,7494516	6,75883257	4	5	4	651	74,594	MELK	-0,17	-0,71	0,54	0
High	Q96RL1	BRCA1-A complex subunit RAP80 [OS=Homo sapiens]	13,7820218	6,39777469	3	5	3	719	79,678	UIMC1	0,21	-0,73	0,95	0
High	Q8NE71-1	ATP-binding cassette sub-family F member 1 [OS=Homo sapiens]	57,0634391	22,0118343	12	20	12	845	95,866	ABCF1	-0,42	-0,75	0,33	0
High	Q8IVF7	Formin-like protein 3 [OS=Homo sapiens]	13,0734134	5,15564202	5	5	5	1028	117,139	FMNL3	-0,49	-0,75	0,25	0
Medium	Q8TCC3-2	Isoform 2 of 39S ribosomal protein L30, mitochondrial [OS=Homo sapiens]	2,31774704	15,1832461	2	2	2	191	21,825		0,21	-0,75	0,95	0
High	Q9H4L5	Oxysterol-binding protein-related protein 3 [OS=Homo sapiens]	427,488524	73,6189402	52	118	49	887	101,16	OSBPL3	-1,1	-0,76	-0,34	4
High	Q13823	Nucleolar GTP-binding protein 2 [OS=Homo sapiens]	85,0597925	24,3502052	15	27	15	731	83,603	GNL2	-0,58	-0,76	0,18	0
High	Q9NVN8	Guanine nucleotide-binding protein-like 3-like protein [OS=Homo sapiens]	20,4851469	11,5120275	6	13	5	582	65,532	GNL3L	-0,38	-0,76	0,38	0
Medium	Q14152	Eukaryotic translation initiation factor 3 subunit A [OS=Homo sapiens]	3,13161222	1,0130246	2	2	2	1382	166,468	EIF3A	-0,92	-0,76	-0,17	0
High	Q9BUF5	Tubulin beta-6 chain [OS=Homo sapiens]	227,858287	40,3587444	13	128	2	446	49,825	TUBB6	-1,7	-0,77	-0,93	0
High	Q8IWK6	Adhesion G protein-coupled receptor A3 [OS=Homo sapiens]	122,388766	25,8894777	30	63	30	1321	146,058	ADGRA3; GPR125; ADGRA	-0,64	-0,77	0,12	0
High	Q9BZE4	Nucleolar GTP-binding protein 1 [OS=Homo sapiens]	110,986421	33,2807571	20	45	20	634	73,918	GTPBP4	-0,3	-0,77	0,47	0
High	Q1KMD3	heterogeneous nuclear ribonucleoprotein U-like protein 2 [OS=Homo sapiens]	40,0576761	18,0722892	11	14	11	747	85,052	HNRNPUL2	-1,13	-0,77	-0,36	0
High	Q9NTW7	Zinc finger protein 64 homolog, isoforms 3 and 4 [OS=Homo sapiens]	7,65230215	5,11627907	2	3	2	645	72,17	ZFP64	-1,22	-0,77	-0,45	0
Medium	O14641	Segment polarity protein dishevelled homolog DVL-2 [OS=Homo sapiens]	4,60156275	1,63043478	1	2	1	736	78,899	DVL2	-0,33	-0,77	0,44	0
High	Q13888-1	General transcription factor IIH subunit 2 [OS=Homo sapiens]	10,343519	5,82278481	2	2	2	395	44,39	GTF2H2; GTF2H	1,98	-0,78	2,76	0

High	Q8NHQ9	ATP-dependent RNA helicase DDX55 [OS=Homo sapiens]	39,3723594	17,6666667	10	13	10	600	68,503	DDX55	-0,7	-0,79	0,09	0
High	Q9NPF4	Probable tRNA N6-adenosine threonylcarbamoyltransferase [OS=Homo sapiens	6,30436626	8,95522388	2	2	2	335	36,403	OSGEP	-1,09	-0,79	-0,3	0
High	P18583-9	Isoform I of Protein SON [OS=Homo sapiens]	202,441342	19,1403082	32	86	32	2466	267,923		-1,1	-0,8	-0,3	0
High	O75382-1	Tripartite motif-containing protein 3 [OS=Homo sapiens]	13,0307723	5,37634409	3	5	3	744	80,779	TRIM3	-0,08	-0,8	0,72	0
Medium	P00558	phosphoglycerate kinase 1 [OS=Homo sapiens]	2,69580341	2,15827338	1	2	1	417	44,586	PGK1	-8,9	-0,8	-8,11	0
High	Q9UNF1	Melanoma-associated antigen D2 [OS=Homo sapiens]	15,288748	5,61056106	4	7	4	606	64,914	MAGED2	-0,68	-0,81	0,12	0
High	Q99697-2	Isoform Ptx2C of Pituitary homeobox 2 [OS=Homo sapiens]	8,80130223	8,64197531	2	2	2	324	35,773	PITX2	0,19	-0,81	1	0
High	Q02040-1	A-kinase anchor protein 17A [OS=Homo sapiens]	383,63191	45,7553957	42	193	42	695	80,686	AKAP17A	-0,9	-0,82	-0,08	0
High	Q9NNW5	WD repeat-containing protein 6 [OS=Homo sapiens]	19,0450351	8,9206066	7	7	7	1121	121,647	WDR6	-0,56	-0,82	0,26	0
High	Q9Y3A4	Ribosomal RNA-processing protein 7 homolog A [OS=Homo sapiens]	111,706129	53,5714286	12	28	12	280	32,314	RRP7A	-0,56	-0,83	0,27	0
High	Q9UK58	Cyclin-L1 [OS=Homo sapiens]	8,15312335	7,03422053	3	3	3	526	59,597	CCNL1	0,92	-0,83	1,75	0
High	Q9NPI1-2	Isoform 2 of Bromodomain-containing protein 7 [OS=Homo sapiens]	7,76782307	7,36196319	3	5	3	652	74,22	BRD7	-1,36	-0,83	-0,52	0
High	Q8TDD1-2	Isoform 2 of ATP-dependent RNA helicase DDX54 [OS=Homo sapiens]	276,795506	62,0181406	45	83	1	882	98,605	DDX54	-0,43	-0,84	0,41	0
High	Q8TAD8	Smad nuclear-interacting protein 1 [OS=Homo sapiens]	64,0363623	39,1414141	13	23	13	396	45,75	SNIP1	-0,45	-0,84	0,39	0
High	Q13427	peptidyl-prolyl cis-trans isomerase g [OS=Homo sapiens]	27,394432	11,8037135	8	18	8	754	88,564	PPIG	-0,76	-0,84	0,07	0
High	Q8WVD3-1	E3 ubiquitin-protein ligase RNF138 [OS=Homo sapiens]	12,1348047	16,3265306	4	4	4	245	28,174	RNF138	-0,34	-0,84	0,5	0
High	P11021	78 kDa glucose-regulated protein [OS=Homo sapiens]	330,041584	55,6574924	33	99	31	654	72,288	HSPA5	-0,96	-0,86	-0,1	0
High	Q96CB9	5-methylcytosine rRNA methyltransferase NSUN4 [OS=Homo sapiens]	12,7704157	10,15625	4	6	4	384	43,061	NSUN4	-1,02	-0,86	-0,15	0
High	Q9P0U4-2	Isoform 2 of CXXC-type zinc finger protein 1 [OS=Homo sapiens]	6,49176468	5,3030303	3	3	3	660	76,178	CXXC1	-0,85	-0,86	0,01	0
Low	Q9Y294	Histone chaperone ASF1A [OS=Homo sapiens]	1,54166437	3,92156863	1	1	1	204	22,954	ASF1A	-0,34	-0,86	0,52	0
High	Q9NWB6	Arginine and glutamate-rich protein 1 [OS=Homo sapiens]	193,121243	46,8864469	25	118	25	273	33,197	ARGLU1	-0,81	-0,88	0,07	0
High	O95478	Ribosome biogenesis protein NSA2 homolog [OS=Homo sapiens]	17,2643474	20	6	7	6	260	30,047	NSA2	-0,83	-0,88	0,05	0
Medium	Q9H5U6-1	Zinc finger CCHC domain-containing protein 4 [OS=Homo sapiens]	3,09750154	3,31384016	2	2	2	513	58,971	ZCCHC4	-1,02	-0,88	-0,14	0
High	Q5T8P6	RNA-binding protein 26 [OS=Homo sapiens]	221,207603	31,1817279	34	69	0	1007	113,527	RBM26	-0,73	-0,89	0,16	28
High	Q7KZI7-1	Serine/threonine-protein kinase MARK2 [OS=Homo sapiens]	120,52179	35,2791878	21	36	13	788	87,856	MARK2	-0,43	-0,89	0,46	0
High	P45880-1	Isoform 1 of Voltage-dependent anion-selective channel protein 2 [OS=Homo sa	12,7750845	11,6504854	3	4	3	309	33,351	VDAC2	-0,73	-0,89	0,16	0
Medium	Q00403	Transcription initiation factor IIB [OS=Homo sapiens]	4,40557292	8,2278481	3	3	3	316	34,811	GTF2B	-0,17	-0,89	0,71	0
High	Q9H6R4-1	Nucleolar protein 6 [OS=Homo sapiens]	235,168713	43,8045375	35	62	35	1146	127,513	NOL6	-0,12	-0,91	0,79	0
High	Q9BUQ8	Probable ATP-dependent RNA helicase DDX23 [OS=Homo sapiens]	36,7642383	15,3658537	11	14	11	820	95,524	DDX23	-1,26	-0,91	-0,35	0
High	Q6IAN0	Dehydrogenase/reductase SDR family member 7B [OS=Homo sapiens]	5,8410463	8,30769231	2	2	2	325	35,097	DHRS7B	-0,82	-0,91	0,09	0
High	Q9UJV9	Probable ATP-dependent RNA helicase DDX41 [OS=Homo sapiens]	764,716405	88,1028939	62	268	62	622	69,793	DDX41	-0,81	-0,92	0,11	0
High	Q5BKY9-1	Protein FAM133B [OS=Homo sapiens]	30,289539	25,1012146	5	16	3	247	28,368	FAM133B	-0,48	-0,92	0,44	2
Medium	O75530-2	Isoform 2 of Polycomb protein EED [OS=Homo sapiens]	3,78166935	4,72103004	2	2	2	466	53,027	EED	-0,8	-0,92	0,13	0
Low	Q9UPT9-1	ubiquitin carboxyl-terminal hydrolase 22 [OS=Homo sapiens]	1,43415218	1,33333333	1	1	1	525	59,921	USP22	-0,59	-0,92	0,33	0
High	Q9UDY2	Tight junction protein ZO-2 [OS=Homo sapiens]	233,024375	44,2857143	47	118	47	1190	133,876	TJP2	-0,91	-0,93	0,01	0
High	Q96ME7	Zinc finger protein 512 [OS=Homo sapiens]	126,124945	42,3280423	18	35	18	567	64,641	ZNF512	-0,81	-0,93	0,13	0
High	Q9BYW2	Histone-lysine N-methyltransferase SETD2 [OS=Homo sapiens]	46,0390294	8,54134165	20	20	20	2564	287,418	SETD2	-0,75	-0,93	0,18	0
High	Q9NWQ4	G patch domain-containing protein 2-like [OS=Homo sapiens]	21,0349046	12,6556017	6	8	6	482	54,226	GPATCH2L	-0,8	-0,93	0,14	0
High	Q6PCB5-1	Round spermatid basic protein 1-like protein [OS=Homo sapiens]	14,8224431	6,61938534	5	5	5	846	94,81	RSBN1L	-1,05	-0,93	-0,12	0
High	Q9Y5J1	U3 small nucleolar RNA-associated protein 18 homolog [OS=Homo sapiens]	38,8179592	20,5035971	7	9	7	556	61,964	UTP18	0,12	-0,94	1,06	0
High	Q12894-2	Isoform 2 of Interferon-related developmental regulator 2 [OS=Homo sapiens]	5,82679718	1,48026316	1	3	1	608	65,557	IFRD2	-0,75	-0,94	0,19	0
Medium	A8MWD9	Putative small nuclear ribonucleoprotein G-like protein 15 [OS=Homo sapiens]	3,80219695	17,1052632	1	2	1	76	8,538	0130932; SNR	-0,44	-0,94	0,5	0
High	Q8TDD1	ATP-dependent RNA helicase DDX54 [OS=Homo sapiens]	270,413359	61,9750284	45	81	1	881	98,534	DDX54	-0,75	-0,95	0,2	40
High	P48735	Isocitrate dehydrogenase [NADP], mitochondrial [OS=Homo sapiens]	22,3102924	13,4955752	5	6	5	452	50,877	IDH2	-1,23	-0,95	-0,28	0
High	P14618	Pyruvate kinase PKM [OS=Homo sapiens]	12,7236813	7,53295669	4	4	4	531	57,9	PKM	-2,34	-0,95	-1,39	0
High	Q9BVP2	Guanine nucleotide-binding protein-like 3 [OS=Homo sapiens]	902,607587	65,9380692	45	376	44	549	61,954	GNL3	-1,08	-0,96	-0,12	2
High	O75319-1	RNA/RNP complex-1-interacting phosphatase [OS=Homo sapiens]	27,5205605	24,5454545	6	7	6	330	38,915	DUSP11	-0,63	-0,96	0,33	0
High	Q8WXX5	dnaJ homolog subfamily C member 9 [OS=Homo sapiens]	25,2446028	15,3846154	4	8	4	260	29,891	DNAJC9	0,07	-0,96	1,03	0
Medium	Q9UDR5	Alpha-aminoadipic semialdehyde synthase, mitochondrial [OS=Homo sapiens]	4,40082383	3,67170626	2	2	2	926	102,066	AASS	-0,59	-0,96	0,37	0
High	Q7Z7C8-4	Isoform 3 of Transcription initiation factor TFIID subunit 8 [OS=Homo sapiens]	42,8250457	16,2721893	3	9	3	338	37,388	TAF8	-0,99	-0,97	-0,02	0
Medium	O75880	Protein SCO1 homolog, mitochondrial [OS=Homo sapiens]	2,86327943	5,31561462	1	1	1	301	33,793	SCO1	-0,39	-0,97	0,58	0
High	Q9H8G2-1	Caspase activity and apoptosis inhibitor 1 [OS=Homo sapiens]	162,422119	47,9224377	18	50	18	361	38,344	CAAP1	-1,11	-0,98	-0,13	0
Medium	Q96IU4	Alpha/beta hydrolase domain-containing protein 14B [OS=Homo sapiens]	2,46117501	6,19047619	1	1	1	210	22,332	ABHD14B	-0,87	-0,98	0,11	0
Low	Q9BXW9-1	Isoform 1 of Fanconi anemia group D2 protein [OS=Homo sapiens]	1,90239567	0,67980965	1	1	1	1471	166,356	FANCD2	-1,84	-0,98	-0,86	0
High	P15924-1	Desmoplakin [OS=Homo sapiens]	43,2111079	7,035876	20	20	20	2871	331,569	DSP	-1,91	-0,99	-0,91	0
High	Q9HCM4	Band 4.1-like protein 5 [OS=Homo sapiens]	495,432427	72,3055935	41	190	15	733	81,805	EPB41L5	-0,31	-1,01	0,7	41
High	P43490	nicotinamide phosphoribosyltransferase [OS=Homo sapiens]	10,4363201	8,14663951	4	4	4	491	55,487	NAMPT	-0,42	-1,01	0,59	0
High	Q8WVK2	U4/U6.U5 small nuclear ribonucleoprotein 27 kDa protein [OS=Homo sapiens]	19,4308002	23,2258065	3	4	3	155	18,849	SNRNP27	-0,6	-1,03	0,42	0
Medium	P00966	Argininosuccinate synthase [OS=Homo sapiens]	2,31318505	1,69902913	1	2	1	412	46,501	ASS1	-0,68	-1,03	0,35	0
High	Q5T8P6-2	Isoform 2 of RNA-binding protein 26 [OS=Homo sapiens]	225,983664	32,5534079	34	69	1	983	110,956	RBM26	-0,65	-1,04	0,39	0
High	Q13393-2	Isoform PLD1B of Phospholipase D1 [OS=Homo sapiens]	80,2908969	23,1660232	19	28	19	1036	119,618	PLD1	-0,74	-1,04	0,3	0
High	Q66PJ3-2	Isoform 2 of ADP-ribosylation factor-like protein 6-interacting protein 4 [OS=Ho	50,8855477	18,6440678	8	28	3	413	44,132	ARL6IP4	-0,98	-1,05	0,06	10
High	Q9NY93	Probable ATP-dependent RNA helicase DDX56 [OS=Homo sapiens]	37,4426797	16,8190128	8	12	8	547	61,551	DDX56	0,01	-1,05	1,06	0
High	P07305	Histone H1.0 [OS=Homo sapiens]	74,0210513	32,4742268	8	38	8	194	20,85	H1F0	-0,94	-1,06	0,12	0

High	Q99590-1	protein SCAF11 [OS=Homo sapiens]	16,1206392	5,80997949	8	8	8	1463	164,551	SCAF11	-1,29	-1,06	-0,24	0
High	Q02978	Mitochondrial 2-oxoglutarate/malate carrier protein [OS=Homo sapiens]	155,405456	66,2420382	17	60	17	314	34,04	SLC25A11	-1,1	-1,07	-0,03	0
Medium	Q93034	Cullin-5 [OS=Homo sapiens]	2,83209219	1,53846154	1	1	1	780	90,897	CUL5	-0,33	-1,07	0,73	0
High	Q9Y324	rRNA-processing protein FCF1 homolog [OS=Homo sapiens]	75,1012826	34,8484848	8	19	8	198	23,354	FCF1	-0,07	-1,08	1,01	0
High	O95373	Importin-7 [OS=Homo sapiens]	36,1481156	11,3680154	8	11	7	1038	119,44	IPO7	-0,7	-1,08	0,38	1
Medium	Q5VUG0	Scm-like with four MBT domains protein 2 [OS=Homo sapiens]	3,82613696	1,67785235	2	2	2	894	100,498	SFMBT2	-0,62	-1,08	0,46	0
High	Q3KQU3	MAP7 domain-containing protein 1 [OS=Homo sapiens]	24,2755929	14,863258	9	10	8	841	92,764	MAP7D1	-0,87	-1,09	0,22	0
High	Q9BVJ6-1	U3 small nucleolar RNA-associated protein 14 homolog A [OS=Homo sapiens]	88,0799249	39,8184176	24	31	24	771	87,924	UTP14A	-0,25	-1,1	0,85	0
Medium	Q96AG4	Leucine-rich repeat-containing protein 59 [OS=Homo sapiens]	4,38197014	6,84039088	2	3	2	307	34,909	LRRC59	-0,06	-1,1	1,04	0
Medium	P42224-1	Signal transducer and activator of transcription 1-alpha/beta [OS=Homo sapien	2,54821356	1,73333333	1	1	1	750	87,28	STAT1	-0,44	-1,1	0,67	0
High	Q9BQ39	ATP-dependent RNA helicase DDX50 [OS=Homo sapiens]	142,925692	33,7856174	21	48	18	737	82,514	DDX50	-1,11	-1,11	0	2
High	P49761	Dual specificity protein kinase CLK3 [OS=Homo sapiens]	83,6663174	21,4733542	13	28	13	638	73,469	CLK3	-0,91	-1,11	0,2	0
High	Q9BVA1	Tubulin beta-2B chain [OS=Homo sapiens]	785,562376	75,9550562	29	366	1	445	49,921	TUBB2B	-1,49	-1,12	-0,37	6
High	O94813	Slit homolog 2 protein [OS=Homo sapiens]	407,038221	40,8109876	55	155	55	1529	169,759	SLIT2	-0,16	-1,12	0,96	0
High	Q9BZF3	Oxysterol-binding protein-related protein 6 [OS=Homo sapiens]	263,262962	57,0663812	41	76	1	934	106,239	OSBPL6	-1,61	-1,12	-0,49	0
High	P11310-2	Isoform 2 of Medium-chain specific acyl-CoA dehydrogenase, mitochondrial [OS	30,4246016	23,7647059	8	11	8	425	46,99	ACADM	-0,76	-1,12	0,36	0
High	Q9BVS4	Serine/threonine-protein kinase rio2 [OS=Homo sapiens]	18,5939794	12,1376812	5	5	5	552	63,243	RIOK2	-0,51	-1,12	0,62	0
High	Q2NL82	Pre-rRNA-processing protein TSR1 homolog [OS=Homo sapiens]	301,305036	52,1144279	38	87	38	804	91,752	TSR1	-0,97	-1,14	0,18	0
High	Q6ZUT1-2	Isoform 2 of Uncharacterized protein C11orf57 [OS=Homo sapiens]	123,875394	39,5904437	14	34	14	293	34,176	C11orf57	-1,07	-1,15	0,08	0
High	Q86Y91-4	Isoform 4 of Kinesin-like protein KIF18B [OS=Homo sapiens]	12,6066915	4,9255441	4	4	4	873	95,069		-0,68	-1,15	0,47	0
High	Q9UPQ9-1	Isoform 2 of Trinucleotide repeat-containing gene 6B protein [OS=Homo sapien	23,3579933	5,39756239	7	10	7	1723	182,703	TNRC6B	-0,92	-1,17	0,25	0
High	E9PAV3	Nascent polypeptide-associated complex subunit alpha, muscle-specific form [C	7,07798338	1,29932628	2	3	2	2078	205,295	NACA	-1,41	-1,17	-0,25	0
High	Q9Y5V3-2	Isoform 2 of Melanoma-associated antigen D1 [OS=Homo sapiens]	5,58633162	5,63549161	3	3	3	834	91,901	MAGED1	-1,95	-1,17	-0,77	0
High	Q8IY81	pre-rRNA processing protein FTSJ3 [OS=Homo sapiens]	219,464163	45,4545455	36	66	36	847	96,499	FTSJ3	-0,62	-1,19	0,57	0
High	P04406-1	glyceraldehyde-3-phosphate dehydrogenase [OS=Homo sapiens]	80,4054294	56,119403	11	23	11	335	36,03	GAPDH	-2,79	-1,19	-1,6	0
High	Q8WXA9-2	Isoform 2 of Splicing regulatory glutamine/lysine-rich protein 1 [OS=Homo sapie	19,4037965	4,6474359	2	6	2	624	71,606	SREK1	-0,82	-1,19	0,37	0
High	Q71RC2-4	Isoform 4 of La-related protein 4 [OS=Homo sapiens]	10,5605258	4,79452055	2	4	2	730	81,193	LARP4	-0,36	-1,19	0,82	0
Medium	Q7Z4Q2	HEAT repeat-containing protein 3 [OS=Homo sapiens]	2,35634996	1,91176471	1	1	1	680	74,535	HEATR3	0,02	-1,19	1,2	0
Low	Q8IXI2-3	Isoform 3 of Mitochondrial Rho GTPase 1 [OS=Homo sapiens]	1,18269912	1,1577424	1	1	1	691	79,496	RHOT1	-1,28	-1,19	-0,09	0
High	O95104	Splicing factor, arginine/serine-rich 15 [OS=Homo sapiens]	97,5751769	22,929381	20	45	20	1147	125,79	SCAF4	-1,19	-1,2	0,01	0
High	Q8N3E9	1-phosphatidylinositol 4,5-bisphosphate phosphodiesterase delta-3 [OS=Homo	440,090793	70,2154626	43	113	43	789	89,202	PLCD3	-1,16	-1,21	0,05	0
High	Q8TER5-4	Isoform 4 of Rho guanine nucleotide exchange factor 40 [OS=Homo sapiens]	60,239074	16,1114888	19	27	19	1471	159,599	ARHGEF40	-0,34	-1,21	0,86	0
High	Q8N9Q2	protein SREK1IP1 [OS=Homo sapiens]	38,3282055	26,4516129	6	24	6	155	18,166	SREK1IP1	-0,24	-1,21	0,96	0
High	Q8N1G0	zinc finger protein 687 [OS=Homo sapiens]	15,6194627	4,04203719	4	8	4	1237	129,446	ZNF687	-0,68	-1,21	0,53	0
Medium	Q9NR12-1	PDZ and LIM domain protein 7 [OS=Homo sapiens]	2,75080164	2,62582057	1	1	1	457	49,813	PDLIM7	-1,25	-1,21	-0,04	0
High	Q8IZ69	tRNA (uracil-5-)-methyltransferase homolog A [OS=Homo sapiens]	16,4974639	6,56	4	6	4	625	68,682	TRMT2A	-0,59	-1,22	0,63	0
Medium	Q96EK4	THAP domain-containing protein 11 [OS=Homo sapiens]	4,30149484	2,5477707	1	2	1	314	34,433	THAP11	-0,49	-1,22	0,73	0
High	Q15154-1	Pericentriolar material 1 protein [OS=Homo sapiens]	184,377932	29,1007905	40	56	40	2024	228,392	PCM1	-1,64	-1,24	-0,4	0
High	Q9H5H4	Zinc finger protein 768 [OS=Homo sapiens]	31,3409066	15,9259259	8	10	8	540	60,191	ZNF768	-0,61	-1,24	0,62	0
High	Q7Z7H8-2	Isoform 2 of 39S ribosomal protein L10, mitochondrial [OS=Homo sapiens]	5,58787559	7,01107011	1	1	1	271	30,288	MRPL10	-1,11	-1,24	0,13	0
Low	P49848-3	Isoform 3 of Transcription initiation factor TFIID subunit 6 [OS=Homo sapiens]	1,24389663	1,12044818	1	1	1	714	76,947	TAF6	-1,72	-1,24	-0,47	0
High	Q13428-3	Isoform 3 of Treacle protein [OS=Homo sapiens]	125,507398	17,5285426	25	60	25	1489	152,114	TCOF1	-2,87	-1,26	-1,61	0
High	P11171-1	protein 4.1 [OS=Homo sapiens]	21,9606686	10,0694444	7	9	6	864	96,957	EPB41	-1,09	-1,26	0,17	0
High	Q9UJZ1	Stomatin-like protein 2, mitochondrial [OS=Homo sapiens]	7,93655518	8,70786517	2	3	2	356	38,51	STOML2	-2,01	-1,26	-0,76	0
Medium	P24928	DNA-directed RNA polymerase II subunit RPB1 [OS=Homo sapiens]	3,28166833	1,72588832	2	2	2	1970	217,039	POLR2A	-6,95	-1,26	-5,69	0
High	Q96P11-2	Isoform 2 of Probable 28S rRNA (cytosine-C(5))-methyltransferase [OS=Homo sa	43,0223974	26,6094421	10	13	10	466	50,379	NSUN5	-1,09	-1,28	0,19	0
High	Q96I25	Splicing factor 45 [OS=Homo sapiens]	39,3802565	20,9476309	7	12	6	401	44,934	RBM17	-1,22	-1,28	0,06	2
Medium	O60701	UDP-glucose 6-dehydrogenase [OS=Homo sapiens]	4,25845448	2,0242915	1	1	1	494	54,989	UGDH	-2,24	-1,28	-0,95	0
High	O14981	TATA-binding protein-associated factor 172 [OS=Homo sapiens]	5,76649076	2,3255814	3	3	3	1849	206,756	BTAF1	-0,75	-1,29	0,53	0
High	Q14562	ATP-dependent RNA helicase dhx8 [OS=Homo sapiens]	302,183724	56,557377	55	102	53	1220	139,227	DHX8	-0,93	-1,3	0,37	0
High	Q14331	Protein FRG1 [OS=Homo sapiens]	19,2044713	17,4418605	4	5	4	258	29,154	FRG1	-1,15	-1,3	0,15	0
Medium	Q14966-1	Zinc finger protein 638 [OS=Homo sapiens]	2,64282774	0,85945399	1	1	1	1978	220,488	ZNF638	-0,73	-1,3	0,57	0
High	O43709-1	Probable 18S rRNA (guanine-N(7))-methyltransferase [OS=Homo sapiens]	7,64926437	12,0996441	2	2	2	281	31,86	WBSCR22	-1,17	-1,32	0,14	0
High	P63208	s-phase kinase-associated protein 1 [OS=Homo sapiens]	22,0180564	40,4907975	6	6	6	163	18,646	SKP1	-1,09	-1,33	0,23	0
High	P62314	Small nuclear ribonucleoprotein Sm D1 [OS=Homo sapiens]	24,168948	27,7310924	2	6	2	119	13,273	SNRPD1	-1,4	-1,34	-0,06	0
High	Q9NP64	nucleolar protein of 40 kDa [OS=Homo sapiens]	336,765654	63,9004149	19	130	19	241	27,552	ZCCHC17	-1,27	-1,36	0,08	0
High	P55081	microfibrillar-associated protein 1 [OS=Homo sapiens]	128,569572	45,1025057	18	33	18	439	51,927	MFAP1	-0,54	-1,36	0,82	0
Medium	O43172-1	U4/U6 small nuclear ribonucleoprotein Prp4 [OS=Homo sapiens]	3,05581354	2,68199234	1	1	1	522	58,412	PRPF4	-1,23	-1,36	0,13	0
High	O00268	Transcription initiation factor TFIID subunit 4 [OS=Homo sapiens]	11,1927819	3,22580645	3	3	3	1085	110,047	TAF4	-1,3	-1,37	0,06	0
High	Q86U06-1	probable RNA-binding protein 23 [OS=Homo sapiens]	96,9528709	33,4851936	12	45	9	439	48,701	RBM23	-1,06	-1,38	0,32	0
High	Q7Z7K6-3	Isoform 3 of Centromere protein V [OS=Homo sapiens]	78,7266632	51,4705882	11	20	1	272	29,712	CENPV	-1,25	-1,39	0,14	11
High	Q9P1Y6-1	PHD and RING finger domain-containing protein 1 [OS=Homo sapiens]	60,8163015	13,4627047	16	29	15	1649	178,557	PHRF1	-1,54	-1,39	-0,15	1
High	P09543-1	2',3'-cyclic-nucleotide 3'-phosphodiesterase [OS=Homo sapiens]	7,14266195	8,0760095	2	2	2	421	47,549	CNP	-1,58	-1,4	-0,18	0
High	O15042	U2 snRNP-associated SURP motif-containing protein [OS=Homo sapiens]	144,644309	39,941691	33	60	33	1029	118,219	U2SURP	-1,62	-1,41	-0,21	0

High	O75815-1	Breast cancer anti-estrogen resistance protein 3 [OS=Homo sapiens]	139,166545	44,1212121	30	43	29	825	92,507	BCAR3	-1	-1,41	0,41	1
High	A8MW92-2	Isoform 2 of PHD finger protein 20-like protein 1 [OS=Homo sapiens]	18,3979617	28,0701754	7	7	1	285	32,805	PHF20L1	-2,62	-1,43	-1,2	0
Low	Q53GS9	U4/U6.U5 tri-snRNP-associated protein 2 [OS=Homo sapiens]	1,90274269	3,36283186	1	1	1	565	65,34	USP39	-1,4	-1,43	0,03	0
High	P21741	Midkine [OS=Homo sapiens]	45,2857759	48,951049	6	14	6	143	15,575	MDK	-1,53	-1,45	-0,08	0
High	P50454	Serpin H1 [OS=Homo sapiens]	15,8523594	16,507177	4	4	4	418	46,411	SERPINH1	-0,82	-1,45	0,63	0
High	O14773	Tripeptidyl-peptidase 1 [OS=Homo sapiens]	5,50612389	2,48667851	1	2	1	563	61,21	TPP1	-2,05	-1,47	-0,58	0
High	Q8NAV1-1	Pre-mRNA-splicing factor 38A [OS=Homo sapiens]	27,8947465	27,5641026	7	9	7	312	37,453	PRPF38A	-0,82	-1,5	0,68	0
Medium	Q9UL40-2	Isoform 2 of Zinc finger protein 346 [OS=Homo sapiens]	4,2276699	7,8369906	2	2	2	319	35,748	ZNF346	-0,08	-1,5	1,42	0
High	Q8TA86	retinitis pigmentosa 9 protein [OS=Homo sapiens]	54,1948098	31,2217195	9	26	9	221	26,091	RP9	-0,7	-1,51	0,81	0
High	Q12962	transcription initiation factor TFIID subunit 10 [OS=Homo sapiens]	4,801893	6,42201835	1	1	1	218	21,698	TAF10	-1,85	-1,51	-0,34	0
High	Q9UBU9-1	nuclear RNA export factor 1 [OS=Homo sapiens]	28,5362736	10,5008078	5	8	5	619	70,139	NXF1	-1,25	-1,52	0,27	0
High	Q05707-1	Collagen alpha-1(XIV) chain [OS=Homo sapiens]	17,1579754	5,56792873	8	8	8	1796	193,394	COL14A1	-0,61	-1,52	0,91	0
Low	Q6IEG0-1	U11/U12 small nuclear ribonucleoprotein 48 kDa protein [OS=Homo sapiens]	1,0616304	3,83480826	1	1	1	339	39,941	SNRNP48	-0,02	-1,52	1,5	0
High	Q13885	Tubulin beta-2A chain [OS=Homo sapiens]	780,378483	67,1910112	28	363	1	445	49,875	TUBB2A	-1,41	-1,54	0,13	0
Medium	O00410-3	Isoform 3 of Importin-5 [OS=Homo sapiens]	4,20205142	2,33183857	2	2	2	1115	125,464	IPO5	-2,15	-1,54	-0,61	0
Low	Q96SK2	Transmembrane protein 209 [OS=Homo sapiens]	1,3638131	2,85204991	1	1	1	561	62,881	TMEM209	-0,87	-1,57	0,7	0
High	O15397-1	Importin-8 [OS=Homo sapiens]	14,0269027	3,08582449	3	5	2	1037	119,861	IPO8	-1,59	-1,58	-0,01	0
High	P30414	NK-tumor recognition protein [OS=Homo sapiens]	8,33045913	2,73597811	3	3	3	1462	165,577	NKTR	-1,74	-1,58	-0,16	0
High	P35579-1	Myosin-9 [OS=Homo sapiens]	558,932482	54,744898	103	170	90	1960	226,392	MYH9	-2,68	-1,59	-1,09	11
High	Q9NVF7-1	F-box only protein 28 [OS=Homo sapiens]	126,800917	47,2826087	19	48	19	368	41,123	FBXO28	-0,74	-1,59	0,85	0
High	A8MW92	PHD finger protein 20-like protein 1 [OS=Homo sapiens]	37,7801303	16,4208456	12	12	6	1017	114,938	PHF20L1	-2,09	-1,59	-0,5	4
High	Q9H9Y2	Ribosome production factor 1 [OS=Homo sapiens]	13,2036689	9,16905444	3	4	3	349	40,086	RPF1	-1,01	-1,59	0,58	0
Medium	Q9UI10-2	Isoform 2 of Translation initiation factor eIF-2B subunit delta [OS=Homo sapien	2,9303319	2,57826888	1	1	1	543	59,578	EIF2B4	-0,73	-1,59	0,86	0
High	Q6DKI1	60S ribosomal protein L7-like 1 [OS=Homo sapiens]	8,69757192	15,4471545	3	3	3	246	28,643	RPL7L1	-1,94	-1,6	-0,34	0
High	Q8N5F7	NF-kappa-B-activating protein [OS=Homo sapiens]	69,1390875	24,8192771	9	31	9	415	47,11	NKAP	-0,86	-1,62	0,76	0
High	P50897	Palmitoyl-protein thioesterase 1 [OS=Homo sapiens]	19,6443201	7,84313725	2	4	2	306	34,171	PPT1	-1,48	-1,63	0,15	0
High	Q9NVI1-3	Fanconi anemia group I protein [OS=Homo sapiens]	5,2692987	2,10843373	3	3	3	1328	149,229	FANCI	-1,32	-1,65	0,33	0
High	Q96GQ7	Probable ATP-dependent RNA helicase DDX27 [OS=Homo sapiens]	84,9716213	29,3969849	21	30	21	796	89,779	DDX27	-1,09	-1,66	0,57	0
High	Q6B0I6	Lysine-specific demethylase 4D [OS=Homo sapiens]	12,9343582	10,5162524	4	4	4	523	58,565	KDM4D	-1,39	-1,66	0,27	0
High	Q9Y3A2	Probable U3 small nucleolar RNA-associated protein 11 [OS=Homo sapiens]	37,6853831	33,9920949	10	14	10	253	30,428	UTP11L; UTP1	-1,29	-1,67	0,39	0
High	Q86YT6	E3 ubiquitin-protein ligase mib1 [OS=Homo sapiens]	31,9749335	11,6302187	10	10	10	1006	110,066	MIB1	-2,18	-1,72	-0,46	0
High	Q13206	probable ATP-dependent RNA helicase DDX10 [OS=Homo sapiens]	9,59778935	4,11428571	3	3	3	875	100,825	DDX10	0,09	-1,74	1,83	0
High	O94876	Transmembrane and coiled-coil domains protein 1 [OS=Homo sapiens]	5,25178933	2,29709035	1	2	1	653	72,038	TMCC1	-0,65	-1,8	1,15	0
High	Q9ULS5	Transmembrane and coiled-coil domains protein 3 [OS=Homo sapiens]	189,445114	52,2012579	25	75	25	477	53,752	TMCC3	-1,35	-1,81	0,45	0
High	O43795	Unconventional myosin-Ib [OS=Homo sapiens]	5,12758788	2,64084507	3	3	3	1136	131,902	MYO1B	-3,72	-1,81	-1,91	0
High	Q9UBM7	7-dehydrocholesterol reductase [OS=Homo sapiens]	33,5439749	12,4210526	6	11	6	475	54,454	DHCR7	-1,77	-1,83	0,06	0
High	Q9Y2L1-1	exosome complex exonuclease RRP44 [OS=Homo sapiens]	62,6392095	21,8162839	17	20	17	958	108,934	DIS3	-2,52	-1,85	-0,67	0
High	Q99959	Plakophilin-2 [OS=Homo sapiens]	24,5654549	11,0102157	8	8	8	881	97,355	PKP2	-2,17	-1,87	-0,3	0
Low	O95071	E3 ubiquitin-protein ligase UBR5 [OS=Homo sapiens]	2,13065092	0,28581636	1	1	1	2799	309,158	UBR5	-0,95	-1,87	0,92	0
High	Q96JM3	Chromosome alignment-maintaining phosphoprotein 1 [OS=Homo sapiens]	13,3404779	9,85221675	5	5	5	812	89,043	CHAMP1	-1,75	-1,95	0,19	0
High	Q9BXS6	Nucleolar and spindle-associated protein 1 [OS=Homo sapiens]	99,2824854	47,3922902	19	30	3	441	49,422	NUSAP1	-1,66	-1,96	0,3	12
Medium	Q96QZ7	Membrane-associated guanylate kinase, WW and PDZ domain-containing prote	4,26351171	1,54258887	2	2	2	1491	164,481	MAGI1	-1,68	-2	0,31	0
Low	Q9NV70-1	exocyst complex component 1 [OS=Homo sapiens]	1,80437706	1,23042506	1	1	1	894	101,917	EXOC1	-0,35	-2	1,65	0
High	Q6PJP8	DNA cross-link repair 1A protein [OS=Homo sapiens]	5,29503299	3,07692308	2	2	2	1040	116,326	DCLRE1A	-2,37	-2,02	-0,36	0
Low	Q9Y6K0	Choline/ethanolaminephosphotransferase 1 [OS=Homo sapiens]	1,46306298	2,64423077	1	1	1	416	46,523	CEPT1	-1,17	-2,04	0,87	0
High	Q9HAZ1	dual specificity protein kinase CLK4 [OS=Homo sapiens]	12,8622695	7,9002079	3	3	1	481	57,455	CLK4	-0,92	-2,05	1,13	0
Low	A0JLT2	Mediator of RNA polymerase II transcription subunit 19 [OS=Homo sapiens]	2,01295971	4,50819672	1	1	1	244	26,257	MED19	-2,1	-2,07	-0,03	0
High	Q92620	Pre-mRNA-splicing factor ATP-dependent RNA helicase PRP16 [OS=Homo sapie	5,2101111	1,62999185	2	3	1	1227	140,415	DHX38	-1,11	-2,14	1,03	0
High	Q9NZM5	Glioma tumor suppressor candidate region gene 2 protein [OS=Homo sapiens]	68,863651	24,0585774	11	20	11	478	54,356	GLTSCR2	-1,81	-2,16	0,35	0
High	P63241-2	Isoform 2 of Eukaryotic translation initiation factor 5A-1 [OS=Homo sapiens]	4,88306301	19,5652174	2	2	2	184	20,157	EIF5A	-2,96	-2,16	-0,8	0
High	Q96GD4-5	Isoform 5 of Aurora kinase B [OS=Homo sapiens]	14,3924954	12,4637681	4	4	4	345	39,442	AURKB	-1,72	-2,18	0,46	0
High	Q96EH5	60S ribosomal protein L39-like [OS=Homo sapiens]	11,0581751	31,372549	1	2	1	51	6,289	RPL39L	-2,12	-2,19	0,07	0
High	Q8NFW8	N-acylneuraminate cytidylyltransferase [OS=Homo sapiens]	60,2964364	35,483871	12	15	12	434	48,349	CMAS	-1,52	-2,2	0,68	0
High	Q9H0W5	Coiled-coil domain-containing protein 8 [OS=Homo sapiens]	16,4016667	10,9665428	3	6	3	538	59,339	CCDC8	-0,13	-2,2	2,07	0
High	Q8IYB3	Serine/arginine repetitive matrix protein 1 [OS=Homo sapiens]	149,484163	22,0132743	16	56	16	904	102,274	SRRM1	-1,81	-2,21	0,41	0
Low	Q9BSJ2-4	Isoform 3 of Gamma-tubulin complex component 2 [OS=Homo sapiens]	1,06343599	0,75268817	1	1	1	930	105,561	TUBGCP2	-0,37	-2,33	1,97	0
High	Q15334	Lethal(2) giant larvae protein homolog 1 [OS=Homo sapiens]	120,75181	34,6804511	27	33	27	1064	115,346	LLGL1	-2,16	-2,37	0,21	0
High	Q9HCS5	band 4.1-like protein 4A [OS=Homo sapiens]	6,23087091	3,06122449	2	2	2	686	79,01	EPB41L4A	-2,46	-2,43	-0,03	0
Low	Q5VT25-6	Isoform 6 of Serine/threonine-protein kinase MRCK alpha [OS=Homo sapiens]	1,37840832	0,50533408	1	1	1	1781	202,684	CDC42BPA	-0,27	-2,43	2,15	0
Low	O60921	checkpoint protein HUS1 [OS=Homo sapiens]	1,3375255	7,14285714	1	1	1	280	31,67	HUS1	-0,92	-2,43	1,52	0
High	Q9ULK5	Vang-like protein 2 [OS=Homo sapiens]	8,83900608	6,14203455	3	3	3	521	59,677	VANGL2	-1,68	-2,45	0,76	0
Low	Q86US8-1	Telomerase-binding protein EST1A [OS=Homo sapiens]	1,70245833	0,91613813	1	1	1	1419	160,362	SMG6	-2,09	-2,45	0,36	0
High	Q9Y4F1	FERM, RhoGEF and pleckstrin domain-containing protein 1 [OS=Homo sapiens]	36,5168593	14,8325359	13	13	13	1045	118,559	FARP1	-2,7	-2,51	-0,19	0
High	Q9UBC1-1	NF-kappa-B inhibitor-like protein 1 [OS=Homo sapiens]	11,852237	12,335958	4	5	4	381	43,177	NFKBIL1	-2,29	-2,53	0,24	0

High	Q6P1M3-1	Lethal(2) giant larvae protein homolog 2 [OS=Homo sapiens]	92,5043502	31,5686275	24	27	24	1020	113,377	LLGL2	-2,05	-2,54	0,49	0
High	Q9UPS8-1	Ankyrin repeat domain-containing protein 26 [OS=Homo sapiens]	423,049589	67,1152721	96	148	1	1709	196,202	ANKRD26	-2,52	-2,86	0,34	65
High	O00458	Interferon-related developmental regulator 1 [OS=Homo sapiens]	17,7634515	15,0776053	5	6	5	451	50,236	IFRD1	-3,34	-2,97	-0,37	0
High	Q9UPV0	centrosomal protein of 164 kDa [OS=Homo sapiens]	10,7639195	5,47945205	6	6	6	1460	164,214	CEP164	-3,21	-2,99	-0,22	0
High	Q9NZ45	CDGSH iron-sulfur domain-containing protein 1 [OS=Homo sapiens]	8,0793108	26,8518519	3	3	3	108	12,191	CISD1	-2,1	-3,08	0,99	0
High	Q9UNL2-2	Isoform 2 of Translocon-associated protein subunit gamma [OS=Homo sapiens]	6,67325462	7,07070707	1	1	1	198	22,596	SSR3	0,26	-3,1	3,36	0
High	Q9GZT4	serine racemase [OS=Homo sapiens]	13,9254633	17,9411765	3	4	3	340	36,543	SRR	-2,14	-3,15	1,01	0
High	P35580-4	Isoform 4 of Myosin-10 [OS=Homo sapiens]	224,604036	34,1803687	57	67	44	2007	232,385	MYH10	-4,98	-3,56	-1,42	0
Medium	Q9BXW7	Cat eye syndrome critical region protein 5 [OS=Homo sapiens]	3,00318198	2,12765957	1	1	1	423	46,292	CECR5	-3,63	-3,67	0,03	0
High	Q8NHP8	Putative phospholipase B-like 2 [OS=Homo sapiens]	41,3539909	21,0526316	11	12	11	589	65,43	PLBD2	-4,14	-3,99	-0,16	0
High	P02533	Keratin, type I cytoskeletal 14 [OS=Homo sapiens]	132,508456	64,6186441	29	94	9	472	51,529	KRT14	-5,77	-4,05	-1,72	9
High	Q9H1J1-1	Regulator of nonsense transcripts 3A [OS=Homo sapiens]	9,96657444	6,93277311	3	4	3	476	54,663	UPF3A	-3,46	-4,51	1,05	0
High	P41743	Protein kinase c iota type [OS=Homo sapiens]	21,6392887	11,2416107	4	4	4	596	68,218	PRKCI	-3,94	-5,28	1,34	0
Low	Q68E01	Integrator complex subunit 3 [OS=Homo sapiens]	2,20446756	1,62991371	1	1	1	1043	117,994	INTS3	-6,99	-6,92	-0,07	0
Low	O60716-1	Catenin delta-1 [OS=Homo sapiens]	1,2645608	1,23966942	1	1	1	968	108,103	CTNND1	-7,33	-7,26	-0,07	0
High	P07355-2	Isoform 2 of Annexin A2 [OS=Homo sapiens]	48,4627971	32,4929972	9	12	9	357	40,386	ANXA2	-7,87	-7,32	-0,54	0
High	Q02413	Desmoglein-1 [OS=Homo sapiens]	9,92227773	5,52907531	4	4	4	1049	113,676	DSG1	-7,58	-7,51	-0,07	0
Medium	P23528	Cofilin-1 [OS=Homo sapiens]	2,49227902	10,2409639	1	1	1	166	18,491	CFL1	-7,96	-7,9	-0,07	0
High	O95049-3	Isoform 3 of Tight junction protein ZO-3 [OS=Homo sapiens]	5,28898281	2,34541578	2	2	2	938	103,361	TJP3	-8,05	-7,98	-0,07	0
Medium	Q2QGD7	Zinc finger protein ZXDC [OS=Homo sapiens]	2,38636957	1,51515152	1	1	1	858	89,932	ZXDC	-8,16	-8,09	-0,07	0
Low	Q99829	Copine-1 [OS=Homo sapiens]	1,81616096	3,72439479	1	1	1	537	59,022	CPNE1	-8,16	-8,09	-0,07	0
Low	O43395	U4/U6 small nuclear ribonucleoprotein Prp3 [OS=Homo sapiens]	1,43309134	3,51390922	1	1	1	683	77,481	PRPF3	-8,28	-8,22	-0,07	0
High	O00159-1	Unconventional myosin-Ic [OS=Homo sapiens]	6,13132896	3,57478833	3	3	3	1063	121,606	MYO1C	-8,29	-8,23	-0,07	0
Low	Q8N0Y2-1	zinc finger protein 444 [OS=Homo sapiens]	1,92226882	4,89296636	1	1	1	327	35,182	ZNF444	-8,38	-8,31	-0,07	0
Medium	Q7Z4L5	Tetratricopeptide repeat protein 21B [OS=Homo sapiens]	3,1024815	2,3556231	2	3	2	1316	150,84	TTC21B	-8,4	-8,33	-0,07	0
Medium	P14923	Junction plakoglobin [OS=Homo sapiens]	3,14138389	2,95302013	2	2	2	745	81,693	JUP	-8,41	-8,35	-0,07	0
Medium	Q96DT7	Zinc finger and BTB domain-containing protein 10 [OS=Homo sapiens]	3,84649001	2,98507463	1	1	1	871	94,835	ZBTB10	-8,51	-8,45	-0,07	0
Medium	P51530	DNA replication ATP-dependent helicase/nuclease DNA2 [OS=Homo sapiens]	4,19889116	2,0754717	2	2	2	1060	120,337	DNA2	-8,73	-8,67	-0,07	0
High	P0C0L4-1	Complement C4-A [OS=Homo sapiens]	14,7137329	2,17889908	3	7	3	1744	192,664	C4A	-8,91	-8,84	-0,07	0
High	P13645	Keratin, type I cytoskeletal 10 [OS=Homo sapiens]	267,397216	62,6712329	35	221	30	584	58,792	KRT10	-11,69	-8,91	-2,78	4
High	Q9UH99-2	Isoform 2 of SUN domain-containing protein 2 [OS=Homo sapiens]	6,0475044	4,06504065	2	3	2	738	82,452	SUN2	-8,98	-8,92	-0,07	0
Medium	P04114	apolipoprotein B-100 [OS=Homo sapiens]	4,35435686	0,74512382	3	4	3	4563	515,283	APOB	-9,17	-9,1	-0,07	0
High	P02751-15	Isoform 15 of Fibronectin [OS=Homo sapiens]	7,15333296	1,33225676	3	3	3	2477	272,15		-9,24	-9,17	-0,07	0
High	Q86YZ3	Hornerin [OS=Homo sapiens]	75,6010623	20,7719298	17	25	17	2850	282,228	HRNR	-9,34	-9,28	-0,07	0
Low	P62312	U6 snRNA-associated Sm-like protein LSm6 [OS=Homo sapiens]	1,36061313	13,75	1	1	1	80	9,122	LSM6	-9,36	-9,29	-0,07	0
Medium	Q96JM7	Lethal(3)malignant brain tumor-like protein 3 [OS=Homo sapiens]	2,66054856	1,02564103	1	1	1	780	88,28	L3MBTL3	-9,4	-9,34	-0,07	0
High	P09622	Dihydrolipoyl dehydrogenase, mitochondrial [OS=Homo sapiens]	5,38316711	4,7151277	2	2	2	509	54,143	DLD	-9,43	-9,36	-0,07	0
High	P60660	Myosin light polypeptide 6 [OS=Homo sapiens]	15,4817908	35,0993377	4	7	4	151	16,919	MYL6	-9,5	-9,43	-0,07	0
Low	P24752	Acetyl-CoA acetyltransferase, mitochondrial [OS=Homo sapiens]	1,67902332	3,98126464	1	1	1	427	45,171	ACAT1	-9,56	-9,49	-0,07	0
Medium	Q6R2W3	SCAN domain-containing protein 3 [OS=Homo sapiens]	2,38933984	0,52830189	1	1	1	1325	151,57	CAND3; ZBED	-9,61	-9,54	-0,07	0
Low	P30101	Protein disulfide-isomerase A3 [OS=Homo sapiens]	1,94923369	2,17821782	1	1	1	505	56,747	PDIA3	-9,63	-9,57	-0,07	0
Low	Q9NW08	DNA-directed RNA polymerase III subunit RPC2 [OS=Homo sapiens]	1,16008222	0,61782877	1	1	1	1133	127,702	POLR3B	-9,63	-9,57	-0,07	0
High	Q8WUY9	DEP domain-containing protein 1B [OS=Homo sapiens]	5,21638223	2,64650284	1	1	1	529	61,731	DEPDC1B	-9,67	-9,6	-0,07	0
High	P06702	Protein S100-A9 [OS=Homo sapiens]	19,7798749	37,7192982	4	6	4	114	13,234	S100A9	-9,7	-9,63	-0,07	0
High	Q06033-1	Inter-alpha-trypsin inhibitor heavy chain H3 [OS=Homo sapiens]	5,15645579	1,46067416	1	1	1	890	99,787	ITIH3	-9,81	-9,74	-0,07	0
High	Q04695	Keratin, type I cytoskeletal 17 [OS=Homo sapiens]	54,2191556	30,0925926	15	52	4	432	48,076	KRT17	-9,89	-9,83	-0,07	0
High	P35908	Keratin, type II cytoskeletal 2 epidermal [OS=Homo sapiens]	273,839083	77,4647887	50	178	37	639	65,393	KRT2	-10,64	-9,99	-0,65	6
Medium	P29508	Serpin B3 [OS=Homo sapiens]	2,34084472	1,79487179	1	1	1	390	44,537	SERPINB3	-10,16	-10,1	-0,07	0
High	Q5D862	Filaggrin-2 [OS=Homo sapiens]	5,90051425	0,8782936	2	3	2	2391	247,928	FLG2	-10,19	-10,13	-0,07	0
Medium	Q9Y5P6-2	Isoform 2 of Mannose-1-phosphate guanyltransferase beta [OS=Homo sapiens]	4,43264398	6,20155039	2	2	2	387	42,594	GMPPB	-10,22	-10,16	-0,07	0
Low	P23435	Cerebellin-1 [OS=Homo sapiens]	1,95350484	3,62694301	1	7	1	193	21,084	CBLN1	-10,23	-10,16	-0,07	0
Medium	O75190	DnaJ homolog subfamily B member 6 [OS=Homo sapiens]	4,22148699	5,21472393	1	1	1	326	36,065	DNAJB6	-10,26	-10,19	-0,07	0
High	Q8IWS0-2	Isoform 2 of PHD finger protein 6 [OS=Homo sapiens]	153,832909	50,9615385	14	69	1	312	35,306	PHF6	-10,33	-10,27	-0,07	0
High	Q8N5H7-1	SH2 domain-containing protein 3C [OS=Homo sapiens]	23,0773104	10,5813953	7	10	6	860	94,352	SH2D3C	-10,36	-10,3	-0,07	0
Low	Q5T750	Skin-specific protein 32 [OS=Homo sapiens]	1,36632959	3,2	1	1	1	250	26,219	C1orf68	-10,36	-10,3	-0,07	0
Low	P04083	annexin A1 [OS=Homo sapiens]	1,91150953	2,60115607	1	1	1	346	38,69	ANXA1	-10,7	-10,64	-0,07	0
High	Q5T8P6-4	Isoform 4 of RNA-binding protein 26 [OS=Homo sapiens]	144,460222	42,6523297	26	42	1	558	62,542	RBM26	-10,72	-10,65	-0,07	0
High	P40925-3	Isoform 3 of Malate dehydrogenase, cytoplasmic [OS=Homo sapiens]	13,5886492	7,38636364	2	3	2	352	38,603	MDH1	-10,88	-10,82	-0,07	0
Low	Q9HC10	Otoferlin [OS=Homo sapiens]	1,26536016	0,75112669	1	2	1	1997	226,61	OTOF	-10,98	-10,91	-0,07	0
Low	Q9Y6X0-1	SET-binding protein [OS=Homo sapiens]	1,18329482	0,43859649	1	1	1	1596	174,899	SETBP1	-11,04	-10,98	-0,07	0
High	P08779	Keratin, type I cytoskeletal 16 [OS=Homo sapiens]	99,7235147	56,6596195	25	77	10	473	51,236	KRT16	-11,26	-11,2	-0,07	0
Low	Q9NP78	ATP-binding cassette sub-family B member 9 [OS=Homo sapiens]	1,42701229	0,91383812	1	2	1	766	84,421	ABCB9	-11,39	-11,32	-0,07	0
High	P31151	Protein S100-A7 [OS=Homo sapiens]	9,90553302	22,7722772	3	4	3	101	11,464	S100A7	-11,43	-11,36	-0,07	0
High	P02538	Keratin, type II cytoskeletal 6A [OS=Homo sapiens]	143,672933	51,9503546	37	106	2	564	60,008	KRT6A	-11,46	-11,39	-0,07	1

High	O15479	Melanoma-associated antigen B2 [OS=Homo sapiens]	9,37059898	8,15047022	3	3	3	319	35,255	MAGEB2	-11,48	-11,41	-0,07	0
High	Q7Z7K6-1	Centromere protein V [OS=Homo sapiens]	80,2317865	51,6363636	11	21	1	275	29,927	CENPV	-11,62	-11,55	-0,07	0
High	P02768-1	Serum albumin [OS=Homo sapiens]	12,2750214	6,73234811	4	8	4	609	69,321	ALB	-11,61	-11,55	-0,07	0
High	P13647	keratin, type II cytoskeletal 5 [OS=Homo sapiens]	113,052367	43,0508475	32	95	15	590	62,34	KRT5	-11,68	-11,61	-0,07	0
High	P02765	Alpha-2-HS-glycoprotein [OS=Homo sapiens]	8,07747799	5,17711172	2	2	2	367	39,3	AHSG	-11,81	-11,75	-0,07	0
High	P04004	Vitronectin [OS=Homo sapiens]	4,7878124	3,13807531	1	1	1	478	54,271	VTN	-11,95	-11,89	-0,07	0
High	P01024	Complement C3 [OS=Homo sapiens]	34,3838108	5,77269994	9	15	9	1663	187,03	C3	-11,98	-11,92	-0,07	0
High	P01023	alpha-2-macroglobulin [OS=Homo sapiens]	9,75991125	2,6458616	4	6	4	1474	163,188	A2M	-12	-11,93	-0,07	0
Medium	P00736	Complement C1r subcomponent [OS=Homo sapiens]	3,08358593	2,26950355	2	2	2	705	80,067	C1R	-12	-11,94	-0,07	0
Low	O60318	Germinal-center associated nuclear protein [OS=Homo sapiens]	1,20683847	1,21212121	1	1	1	1980	218,267	MCM3AP	-12	-11,94	-0,07	0
Low	Q9NVV4-2	Isoform 2 of Poly(A) RNA polymerase, mitochondrial [OS=Homo sapiens]	1,17685194	1,26404494	1	1	1	712	78,784		-12,02	-11,95	-0,07	0
High	P05109	Protein S100-A8 [OS=Homo sapiens]	11,7398865	52,688172	5	7	5	93	10,828	S100A8	-12,12	-12,05	-0,07	0
High	P07477	Trypsin-1 [OS=Homo sapiens]	6,60781994	11,3360324	2	5	2	247	26,541	PRSS1	-12,15	-12,09	-0,07	0
High	P04259	keratin, type II cytoskeletal 6B [OS=Homo sapiens]	140,408359	50,7092199	37	103	2	564	60,03	KRT6B	-12,55	-12,48	-0,07	12
High	P02746	Complement C1q subcomponent subunit B [OS=Homo sapiens]	14,8911812	5,53359684	1	7	1	253	26,704	C1QB	-13,24	-13,17	-0,07	0
Low	P02042	Hemoglobin subunit delta [OS=Homo sapiens]	2,25173443	6,80272109	1	3	1	147	16,045	HBD	-13,29	-13,22	-0,07	0
High	P35527	Keratin, type I cytoskeletal 9 [OS=Homo sapiens]	264,902853	78,0096308	35	188	34	623	62,027	KRT9	-13,44	-13,37	-0,07	0
High	P04264	Keratin, type II cytoskeletal 1 [OS=Homo sapiens]	396,145244	69,5652174	55	332	46	644	65,999	KRT1	-13,71	-13,64	-0,07	5
High	P06314	Ig kappa chain V-IV region B17 [OS=Homo sapiens]	13,1427255	17,9104478	2	10	2	134	14,956		-14,79	-14,73	-0,07	0
High	P01605	Ig kappa chain V-I region Lay [OS=Homo sapiens]	14,9505445	25	2	6	2	108	11,827		-15,19	-15,13	-0,07	0
Low	Q7Z6K1	THAP domain-containing protein 5 [OS=Homo sapiens]	2,08460016	1,7721519	1	10	1	395	45,388	THAP5	-15,29	-15,22	-0,07	0
High	P01859	Ig gamma-2 chain C region [OS=Homo sapiens]	4,90146824	10,7361963	2	6	2	326	35,878	IGHG2	-15,96	-15,9	-0,07	0
Low	P14314	Glucosidase 2 subunit beta [OS=Homo sapiens]	1,41691463	4,92424242	1	1	1	528	59,388	PRKCSH	-16,61	-16,61	-0,07	0
Low	P46019	Phosphorylase b kinase regulatory subunit alpha, liver isoform [OS=Homo sapie	1,35261703	1,45748988	1	1	1	1235	138,32	PHKA2	-16,61	-16,61	-0,07	0

Annex Table III: Liquid chromatography-tandem mass spectrometry (LC-MS/MS) data from SILAC (UV treatment). The data were analyzed using SEQUEST in Proteome Discoverer 2.1 and searched in the complete human proteome database (Swiss-Prot). Peptide identification was filtered at a false discovery rate (FDR) < 1%. Coverage: percentage of the protein sequence covered by identified peptides (confident coverage threshold >1). Peptides: total number of distinct peptide sequences identified in the protein group. PSMs: total number of identified peptide spectra matched for the protein. Unique peptides: The number of peptide sequences that are unique to a protein group. MW: molecular weight. Abundance ratios are calculated based on light (for XPF-KO cells untreated), medium (for XPF-KO + XPF-Wt treated with UV 40J/m2, 1h of recovery), heavy (for XPF-KO + XPF-Wt untreated) forms of lysine and arginine. Razor peptides: peptides that can be assigned to more than one protein.

Protein FDR Confidence	Accession	Description	Sum PEP Score	Coverage	# Peptides	# PSMs	# Unique Peptides	# AAs	MW [kDa]	Gene ID	Abundance Ratio (log2): (Medium) / (Light)	Abundance Ratio (log2): (Heavy) / (Light)	Abundance Ratio (log2): (Medium) / (Heavy)	# Razor Peptides
High	Q96CN7	Isochorismatase domain-containing protein 1 [OS=Homo sapiens]	51,9804541	39,9328859	8	14	8	298	32,216	ISOC1	11,65	11,92	-0,27	0
High	Q9NZ56	Formin-2 [OS=Homo sapiens]	6,74534362	0,92915215	1	3	1	1722	179,993	FMN2	11,87	11,92	-0,05	0
High	Q5VYV7	protein SLX4IP [OS=Homo sapiens]	13,4891316	13,9705882	4	5	4	408	45,524	SLX4IP	10,23	9,81	0,43	0
Medium	Q9BUZ4	TNF receptor-associated factor 4 [OS=Homo sapiens]	3,50206749	1,4893617	1	2	1	470	53,507	TRAF4	9,4	8,83	0,57	0
High	P51784	Ubiquitin carboxyl-terminal hydrolase 11 [OS=Homo sapiens]	8,51782722	3,1152648	3	3	3	963	109,747	USP11	8,12	7,63	0,49	0
High	P07992-1	DNA excision repair protein ERCC-1 [OS=Homo sapiens]	454,541232	74,4107744	29	341	29	297	32,542	ERCC1	5,31	5,4	-0,09	0
High	Q709F0-1	acyl-CoA dehydrogenase family member 11 [OS=Homo sapiens]	135,823536	30,3846154	24	62	24	780	87,228	ACAD11	4,65	5,15	-0,5	0
High	Q8IY92	Structure-specific endonuclease subunit SLX4 [OS=Homo sapiens]	699,781887	40,4580153	76	433	76	1834	199,889	SLX4	4,23	3,53	0,69	0
High	Q92889	DNA repair endonuclease XPF [OS=Homo sapiens]	1623,85672	75,6550218	97	2250	97	916	104,42	ERCC4	4,35	3,52	0,83	0
High	Q9BQ83-1	Structure-specific endonuclease subunit SLX1 [OS=Homo sapiens]	17,8694641	15,6363636	3	5	3	275	30,751	SLX1B; SLX1A	2,9	2,85	0,05	0
High	Q9H1R3	Myosin light chain kinase 2, skeletal/cardiac muscle [OS=Homo sapiens]	30,8644891	2,18120805	3	48	3	596	64,644	MYLK2	2,77	2,81	-0,04	0
High	Q9BQ75	Protein CMSS1 [OS=Homo sapiens]	5,33953232	6,81003584	2	3	2	279	31,864	CMSS1	2,02	2,8	-0,78	0
High	Q96HS1-1	Serine/threonine-protein phosphatase Pgam5, mitochondrial [OS=Homo sapier	77,0766606	39,7923875	14	46	14	289	31,985	PGAM5	3,06	2,51	0,55	0
High	Q02543	60S ribosomal protein L18a [OS=Homo sapiens]	6,21212243	11,9318182	2	2	2	176	20,749	RPL18A	2,48	2,5	-0,02	0
High	P36578	60S ribosomal protein L4 [OS=Homo sapiens]	40,9905461	15,4566745	7	17	7	427	47,667	RPL4	2,25	2,44	-0,19	0
High	P05387	60S acidic ribosomal protein P2 [OS=Homo sapiens]	39,1242838	41,7391304	4	9	4	115	11,658	RPLP2	2,35	2,42	-0,06	0
High	P05386	60S acidic ribosomal protein P1 [OS=Homo sapiens]	11,4748249	14,0350877	1	3	1	114	11,507	RPLP1	1,64	2,4	-0,76	0
High	Q15233	Non-POU domain-containing octamer-binding protein [OS=Homo sapiens]	8,15039186	2,33545648	1	2	1	471	54,197	NONO	1,73	2,34	-0,61	0
High	P11310-2	Isoform 2 of Medium-chain specific acyl-CoA dehydrogenase, mitochondrial [O	39,1152081	16,2352941	6	9	6	425	46,99	ACADM	2,42	2,32	0,1	0
High	Q9NVP1	ATP-dependent RNA helicase DDX18 [OS=Homo sapiens]	334,25907	62,238806	34	190	34	670	75,359	DDX18	0,72	2,18	-1,46	0
High	Q14204	Cytoplasmic dynein 1 heavy chain 1 [OS=Homo sapiens]	16,8504643	1,89410245	8	9	8	4646	532,072	DYNC1H1	2,04	2,06	-0,02	0
Low	Q96PQ7-3	Isoform 3 of Kelch-like protein 5 [OS=Homo sapiens]	1,17600441	1,55844156	1	1	1	770	86,605		0,88	2,06	-1,18	0
High	P61313-1	60S ribosomal protein L15 [OS=Homo sapiens]	29,5569598	20,5882353	4	13	4	204	24,131	RPL15	1,8	2,01	-0,2	0
High	P18124	60S ribosomal protein L7 [OS=Homo sapiens]	80,6364176	49,1935484	13	30	13	248	29,207	RPL7	1,82	1,95	-0,13	0
High	P50914	60S ribosomal protein L14 [OS=Homo sapiens]	32,3463162	19,5348837	4	9	4	215	23,417	RPL14	1,88	1,95	-0,07	0
High	Q6P5R6	60S ribosomal protein L22-like 1 [OS=Homo sapiens]	97,1588866	52,4590164	6	52	4	122	14,598	RPL22L1	1,89	1,93	-0,04	3
High	Q9BYD2	39S ribosomal protein L9, mitochondrial [OS=Homo sapiens]	8,91942683	3,37078652	1	3	1	267	30,224	MRPL9	-0,03	1,92	-1,95	0
High	Q96NY9	crossover junction endonuclease MUS81 [OS=Homo sapiens]	61,9513325	21,9600726	10	33	10	551	61,135	MUS81	1,75	1,78	-0,03	0
High	Q9BRG2	SH2 domain-containing protein 3A [OS=Homo sapiens]	9,99678651	6,77083333	3	7	3	576	63,054	SH2D3A	2,88	1,77	1,11	0
High	Q06787	fragile X mental retardation protein 1 [OS=Homo sapiens]	26,9604055	9,17721519	6	16	5	632	71,131	FMR1	1,64	1,72	-0,08	2
High	O43390-2	Isoform 2 of Heterogeneous nuclear ribonucleoprotein R [OS=Homo sapiens]	5,37476803	1,88679245	1	2	1	636	71,17	HNRNPR	0,23	1,59	-1,36	0
High	P40429	60S ribosomal protein L13a [OS=Homo sapiens]	22,4337069	16,7487685	4	10	4	203	23,562	RPL13A	1,43	1,54	-0,11	0
High	O75676	Ribosomal protein S6 kinase alpha-4 [OS=Homo sapiens]	11,453093	7,12435233	5	8	5	772	85,552	RPS6KA4	1,41	1,52	-0,11	0
High	P49368-1	T-complex protein 1 subunit gamma [OS=Homo sapiens]	58,9455601	18,1651376	9	22	9	545	60,495	CCT3	0,71	1,49	-0,77	0
High	Q07020	60S ribosomal protein L18 [OS=Homo sapiens]	40,7939192	37,2340426	6	15	6	188	21,621	RPL18	1,3	1,49	-0,19	0
High	Q02878	60S ribosomal protein L6 [OS=Homo sapiens]	98,0284244	44,0972222	14	46	14	288	32,708	RPL6	1,26	1,48	-0,22	0
High	Q15149-1	plectin [OS=Homo sapiens]	7,75103027	0,55508113	2	6	2	4684	531,466	PLEC	1,54	1,47	0,07	0
High	Q9NPL8	Complex I assembly factor TIMMDC1, mitochondrial [OS=Homo sapiens]	4,68169259	7,01754386	2	2	2	285	32,158	TIMMDC1	1,07	1,47	-0,4	0
High	P40939	Trifunctional enzyme subunit alpha, mitochondrial [OS=Homo sapiens]	133,428399	33,9449541	22	60	22	763	82,947	HADHA	0,84	1,45	-0,61	0
High	O00567	Nucleolar protein 56 [OS=Homo sapiens]	16,2026264	6,22895623	4	6	4	594	66,009	NOP56	2,21	1,45	0,76	0
High	P28288	ATP-binding cassette sub-family D member 3 [OS=Homo sapiens]	4,66265337	1,82094082	1	2	1	659	75,428	ABCD3	1,42	1,43	-0,01	0
Medium	Q9ULX6	A-kinase anchor protein 8-like [OS=Homo sapiens]	4,22371101	3,25077399	2	2	2	646	71,604	AKAP8L	0,93	1,42	-0,48	0
High	P18074-1	Tfiih basal transcription factor complex helicase xpd subunit [OS=Homo sapiens	20,5031099	6,97368421	6	8	6	760	86,854	ERCC2	1,23	1,41	-0,18	0
High	P11940-1	Polyadenylate-binding protein 1 [OS=Homo sapiens]	158,7424	36,3207547	21	60	21	636	70,626	PABPC1	1,47	1,4	0,06	0
Medium	Q96TA2-1	ATP-dependent zinc metalloprotease YME1L1 [OS=Homo sapiens]	2,84924356	1,16429495	1	1	1	773	86,401	YME1L1	0,25	1,4	-1,15	0
High	Q12996-1	Cleavage stimulation factor subunit 3 [OS=Homo sapiens]	7,49783203	2,78940028	2	3	2	717	82,869	CSTF3	1,76	1,39	0,37	0
High	P49959-3	Isoform 3 of Double-strand break repair protein MRE11A [OS=Homo sapiens]	18,4176423	7,59493671	4	7	4	711	81,02	MRE11A	1,25	1,35	-0,09	0
High	Q96AY2-2	Isoform 2 of Crossover junction endonuclease EME1 [OS=Homo sapiens]	33,5536683	14,0651801	8	18	8	583	64,738	EME1	1,41	1,32	0,09	0
High	Q9NR30-1	Nucleolar RNA helicase 2 [OS=Homo sapiens]	25,125144	5,74712644	4	11	1	783	87,29	DDX21	1,72	1,25	0,47	0
High	Q9NRA0-5	Isoform 5 of Sphingosine kinase 2 [OS=Homo sapiens]	46,4680522	8,80420499	6	15	6	761	80,154	SPHK2	1,16	1,21	-0,05	0
High	Q9NZ01-1	Very-long-chain enoyl-CoA reductase [OS=Homo sapiens]	37,8873051	12,6623377	5	10	5	308	36,011	TECR	0,83	1,19	-0,36	0
High	P33992	DNA replication licensing factor mcm5 [OS=Homo sapiens]	63,5951497	22,479564	16	28	16	734	82,233	MCM5	1,09	1,18	-0,09	0
High	Q92499	ATP-dependent RNA helicase DDX1 [OS=Homo sapiens]	17,1424771	10,1351351	7	9	7	740	82,38	DDX1	1,02	1,18	-0,16	0
High	O14654	insulin receptor substrate 4 [OS=Homo sapiens]	112,567986	20,1272872	24	61	24	1257	133,685	IRS4	1,07	1,17	-0,11	0
High	Q9H5Z1	Probable ATP-dependent RNA helicase DHX35 [OS=Homo sapiens]	33,4492228	12,802276	9	17	9	703	78,86	DHX35	0,4	1,17	-0,77	0
Low	P55084	Trifunctional enzyme subunit beta, mitochondrial [OS=Homo sapiens]	1,56976365	1,89873418	1	1	1	474	51,262	HADHB	0,62	1,16	-0,54	0
High	P11142-1	Heat shock cognate 71 kDa protein [OS=Homo sapiens]	777,753406	57,8947368	44	363	33	646	70,854	HSPA8	1,3	1,15	0,15	2

High	P49327	Fatty acid synthase [OS=Homo sapiens]	9,24333484	1,39386699	3	4	3	2511	273,254	FASN	0,56	1,14	-0,58	0
Low	Q9NVV4-2	Isoform 2 of Poly(A) RNA polymerase, mitochondrial [OS=Homo sapiens]	2,17509353	0,98314607	1	1	1	712	78,784		0,73	1,12	-0,39	0
High	P07900-2	Isoform 2 of Heat shock protein HSP 90-alpha [OS=Homo sapiens]	122,30819	18,969555	16	53	6	854	98,099	HSP90AA1	0,94	1,11	-0,18	0
High	Q14119	Vascular endothelial zinc finger 1 [OS=Homo sapiens]	4,6867047	5,56621881	2	2	2	521	56,895	VEZF1	9,37	1,1	8,26	0
Medium	P18077	60S ribosomal protein L35a [OS=Homo sapiens]	2,6892711	18,1818182	2	2	2	110	12,53	RPL35A	0,53	1,09	-0,56	0
High	P10809	60 kDa heat shock protein, mitochondrial [OS=Homo sapiens]	67,3677612	27,2251309	14	24	14	573	61,016	HSPD1	1,13	1,08	0,05	0
High	P19447	TFIIH basal transcription factor complex helicase XPB subunit [OS=Homo sapien	20,7436448	11,3810742	8	10	8	782	89,221	ERCC3	0,69	1,07	-0,38	0
High	P52272	Heterogeneous nuclear ribonucleoprotein M [OS=Homo sapiens]	270,498535	48,3561644	36	204	36	730	77,464	HNRNPM	0,98	1,03	-0,05	0
High	Q92841	Probable ATP-dependent RNA helicase DDX17 [OS=Homo sapiens]	104,320488	19,2043896	13	52	8	729	80,222	DDX17	0,99	1,03	-0,04	0
Medium	Q9UNK9	Protein angel homolog 1 [OS=Homo sapiens]	4,11571454	2,08955224	1	1	1	670	75,227	ANGEL1	10,88	1,02	9,86	0
High	O00425	Insulin-like growth factor 2 mRNA-binding protein 3 [OS=Homo sapiens]	8,60842872	3,45423143	2	4	1	579	63,666	IGF2BP3	0,77	1,01	-0,23	0
High	Q08945	FACT complex subunit SSRP1 [OS=Homo sapiens]	5,28460918	4,93653032	3	3	3	709	81,024	SSRP1	0,95	1,01	-0,06	0
High	Q9HDC5	junctophilin-1 [OS=Homo sapiens]	104,475071	27,0801815	19	63	19	661	71,642	JPH1	0,98	1	-0,02	0
High	P05388	60S acidic ribosomal protein P0 [OS=Homo sapiens]	45,5609769	22,3974763	6	17	6	317	34,252	RPLP0	0,7	1	-0,29	0
High	Q9Y5Y2	Cytosolic Fe-S cluster assembly factor NUBP2 [OS=Homo sapiens]	7,95508451	3,32103321	1	2	1	271	28,807	NUBP2	0,64	0,97	-0,33	0
High	P50402	Emerin [OS=Homo sapiens]	48,6275794	24,4094488	5	17	5	254	28,976	EMD	1,2	0,96	0,24	0
High	P17844	probable ATP-dependent RNA helicase DDX5 [OS=Homo sapiens]	75,0091662	20,0325733	14	37	9	614	69,105	DDX5	0,99	0,95	0,04	5
High	Q9NUL7	Probable ATP-dependent RNA helicase DDX28 [OS=Homo sapiens]	65,8212083	24,8148148	12	20	12	540	59,545	DDX28	0,79	0,95	-0,16	0
High	Q9UNX3	60S ribosomal protein L26-like 1 [OS=Homo sapiens]	122,411781	52,4137931	11	130	3	145	17,246	RPL26L1	0,92	0,91	0,02	0
High	P62424	60S ribosomal protein L7a [OS=Homo sapiens]	131,771446	42,8571429	15	43	15	266	29,977	RPL7A	0,87	0,9	-0,03	0
High	Q9UG63-2	Isoform 2 of ATP-binding cassette sub-family F member 2 [OS=Homo sapiens]	61,4031092	15,615142	9	22	9	634	72,397	ABCF2	0,84	0,86	-0,02	0
High	O43143	Pre-mRNA-splicing factor ATP-dependent RNA helicase DHX15 [OS=Homo sapie	192,37662	33,3333333	25	73	25	795	90,875	DHX15	0,62	0,85	-0,23	0
High	P56270-2	Isoform 2 of Myc-associated zinc finger protein [OS=Homo sapiens]	20,8398963	6,69371197	3	9	3	493	51,04	MAZ	1,26	0,85	0,41	0
High	Q8WWY3	U4/U6 small nuclear ribonucleoprotein Prp31 [OS=Homo sapiens]	4,59991018	3,80761523	2	2	2	499	55,421	PRPF31	0,45	0,85	-0,4	0
High	Q09161	Nuclear cap-binding protein subunit 1 [OS=Homo sapiens]	21,1464027	7,59493671	6	9	6	790	91,781	NCBP1	0,91	0,84	0,08	0
Medium	Q9Y6J9	TAF6-like RNA polymerase II p300/CBP-associated factor-associated factor 65 k	2,33526403	1,76848875	1	1	1	622	67,772	TAF6L	1,98	0,84	1,14	0
High	Q9NZI8	Insulin-like growth factor 2 mRNA-binding protein 1 [OS=Homo sapiens]	22,212904	9,87868284	5	9	4	577	63,441	IGF2BP1	0,56	0,82	-0,26	1
High	Q96JP5-1	E3 ubiquitin-protein ligase ZFP91 [OS=Homo sapiens]	134,280352	29,6491228	16	60	16	570	63,406	ZFP91	1,04	0,81	0,24	0
High	Q9H6H4-1	Receptor expression-enhancing protein 4 [OS=Homo sapiens]	89,8514637	45,5252918	11	34	11	257	29,376	REEP4	0,99	0,81	0,18	0
High	P38646	Stress-70 protein, mitochondrial [OS=Homo sapiens]	290,015909	43,4462445	32	131	31	679	73,635	HSPA9	0,78	0,8	-0,02	0
High	O00139-2	Isoform 2 of Kinesin-like protein KIF2A [OS=Homo sapiens]	98,0680154	27,7272727	19	44	19	660	74,996	KIF2A	0,64	0,8	-0,16	0
High	P17812	CTP synthase 1 [OS=Homo sapiens]	43,3249301	15,9052453	9	19	9	591	66,648	CTPS1	0,47	0,8	-0,34	0
High	P38159-1	RNA-binding motif protein, X chromosome [OS=Homo sapiens]	15,8224287	3,32480818	1	3	1	391	42,306	RBMX	0,6	0,8	-0,2	0
High	Q96L34-1	Map/microtubule affinity-regulating kinase 4 [OS=Homo sapiens]	133,486021	37,7659574	24	64	22	752	82,468	MARK4	0,84	0,79	0,04	0
High	P53007	Tricarboxylate transport protein, mitochondrial [OS=Homo sapiens]	124,190455	41,8006431	12	64	12	311	33,991	SLC25A1	0,85	0,79	0,06	0
High	Q16629	serine/arginine-rich splicing factor 7 [OS=Homo sapiens]	32,500365	27,7310924	5	10	5	238	27,35	SRSF7	1,91	0,79	1,12	0
Low	Q15392	Delta(24)-sterol reductase [OS=Homo sapiens]	1,17528856	1,74418605	1	1	1	516	60,062	DHCR24	0,16	0,78	-0,63	0
High	O60762	Dolichol-phosphate mannosyltransferase subunit 1 [OS=Homo sapiens]	122,436018	65,7692308	14	45	14	260	29,616	DPM1	2,67	0,77	1,9	0
High	P62987	Ubiquitin-60S ribosomal protein L40 [OS=Homo sapiens]	49,1357029	37,5	4	48	1	128	14,719	UBA52	0,55	0,77	-0,22	0
High	P54886	delta-1-pyrroline-5-carboxylate synthase [OS=Homo sapiens]	11,7379122	5,40880503	4	5	4	795	87,248	ALDH18A1	1,62	0,77	0,85	0
High	P04350	Tubulin beta-4A chain [OS=Homo sapiens]	689,999952	75,9009009	28	430	2	444	49,554	TUBB4A	0,73	0,75	-0,02	2
High	Q9BQE3	Tubulin alpha-1C chain [OS=Homo sapiens]	544,745632	63,9198218	29	269	4	449	49,863	TUBA1C	0,27	0,74	-0,47	0
High	P13010	X-ray repair cross-complementing protein 5 [OS=Homo sapiens]	76,2965189	20,9016393	15	27	15	732	82,652	XRCC5	0,54	0,74	-0,2	0
High	P49593	Protein phosphatase 1F [OS=Homo sapiens]	16,372887	2,64317181	1	4	1	454	49,8	PPM1F	0,55	0,74	-0,19	0
High	Q05823	2-5A-dependent ribonuclease [OS=Homo sapiens]	9,05871193	3,91363023	3	4	3	741	83,481	RNASEL	0,79	0,74	0,05	0
High	Q49A26-1	Putative oxidoreductase GLYR1 [OS=Homo sapiens]	23,1148131	14,2857143	6	11	6	553	60,518	GLYR1	1,09	0,73	0,37	0
High	P39023	60S ribosomal protein L3 [OS=Homo sapiens]	48,5532685	20,0992556	9	23	9	403	46,08	RPL3	0,48	0,72	-0,24	0
High	P19338	Nucleolin [OS=Homo sapiens]	46,0277625	13,943662	10	20	10	710	76,568	NCL	0,2	0,72	-0,52	0
Low	Q9Y619	mitochondrial ornithine transporter 1 [OS=Homo sapiens]	1,27310986	2,3255814	1	1	1	301	32,715	SLC25A15	0,66	0,71	-0,06	0
High	P53621-2	Isoform 2 of Coatomer subunit alpha [OS=Homo sapiens]	26,4342546	5,75831306	7	11	7	1233	139,235	COPA	-0,28	0,69	-0,97	0
High	P04843	Dolichyl-diphosphooligosaccharide--protein glycosyltransferase subunit 1 [OS=	6,80745267	4,28336079	3	4	3	607	68,527	RPN1	0,83	0,69	0,14	0
High	Q9NVU7	Protein SDA1 homolog [OS=Homo sapiens]	74,7041691	14,7016012	11	38	11	687	79,82	SDAD1	0,53	0,68	-0,15	0
High	Q9Y483	Metal-response element-binding transcription factor 2 [OS=Homo sapiens]	25,4721072	15,682968	7	11	7	593	67,063	MTF2	0,56	0,68	-0,11	0
High	Q9NXE4-4	Isoform 4 of Sphingomyelin phosphodiesterase 4 [OS=Homo sapiens]	6,70641199	3,20733104	3	3	3	873	98,086		0,12	0,68	-0,56	0
High	P10412	Histone H1.4 [OS=Homo sapiens]	173,546553	39,7260274	13	174	3	219	21,852	HIST1H1E	0,8	0,67	0,12	15
High	P42677	40S ribosomal protein S27 [OS=Homo sapiens]	121,015786	42,8571429	6	46	2	84	9,455	RPS27	0,54	0,67	-0,13	6
Medium	Q96I25	Splicing factor 45 [OS=Homo sapiens]	4,15289335	4,2394015	2	2	1	401	44,934	RBM17	9,21	0,67	8,54	0
High	O75746	Calcium-binding mitochondrial carrier protein Aralar1 [OS=Homo sapiens]	71,914328	17,9941003	11	28	6	678	74,715	SLC25A12	0,86	0,66	0,2	0
High	O60884	DnaJ homolog subfamily A member 2 [OS=Homo sapiens]	13,9066736	5,09708738	2	6	2	412	45,717	DNAJA2	0,63	0,66	-0,03	0
Low	Q5JTW2-2	Isoform 2 of Centrosomal protein of 78 kDa [OS=Homo sapiens]	1,75374769	0,83102493	1	1	1	722	80,023	CEP78	0,99	0,66	0,33	0
High	Q96A33-1	Coiled-coil domain-containing protein 47 [OS=Homo sapiens]	28,1818193	12,6293996	6	12	6	483	55,838	CCDC47	0,54	0,65	-0,11	0

High	Q92878-2	Isoform 2 of DNA repair protein RAD50 [OS=Homo sapiens]	19,8210171	5,00758725	6	8	6	1318	154,491		0,5	0,65	-0,15	0
High	O75419-3	Isoform 3 of Cell division control protein 45 homolog [OS=Homo sapiens]	9,67776526	6,02006689	3	4	3	598	68,724	CDC45	0,81	0,65	0,15	0
High	Q96CM3	RNA pseudouridylate synthase domain-containing protein 4 [OS=Homo sapiens	7,42670958	6,89655172	3	4	3	377	42,178	RPUSD4	0,4	0,65	-0,25	0
High	Q07955-1	Serine/arginine-rich splicing factor 1 [OS=Homo sapiens]	12,7372961	20,9677419	4	6	4	248	27,728	SRSF1	0,32	0,64	-0,31	0
High	Q9Y678	Coatomer subunit gamma-1 [OS=Homo sapiens]	8,12522127	2,28832952	2	3	2	874	97,655	COPG1	0,54	0,63	-0,1	0
High	O95347-1	structural maintenance of chromosomes protein 2 [OS=Homo sapiens]	6,18245636	2,33918129	3	3	3	1197	135,572	SMC2	0,1	0,63	-0,53	0
High	Q8IXI1	Mitochondrial Rho GTPase 2 [OS=Homo sapiens]	15,7235563	7,2815534	4	8	4	618	68,075	RHOT2	0,79	0,62	0,18	0
High	Q8IUF8	Bifunctional lysine-specific demethylase and histidyl-hydroxylase MINA [OS=Ho	8,64371304	2,3655914	2	3	2	465	52,767	MINA	1,17	0,62	0,54	0
High	P33993-1	DNA replication licensing factor MCM7 [OS=Homo sapiens]	336,658735	58,8317107	37	137	37	719	81,257	MCM7	0,54	0,61	-0,06	0
High	P22695	Cytochrome b-c1 complex subunit 2, mitochondrial [OS=Homo sapiens]	53,8790178	19,4260486	9	19	9	453	48,413	UQCRC2	0,69	0,6	0,09	0
High	Q96EY1-1	DnaJ homolog subfamily A member 3, mitochondrial [OS=Homo sapiens]	34,2257629	21,875	8	12	8	480	52,456	DNAJA3	1,02	0,6	0,42	0
High	O75306-1	NADH dehydrogenase [ubiquinone] iron-sulfur protein 2, mitochondrial [OS=Ho	4,85954809	1,72786177	1	2	1	463	52,512	NDUFS2	0,14	0,59	-0,45	0
High	P16403	Histone H1.2 [OS=Homo sapiens]	174,045804	37,5586854	12	180	2	213	21,352	HIST1H1C	0,55	0,58	-0,03	0
High	Q9UBM7	7-dehydrocholesterol reductase [OS=Homo sapiens]	24,8057265	9,26315789	5	10	5	475	54,454	DHCR7	0,44	0,58	-0,15	0
High	Q96S44	TP53-regulating kinase [OS=Homo sapiens]	6,24429057	10,6719368	2	3	2	253	28,143	TP53RK	0,23	0,58	-0,34	0
High	Q9BZI7-1	Regulator of nonsense transcripts 3B [OS=Homo sapiens]	149,314571	46,5838509	22	74	22	483	57,727	UPF3B	0,58	0,57	0,02	0
High	Q9NTJ3-1	Structural maintenance of chromosomes protein 4 [OS=Homo sapiens]	27,6796846	6,83229814	9	13	9	1288	147,091	SMC4	0,64	0,57	0,07	0
Medium	Q9UH62	Armadillo repeat-containing X-linked protein 3 [OS=Homo sapiens]	3,82447297	4,74934037	2	2	2	379	42,474	ARMCX3	0,63	0,56	0,08	0
High	O00571	ATP-dependent RNA helicase DDX3X [OS=Homo sapiens]	422,366594	59,6676737	40	191	40	662	73,198	DDX3X	0,38	0,55	-0,17	0
High	P49411	elongation factor Tu, mitochondrial [OS=Homo sapiens]	317,45722	47,1238938	19	90	19	452	49,51	TUFM	0,44	0,55	-0,12	0
High	Q13724-1	Mannosyl-oligosaccharide glucosidase [OS=Homo sapiens]	99,086285	23,297491	16	44	16	837	91,861	MOGS	0,64	0,55	0,09	0
High	P62906	60S ribosomal protein L10A [OS=Homo sapiens]	48,13563	44,2396313	9	20	9	217	24,816	RPL10A	0,79	0,55	0,24	0
High	P51116	Fragile X mental retardation syndrome-related protein 2 [OS=Homo sapiens]	14,9060101	4,90341753	3	8	2	673	74,178	FXR2	0,43	0,55	-0,11	0
Low	Q9UK58	Cyclin-L1 [OS=Homo sapiens]	1,53402263	1,14068441	1	1	1	526	59,597	CCNL1	-0,15	0,55	-0,7	0
High	P17987	T-complex protein 1 subunit alpha [OS=Homo sapiens]	193,045162	45,5035971	23	70	23	556	60,306	TCP1	0,63	0,54	0,09	0
High	Q9NVI7-2	Isoform 2 of ATPase family AAA domain-containing protein 3A [OS=Homo sapie	43,4767352	21,8430034	15	23	15	586	66,177	ATAD3A	0,46	0,54	-0,08	0
High	Q8N2M8	CLK4-associating serine/arginine rich protein [OS=Homo sapiens]	46,5614203	13,9465875	8	23	8	674	77,115	CLASRP	0,28	0,53	-0,25	0
High	Q9Y4R8	telomere length regulation protein TEL2 homolog [OS=Homo sapiens]	5,66387218	3,22580645	3	3	3	837	91,689	TELO2	-0,04	0,52	-0,56	0
High	O14880	Microsomal glutathione S-transferase 3 [OS=Homo sapiens]	21,820657	8,55263158	1	5	1	152	16,506	MGST3	1,01	0,51	0,5	0
High	Q14739	Lamin-B receptor [OS=Homo sapiens]	20,8229426	7,64227642	4	5	4	615	70,658	LBR	0,34	0,51	-0,18	0
Medium	P63167	Dynein light chain 1, cytoplasmic [OS=Homo sapiens]	3,57073233	13,4831461	1	1	1	89	10,359	DYNLL1	-9,93	0,51	-10,44	0
Low	Q8IXB1-1	DnaJ homolog subfamily C member 10 [OS=Homo sapiens]	1,84771166	1,26103405	1	1	1	793	91,021	DNAJC10	0,48	0,5	-0,02	0
High	P78527	DNA-dependent protein kinase catalytic subunit [OS=Homo sapiens]	338,172021	20,373062	77	214	77	4128	468,788	PRKDC	0,47	0,48	0	0
High	Q9BQ70	Transcription factor 25 [OS=Homo sapiens]	4,88958115	3,69822485	2	2	2	676	76,619	TCF25	1,29	0,48	0,81	0
Medium	Q15070-1	Mitochondrial inner membrane protein OXA1L [OS=Homo sapiens]	3,50916538	2,29885057	1	2	1	435	48,516	OXA1L	0,16	0,48	-0,32	0
High	P05141	ADP/ATP translocase 2 [OS=Homo sapiens]	589,161468	61,0738255	26	352	8	298	32,831	SLC25A5	0,55	0,47	0,07	38
High	Q9Y3Z3	deoxynucleoside triphosphate triphosphohydrolase SAMHD1 [OS=Homo sapier	54,3590429	16,6134185	10	20	10	626	72,155	SAMHD1	0,43	0,47	-0,03	0
High	P25490	Transcriptional repressor protein YY1 [OS=Homo sapiens]	28,3829123	8,21256039	5	15	5	414	44,685	YY1	0,27	0,47	-0,2	0
High	P12956	X-ray repair cross-complementing protein 6 [OS=Homo sapiens]	16,2065023	10,0164204	5	7	5	609	69,799	XRCC6	0,36	0,47	-0,11	0
Low	Q7Z736	Pleckstrin homology domain-containing family H member 3 [OS=Homo sapiens	2,2541448	1,13493064	1	1	1	793	85,264	PLEKHH3	-0,45	0,47	-0,92	0
High	P52597	Heterogeneous nuclear ribonucleoprotein F [OS=Homo sapiens]	14,3310385	7,95180723	2	4	1	415	45,643	HNRNPF	0,66	0,46	0,2	0
Medium	O95816	BAG family molecular chaperone regulator 2 [OS=Homo sapiens]	3,34969248	5,21327014	1	1	1	211	23,757	BAG2	11,8	0,46	11,34	0
High	Q9UHR5-1	SAP30-binding protein [OS=Homo sapiens]	12,909052	9,09090909	3	6	3	308	33,85	SAP30BP	-0,26	0,45	-0,72	0
High	Q9Y2X3	Nucleolar protein 58 [OS=Homo sapiens]	57,1835613	24,952741	10	21	10	529	59,541	NOP58	0,77	0,44	0,33	0
Medium	Q96CW1	AP-2 complex subunit mu [OS=Homo sapiens]	3,67289211	3,67816092	2	3	2	435	49,623	AP2M1	0,46	0,44	0,02	0
Medium	Q99805	Transmembrane 9 superfamily member 2 [OS=Homo sapiens]	3,38383969	1,2066365	1	2	1	663	75,725	TM9SF2	0,12	0,44	-0,32	0
High	Q9UKV8	Protein argonaute-2 [OS=Homo sapiens]	384,364734	51,5715949	40	198	40	859	97,146	AGO2; EIF2C2	0,29	0,42	-0,13	0
High	Q9Y4W2	Ribosomal biogenesis protein LAS1L [OS=Homo sapiens]	67,9070173	25,3405995	16	31	16	734	83,013	LAS1L	0,71	0,42	0,29	0
High	Q9NWQ4	G patch domain-containing protein 2-like [OS=Homo sapiens]	40,0150493	15,1452282	7	13	7	482	54,226	GPATCH2L	0,83	0,42	0,41	0
High	Q5SSJ5-1	Heterochromatin protein 1-binding protein 3 [OS=Homo sapiens]	35,8850489	16,2748644	9	15	9	553	61,169	HP1BP3	0,72	0,42	0,3	0
High	Q9NWK9	Box C/D snoRNA protein 1 [OS=Homo sapiens]	6,65651818	4,68085106	2	4	2	470	53,884	ZNHIT6	0,67	0,42	0,25	0
Medium	O60934	Nibrin [OS=Homo sapiens]	4,42158269	1,06100796	1	2	1	754	84,906	NBN	0,85	0,42	0,43	0
High	O96028-1	Histone-lysine N-methyltransferase NSD2 [OS=Homo sapiens]	6,01952393	0,65934066	1	3	1	1365	152,16	WHSC1	0,54	0,41	0,13	0
Low	Q14592	Zinc finger protein 460 [OS=Homo sapiens]	1,36011526	1,42348754	1	1	1	562	63,624	ZNF460	0,2	0,41	-0,22	0
High	Q16891	MICOS complex subunit Mic60 [OS=Homo sapiens]	34,9039559	10,6860158	8	16	8	758	83,626	IMMT	0,49	0,4	0,09	0
Medium	P78371-1	T-complex protein 1 subunit beta [OS=Homo sapiens]	2,57954914	2,24299065	1	1	1	535	57,452	CCT2	0,36	0,4	-0,05	0
High	Q8N1F7-1	Nuclear pore complex protein Nup93 [OS=Homo sapiens]	176,684874	41,2698413	31	89	31	819	93,43	NUP93	0,5	0,39	0,11	0
High	P50991	T-complex protein 1 subunit delta [OS=Homo sapiens]	31,534444	12,0593692	6	13	6	539	57,888	CCT4	0,95	0,39	0,56	0
Low	Q9P0J6	39S ribosomal protein L36, mitochondrial [OS=Homo sapiens]	1,38573571	5,82524272	1	2	1	103	11,777	MRPL36	0,24	0,39	-0,16	0
High	Q08211	Atp-dependent rna helicase a [OS=Homo sapiens]	13,1275055	4,17322835	5	7	5	1270	140,869	DHX9	0,3	0,38	-0,08	0
High	Q96EY4	translation machinery-associated protein 16 [OS=Homo sapiens]	139,800576	46,7980296	13	73	13	203	23,849	TMA16	0,63	0,37	0,27	0

Low	Q14257-2	Isoform 2 of Reticulocalbin-2 [OS=Homo sapiens]	1,72955409	2,3880597	1	1	1	335	39,115	RCN2	-0,3	0,37	-0,67	0
Medium	Q9H6F5	Coiled-coil domain-containing protein 86 [OS=Homo sapiens]	3,95130966	5,27777778	2	2	2	360	40,211	CCDC86	0,62	0,36	0,26	0
Low	Q05BV3-5	Isoform 5 of Echinoderm microtubule-associated protein-like 5 [OS=Homo sapi	1,20377269	0,40465352	1	1	1	1977	220,126	EML5	-0,16	0,36	-0,52	0
High	Q9UJS0-2	Isoform 2 of Calcium-binding mitochondrial carrier protein Aralar2 [OS=Homo	165,455968	41,2721893	20	65	15	676	74,257	SLC25A13	0,27	0,35	-0,08	5
High	Q9GZS1-1	DNA-directed RNA polymerase I subunit RPA49 [OS=Homo sapiens]	15,8396123	6,02910603	3	7	3	481	53,928	POLR1E	0,69	0,35	0,34	0
High	O14949	Cytochrome b-c1 complex subunit 8 [OS=Homo sapiens]	6,6453999	15,8536585	1	2	1	82	9,9	UQCRQ	0,63	0,35	0,27	0
High	P27448-5	MAP/microtubule affinity-regulating kinase 3 [OS=Homo sapiens]	304,627752	55,7768924	36	128	2	753	84,436	MARK3	0,42	0,34	0,08	29
High	Q7L3S4	Zinc finger protein 771 [OS=Homo sapiens]	157,629962	50,1577287	20	65	20	317	35,679	ZNF771	0,26	0,34	-0,08	0
High	O43660-1	Pleiotropic regulator 1 [OS=Homo sapiens]	20,3624524	19,0661479	9	10	9	514	57,158	PLRG1	0,32	0,34	-0,02	0
High	Q8TCJ2	Dolichyl-diphosphooligosaccharide--protein glycosyltransferase subunit STT3B	8,44655769	5,08474576	3	3	3	826	93,614	STT3B	0,27	0,34	-0,07	0
High	O75533-1	splicing factor 3B subunit 1 [OS=Homo sapiens]	43,2838375	10,4294479	11	18	11	1304	145,738	SF3B1	-0,14	0,33	-0,47	0
High	Q9H0U3	Magnesium transporter protein 1 [OS=Homo sapiens]	7,57135398	8,05970149	3	3	3	335	38,011	MAGT1	0,37	0,33	0,04	0
High	Q13247	Serine/arginine-rich splicing factor 6 [OS=Homo sapiens]	11,6691668	6,68604651	3	4	3	344	39,563	SRSF6	0,24	0,32	-0,08	0
High	Q9H2S9	Zinc finger protein Eos [OS=Homo sapiens]	21,0041293	14,8717949	7	8	7	585	64,065	IKZF4	0,78	0,31	0,47	0
Medium	O75530-2	Isoform 2 of Polycomb protein EED [OS=Homo sapiens]	3,15244696	5,57939914	2	2	2	466	53,027	EED	0,58	0,31	0,28	0
High	Q9UHX1-2	Isoform 2 of Poly(U)-binding-splicing factor PUF60 [OS=Homo sapiens]	311,059489	68,0811808	26	136	26	542	58,135	PUF60	0,43	0,29	0,14	0
High	Q9NSD4	zinc finger protein 275 [OS=Homo sapiens]	16,7628187	10,955711	5	9	5	429	48,412	ZNF275	0,6	0,29	0,31	0
High	Q9Y5A9-1	YTH domain-containing family protein 2 [OS=Homo sapiens]	7,82491158	5,87219344	3	4	3	579	62,296	YTHDF2	0,35	0,29	0,07	0
High	Q14680	Maternal embryonic leucine zipper kinase [OS=Homo sapiens]	11,2073142	5,99078341	4	5	3	651	74,594	MELK	0,48	0,28	0,21	1
High	O14641	Segment polarity protein dishevelled homolog DVL-2 [OS=Homo sapiens]	5,24683305	1,63043478	1	2	1	736	78,899	DVL2	0,04	0,27	-0,22	0
High	Q6UN15-3	Isoform 3 of Pre-mRNA 3'-end-processing factor FIP1 [OS=Homo sapiens]	532,425179	54,8076923	31	417	1	520	58,341	FIP1L1	0,4	0,26	0,15	0
High	P61513	60S ribosomal protein L37a [OS=Homo sapiens]	86,18308	52,173913	6	44	6	92	10,268	RPL37A	0,14	0,26	-0,12	0
High	Q9H936	Mitochondrial glutamate carrier 1 [OS=Homo sapiens]	4,92860748	4,95356037	2	2	2	323	34,448	SLC25A22	-0,13	0,26	-0,38	0
High	Q9NX20	39S ribosomal protein L16, mitochondrial [OS=Homo sapiens]	8,25543681	8,36653386	2	2	2	251	28,431	MRPL16	0,22	0,25	-0,03	0
Medium	P42695	condensin-2 complex subunit D3 [OS=Homo sapiens]	4,46354636	1,8024032	2	2	2	1498	168,783	NCAPD3	-0,26	0,25	-0,52	0
High	Q2TAK8-1	PWWP domain-containing protein MUM1 [OS=Homo sapiens]	38,2226844	14,084507	10	16	10	710	78,587	MUM1	0,59	0,24	0,35	0
High	Q9Y3T9	Nucleolar complex protein 2 homolog [OS=Homo sapiens]	10,8274146	2,67022697	2	3	2	749	84,866	NOC2L	0,72	0,24	0,48	0
High	P62805	histone H4 [OS=Homo sapiens]	127,070315	52,4271845	7	44	7	103	11,36	ST1H4H; HIST1	0,22	0,23	-0,01	0
High	O14545	TRAF-type zinc finger domain-containing protein 1 [OS=Homo sapiens]	5,64949013	3,26460481	2	2	2	582	64,8	TRAFD1	0,5	0,23	0,27	0
High	P07814	Bifunctional glutamate/proline--tRNA ligase [OS=Homo sapiens]	4,96421477	0,5952381	1	3	1	1512	170,483	EPRS	-0,16	0,23	-0,39	0
High	Q9BXS5-2	Isoform 2 of AP-1 complex subunit mu-1 [OS=Homo sapiens]	4,71990771	1,6091954	1	3	1	435	49,809	AP1M1	0,01	0,23	-0,22	0
High	P08238	Heat shock protein HSP 90-beta [OS=Homo sapiens]	155,499021	33,0110497	22	65	11	724	83,212	HSP90AB1	-0,06	0,22	-0,27	12
High	P06733-1	alpha-enolase [OS=Homo sapiens]	40,6761762	14,0552995	7	16	7	434	47,139	ENO1	-0,16	0,22	-0,37	0
High	P68431	Histone H3.1 [OS=Homo sapiens]	15,5322695	16,9117647	3	16	3	136	15,394	ST1H3H; HIST1	0,15	0,22	-0,07	0
High	P15531-2	Isoform 2 of Nucleoside diphosphate kinase A [OS=Homo sapiens]	4,82131076	6,77966102	1	1	1	177	19,641	NME1	0,37	0,22	0,15	0
High	Q9H8H2	Probable ATP-dependent RNA helicase DDX31 [OS=Homo sapiens]	4,77768214	3,40775558	2	2	2	851	94,029	DDX31	0,32	0,22	0,1	0
High	Q9UKF6	Cleavage and polyadenylation specificity factor subunit 3 [OS=Homo sapiens]	53,7017994	22,8070175	13	30	13	684	77,436	CPSF3	0,43	0,21	0,22	0
High	P22087	rRNA 2'-O-methyltransferase fibrillarin [OS=Homo sapiens]	5,82600955	4,36137072	2	2	2	321	33,763	FBL	0,8	0,21	0,6	0
Low	Q99728	BRCA1-associated RING domain protein 1 [OS=Homo sapiens]	1,47404866	1,54440154	1	1	1	777	86,593	BARD1	0,19	0,21	-0,03	0
High	P62273-1	40S ribosomal protein S29 [OS=Homo sapiens]	12,8595986	26,7857143	2	25	2	56	6,672	RPS29	0,1	0,2	-0,1	0
High	Q8N357	Solute carrier family 35 member F6 [OS=Homo sapiens]	5,00907609	5,1212938	2	2	2	371	40,188	2orf18; SLC35F	0,71	0,2	0,51	0
High	P62913	60S ribosomal protein L11 [OS=Homo sapiens]	177,663272	66,8539326	13	189	13	178	20,24	RPL11	-0,06	0,19	-0,25	0
High	P32969	60S ribosomal protein L9 [OS=Homo sapiens]	114,201463	49,4791667	6	29	6	192	21,85	RPL9	0,01	0,19	-0,18	0
High	P62861	40S ribosomal protein S30 [OS=Homo sapiens]	66,5719454	33,8983051	6	59	6	59	6,644	FAU	0,1	0,19	-0,09	0
High	O15235	28S ribosomal protein S12, mitochondrial [OS=Homo sapiens]	63,7979846	44,2028986	5	26	5	138	15,163	MRPS12	0,13	0,19	-0,06	0
High	Q9P258	Protein RCC2 [OS=Homo sapiens]	21,5626035	17,4329502	8	11	8	522	56,049	RCC2	0,29	0,19	0,09	0
Medium	Q9HC62	Sentrin-specific protease 2 [OS=Homo sapiens]	3,70991871	2,5466893	2	2	2	589	67,812	SENP2	0,03	0,19	-0,16	0
High	O00541-1	Pescadillo homolog [OS=Homo sapiens]	229,911752	45,7482993	30	111	30	588	67,96	PES1	0,3	0,18	0,12	0
High	P62277	40S ribosomal protein S13 [OS=Homo sapiens]	227,086541	51,6556291	13	155	13	151	17,212	RPS13	-0,07	0,18	-0,26	0
High	Q8N257	Histone H2B type 3-B [OS=Homo sapiens]	115,002113	46,8253968	7	64	2	126	13,9	HIST3H2BB	0,28	0,18	0,1	0
High	P04637	Cellular tumor antigen p53 [OS=Homo sapiens]	36,9888621	25,9541985	10	15	10	393	43,625	TP53	-0,26	0,18	-0,43	0
High	P49458	Signal recognition particle 9 kDa protein [OS=Homo sapiens]	33,2719809	32,5581395	3	15	3	86	10,105	SRP9; SRP9P1	0,22	0,18	0,04	0
High	Q00325-2	Isoform B of Phosphate carrier protein, mitochondrial [OS=Homo sapiens]	230,738215	45,7063712	17	124	17	361	39,933	SLC25A3	0,15	0,17	-0,02	0
High	Q9BX10	GTP-binding protein 2 [OS=Homo sapiens]	39,579444	18,1063123	10	13	10	602	65,727	GTPBP2	0,14	0,17	-0,04	0
High	O75382-1	Tripartite motif-containing protein 3 [OS=Homo sapiens]	23,098127	14,6505376	8	9	8	744	80,779	TRIM3	0,79	0,17	0,62	0
High	Q9H5V9-1	UPF0428 protein CXorf56 [OS=Homo sapiens]	95,9457348	43,2432432	9	35	9	222	25,608	CXorf56	0,28	0,16	0,12	0
High	P14678-3	Isoform SM-B1 of Small nuclear ribonucleoprotein-associated proteins B and B'	5,70530729	7,61245675	3	4	3	289	30,012		-0,07	0,16	-0,23	0
Medium	O00743-3	Isoform 3 of Serine/threonine-protein phosphatase 6 catalytic subunit [OS=Hor	4,5503982	5,84795322	2	2	2	342	38,921	PPP6C	0,25	0,16	0,09	0
High	Q9UGN5-1	Poly [ADP-ribose] polymerase 2 [OS=Homo sapiens]	243,220267	49,2281304	30	109	30	583	66,164	PARP2	-0,03	0,15	-0,17	0
High	P32322-3	Isoform 3 of Pyrroline-5-carboxylate reductase 1, mitochondrial [OS=Homo sap	35,3092422	12,4277457	4	11	3	346	35,958	PYCR1	0,02	0,15	-0,13	1
High	P13639	Elongation factor 2 [OS=Homo sapiens]	6,61817663	4,07925408	3	3	3	858	95,277	EEF2	0,14	0,15	-0,01	0

High	Q9UET6	Putative tRNA (cytidine(32)/guanosine(34)-2'-O)-methyltransferase [OS=Homo	5,9344437	8,20668693	2	2	2	329	36,056	FTSJ1	-1,43	0,15	-1,58	0
High	P18621-3	Isoform 3 of 60S ribosomal protein L17 [OS=Homo sapiens]	641,552393	56,5789474	22	898	21	228	26,356	PL17-C18ORF3	0,02	0,14	-0,13	2
High	P62899-2	Isoform 2 of 60S ribosomal protein L31 [OS=Homo sapiens]	103,997176	40,625	9	64	9	128	14,623	RPL31	0,08	0,14	-0,07	0
High	Q9H8M2-5	Bromodomain-containing protein 9 [OS=Homo sapiens]	109,618558	40,3685092	17	62	17	597	66,958	BRD9	-0,12	0,13	-0,24	0
High	P17858-1	ATP-dependent 6-phosphofructokinase, liver type [OS=Homo sapiens]	54,5860376	24,7435897	16	26	12	780	84,964	PFKL	-0,46	0,13	-0,59	3
High	Q9NQ29	putative RNA-binding protein Luc7-like 1 [OS=Homo sapiens]	427,276402	49,8652291	30	313	21	371	43,701	LUC7L	0,13	0,12	0	0
High	Q9BXF6	Rab11 family-interacting protein 5 [OS=Homo sapiens]	254,093484	53,1393568	28	105	28	653	70,372	RAB11FIP5	0,29	0,11	0,18	0
High	Q8IWA0	WD repeat-containing protein 75 [OS=Homo sapiens]	9,85325563	5,54216867	4	4	4	830	94,438	WDR75	0,3	0,11	0,19	0
Medium	Q92769	Histone deacetylase 2 [OS=Homo sapiens]	3,30636977	2,45901639	1	2	1	488	55,329	HDAC2	0,43	0,11	0,32	0
High	Q16630-2	Isoform 2 of Cleavage and polyadenylation specificity factor subunit 6 [OS=Hon	241,75803	32,1428571	20	84	20	588	63,432	CPSF6	0,07	0,1	-0,03	0
High	Q8WVM0	Dimethyladenosine transferase 1, mitochondrial [OS=Homo sapiens]	172,144392	76,5895954	21	79	21	346	39,518	TFB1M	-0,1	0,1	-0,2	0
Low	Q9UKM9-1	RNA-binding protein Raly [OS=Homo sapiens]	1,36211018	2,94117647	1	1	1	306	32,444	RALY	-0,11	0,1	-0,22	0
High	Q96K58-2	Isoform 2 of Zinc finger protein 668 [OS=Homo sapiens]	26,9763819	17,2897196	8	14	8	642	70,46		0,07	0,09	-0,01	0
High	Q9NVN8	Guanine nucleotide-binding protein-like 3-like protein [OS=Homo sapiens]	12,0642354	4,63917526	3	14	2	582	65,532	GNL3L	0,17	0,09	0,07	0
High	P42766	60S ribosomal protein L35 [OS=Homo sapiens]	285,227524	49,5934959	13	201	13	123	14,543	RPL35	0,03	0,08	-0,05	0
High	P27708	CAD protein [OS=Homo sapiens]	119,613577	15,0561798	28	54	28	2225	242,829	CAD	-0,11	0,08	-0,19	0
Medium	Q9BQ67	Glutamate-rich WD repeat-containing protein 1 [OS=Homo sapiens]	4,41920567	1,79372197	1	2	1	446	49,388	GRWD1	-0,07	0,08	-0,15	0
High	Q9NXF1	Testis-expressed sequence 10 protein [OS=Homo sapiens]	229,625453	38,2131324	30	93	30	929	105,608	TEX10	0,3	0,07	0,23	0
High	P61927	60S ribosomal protein L37 [OS=Homo sapiens]	21,3795605	40,2061856	6	49	6	97	11,071	RPL37	0,08	0,07	0,01	0
High	P62995	transformer-2 protein homolog beta [OS=Homo sapiens]	27,4201108	17,7083333	5	13	5	288	33,646	TRA2B	0,07	0,06	0,01	0
High	Q5T3I0-3	Isoform 3 of G patch domain-containing protein 4 [OS=Homo sapiens]	24,1982583	7,76053215	4	10	4	451	50,897	GPATCH4	0,61	0,06	0,55	0
High	P36542-1	ATP synthase subunit gamma, mitochondrial [OS=Homo sapiens]	181,999865	54,3624161	17	75	17	298	32,975	ATP5C1	0,11	0,05	0,06	0
High	Q9Y285	Phenylalanine--tRNA ligase alpha subunit [OS=Homo sapiens]	153,326948	38,976378	16	62	16	508	57,528	FARSA	0,59	0,05	0,54	0
High	P39019	40S ribosomal protein S19 [OS=Homo sapiens]	99,4424982	50,3448276	10	40	10	145	16,051	RPS19	0	0,05	-0,04	0
High	Q7L0Y3	Mitochondrial ribonuclease P protein 1 [OS=Homo sapiens]	13,0287609	7,94044665	3	4	3	403	47,317	TRMT10C	-0,05	0,05	-0,1	0
High	Q9H7H0-3	Isoform 3 of Methyltransferase-like protein 17, mitochondrial [OS=Homo sapie	10,4782544	5,85774059	3	5	3	478	53,017	METTL17	0	0,05	-0,06	0
High	P13674-2	Isoform 2 of Prolyl 4-hydroxylase subunit alpha-1 [OS=Homo sapiens]	8,48459247	6,92883895	4	5	4	534	60,929	P4HA1	1	0,05	0,95	0
High	P23025	DNA repair protein complementing XP-A cells [OS=Homo sapiens]	8,40592915	7,69230769	1	2	1	273	31,348	XPA	10,27	0,05	10,22	0
Medium	Q96G21	U3 small nucleolar ribonucleoprotein protein IMP4 [OS=Homo sapiens]	2,41217683	4,81099656	1	1	1	291	33,736	IMP4	10,86	0,05	10,81	0
Low	P09543-1	2',3'-cyclic-nucleotide 3'-phosphodiesterase [OS=Homo sapiens]	1,45173345	2,6128266	1	1	1	421	47,549	CNP	-0,5	0,05	-0,55	0
High	P62829	60S ribosomal protein L23 [OS=Homo sapiens]	666,50464	77,1428571	17	678	17	140	14,856	RPL23	0,01	0,04	-0,03	0
High	P62269	40S ribosomal protein S18 [OS=Homo sapiens]	398,246245	59,8684211	25	350	25	152	17,708	RPS18	0,08	0,04	0,03	0
High	Q01813	ATP-dependent 6-phosphofructokinase, platelet type [OS=Homo sapiens]	25,01605	9,94897959	8	14	4	784	85,542	PFKP	0,07	0,04	0,03	0
High	Q9BRX9	WD repeat domain-containing protein 83 [OS=Homo sapiens]	6,58452767	5,3968254	2	4	2	315	34,321	WDR83	-0,58	0,04	-0,63	0
High	P46783	40S ribosomal protein S10 [OS=Homo sapiens]	80,2034269	53,9393939	11	37	11	165	18,886	RPS10	0,09	0,03	0,07	0
High	P56182	Ribosomal RNA processing protein 1 homolog A [OS=Homo sapiens]	52,5116591	18,8720174	9	27	9	461	52,807	RRP1	0,09	0,03	0,06	0
High	P61353	60S ribosomal protein L27 [OS=Homo sapiens]	48,820781	54,4117647	9	24	9	136	15,788	RPL27	0,6	0,03	0,57	0
High	Q96HA1-1	Nuclear envelope pore membrane protein POM 121 [OS=Homo sapiens]	5,11616988	0,88070456	1	2	1	1249	127,642	POM121	0,26	0,03	0,23	0
High	P62280	40S ribosomal protein S11 [OS=Homo sapiens]	291,471926	59,4936709	18	395	18	158	18,419	RPS11	-0,11	0,02	-0,13	0
High	O60783	28S ribosomal protein S14, mitochondrial [OS=Homo sapiens]	42,314184	28,125	3	11	3	128	15,129	MRPS14	0,16	0,02	0,14	0
High	P49755	Transmembrane emp24 domain-containing protein 10 [OS=Homo sapiens]	5,00004343	5,02283105	1	1	1	219	24,96	TMED10	0,45	0,02	0,43	0
Low	Q13573	SNW domain-containing protein 1 [OS=Homo sapiens]	1,72376804	1,86567164	1	1	1	536	61,456	SNW1	0,32	0,02	0,31	0
High	P27635	60S ribosomal protein L10 [OS=Homo sapiens]	556,166375	64,0186916	19	732	19	214	24,588	RPL10	-0,04	0,01	-0,05	0
High	P62081	40S ribosomal protein S7 [OS=Homo sapiens]	411,385447	74,2268041	20	316	20	194	22,113	RPS7	0,12	0,01	0,11	0
High	Q8NHQ9	ATP-dependent RNA helicase DDX55 [OS=Homo sapiens]	87,2679814	23,5	13	32	13	600	68,503	DDX55	0	0,01	-0,01	0
High	Q86Y79	Probable peptidyl-tRNA hydrolase [OS=Homo sapiens]	4,95428594	11,682243	1	1	1	214	22,922	PTRH1	-0,27	0,01	-0,28	0
High	P62857	40S ribosomal protein S28 [OS=Homo sapiens]	138,905241	56,5217391	6	71	6	69	7,836	RPS28	0,09	0	0,09	0
High	Q9UBU9-1	nuclear RNA export factor 1 [OS=Homo sapiens]	79,6900729	33,4410339	15	29	15	619	70,139	NXF1	0,51	0	0,5	0
High	P46778	60S ribosomal protein L21 [OS=Homo sapiens]	78,2538679	40,625	7	33	7	160	18,553	RPL21	0,04	0	0,04	0
High	Q9Y4W6	AFG3-like protein 2 [OS=Homo sapiens]	39,4128957	11,5432873	8	13	8	797	88,528	AFG3L2	0,02	0	0,02	0
High	P84103	Serine/arginine-rich splicing factor 3 [OS=Homo sapiens]	6,35316326	5,48780488	1	4	1	164	19,318	SRSF3	-0,27	0	-0,27	0
High	P62249	40S ribosomal protein S16 [OS=Homo sapiens]	250,936893	73,2876712	17	314	17	146	16,435	RPS16	-0,04	-0,01	-0,03	0
High	Q8N6R0-5	Methyltransferase-like protein 13 [OS=Homo sapiens]	98,5735431	28,8984263	18	36	18	699	78,718	METTL13	0,2	-0,01	0,21	0
High	Q8IY37	Probable ATP-dependent RNA helicase DHX37 [OS=Homo sapiens]	24,2322647	6,65514261	8	11	8	1157	129,464	DHX37	-0,03	-0,01	-0,03	0
High	P48047	ATP synthase subunit O, mitochondrial [OS=Homo sapiens]	18,3737571	25,3521127	5	5	5	213	23,263	ATP5O	0,33	-0,01	0,34	0
High	Q9BTC0	Death-inducer obliterator 1 [OS=Homo sapiens]	8,3355216	1,65178571	4	5	4	2240	243,723	DIDO1	0,29	-0,01	0,3	0
High	P12236	ADP/ATP translocase 3 [OS=Homo sapiens]	390,362187	67,4496644	24	283	4	298	32,845	SLC25A6	-0,05	-0,02	-0,03	5
High	P83731	60S ribosomal protein L24 [OS=Homo sapiens]	154,070702	48,4076433	15	239	15	157	17,768	RPL24	0,08	-0,02	0,1	0
High	O43663-1	Protein regulator of cytokinesis 1 [OS=Homo sapiens]	48,3442081	19,6774194	11	23	10	620	71,562	PRC1	0,3	-0,02	0,33	0
High	P62244	40S ribosomal protein S15a [OS=Homo sapiens]	269,853761	75,3846154	13	141	13	130	14,83	RPS15A	-0,15	-0,03	-0,12	0
High	P63173	60s ribosomal protein l38 [OS=Homo sapiens]	84,9443821	52,8571429	6	66	6	70	8,213	RPL38	0,02	-0,03	0,05	0

High	O95470	sphingosine-1-phosphate lyase 1 [OS=Homo sapiens]	7,93936962	4,40140845	3	4	3	568	63,483	SGPL1	-0,1	-0,03	-0,07	0
High	P62266	40S ribosomal protein S23 [OS=Homo sapiens]	371,017231	72,027972	17	1188	17	143	15,798	RPS23	-0,08	-0,04	-0,04	0
High	P83881	60S ribosomal protein L36a [OS=Homo sapiens]	160,856691	53,7735849	13	191	4	106	12,433	RPL36A	0,03	-0,04	0,07	16
High	Q9Y6A4	Cilia- and flagella-associated protein 20 [OS=Homo sapiens]	26,1343312	23,3160622	5	9	5	193	22,76	16orf80; CFAP2	0,27	-0,04	0,31	0
High	P46777	60S ribosomal protein L5 [OS=Homo sapiens]	5,22047176	5,38720539	2	2	2	297	34,341	RPL5	-0,38	-0,04	-0,34	0
High	P41252	isoleucine--tRNA ligase, cytoplasmic [OS=Homo sapiens]	4,98886525	2,13946117	3	3	3	1262	144,406	IARS	-0,27	-0,04	-0,23	0
Low	P49321-3	Isoform 3 of Nuclear autoantigenic sperm protein [OS=Homo sapiens]	1,24366823	0,88607595	1	1	1	790	86,216	NASP	0,03	-0,04	0,07	0
High	P60866-2	Isoform 2 of 40S ribosomal protein S20 [OS=Homo sapiens]	109,22262	36,6197183	7	49	7	142	15,995	RPS20	-0,11	-0,05	-0,06	0
High	Q14683	structural maintenance of chromosomes protein 1a [OS=Homo sapiens]	66,7068715	14,2741281	17	28	17	1233	143,144	SMC1A	0,1	-0,05	0,15	0
High	P08670	Vimentin [OS=Homo sapiens]	32,4553228	12,4463519	6	17	5	466	53,619	VIM	-0,14	-0,05	-0,09	0
High	Q9NQZ2	Something about silencing protein 10 [OS=Homo sapiens]	12,92576	9,39457203	4	7	4	479	54,525	UTP3	0,17	-0,05	0,22	0
Low	Q9BWC9	Coiled-coil domain-containing protein 106 [OS=Homo sapiens]	2,05178271	2,85714286	1	1	1	280	32,012	CCDC106	0,65	-0,05	0,71	0
High	P07437	tubulin beta chain [OS=Homo sapiens]	932,87256	84,009009	33	542	5	444	49,639	TUBB	-0,05	-0,06	0,01	2
High	P46782	40S ribosomal protein S5 [OS=Homo sapiens]	386,784851	72,0588235	17	477	17	204	22,862	RPS5	-0,07	-0,06	-0,02	0
High	Q8IWS0-1	PHD finger protein 6 [OS=Homo sapiens]	234,993548	45,4794521	20	112	20	365	41,264	PHF6	-0,31	-0,06	-0,25	0
High	Q05519	serine/arginine-rich splicing factor 11 [OS=Homo sapiens]	18,8808565	13,4297521	4	8	4	484	53,51	SRSF11	0,46	-0,06	0,52	0
High	P11021	78 kDa glucose-regulated protein [OS=Homo sapiens]	456,642055	57,1865443	40	190	37	654	72,288	HSPA5	-0,56	-0,07	-0,49	0
High	Q53GQ0	Very-long-chain 3-oxoacyl-CoA reductase [OS=Homo sapiens]	82,08143	34,9358974	9	28	9	312	34,302	HSD17B12	0,01	-0,07	0,08	0
High	Q9Y5J1	U3 small nucleolar RNA-associated protein 18 homolog [OS=Homo sapiens]	65,9566942	24,4604317	10	20	10	556	61,964	UTP18	0,14	-0,07	0,2	0
High	O43175	D-3-phosphoglycerate dehydrogenase [OS=Homo sapiens]	31,3616884	12,0075047	7	15	7	533	56,614	PHGDH	0,2	-0,07	0,27	0
High	Q14498-2	Isoform 2 of RNA-binding protein 39 [OS=Homo sapiens]	622,175138	60,1145038	32	342	29	524	58,62	RBM39	0	-0,08	0,08	4
High	P62910	60S ribosomal protein L32 [OS=Homo sapiens]	119,161638	50,3703704	8	51	8	135	15,85	RPL32	0	-0,08	0,08	0
High	P07910-1	Heterogeneous nuclear ribonucleoproteins C1/C2 [OS=Homo sapiens]	94,4708534	39,2156863	15	42	15	306	33,65	HNRNPC	-0,37	-0,08	-0,29	0
High	P08708	40S ribosomal protein S17 [OS=Homo sapiens]	572,553962	73,3333333	17	474	17	135	15,54	RPS17; RPS17L	-0,16	-0,09	-0,07	0
High	P62847-4	Isoform 4 of 40S ribosomal protein S24 [OS=Homo sapiens]	282,503277	21,1072664	8	190	8	289	32,41	RPS24	0,16	-0,09	0,26	0
High	P46779	60S ribosomal protein L28 [OS=Homo sapiens]	65,0565305	38,6861314	7	47	7	137	15,738	RPL28	-0,03	-0,09	0,06	0
High	Q9P0U4-2	Isoform 2 of CXXC-type zinc finger protein 1 [OS=Homo sapiens]	14,7961915	10,1515152	6	9	6	660	76,178	CXXC1	-0,53	-0,09	-0,45	0
Low	Q92797-1	Symplekin [OS=Homo sapiens]	1,55083027	0,86342229	1	1	1	1274	141,059	SYMPK	-0,06	-0,09	0,03	0
High	Q6UN15-1	Pre-mRNA 3'-end-processing factor FIP1 [OS=Homo sapiens]	634,587021	68,6868687	40	482	10	594	66,487	FIP1L1	0,17	-0,1	0,27	44
High	Q5QNW6-2	Isoform 2 of Histone H2B type 2-F [OS=Homo sapiens]	134,62001	49,2537313	8	82	1	134	14,832	HIST2H2BF	0,02	-0,1	0,11	12
High	Q8N684-3	Isoform 3 of Cleavage and polyadenylation specificity factor subunit 7 [OS=Hon	23,7328409	13,618677	6	17	6	514	56,341	CPSF7	-0,04	-0,1	0,06	0
High	Q8WWC4	Uncharacterized protein C2orf47, mitochondrial [OS=Homo sapiens]	13,1980565	10,652921	3	5	3	291	32,524	C2orf47	0,07	-0,1	0,17	0
High	A0FGR8-6	Isoform 6 of Extended synaptotagmin-2 [OS=Homo sapiens]	12,813607	3,71549894	4	6	4	942	104,643		-0,15	-0,1	-0,05	0
High	P43307	Translocon-associated protein subunit alpha [OS=Homo sapiens]	7,23864742	2,7972028	1	3	1	286	32,215	SSR1	-0,35	-0,1	-0,25	0
High	P84098	60S ribosomal protein L19 [OS=Homo sapiens]	136,170823	33,1632653	12	75	12	196	23,451	RPL19	-0,05	-0,11	0,06	0
High	Q9NZM5	Glioma tumor suppressor candidate region gene 2 protein [OS=Homo sapiens]	126,909919	43,5146444	19	62	19	478	54,356	GLTSCR2	0,05	-0,11	0,15	0
High	P20700	Lamin-B1 [OS=Homo sapiens]	68,769292	22,0136519	13	26	12	586	66,368	LMNB1	0,37	-0,11	0,47	0
High	P46776	60S ribosomal protein L27a [OS=Homo sapiens]	98,3929002	34,4594595	6	144	6	148	16,551	RPL27A	-0,14	-0,12	-0,02	0
High	P16104	Histone H2AX [OS=Homo sapiens]	62,3567585	37,7622378	6	59	1	143	15,135	H2AFX	-0,27	-0,12	-0,15	2
High	Q9NPI1-2	Isoform 2 of Bromodomain-containing protein 7 [OS=Homo sapiens]	59,8595707	23,1595092	13	29	13	652	74,22	BRD7	-0,46	-0,12	-0,33	0
High	P31689-1	DnaJ homolog subfamily A member 1 [OS=Homo sapiens]	54,3265007	24,1813602	7	15	7	397	44,839	DNAJA1	0	-0,13	0,12	0
Medium	Q9P035	Very-long-chain (3R)-3-hydroxyacyl-CoA dehydratase 3 [OS=Homo sapiens]	2,37975981	1,93370166	1	1	1	362	43,132	PTPLAD1; HACD	0,29	-0,13	0,42	0
High	P61247	40S ribosomal protein S3a [OS=Homo sapiens]	526,420405	74,6212121	30	306	30	264	29,926	RPS3A	-0,14	-0,14	0,01	0
High	Q10570	Cleavage and polyadenylation specificity factor subunit 1 [OS=Homo sapiens]	525,611991	45,1143451	62	243	62	1443	160,782	CPSF1	-0,09	-0,14	0,05	0
High	P04908	histone H2A type 1-B/E [OS=Homo sapiens]	104,964422	36,1538462	8	70	2	130	14,127	T1H2AB; HIST1H	-0,03	-0,14	0,11	8
High	P37108	Signal recognition particle 14 kDa protein [OS=Homo sapiens]	57,444773	41,9117647	7	25	7	136	14,561	SRP14	0,02	-0,14	0,16	0
High	Q14839-2	Isoform 2 of Chromodomain-helicase-DNA-binding protein 4 [OS=Homo sapien	5,62497206	2,21649485	4	4	4	1940	220,709	CHD4	0,09	-0,14	0,23	0
Medium	P22061-2	Isoform 2 of Protein-L-isoaspartate(D-aspartate) O-methyltransferase [OS=Hom	4,21745572	6,57894737	1	1	1	228	24,664	PCMT1	-0,23	-0,14	-0,08	0
Medium	O43772	mitochondrial carnitine/acylcarnitine carrier protein [OS=Homo sapiens]	3,47990967	2,99003322	1	1	1	301	32,922	SLC25A20	-0,19	-0,14	-0,05	0
High	P0C0S8	histone H2A type 1 [OS=Homo sapiens]	151,483093	36,1538462	8	90	2	130	14,083	M; HIST1H2AI;	-0,07	-0,15	0,08	0
High	Q9P2N5	RNA-binding protein 27 [OS=Homo sapiens]	53,7606242	16,1320755	14	31	13	1060	118,645	RBM27	-0,8	-0,15	-0,66	0
High	Q7KZI7-1	Serine/threonine-protein kinase MARK2 [OS=Homo sapiens]	170,25147	37,9441624	23	72	2	788	87,856	MARK2	0,09	-0,16	0,25	11
High	Q9Y3C1	nucleolar protein 16 [OS=Homo sapiens]	173,225736	56,741573	13	61	13	178	21,175	NOP16	-0,31	-0,17	-0,15	0
Low	Q9BQC6	Ribosomal protein 63, mitochondrial [OS=Homo sapiens]	1,67060212	12,745098	1	1	1	102	12,259	MRP63; MRPL5	-0,07	-0,17	0,1	0
High	P0DMV8	heat shock 70 kDa protein 1A [OS=Homo sapiens]	622,886515	68,798752	45	301	36	641	70,009	HSPA1B; HSPA1	0,21	-0,18	0,38	17
High	O95232-1	Luc7-like protein 3 [OS=Homo sapiens]	406,978784	43,9814815	28	453	28	432	51,435	LUC7L3	0,1	-0,18	0,28	0
High	O94761	ATP-dependent DNA helicase Q4 [OS=Homo sapiens]	53,6822256	10,7615894	11	22	11	1208	132,993	RECQL4	-0,02	-0,18	0,16	0
High	Q9H0W5	Coiled-coil domain-containing protein 8 [OS=Homo sapiens]	18,3573614	11,33829	4	8	4	538	59,339	CCDC8	0,11	-0,18	0,29	0
High	Q9BQG0-2	Isoform 2 of Myb-binding protein 1A [OS=Homo sapiens]	16,3042154	2,77777778	4	8	4	1332	149,274	MYBBP1A	-0,02	-0,18	0,16	0
Medium	O95391	Pre-mRNA-splicing factor SLU7 [OS=Homo sapiens]	2,65423431	1,53583618	1	1	1	586	68,344	SLU7	0,36	-0,18	0,54	0
High	P62854	40S ribosomal protein S26 [OS=Homo sapiens]	171,275376	52,173913	6	171	6	115	13,007	OC101929876;	-0,22	-0,19	-0,03	0

High	Q9Y3U8	60S ribosomal protein L36 [OS=Homo sapiens]	51,2706185	30,4761905	4	23	4	105	12,246	RPL36	-0,07	-0,19	0,12	0
High	P53985	Monocarboxylate transporter 1 [OS=Homo sapiens]	26,1101033	6,6	3	5	3	500	53,909	SLC16A1	-0,31	-0,19	-0,12	0
High	P12235	ADP/ATP translocase 1 [OS=Homo sapiens]	395,37639	68,1208054	23	257	4	298	33,043	SLC25A4	-0,01	-0,2	0,19	0
High	Q9UGY1	Nucleolar protein 12 [OS=Homo sapiens]	127,458048	49,7652582	11	40	11	213	24,648	NOL12	-0,24	-0,2	-0,03	0
High	Q9BSC4-1	Nucleolar protein 10 [OS=Homo sapiens]	19,1799598	6,83139535	5	7	5	688	80,251	NOL10	-0,7	-0,2	-0,5	0
High	P23396-1	40S ribosomal protein S3 [OS=Homo sapiens]	419,003023	83,9506173	26	285	26	243	26,671	RPS3	-0,13	-0,21	0,08	0
High	P49207	60S ribosomal protein L34 [OS=Homo sapiens]	56,4094084	38,4615385	8	49	8	117	13,284	RPL34	-0,5	-0,21	-0,29	0
Medium	Q6KCM7-3	Isoform 3 of Calcium-binding mitochondrial carrier protein SCaMC-2 [OS=Homo	2,50003813	2,52427184	1	1	1	515	56,846	SLC25A25	-0,53	-0,21	-0,32	0
High	P62753	40S RIBOSOMAL PROTEIN S6 [OS=Homo sapiens]	636,656637	49,3975904	21	534	21	249	28,663	RPS6	-0,06	-0,23	0,17	0
High	Q6P2Q9	Pre-mRNA-processing-splicing factor 8 [OS=Homo sapiens]	92,5078058	7,06638116	16	39	16	2335	273,427	PRPF8	-0,38	-0,23	-0,15	0
High	Q8N5H7-1	SH2 domain-containing protein 3C [OS=Homo sapiens]	63,8335089	16,744186	13	35	12	860	94,352	SH2D3C	0,4	-0,23	0,63	0
High	P62318	small nuclear ribonucleoprotein sm d3 [OS=Homo sapiens]	10,0373706	7,14285714	1	4	1	126	13,907	SNRPD3	-0,35	-0,23	-0,13	0
Low	Q96RL1	BRCA1-A complex subunit RAP80 [OS=Homo sapiens]	1,28382965	1,25173853	1	1	1	719	79,678	UIMC1	-0,12	-0,23	0,1	0
High	P62701	40S ribosomal protein S4, X isoform [OS=Homo sapiens]	553,228587	73,7642586	26	451	26	263	29,579	RPS4X	-0,27	-0,24	-0,03	0
High	Q8IUE6	Histone H2A type 2-B [OS=Homo sapiens]	29,5546623	35,3846154	4	33	1	130	13,987	HIST2H2AB	0,03	-0,24	0,27	0
High	P60891	ribose-phosphate pyrophosphokinase 1 [OS=Homo sapiens]	18,0490297	14,4654088	4	5	4	318	34,812	PRPS1	-0,33	-0,25	-0,08	0
High	Q8N1G4	Leucine-rich repeat-containing protein 47 [OS=Homo sapiens]	16,2253881	8,9193825	4	6	4	583	63,434	LRRC47	0,07	-0,25	0,32	0
High	Q9Y383	Putative RNA-binding protein Luc7-like 2 [OS=Homo sapiens]	781,30089	64,2857143	40	641	31	392	46,486	LUC7L2	0,42	-0,26	0,68	20
High	P46781	40S ribosomal protein S9 [OS=Homo sapiens]	305,111856	59,2783505	23	306	23	194	22,578	RPS9	-0,28	-0,26	-0,01	0
High	P61254	60S ribosomal protein L26 [OS=Homo sapiens]	160,012	53,1034483	13	179	5	145	17,248	RPL26	-0,21	-0,26	0,05	16
High	Q9Y2R4	Probable ATP-dependent RNA helicase DDX52 [OS=Homo sapiens]	21,7962365	7,01168614	4	11	3	599	67,456	DDX52	0,36	-0,26	0,63	0
High	P06493	Cyclin-dependent kinase 1 [OS=Homo sapiens]	17,4445711	11,1111111	3	5	2	297	34,074	CDK1	0,25	-0,26	0,51	0
High	O00483	Cytochrome c oxidase subunit NDUFA4 [OS=Homo sapiens]	15,5485917	46,9135802	4	7	4	81	9,364	NDUFA4	0,37	-0,26	0,63	0
High	P62917	60S ribosomal protein L8 [OS=Homo sapiens]	300,724581	67,7042802	20	140	20	257	28,007	RPL8	-0,18	-0,27	0,1	0
High	P62888	60S ribosomal protein L30 [OS=Homo sapiens]	93,561983	66,0869565	7	33	7	115	12,776	RPL30	-0,39	-0,27	-0,11	0
High	Q92621	Nuclear pore complex protein Nup205 [OS=Homo sapiens]	16,6133351	2,48508946	5	8	5	2012	227,776	NUP205	-0,46	-0,27	-0,19	0
High	P31947-1	14-3-3 protein sigma [OS=Homo sapiens]	9,3428917	6,4516129	2	4	1	248	27,757	SFN	-0,19	-0,27	0,08	1
High	P62750	60S ribosomal protein L23a [OS=Homo sapiens]	302,215925	48,0769231	14	223	14	156	17,684	RPL23A	-0,13	-0,28	0,14	0
High	P29372-2	Isoform 2 of DNA-3-methyladenine glycosylase [OS=Homo sapiens]	92,6985759	47,440273	11	37	11	293	32,16	MPG	-0,11	-0,28	0,17	0
High	P61964	WD repeat-containing protein 5 [OS=Homo sapiens]	22,183194	15,2694611	4	8	4	334	36,565	WDR5	-0,08	-0,28	0,2	0
High	P25705-1	ATP synthase subunit alpha, mitochondrial [OS=Homo sapiens]	148,154238	49,5479204	26	59	26	553	59,714	ATP5A1	-0,31	-0,29	-0,02	0
High	Q969Q0	60S ribosomal protein L36a-like [OS=Homo sapiens]	142,378677	50,9433962	11	174	2	106	12,461	RPL36AL	-0,05	-0,29	0,25	0
High	P82914	28S ribosomal protein S15, mitochondrial [OS=Homo sapiens]	23,7470479	24,1245136	7	14	7	257	29,823	MRPS15	1,33	-0,29	1,61	0
High	Q6P1X5	Transcription initiation factor TFIID subunit 2 [OS=Homo sapiens]	912,300186	63,2193495	79	574	79	1199	136,883	TAF2	-0,43	-0,3	-0,13	0
High	Q5JTH9-1	RRP12-like protein [OS=Homo sapiens]	249,507338	34,387047	38	115	38	1297	143,611	RRP12	-0,31	-0,32	0,01	0
High	P62263	40S ribosomal protein S14 [OS=Homo sapiens]	237,459585	41,7218543	9	114	9	151	16,263	RPS14	-0,26	-0,32	0,06	0
High	P12004	proliferating cell nuclear antigen [OS=Homo sapiens]	86,7085997	54,0229885	13	41	13	261	28,75	PCNA	-0,2	-0,32	0,11	0
High	Q9UBX3-2	Isoform 2 of Mitochondrial dicarboxylate carrier [OS=Homo sapiens]	81,5951815	43,9189189	11	27	11	296	32,125	SLC25A10	-0,34	-0,32	-0,02	0
High	Q9H5H4	Zinc finger protein 768 [OS=Homo sapiens]	30,9816255	21,1111111	10	14	10	540	60,191	ZNF768	-0,26	-0,32	0,07	0
High	P51571	translocon-associated protein subunit delta [OS=Homo sapiens]	30,716098	18,4971098	4	9	4	173	18,987	SSR4	-0,07	-0,32	0,24	0
High	P0C7P4	Putative cytochrome b-c1 complex subunit Rieske-like protein 1 [OS=Homo sap	8,11046931	4,94699647	1	6	1	283	30,796	UQCRFS1P1	-0,19	-0,32	0,13	0
High	Q13509	tubulin beta-3 chain [OS=Homo sapiens]	474,482268	38	17	284	1	450	50,4	TUBB3	-0,43	-0,33	-0,11	1
High	Q96ME7	Zinc finger protein 512 [OS=Homo sapiens]	67,9333388	35,8024691	13	37	13	567	64,641	ZNF512	-0,26	-0,33	0,07	0
High	Q12906-7	Isoform 7 of Interleukin enhancer-binding factor 3 [OS=Homo sapiens]	4,63922477	3,56347439	3	3	3	898	95,748	ILF3	-0,43	-0,33	-0,1	0
High	P27448-6	Isoform 5 of MAP/microtubule affinity-regulating kinase 3 [OS=Homo sapiens]	278,387019	56,6619916	35	125	1	713	79,886	MARK3	0,11	-0,34	0,45	0
High	Q5SY16	Polynucleotide 5'-hydroxyl-kinase NOL9 [OS=Homo sapiens]	72,6521207	24,2165242	12	31	12	702	79,272	NOL9	0,34	-0,34	0,67	0
Medium	O95163	Elongator complex protein 1 [OS=Homo sapiens]	3,03409308	0,67567568	1	1	1	1332	150,159	IKBKAP	0,27	-0,34	0,6	0
High	P30050-1	60S ribosomal protein L12 [OS=Homo sapiens]	29,6793036	33,3333333	4	10	4	165	17,808	RPL12	0,15	-0,35	0,5	0
High	Q96MU7-1	YTH domain-containing protein 1 [OS=Homo sapiens]	13,5797878	5,36451169	4	7	4	727	84,649	YTHDC1	-0,51	-0,35	-0,16	0
High	O95639	Cleavage and polyadenylation specificity factor subunit 4 [OS=Homo sapiens]	253,174746	75,464684	18	108	2	269	30,235	CPSF4	-0,25	-0,36	0,12	24
High	Q9Y2W1	Thyroid hormone receptor-associated protein 3 [OS=Homo sapiens]	95,8083983	20,8376963	20	48	18	955	108,601	THRAP3	-0,3	-0,37	0,08	0
High	Q14684	Ribosomal RNA processing protein 1 homolog B [OS=Homo sapiens]	15,3399642	6,72823219	4	7	4	758	84,375	RRP1B	0,13	-0,38	0,5	0
High	P62851	40S ribosomal protein S25 [OS=Homo sapiens]	99,8869879	39,2	8	105	8	125	13,734	RPS25	-0,04	-0,39	0,35	0
High	O75643-1	U5 small nuclear ribonucleoprotein 200 kDa helicase [OS=Homo sapiens]	83,9720518	9,83146067	16	34	16	2136	244,353	SNRNP200	-0,71	-0,39	-0,32	0
High	P63244	Guanine nucleotide-binding protein subunit beta-2-like 1 [OS=Homo sapiens]	22,67439	25,8675079	8	8	8	317	35,055	GNB2L1; RACK1	-0,69	-0,39	-0,31	0
High	Q9UQE7	Structural maintenance of chromosomes protein 3 [OS=Homo sapiens]	22,5294284	5,42317173	7	12	7	1217	141,454	SMC3	0,03	-0,39	0,42	0
High	P46734-3	Isoform 2 of Dual specificity mitogen-activated protein kinase kinase 3 [OS=Hor	14,7805642	13,9204545	5	7	5	352	39,914		-0,41	-0,39	-0,01	0
High	Q6P3X3	tetratricopeptide repeat protein 27 [OS=Homo sapiens]	6,6760827	4,15183867	3	3	3	843	96,571	TTC27	1,38	-0,39	1,77	0
High	Q9HCM4-2	Isoform 2 of Band 4.1-like protein 5 [OS=Homo sapiens]	394,58991	72,8712871	30	339	6	505	57,849	EPB41L5	-0,24	-0,4	0,16	0
High	Q00839	Heterogeneous nuclear ribonucleoprotein U [OS=Homo sapiens]	106,512561	23,5151515	17	45	17	825	90,528	HNRNPU	1,68	-0,4	2,08	0
High	P55081	microfibrillar-associated protein 1 [OS=Homo sapiens]	102,550418	48,5193622	19	46	19	439	51,927	MFAP1	-0,47	-0,4	-0,07	0

High	Q92522	Histone H1x [OS=Homo sapiens]	100,945818	37,0892019	10	41	10	213	22,474	H1FX	-0,22	-0,4	0,18	0
High	P06748	Nucleophosmin [OS=Homo sapiens]	14,5917647	16,6666667	3	4	3	294	32,555	NPM1	-0,49	-0,4	-0,1	0
High	P26368	Splicing factor U2AF 65 kDa subunit [OS=Homo sapiens]	554,117764	67,1578947	29	384	29	475	53,467	U2AF2	-0,24	-0,41	0,17	0
High	Q9UJK0	Ribosome biogenesis protein TSR3 homolog [OS=Homo sapiens]	123,403015	48,0769231	11	45	11	312	33,575	TSR3	-0,25	-0,41	0,16	0
High	Q53H12	Acylglycerol kinase, mitochondrial [OS=Homo sapiens]	14,0766899	11,6113744	4	5	4	422	47,107	AGK	-0,56	-0,41	-0,15	0
High	Q14974	Importin subunit beta-1 [OS=Homo sapiens]	9,59774362	5,59360731	5	6	5	876	97,108	KPNB1	-0,3	-0,41	0,1	0
High	P62841	40S ribosomal protein S15 [OS=Homo sapiens]	685,822563	73,1034483	9	487	9	145	17,029	RPS15	-0,41	-0,42	0,01	0
High	Q9BYT3-1	Serine/threonine-protein kinase 33 [OS=Homo sapiens]	39,9578826	24,3190661	11	22	11	514	57,794	STK33	0,23	-0,42	0,65	0
High	Q9UNF1	Melanoma-associated antigen D2 [OS=Homo sapiens]	14,6077003	10,5610561	5	7	5	606	64,914	MAGED2	-0,21	-0,42	0,21	0
High	P15880	40S ribosomal protein S2 [OS=Homo sapiens]	282,905051	59,3856655	18	136	18	293	31,305	RPS2	-0,66	-0,43	-0,23	0
High	Q9UNQ2	Probable dimethyladenosine transferase [OS=Homo sapiens]	160,655479	73,8019169	21	94	21	313	35,214	DIMT1	-0,71	-0,43	-0,28	0
High	Q86Y39-1	NADH dehydrogenase [ubiquinone] 1 alpha subcomplex subunit 11 [OS=Homo	35,8844749	48,2269504	4	11	4	141	14,843	NDUFA11	-0,03	-0,43	0,4	0
High	O14776-1	Transcription elongation regulator 1 [OS=Homo sapiens]	20,5210734	4,18943534	4	8	4	1098	123,823	TCERG1	-0,7	-0,43	-0,27	0
Low	Q96GY0	Zinc finger C2HC domain-containing protein 1A [OS=Homo sapiens]	1,95506845	1,84615385	1	1	1	325	35,07	ZC2HC1A	-0,3	-0,44	0,14	0
High	P62891	60S ribosomal protein L39 [OS=Homo sapiens]	37,8380653	25,4901961	3	85	3	51	6,403	RPL39; RPL39P3	-0,41	-0,45	0,04	0
High	P62241	40S ribosomal protein S8 [OS=Homo sapiens]	444,592606	62,9807692	21	282	21	208	24,19	RPS8	-0,49	-0,48	-0,01	0
High	P62826	GTP-binding nuclear protein RAN [OS=Homo sapiens]	63,327485	39,8148148	8	23	8	216	24,408	RAN	-0,62	-0,48	-0,14	0
Medium	Q15054	DNA polymerase delta subunit 3 [OS=Homo sapiens]	4,31680061	2,14592275	1	2	1	466	51,368	POLD3	0,2	-0,49	0,7	0
Low	P53597	Succinyl-CoA ligase [ADP/GDP-forming] subunit alpha, mitochondrial [OS=Hom	1,4609239	2,60115607	1	1	1	346	36,227	SUCLG1	-0,86	-0,49	-0,37	0
High	Q9UMS4	Pre-mRNA-processing factor 19 [OS=Homo sapiens]	33,243656	17,8571429	7	15	7	504	55,146	PRPF19	-0,76	-0,5	-0,27	0
High	Q9BYG3	MKI67 FHA domain-interacting nucleolar phosphoprotein [OS=Homo sapiens]	266,00165	57,337884	17	93	17	293	34,201	MKI67IP; NIFK	-0,36	-0,52	0,17	0
High	P56134	ATP synthase subunit f, mitochondrial [OS=Homo sapiens]	25,7915018	25,5319149	2	7	2	94	10,911	ATP5J2	-0,44	-0,52	0,07	0
Medium	Q9Y5V3-2	Isoform 2 of Melanoma-associated antigen D1 [OS=Homo sapiens]	2,38231301	1,31894484	1	2	1	834	91,901	MAGED1	-0,61	-0,52	-0,1	0
High	P26373-1	60S ribosomal protein L13 [OS=Homo sapiens]	219,690139	52,6066351	17	176	17	211	24,247	RPL13	-0,39	-0,54	0,15	0
High	Q9BZE4	Nucleolar GTP-binding protein 1 [OS=Homo sapiens]	278,225058	60,5678233	36	137	36	634	73,918	GTPBP4	-0,33	-0,55	0,23	0
Low	O43852-3	Isoform 3 of Calumenin [OS=Homo sapiens]	2,20873052	4,0247678	1	2	1	323	38,027	CALU	-0,83	-0,55	-0,28	0
High	Q5T280	putative methyltransferase C9orf114 [OS=Homo sapiens]	86,6327083	36,1702128	10	28	10	376	41,982	C9orf114	-0,36	-0,56	0,2	0
High	Q01081	Splicing factor U2AF 35 kDa subunit [OS=Homo sapiens]	248,880568	56,6666667	12	169	2	240	27,854	OC102724594;	-0,42	-0,57	0,15	18
High	P31943	Heterogeneous nuclear ribonucleoprotein H [OS=Homo sapiens]	19,5015598	13,1403118	4	7	3	449	49,198	HNRNPH1	0,14	-0,57	0,71	1
High	Q9UBS4	DnaJ homolog subfamily B member 11 [OS=Homo sapiens]	5,89216264	4,74860335	2	3	2	358	40,489	DNAJB11	-0,69	-0,57	-0,12	0
High	P62304	small nuclear ribonucleoprotein E [OS=Homo sapiens]	5,76081681	25	2	2	2	92	10,797	SNRPE	-0,5	-0,57	0,06	0
Medium	Q15369-1	Transcription elongation factor B polypeptide 1 [OS=Homo sapiens]	2,39093945	9,82142857	1	1	1	112	12,465	TCEB1	-0,96	-0,57	-0,39	0
High	E9PRG8	Uncharacterized protein C11orf98 [OS=Homo sapiens]	21,1052788	12,295082	2	6	2	122	13,79	02288414; C11	-0,3	-0,58	0,28	0
High	P68363	Tubulin alpha-1B chain [OS=Homo sapiens]	619,13432	63,6363636	29	296	4	451	50,12	TUBA1B	-0,39	-0,59	0,19	37
Low	P08047	Transcription factor Sp1 [OS=Homo sapiens]	1,53491471	0,76433121	1	1	1	785	80,644	SP1	0,75	-0,59	1,34	0
High	Q9H329-2	Isoform 2 of Band 4.1-like protein 4B [OS=Homo sapiens]	174,048135	34,3629344	17	101	15	518	58,529	EPB41L4B	-0,57	-0,6	0,03	0
High	Q9NY93	Probable ATP-dependent RNA helicase DDX56 [OS=Homo sapiens]	68,9153038	29,4332724	12	27	12	547	61,551	DDX56	0,04	-0,6	0,64	0
High	Q14232	Translation initiation factor eIF-2B subunit alpha [OS=Homo sapiens]	23,5398082	13,1147541	4	11	4	305	33,691	EIF2B1	-0,65	-0,6	-0,05	0
High	P61619	Protein transport protein Sec61 subunit alpha isoform 1 [OS=Homo sapiens]	19,4059852	8,61344538	3	6	3	476	52,231	SEC61A1	-0,75	-0,6	-0,15	0
High	P41250	Glycine--tRNA ligase [OS=Homo sapiens]	8,04424838	4,46549391	3	4	3	739	83,113	GARS	-0,11	-0,61	0,5	0
High	Q15365	Poly(RC)-binding protein 1 [OS=Homo sapiens]	137,759411	64,8876404	14	52	9	356	37,474	PCBP1	-0,73	-0,62	-0,11	5
High	Q8TCC3-2	Isoform 2 of 39S ribosomal protein L30, mitochondrial [OS=Homo sapiens]	6,97784759	5,7591623	1	2	1	191	21,825		-0,39	-0,62	0,23	0
High	Q9H8G2-1	Caspase activity and apoptosis inhibitor 1 [OS=Homo sapiens]	112,101084	30,1939058	11	56	11	361	38,344	CAAP1	-0,58	-0,63	0,05	0
High	Q13009	T-lymphoma invasion and metastasis-inducing protein 1 [OS=Homo sapiens]	14,287318	2,95411691	4	6	4	1591	177,398	TIAM1	-0,57	-0,63	0,06	0
High	O75815-1	Breast cancer anti-estrogen resistance protein 3 [OS=Homo sapiens]	159,374866	43,8787879	28	74	27	825	92,507	BCAR3	-0,61	-0,64	0,03	1
High	P62979	Ubiquitin-40S ribosomal protein S27a [OS=Homo sapiens]	280,03675	58,3333333	10	161	7	156	17,953	RPS27A	-0,53	-0,65	0,13	3
High	Q9NRC8	NAD-dependent protein deacetylase sirtuin-7 [OS=Homo sapiens]	101,810576	39,75	13	29	13	400	44,87	SIRT7	-0,34	-0,65	0,32	0
High	O95831-1	Apoptosis-inducing factor 1, mitochondrial [OS=Homo sapiens]	47,9866214	17,7814029	9	16	9	613	66,859	AIFM1	0,76	-0,65	1,41	0
High	Q3ZCQ8-2	Isoform 2 of Mitochondrial import inner membrane translocase subunit TIM50	16,8049315	10,9649123	4	7	4	456	50,433	TIMM50	-0,6	-0,65	0,06	0
High	Q92616	translational activator GCN1 [OS=Homo sapiens]	9,37412495	1,90939723	4	6	4	2671	292,572	GCN1L1; GCN1	-1,04	-0,66	-0,38	0
High	Q9UQ35	serine/arginine repetitive matrix protein 2 [OS=Homo sapiens]	64,3474235	5,37790698	12	43	12	2752	299,438	SRRM2	-0,76	-0,67	-0,09	0
High	Q9BVS4	Serine/threonine-protein kinase rio2 [OS=Homo sapiens]	18,9727468	12,6811594	5	9	5	552	63,243	RIOK2	-0,45	-0,67	0,22	0
High	Q9H9B4	Sideroflexin-1 [OS=Homo sapiens]	27,3758127	18,0124224	5	8	5	322	35,596	SFXN1	-0,44	-0,69	0,25	0
High	P35268	60S ribosomal protein L22 [OS=Homo sapiens]	46,5785545	57,8125	6	28	4	128	14,778	RPL22	-0,77	-0,7	-0,07	0
High	P07305	Histone H1.0 [OS=Homo sapiens]	90,8543468	28,3505155	6	60	6	194	20,85	H1F0	-0,72	-0,72	0	0
High	P47914	60S ribosomal protein L29 [OS=Homo sapiens]	46,7375078	24,5283019	4	44	4	159	17,741	RPL29	-0,31	-0,72	0,41	0
High	P31040	Succinate dehydrogenase [ubiquinone] flavoprotein subunit, mitochondrial [OS	9,50242313	6,92771084	4	4	4	664	72,645	SDHA	0,29	-0,72	1,01	0
High	Q8IY17-4	Isoform 4 of Neuropathy target esterase [OS=Homo sapiens]	5,18603985	1,16363636	1	2	1	1375	150,859	PNPLA6	0,92	-0,72	1,64	0
High	Q15366-2	Isoform 2 of Poly(rC)-binding protein 2 [OS=Homo sapiens]	51,9039976	16,1202186	6	26	1	366	38,627	PCBP2	-1,32	-0,73	-0,59	0
High	O75683	Surfeit locus protein 6 [OS=Homo sapiens]	5,98828022	6,09418283	2	2	2	361	41,426	SURF6	-0,59	-0,73	0,14	0
High	Q8N3E9	1-phosphatidylinositol 4,5-bisphosphate phosphodiesterase delta-3 [OS=Homo	600,078854	72,1166033	43	272	43	789	89,202	PLCD3	-0,75	-0,74	0	0

High	P49756-1	RNA-binding protein 25 [OS=Homo sapiens]	372,825618	46,2633452	44	191	44	843	100,124	RBM25	-0,72	-0,74	0,02	0
High	Q9HCS5	band 4.1-like protein 4A [OS=Homo sapiens]	26,5026399	16,0349854	10	12	10	686	79,01	EPB41L4A	-0,51	-0,75	0,25	0
High	Q96P11-2	Isoform 2 of Probable 28S rRNA (cytosine-C(5))-methyltransferase [OS=Homo s	9,89142389	6,43776824	3	6	3	466	50,379	NSUN5	-0,64	-0,75	0,12	0
Medium	P48444	Coatomer subunit delta [OS=Homo sapiens]	2,81276138	2,15264188	1	1	1	511	57,174	ARCN1	-0,15	-0,75	0,6	0
High	O43809	Cleavage and polyadenylation specificity factor subunit 5 [OS=Homo sapiens]	83,6538858	58,5903084	10	31	10	227	26,211	NUDT21	-0,71	-0,76	0,05	0
High	O95478	Ribosome biogenesis protein NSA2 homolog [OS=Homo sapiens]	60,2542194	34,2307692	10	30	10	260	30,047	NSA2	-0,53	-0,76	0,23	0
High	Q9NPA5-1	Zinc finger protein 64 homolog, isoforms 1 and 2 [OS=Homo sapiens]	9,8349325	5,13950073	3	5	1	681	74,596	ZFP64	-0,75	-0,76	0,02	2
High	Q9BU76-1	Multiple myeloma tumor-associated protein 2 [OS=Homo sapiens]	513,27533	63,878327	29	548	29	263	29,394	C1orf35	-1,11	-0,77	-0,34	0
High	Q96CB9	5-methylcytosine rRNA methyltransferase NSUN4 [OS=Homo sapiens]	15,4210302	10,15625	4	6	4	384	43,061	NSUN4	-0,98	-0,77	-0,21	0
Medium	Q53GL0-1	pleckstrin homology domain-containing family O member 1 [OS=Homo sapiens	2,73189027	3,66748166	1	1	1	409	46,209	PLEKHO1	-0,83	-0,77	-0,06	0
Medium	Q9UHB9	Signal recognition particle subunit SRP68 [OS=Homo sapiens]	3,16358163	2,55183413	2	2	2	627	70,686	SRP68	-1,58	-0,78	-0,8	0
High	Q9Y5B9	FACT complex subunit SPT16 [OS=Homo sapiens]	5,7439714	1,14613181	1	2	1	1047	119,838	SUPT16H	-0,11	-0,79	0,67	0
High	Q9Y3A4	Ribosomal RNA-processing protein 7 homolog A [OS=Homo sapiens]	150,798105	60,3571429	13	73	13	280	32,314	RRP7A	-0,77	-0,81	0,04	0
High	P49759-3	Isoform 3 of Dual specificity protein kinase CLK1 [OS=Homo sapiens]	94,9820311	24,7148289	13	37	12	526	61,718	CLK1	-0,67	-0,81	0,14	1
High	Q02978	Mitochondrial 2-oxoglutarate/malate carrier protein [OS=Homo sapiens]	165,326418	69,1082803	19	79	19	314	34,04	SLC25A11	-0,77	-0,82	0,05	0
High	Q8IYB3	Serine/arginine repetitive matrix protein 1 [OS=Homo sapiens]	150,124778	19,9115044	18	93	18	904	102,274	SRRM1	-1,2	-0,83	-0,37	0
High	Q9H9J4-1	Ubiquitin carboxyl-terminal hydrolase 42 [OS=Homo sapiens]	20,544326	5,89123867	6	10	6	1324	145,302	USP42	-0,54	-0,83	0,29	0
High	P56945-6	Isoform 6 of Breast cancer anti-estrogen resistance protein 1 [OS=Homo sapien	603,224124	61,0262009	45	324	45	916	97,817	BCAR1	-0,61	-0,84	0,24	0
High	P51570-2	Isoform 2 of Galactokinase [OS=Homo sapiens]	28,7593321	13,9810427	6	11	6	422	45,329	GALK1	-0,9	-0,84	-0,07	0
High	Q9BVA1	Tubulin beta-2B chain [OS=Homo sapiens]	749,148827	61,7977528	26	445	1	445	49,921	TUBB2B	-1,1	-0,85	-0,25	0
High	Q6DKI1	60S ribosomal protein L7-like 1 [OS=Homo sapiens]	46,0431928	33,7398374	7	15	7	246	28,643	RPL7L1	-0,53	-0,85	0,32	0
High	P21980	Protein-glutamine gamma-glutamyltransferase 2 [OS=Homo sapiens]	41,5377074	17,6128093	10	16	10	687	77,28	TGM2	-0,92	-0,85	-0,07	0
High	Q9BXS6-2	Isoform 2 of Nucleolar and spindle-associated protein 1 [OS=Homo sapiens]	124,727792	56,8181818	24	71	3	440	49,294	NUSAP1	-0,76	-0,86	0,1	15
High	Q7Z6E9	E3 ubiquitin-protein ligase RBBP6 [OS=Homo sapiens]	77,8415229	13,5044643	24	71	24	1792	201,442	RBBP6	-1,03	-0,87	-0,16	0
High	Q9NYV4-1	Cyclin-dependent kinase 12 [OS=Homo sapiens]	26,6326959	6,91275168	8	14	7	1490	164,054	CDK12	-0,76	-0,87	0,11	1
High	P45954	Short/branched chain specific acyl-CoA dehydrogenase, mitochondrial [OS=Hor	6,08828813	4,16666667	2	2	2	432	47,455	ACADSB	-0,75	-0,87	0,12	0
Medium	P63220	40S ribosomal protein S21 [OS=Homo sapiens]	2,77988574	8,43373494	1	2	1	83	9,106	RPS21	-0,19	-0,87	0,68	0
High	Q8IZ69	tRNA (uracil-5-)-methyltransferase homolog A [OS=Homo sapiens]	23,4183851	11,36	7	11	7	625	68,682	TRMT2A	-0,42	-0,88	0,46	0
High	Q9UI30	Multifunctional methyltransferase subunit TRM112-like protein [OS=Homo sap	14,6924302	31,2	3	4	3	125	14,19	TRMT112	-1,83	-0,88	-0,95	0
High	P41091	eukaryotic translation initiation factor 2 subunit 3 [OS=Homo sapiens]	7,1699599	4,44915254	2	2	2	472	51,077	EIF2S3	-0,74	-0,89	0,15	0
Medium	Q15293	Reticulocalbin-1 [OS=Homo sapiens]	2,48945499	3,92749245	1	1	1	331	38,866	RCN1	-0,81	-0,89	0,09	0
High	Q9P031	Thyroid transcription factor 1-associated protein 26 [OS=Homo sapiens]	55,5274884	37,3443983	9	31	9	241	28,652	CCDC59	-0,68	-0,92	0,25	0
High	P08865	40S ribosomal protein SA [OS=Homo sapiens]	66,9579456	38,9830508	9	24	9	295	32,833	RPSA	-1	-0,93	-0,07	0
High	P68371	Tubulin beta-4B chain [OS=Homo sapiens]	906,868866	83,8202247	33	540	1	445	49,799	TUBB4B	-0,89	-0,94	0,05	71
High	Q9Y3A2	Probable U3 small nucleolar RNA-associated protein 11 [OS=Homo sapiens]	53,7087915	37,5494071	11	23	11	253	30,428	UTP11L; UTP11	-1,16	-0,94	-0,22	0
High	Q8WUQ7-2	Isoform 2 of Cactin [OS=Homo sapiens]	377,879671	36,4705882	33	213	33	935	107,871		-0,97	-0,96	-0,01	0
High	P18085	ADP-ribosylation factor 4 [OS=Homo sapiens]	35,7025829	28,3333333	4	13	3	180	20,498	ARF4	-0,81	-0,96	0,14	1
Medium	Q9H9Y2	Ribosome production factor 1 [OS=Homo sapiens]	3,84043281	3,43839542	1	1	1	349	40,086	RPF1	-1,67	-0,96	-0,71	0
High	Q9NWT8	Aurora kinase A-interacting protein [OS=Homo sapiens]	22,0789435	7,03517588	2	9	2	199	22,34	AURKAIP1	-1,37	-0,97	-0,39	0
High	Q9BQ39	ATP-dependent RNA helicase DDX50 [OS=Homo sapiens]	187,651744	51,0176391	31	99	28	737	82,514	DDX50	-0,71	-0,98	0,28	2
High	P11387	DNA topoisomerase 1 [OS=Homo sapiens]	78,3876966	23,0065359	17	33	17	765	90,669	TOP1	-1,39	-0,98	-0,42	0
High	P16615	Sarcoplasmic/endoplasmic reticulum calcium ATPase 2 [OS=Homo sapiens]	72,9070763	16,9865643	16	34	16	1042	114,683	ATP2A2	-1,02	-0,98	-0,04	0
High	Q8TER5	Rho guanine nucleotide exchange factor 40 [OS=Homo sapiens]	18,2011181	5,13495721	7	9	7	1519	164,555	ARHGEF40	-1,28	-0,98	-0,3	0
High	P49848-3	Isoform 3 of Transcription initiation factor TFIID subunit 6 [OS=Homo sapiens]	4,87605851	2,66106443	2	2	2	714	76,947	TAF6	-0,59	-0,98	0,39	0
High	Q9ULS5	Transmembrane and coiled-coil domains protein 3 [OS=Homo sapiens]	191,017373	48,0083857	26	83	25	477	53,752	TMCC3	-0,8	-0,99	0,19	1
High	P47756-2	Isoform 2 of F-actin-capping protein subunit beta [OS=Homo sapiens]	4,76020018	6,25	2	3	2	272	30,609	CAPZB	-0,39	-0,99	0,6	0
Low	P17026	zinc finger protein 22 [OS=Homo sapiens]	1,42010213	6,69642857	1	1	1	224	25,899	ZNF22	-0,39	-0,99	0,6	0
High	Q8NF37	Lysophosphatidylcholine acyltransferase 1 [OS=Homo sapiens]	6,64042697	2,43445693	1	4	1	534	59,113	LPCAT1	-0,34	-1	0,66	0
High	Q6P087	RNA pseudouridylate synthase domain-containing protein 3 [OS=Homo sapiens	11,5660775	10,2564103	4	5	4	351	38,437	RPUSD3	-1,05	-1,01	-0,05	0
High	Q66PJ3-2	Isoform 2 of ADP-ribosylation factor-like protein 6-interacting protein 4 [OS=Ho	36,3291946	15,2542373	6	16	6	413	44,132	ARL6IP4	-1,72	-1,04	-0,68	0
High	Q8IWK6	Adhesion G protein-coupled receptor A3 [OS=Homo sapiens]	31,2890195	7,41862226	9	19	9	1321	146,058	GPR125; ADGRA	-1,28	-1,04	-0,24	0
High	Q99459	Cell division cycle 5-like protein [OS=Homo sapiens]	123,681495	27,4314214	18	52	18	802	92,194	CDC5L	-1,01	-1,05	0,04	0
High	Q4KMP7	TBC1 domain family member 10B [OS=Homo sapiens]	122,776005	25	18	64	18	808	87,145	TBC1D10B	-1,07	-1,05	-0,02	0
High	Q8WXA9-2	Isoform 2 of Splicing regulatory glutamine/lysine-rich protein 1 [OS=Homo sapi	19,1171269	3,84615385	2	11	2	624	71,606	SREK1	-0,34	-1,07	0,73	0
High	P58557	putative ribonuclease [OS=Homo sapiens]	16,5998751	16,1676647	2	4	2	167	19,286	YBEY	-0,8	-1,07	0,27	0
High	Q13823	Nucleolar GTP-binding protein 2 [OS=Homo sapiens]	106,178521	33,378933	20	49	20	731	83,603	GNL2	-1,39	-1,08	-0,31	0
High	P20719	Homeobox protein Hox-A5 [OS=Homo sapiens]	51,7236564	27,7777778	6	12	6	270	29,327	HOXA5	-1,25	-1,08	-0,17	0
High	P05023	Sodium/potassium-transporting ATPase subunit alpha-1 [OS=Homo sapiens]	147,08925	29,3255132	28	76	25	1023	112,824	ATP1A1	-1,1	-1,12	0,03	3
High	O95299	NADH dehydrogenase [ubiquinone] 1 alpha subcomplex subunit 10, mitochond	13,0317491	14,9295775	4	5	4	355	40,725	NDUFA10	0,06	-1,12	1,18	0
High	Q9H300	Presenilins-associated rhomboid-like protein, mitochondrial [OS=Homo sapiens	10,9987366	10,2902375	3	4	3	379	42,163	PARL	-1,39	-1,12	-0,27	0
Low	P49792	E3 SUMO-protein ligase RanBP2 [OS=Homo sapiens]	1,53655497	0,27915633	1	1	1	3224	357,974	RANBP2	-0,33	-1,12	0,79	0

High	Q8N1G0	zinc finger protein 687 [OS=Homo sapiens]	32,4269297	7,59902991	8	16	8	1237	129,446	ZNF687	-0,63	-1,13	0,5	0
High	O94876	Transmembrane and coiled-coil domains protein 1 [OS=Homo sapiens]	22,149746	8,72894334	6	12	5	653	72,038	TMCC1	-0,49	-1,13	0,64	0
High	O00488	Zinc finger protein 593 [OS=Homo sapiens]	37,2916799	55,2238806	5	10	5	134	15,19	ZNF593	-0,82	-1,14	0,31	0
High	O75964	ATP synthase subunit g, mitochondrial [OS=Homo sapiens]	19,8139827	37,8640777	3	5	3	103	11,421	ATP5L	-0,81	-1,16	0,34	0
High	Q13523	Serine/threonine-protein kinase PRP4 homolog [OS=Homo sapiens]	65,2307608	13,6047666	13	32	13	1007	116,916	PRPF4B	-0,94	-1,18	0,24	0
High	Q9UDY2-7	Isoform 7 of Tight junction protein ZO-2 [OS=Homo sapiens]	196,913853	34,8075348	38	93	38	1221	137,258	TJP2	-1,1	-1,19	0,09	0
High	P26641-2	Isoform 2 of Elongation factor 1-gamma [OS=Homo sapiens]	25,6579682	13,963039	7	9	7	487	56,114	EEF1G	-1,07	-1,19	0,12	0
High	Q9NWU5	39S ribosomal protein L22, mitochondrial [OS=Homo sapiens]	5,13913732	10,1941748	2	2	2	206	23,626	MRPL22	0,59	-1,19	1,78	0
High	Q13428-3	Isoform 3 of Treacle protein [OS=Homo sapiens]	105,488563	17,7300201	26	81	26	1489	152,114	TCOF1	-2,82	-1,2	-1,62	0
High	O75367-1	Core histone macro-H2A.1 [OS=Homo sapiens]	29,2946933	17,7419355	5	8	5	372	39,592	H2AFY	-0,44	-1,21	0,76	0
Medium	P11177	Pyruvate dehydrogenase E1 component subunit beta, mitochondrial [OS=Homo	2,30129065	2,22841226	1	1	1	359	39,208	PDHB	-2,4	-1,22	-1,19	0
High	P11171-1	protein 4.1 [OS=Homo sapiens]	109,276365	27,5462963	20	46	17	864	96,957	EPB41	-1,36	-1,24	-0,12	3
High	P63208	s-phase kinase-associated protein 1 [OS=Homo sapiens]	48,7853619	50,3067485	7	14	7	163	18,646	SKP1	-0,61	-1,24	0,63	0
High	Q9P2I0	Cleavage and polyadenylation specificity factor subunit 2 [OS=Homo sapiens]	267,518448	51,6624041	31	110	31	782	88,431	CPSF2	-0,88	-1,25	0,36	0
High	Q9Y324	rRNA-processing protein FCF1 homolog [OS=Homo sapiens]	112,674787	38,8888889	10	37	10	198	23,354	FCF1	-1,02	-1,28	0,26	0
High	Q7L014	probable ATP-dependent RNA helicase DDX46 [OS=Homo sapiens]	104,408263	20,6595538	20	67	20	1031	117,29	DDX46	-0,94	-1,28	0,34	0
High	Q9BXS6-4	Isoform 4 of Nucleolar and spindle-associated protein 1 [OS=Homo sapiens]	107,842872	55,2941176	22	64	1	425	47,541	NUSAP1	-1,03	-1,29	0,26	0
High	Q8WVD3-1	E3 ubiquitin-protein ligase RNF138 [OS=Homo sapiens]	11,7195111	25,7142857	5	5	5	245	28,174	RNF138	-0,79	-1,29	0,51	0
High	Q9NWB6	Arginine and glutamate-rich protein 1 [OS=Homo sapiens]	202,126562	47,2527473	28	290	28	273	33,197	ARGLU1	-1,25	-1,34	0,09	0
High	P50416	Carnitine O-palmitoyltransferase 1, liver isoform [OS=Homo sapiens]	13,678913	8,92626132	6	7	6	773	88,311	CPT1A	-1,16	-1,34	0,19	0
High	P19474	E3 ubiquitin-protein ligase TRIM21 [OS=Homo sapiens]	532,792206	67,1578947	37	260	37	475	54,135	TRIM21	-0,75	-1,35	0,6	0
Medium	P04792	Heat shock protein beta-1 [OS=Homo sapiens]	3,13259144	6,34146341	1	1	1	205	22,768	HSPB1	-1,91	-1,35	-0,57	0
High	Q86U06-1	probable RNA-binding protein 23 [OS=Homo sapiens]	59,5766925	17,0842825	7	47	4	439	48,701	RBM23	-1,45	-1,38	-0,07	0
Low	Q8N0Y2-1	zinc finger protein 444 [OS=Homo sapiens]	1,82594019	2,14067278	1	1	1	327	35,182	ZNF444	0,18	-1,38	1,57	0
High	Q5C9Z4	nucleolar MIF4G domain-containing protein 1 [OS=Homo sapiens]	112,643033	20,1162791	16	45	16	860	96,198	NOM1	-2,15	-1,4	-0,74	0
High	Q14244	Ensconsin [OS=Homo sapiens]	109,41114	27,9038718	24	54	23	749	84,002	MAP7	-1,17	-1,4	0,23	1
High	Q96D09	G-protein coupled receptor-associated sorting protein 2 [OS=Homo sapiens]	6,97054575	2,2673031	2	5	2	838	93,715	P2; ARMCX5-G	-1,43	-1,4	-0,02	0
High	Q99590-1	protein SCAF11 [OS=Homo sapiens]	7,39781221	2,3923445	3	3	3	1463	164,551	SCAF11	-1,27	-1,42	0,15	0
High	P21127-1	Cyclin-dependent kinase 11B [OS=Homo sapiens]	190,371212	39,7484277	34	114	34	795	92,65	CDK11B	-1,75	-1,43	-0,32	0
Medium	P78549	Endonuclease III-like protein 1 [OS=Homo sapiens]	3,00725045	3,20512821	1	2	1	312	34,368	NTHL1	-0,5	-1,44	0,94	0
Low	Q9UMY1-1	Nucleolar protein 7 [OS=Homo sapiens]	1,67019548	3,89105058	1	1	1	257	29,409	NOL7	-1,39	-1,45	0,06	0
High	Q7Z7C8-4	Isoform 3 of Transcription initiation factor TFIID subunit 8 [OS=Homo sapiens]	53,67072	24,556213	5	15	5	338	37,388	TAF8	-1,7	-1,46	-0,24	0
High	Q9C0J8	pre-mRNA 3' end processing protein WDR33 [OS=Homo sapiens]	192,481051	26,2724551	34	105	34	1336	145,799	WDR33	-1,48	-1,47	-0,02	0
High	Q8IWC1	MAP7 domain-containing protein 3 [OS=Homo sapiens]	20,9192056	7,53424658	7	9	7	876	98,368	MAP7D3	-1,1	-1,47	0,38	0
High	O75400	pre-mRNA-processing factor 40 homolog A [OS=Homo sapiens]	314,244181	33,4378265	32	150	32	957	108,737	PRPF40A	-1,7	-1,48	-0,23	0
Medium	P50897	Palmitoyl-protein thioesterase 1 [OS=Homo sapiens]	4,19885983	7,84313725	2	2	2	306	34,171	PPT1	-1,41	-1,48	0,06	0
High	Q8TAD8	Smad nuclear-interacting protein 1 [OS=Homo sapiens]	18,0131549	9,84848485	3	8	3	396	45,75	SNIP1	-1,45	-1,51	0,06	0
High	Q9BVP2	Guanine nucleotide-binding protein-like 3 [OS=Homo sapiens]	1199,55305	62,8415301	53	682	52	549	61,954	GNL3	-1,59	-1,52	-0,06	2
High	Q8NAV1-1	Pre-mRNA-splicing factor 38A [OS=Homo sapiens]	7,88774982	8,97435897	3	3	3	312	37,453	PRPF38A	-1,79	-1,52	-0,26	0
High	P42704	Leucine-rich PPR motif-containing protein, mitochondrial [OS=Homo sapiens]	35,812574	7,96269727	10	19	10	1394	157,805	LRPPRC	-2,1	-1,55	-0,54	0
High	P17509	Homeobox protein Hox-B6 [OS=Homo sapiens]	19,8827059	34,375	5	6	5	224	25,416	HOXB6	-0,92	-1,57	0,65	0
High	Q9HCM4	Band 4.1-like protein 5 [OS=Homo sapiens]	485,706842	66,9849932	37	389	2	733	81,805	EPB41L5	-1,56	-1,6	0,04	42
High	Q13427	peptidyl-prolyl cis-trans isomerase g [OS=Homo sapiens]	55,738904	15,1193634	11	24	11	754	88,564	PPIG	-1,5	-1,6	0,1	0
High	O95104	Splicing factor, arginine/serine-rich 15 [OS=Homo sapiens]	38,5142534	7,75937228	9	24	9	1147	125,79	SCAF4	-1,46	-1,62	0,16	0
High	Q6B0I6	Lysine-specific demethylase 4D [OS=Homo sapiens]	21,6588322	11,6634799	7	9	7	523	58,565	KDM4D	-0,94	-1,63	0,69	0
High	A8MW92	PHD finger protein 20-like protein 1 [OS=Homo sapiens]	21,607765	10,1278269	8	14	8	1017	114,938	PHF20L1	-2,33	-1,63	-0,7	0
High	P25205-2	Isoform 2 of DNA replication licensing factor MCM3 [OS=Homo sapiens]	7,59484777	0,93786635	1	3	1	853	95,848	MCM3	-1,63	-1,63	0	0
High	Q8NFW8	N-acylneuraminate cytidylyltransferase [OS=Homo sapiens]	38,754413	23,0414747	9	18	9	434	48,349	CMAS	-1,51	-1,64	0,13	0
Low	Q6ZNG9	KRAB-A domain-containing protein 2 [OS=Homo sapiens]	1,80576325	1,2195122	1	3	1	492	56,169	KRBA2	-1,72	-1,65	-0,07	0
High	Q7Z7K6-1	Centromere protein V [OS=Homo sapiens]	110,493775	49,0909091	11	40	2	275	29,927	CENPV	-1,94	-1,69	-0,24	8
High	Q9NVF7-1	F-box only protein 28 [OS=Homo sapiens]	108,069883	38,8586957	15	41	15	368	41,123	FBXO28	-0,88	-1,72	0,84	0
High	Q8N9Q2	protein SREK1IP1 [OS=Homo sapiens]	32,972146	21,2903226	5	22	5	155	18,166	SREK1IP1	-0,92	-1,75	0,83	0
High	Q8WTT2	Nucleolar complex protein 3 homolog [OS=Homo sapiens]	153,772152	38	27	67	27	800	92,49	NOC3L	-1,06	-1,78	0,72	0
High	Q9UKV3-1	Apoptotic chromatin condensation inducer in the nucleus [OS=Homo sapiens]	14,062847	2,31170768	3	4	3	1341	151,771	ACIN1	-1,79	-1,79	0	0
High	Q08J23	tRNA (Cytosine(34)-C(5))-methyltransferase [OS=Homo sapiens]	90,6923432	29,8565841	19	55	19	767	86,416	NSUN2	-1,41	-1,8	0,39	0
Medium	Q8NB90-1	Spermatogenesis-associated protein 5 [OS=Homo sapiens]	3,70831633	2,79955207	2	2	2	893	97,843	SPATA5	5,29	-1,8	7,09	0
Medium	Q92974	Rho guanine nucleotide exchange factor 2 [OS=Homo sapiens]	2,68118548	0,9127789	1	3	1	986	111,473	ARHGEF2	7,29	-1,8	9,08	0
High	Q9BRT6	Protein LLP homolog [OS=Homo sapiens]	61,6713522	34,8837209	5	26	5	129	15,215	LLPH	-1,09	-1,81	0,73	0
High	Q9H4L5	Oxysterol-binding protein-related protein 3 [OS=Homo sapiens]	379,55804	59,7519729	41	162	5	887	101,16	OSBPL3	-1,27	-1,83	0,56	37
High	P63010-2	Isoform 2 of AP-2 complex subunit beta [OS=Homo sapiens]	26,3193666	7,78128286	7	11	7	951	105,625	AP2B1	-1,85	-1,85	0	0
High	Q12986-3	Isoform 3 of Transcriptional repressor NF-X1 [OS=Homo sapiens]	45,6886031	15,4861945	10	26	10	833	92,618	NFX1	-1,18	-1,87	0,69	0

High	Q9Y4X4-1	Krueppel-like factor 12 [OS=Homo sapiens]	10,0586981	6,96517413	3	5	3	402	44,212	KLF12	-1,63	-1,89	0,26	0
High	P18583-9	Isoform I of Protein SON [OS=Homo sapiens]	42,1391604	6,60989457	11	50	11	2466	267,923		-1,98	-1,9	-0,08	0
High	Q07157-2	Isoform Short of Tight junction protein ZO-1 [OS=Homo sapiens]	31,5715932	8,39328537	10	12	10	1668	186,852	TJP1	-1,8	-1,9	0,1	0
High	Q6P5Z2	Serine/threonine-protein kinase N3 [OS=Homo sapiens]	8,62931363	2,24971879	2	4	2	889	99,358	PKN3	-1,82	-1,94	0,12	0
High	O75319-1	RNA/RNP complex-1-interacting phosphatase [OS=Homo sapiens]	46,0557336	41,2121212	10	20	10	330	38,915	DUSP11	-1,55	-1,96	0,42	0
High	Q9NYF8-1	Bcl-2-associated transcription factor 1 [OS=Homo sapiens]	88,3053774	24,1304348	23	52	21	920	106,059	BCLAF1	-2,1	-1,97	-0,13	2
High	Q5BKY9-1	Protein FAM133B [OS=Homo sapiens]	40,8986643	35,6275304	6	23	3	247	28,368	FAM133B	-2,24	-1,98	-0,26	4
High	P52907	F-actin-capping protein subunit alpha-1 [OS=Homo sapiens]	11,7428203	17,8321678	4	4	4	286	32,902	CAPZA1	-1,24	-1,98	0,74	0
High	Q9P1Y6-1	PHD and RING finger domain-containing protein 1 [OS=Homo sapiens]	40,712688	7,39842329	10	22	10	1649	178,557	PHRF1	-1,67	-1,99	0,32	0
High	Q2NL82	Pre-rRNA-processing protein TSR1 homolog [OS=Homo sapiens]	302,506414	40,6716418	35	163	35	804	91,752	TSR1	-2,07	-2,03	-0,04	0
High	Q5T8P6	RNA-binding protein 26 [OS=Homo sapiens]	106,458132	18,7686197	19	55	18	1007	113,527	RBM26	-2,21	-2,05	-0,15	1
High	Q8TA86	retinitis pigmentosa 9 protein [OS=Homo sapiens]	80,1117903	35,7466063	11	57	11	221	26,091	RP9	-1,68	-2,05	0,37	0
High	Q15393-1	Splicing factor 3B subunit 3 [OS=Homo sapiens]	23,4617632	6,16269515	8	11	8	1217	135,492	SF3B3	-1,95	-2,06	0,11	0
High	Q9HC21	Mitochondrial thiamine pyrophosphate carrier [OS=Homo sapiens]	14,6813934	14,375	4	5	4	320	35,488	SLC25A19	-0,84	-2,09	1,25	0
High	Q13263	Transcription intermediary factor 1-beta [OS=Homo sapiens]	14,7595564	5,1497006	5	7	5	835	88,493	TRIM28	-2,34	-2,12	-0,22	0
High	P41743	Protein kinase c iota type [OS=Homo sapiens]	24,5209708	14,9328859	6	7	5	596	68,218	PRKCI	-1,86	-2,13	0,27	0
High	P43243	Matrin-3 [OS=Homo sapiens]	19,3146327	7,55608028	5	9	5	847	94,565	MATR3	-1,8	-2,13	0,34	0
High	P11586	C-1-tetrahydrofolate synthase, cytoplasmic [OS=Homo sapiens]	13,1947664	4,9197861	5	7	5	935	101,495	MTHFD1	-2,44	-2,14	-0,3	0
High	O95782	AP-2 complex subunit alpha-1 [OS=Homo sapiens]	19,9858706	6,44831116	6	8	6	977	107,478	AP2A1	-1,8	-2,15	0,35	0
High	P68104	Elongation factor 1-alpha 1 [OS=Homo sapiens]	109,263809	42,2077922	14	47	14	462	50,109	EEF1A1	-2,51	-2,16	-0,35	0
High	Q02040-1	A-kinase anchor protein 17A [OS=Homo sapiens]	479,443032	47,7697842	47	348	47	695	80,686	AKAP17A	-2,25	-2,17	-0,08	0
High	Q9BRR8	G patch domain-containing protein 1 [OS=Homo sapiens]	55,5245784	16,3265306	11	20	11	931	103,282	GPATCH1	-2,92	-2,17	-0,75	0
Medium	Q15459	splicing factor 3A subunit 1 [OS=Homo sapiens]	2,47938548	0,88272383	1	1	1	793	88,831	SF3A1	-2,3	-2,21	-0,09	0
High	Q8N5F7	NF-kappa-B-activating protein [OS=Homo sapiens]	48,4415526	20,7228916	9	29	9	415	47,11	NKAP	-2,03	-2,22	0,2	0
High	Q8IWX8	Calcium homeostasis endoplasmic reticulum protein [OS=Homo sapiens]	78,3559987	18,4497817	15	30	15	916	103,637	CHERP	-2,66	-2,24	-0,42	0
High	P09874	Poly [ADP-ribose] polymerase 1 [OS=Homo sapiens]	18,0581311	5,0295858	5	8	5	1014	113,012	PARP1	-2	-2,24	0,24	0
High	Q13435	Splicing factor 3b subunit 2 [OS=Homo sapiens]	14,176119	7,03910615	6	8	6	895	100,165	SF3B2	-2,21	-2,25	0,04	0
High	P33991	DNA replication licensing factor MCM4 [OS=Homo sapiens]	28,8535561	10,7763615	8	11	8	863	96,498	MCM4	-2,03	-2,26	0,23	0
Low	Q4KWH8-1	1-phosphatidylinositol 4,5-bisphosphate phosphodiesterase eta-1 [OS=Homo sa	2,18728713	0,41346722	1	1	1	1693	189,104	PLCH1	-1,31	-2,26	0,95	0
High	Q8NHP8	Putative phospholipase B-like 2 [OS=Homo sapiens]	59,1594376	24,7877759	13	25	13	589	65,43	PLBD2	-2,62	-2,27	-0,35	0
High	O00458	Interferon-related developmental regulator 1 [OS=Homo sapiens]	6,7994321	7,09534368	2	2	2	451	50,236	IFRD1	-2,32	-2,27	-0,05	0
High	P68032	Actin, alpha cardiac muscle 1 [OS=Homo sapiens]	171,870728	40,0530504	15	172	2	377	41,992	ACTC1	-1,96	-2,28	0,32	0
High	P46940	Ras GTPase-activating-like protein IQGAP1 [OS=Homo sapiens]	13,0047237	3,43995172	5	5	5	1657	189,134	IQGAP1	-1,63	-2,28	0,65	0
Medium	Q6ZN55-2	Isoform 2 of Zinc finger protein 574 [OS=Homo sapiens]	4,10225418	1,01522843	1	2	1	985	108,504		-1,03	-2,28	1,25	0
High	Q96T37-1	Putative RNA-binding protein 15 [OS=Homo sapiens]	19,1375171	6,03889458	5	7	5	977	107,124	RBM15	-2,06	-2,3	0,24	0
High	O43592	Exportin-T [OS=Homo sapiens]	78,5196947	12,8898129	11	27	11	962	109,893	XPOT	-2,1	-2,31	0,21	0
High	P60709	Actin, cytoplasmic 1 [OS=Homo sapiens]	326,823363	70,9333333	24	240	11	375	41,71	ACTB	-2,36	-2,33	-0,03	21
High	Q9NP64	nucleolar protein of 40 kDa [OS=Homo sapiens]	268,631356	45,2282158	16	210	16	241	27,552	ZCCHC17	-2,52	-2,33	-0,18	0
High	Q3KQU3	MAP7 domain-containing protein 1 [OS=Homo sapiens]	21,5833152	9,75029727	8	14	7	841	92,764	MAP7D1	-1,99	-2,35	0,36	0
High	P29597	Non-receptor tyrosine-protein kinase TYK2 [OS=Homo sapiens]	7,51779871	0,92670598	1	3	1	1187	133,565	TYK2	-2,68	-2,38	-0,3	0
High	Q9UII4	E3 ISG15--protein ligase HERC5 [OS=Homo sapiens]	384,516762	45,9960938	38	148	38	1024	116,777	HERC5	-2,1	-2,39	0,29	0
High	O75147	Obscurin-like protein 1 [OS=Homo sapiens]	30,277096	4,43037975	8	12	8	1896	206,817	OBSL1	-1,62	-2,39	0,77	0
High	P55786	puromycin-sensitive aminopeptidase [OS=Homo sapiens]	22,96397	5,76713819	5	9	5	919	103,211	NPEPPS	-2,08	-2,39	0,31	0
High	Q9UBB9-1	Tuftelin-interacting protein 11 [OS=Homo sapiens]	17,6515062	7,16845878	6	7	6	837	96,758	TFIP11	-2,64	-2,44	-0,2	0
High	Q14241	Transcription elongation factor B polypeptide 3 [OS=Homo sapiens]	17,7514689	6,76691729	5	7	5	798	89,853	TCEB3	-2,2	-2,45	0,25	0
High	P55060-1	Exportin-2 [OS=Homo sapiens]	11,6510409	2,26570546	3	5	3	971	110,346	CSE1L	-2,81	-2,47	-0,34	0
Medium	O43395	U4/U6 small nuclear ribonucleoprotein Prp3 [OS=Homo sapiens]	3,3579388	3,80673499	2	2	2	683	77,481	PRPF3	-1,49	-2,47	0,98	0
Medium	Q86XI2-2	Isoform 2 of Condensin-2 complex subunit G2 [OS=Homo sapiens]	2,78436244	0,77854671	1	1	1	1156	132,111	NCAPG2	-1,94	-2,49	0,55	0
Low	Q9ULD4	Bromodomain and PHD finger-containing protein 3 [OS=Homo sapiens]	1,49363028	0,58091286	1	1	1	1205	135,66	BRPF3	-2,33	-2,5	0,17	0
High	Q9Y388	RNA-binding motif protein, X-linked 2 [OS=Homo sapiens]	43,175556	25,4658385	7	13	7	322	37,313	RBMX2	-2,34	-2,52	0,18	0
High	Q6ZUT1-2	Isoform 2 of Uncharacterized protein C11orf57 [OS=Homo sapiens]	146,721932	40,6143345	15	71	15	293	34,176	C11orf57	-2,3	-2,53	0,23	0
High	Q96GQ7	Probable ATP-dependent RNA helicase DDX27 [OS=Homo sapiens]	91,2597244	29,6482412	23	58	23	796	89,779	DDX27	-1,62	-2,53	0,91	0
High	Q9HCB6	Spondin-1 [OS=Homo sapiens]	7,32827391	2,85006196	2	5	2	807	90,914	SPON1	-2,24	-2,53	0,3	0
High	P56192	Methionine--tRNA ligase, cytoplasmic [OS=Homo sapiens]	39,7217155	13,2222222	11	19	11	900	101,052	MARS	-2,28	-2,54	0,26	0
High	O94906-1	Pre-mRNA-processing factor 6 [OS=Homo sapiens]	20,283645	7,01381509	6	8	6	941	106,858	PRPF6	-2,7	-2,55	-0,15	0
Medium	Q15542	Transcription initiation factor TFIID subunit 5 [OS=Homo sapiens]	3,77469072	1,375	1	1	1	800	86,776	TAF5	-3,55	-2,55	-1	0
High	Q6PJP8	DNA cross-link repair 1A protein [OS=Homo sapiens]	17,1226458	4,90384615	5	5	5	1040	116,326	DCLRE1A	-2,36	-2,58	0,23	0
High	Q99959	Plakophilin-2 [OS=Homo sapiens]	25,7314605	13,3938706	9	12	9	881	97,355	PKP2	-1,81	-2,59	0,78	0
High	Q1KMD3	heterogeneous nuclear ribonucleoprotein U-like protein 2 [OS=Homo sapiens]	40,1856804	17,5368139	11	21	11	747	85,052	HNRNPUL2	-2,23	-2,62	0,39	0
High	Q15029	116 kDa U5 small nuclear ribonucleoprotein component [OS=Homo sapiens]	61,2398766	20,473251	16	25	16	972	109,366	EFTUD2	-2,61	-2,64	0,03	0
High	P49761	Dual specificity protein kinase CLK3 [OS=Homo sapiens]	78,1671703	15,0470219	8	24	8	638	73,469	CLK3	-2,67	-2,65	-0,02	0

High	Q14562	ATP-dependent RNA helicase dhx8 [OS=Homo sapiens]	179,872895	36,3934426	35	83	35	1220	139,227	DHX8	-2,73	-2,68	-0,05	0
High	P53618	Coatomer subunit beta [OS=Homo sapiens]	22,092392	8,91920252	7	9	7	953	107,074	COPB1	-2,73	-2,69	-0,04	0
Medium	Q96T76-8	Isoform 5 of MMS19 nucleotide excision repair protein homolog [OS=Homo sa	2,45792185	0,85632731	1	1	1	1051	115,631		-2,6	-2,7	0,1	0
High	O14980	Exportin-1 [OS=Homo sapiens]	47,8146828	12,605042	12	19	12	1071	123,306	XPO1	-2,82	-2,72	-0,11	0
High	P43246-1	DNA mismatch repair protein MSH2 [OS=Homo sapiens]	14,9839768	4,28265525	4	6	4	934	104,677	MSH2	-1,65	-2,74	1,09	0
High	Q8NE71-1	ATP-binding cassette sub-family F member 1 [OS=Homo sapiens]	13,5419358	4,14201183	3	5	3	845	95,866	ABCF1	-2,67	-2,74	0,07	0
High	Q9NRZ9	Lymphoid-specific helicase [OS=Homo sapiens]	5,4307832	3,69928401	3	3	3	838	97,012	HELLS	-2,31	-2,75	0,44	0
High	Q9Y2J2	Band 4.1-like protein 3 [OS=Homo sapiens]	88,048902	19,9632015	17	31	14	1087	120,603	EPB41L3	-2,41	-2,76	0,35	0
High	Q9BZF3-5	Isoform 5 of Oxysterol-binding protein-related protein 6 [OS=Homo sapiens]	143,684751	30,9697602	24	64	24	959	108,89	OSBPL6	-2,25	-2,77	0,53	0
High	Q8IVF7	Formin-like protein 3 [OS=Homo sapiens]	16,809594	3,21011673	4	6	2	1028	117,139	FMNL3	-2,67	-2,77	0,1	0
High	Q16531	DNA damage-binding protein 1 [OS=Homo sapiens]	49,6494258	11,9298246	12	18	12	1140	126,887	DDB1	-2,96	-2,78	-0,18	0
High	Q9H307	Pinin [OS=Homo sapiens]	22,3555408	7,53138075	6	11	6	717	81,565	PNN	-2,69	-2,78	0,09	0
High	Q14331	Protein FRG1 [OS=Homo sapiens]	33,1767188	21,7054264	6	13	6	258	29,154	FRG1	-2,65	-2,79	0,15	0
High	Q9P015	39S ribosomal protein L15, mitochondrial [OS=Homo sapiens]	9,61307735	14,8648649	4	5	4	296	33,399	MRPL15	-3,12	-2,83	-0,29	0
High	Q9Y5B6	PAX3- and PAX7-binding protein 1 [OS=Homo sapiens]	21,7801759	7,30643402	5	6	5	917	104,739	GCFC1; PAXBP1	-2,36	-2,85	0,49	0
Low	P54198	Protein HIRA [OS=Homo sapiens]	1,40329297	1,179941	1	1	1	1017	111,764	HIRA	-2,16	-2,86	0,7	0
High	Q7Z7K6-3	Isoform 3 of Centromere protein V [OS=Homo sapiens]	105,706017	48,1617647	10	40	1	272	29,712	CENPV	-1,91	-2,87	0,95	0
High	Q9UJV9	Probable ATP-dependent RNA helicase DDX41 [OS=Homo sapiens]	1077,48304	91,9614148	74	675	74	622	69,793	DDX41	-3,57	-2,92	-0,64	0
High	Q96PY5-3	Isoform 2 of Formin-like protein 2 [OS=Homo sapiens]	8,41347337	3,20512821	4	4	2	1092	124,029	FMNL2	-2,73	-2,93	0,2	1
High	Q99697-2	Isoform Ptx2C of Pituitary homeobox 2 [OS=Homo sapiens]	7,48630016	11,7283951	3	3	3	324	35,773	PITX2	-1,67	-2,95	1,27	0
High	Q9H1J1-1	Regulator of nonsense transcripts 3A [OS=Homo sapiens]	11,8167297	10,2941176	5	9	5	476	54,663	UPF3A	-3,3	-2,98	-0,32	0
High	Q9BUQ8	Probable ATP-dependent RNA helicase DDX23 [OS=Homo sapiens]	13,9819576	7,07317073	5	5	5	820	95,524	DDX23	-2,69	-3	0,3	0
High	Q9H0A0	N-acetyltransferase 10 [OS=Homo sapiens]	533,956463	58,9268293	58	227	58	1025	115,657	NAT10	-2,88	-3,01	0,13	0
High	O43290	U4/U6.U5 tri-snRNP-associated protein 1 [OS=Homo sapiens]	64,6313822	20,25	12	25	12	800	90,2	SART1	-3,1	-3,07	-0,03	0
High	P00338-3	Isoform 3 of L-lactate dehydrogenase A chain [OS=Homo sapiens]	10,1133893	8,58725762	3	3	2	361	39,812	LDHA	-3,31	-3,09	-0,22	1
Low	Q9H8V3-3	Isoform 3 of Protein ECT2 [OS=Homo sapiens]	1,59142087	1,35699374	1	1	1	958	108,461	ECT2	-2,53	-3,12	0,58	0
Low	P23458	Tyrosine-protein kinase JAK1 [OS=Homo sapiens]	1,66154351	0,6932409	1	1	1	1154	133,191	JAK1	-2,46	-3,14	0,68	0
High	Q13393-2	Isoform PLD1B of Phospholipase D1 [OS=Homo sapiens]	114,511277	22,6833977	20	44	20	1036	119,618	PLD1	-2,75	-3,22	0,47	0
High	Q9H6R4-1	Nucleolar protein 6 [OS=Homo sapiens]	218,463919	30,2792321	29	88	29	1146	127,513	NOL6	-3,12	-3,23	0,11	0
High	Q9ULK5	Vang-like protein 2 [OS=Homo sapiens]	6,22033029	4,41458733	2	2	2	521	59,677	VANGL2	-2,54	-3,29	0,75	0
High	Q14697-2	Isoform 2 of Neutral alpha-glucosidase AB [OS=Homo sapiens]	4,63735639	1,96687371	2	2	2	966	109,369	GANAB	-2,74	-3,29	0,55	0
High	P78347	General transcription factor II-I [OS=Homo sapiens]	47,4478146	16,9338677	15	19	15	998	112,346	GTF2I	-3,07	-3,33	0,26	0
High	Q9BVJ6-1	U3 small nucleolar RNA-associated protein 14 homolog A [OS=Homo sapiens]	71,3007739	28,4046693	18	30	18	771	87,924	UTP14A	-2,7	-3,35	0,65	0
High	Q14566	DNA replication licensing factor MCM6 [OS=Homo sapiens]	5,49306446	3,04506699	2	2	2	821	92,831	MCM6	-3,4	-3,4	0,01	0
High	Q13206	probable ATP-dependent RNA helicase DDX10 [OS=Homo sapiens]	6,61153906	4,22857143	3	3	3	875	100,825	DDX10	-2,58	-3,43	0,85	0
High	P78316	Nucleolar protein 14 [OS=Homo sapiens]	20,3128562	11,3185531	9	9	9	857	97,607	NOP14	-2,62	-3,48	0,86	0
Medium	Q8WVS4	WD repeat-containing protein 60 [OS=Homo sapiens]	3,73728082	1,31332083	1	2	1	1066	122,496	WDR60	-2,09	-3,5	1,4	0
High	O95696-2	Isoform 2 of Bromodomain-containing protein 1 [OS=Homo sapiens]	5,89359415	1,51387721	2	2	2	1189	133,159	BRD1; LOC9083	-2,04	-3,61	1,56	0
High	P21741	Midkine [OS=Homo sapiens]	55,315584	60,1398601	9	22	9	143	15,575	MDK	-3,9	-3,64	-0,26	0
High	Q8TDD1	ATP-dependent RNA helicase DDX54 [OS=Homo sapiens]	213,72647	53,5754824	38	92	1	881	98,534	DDX54	-3,15	-3,74	0,59	29
High	O94813	Slit homolog 2 protein [OS=Homo sapiens]	228,664929	36,559843	47	112	47	1529	169,759	SLIT2	-3,84	-3,87	0,03	0
Medium	Q9UDR5	Alpha-aminoadipic semialdehyde synthase, mitochondrial [OS=Homo sapiens]	2,80715388	1,07991361	1	1	1	926	102,066	AASS	-2,99	-3,88	0,89	0
High	Q9NNW5	WD repeat-containing protein 6 [OS=Homo sapiens]	12,1064491	3,38983051	4	5	4	1121	121,647	WDR6	-3,39	-3,93	0,53	0
Low	Q96DT7	Zinc finger and BTB domain-containing protein 10 [OS=Homo sapiens]	1,75251774	0,9184845	1	1	1	871	94,835	ZBTB10	-2,85	-3,94	1,1	0
High	Q86YT6	E3 ubiquitin-protein ligase mib1 [OS=Homo sapiens]	22,2950593	7,35586481	6	6	6	1006	110,066	MIB1	-4,86	-4,09	-0,77	0
High	O00566	U3 small nucleolar ribonucleoprotein protein Mpp10 [OS=Homo sapiens]	17,1993603	10,5726872	6	8	6	681	78,816	MPHOSPH10	-4,14	-4,13	0	0
High	P13647	keratin, type II cytoskeletal 5 [OS=Homo sapiens]	89,6782869	29,8305085	23	128	9	590	62,34	KRT5	-4,55	-4,4	-0,16	2
Low	P15924-1	Desmoplakin [OS=Homo sapiens]	1,98422124	0,20898642	1	1	1	2871	331,569	DSP	-4,59	-4,47	-0,12	0
High	Q8IY81	pre-rRNA processing protein FTSJ3 [OS=Homo sapiens]	209,793733	48,7603306	32	95	32	847	96,499	FTSJ3	-4,15	-4,53	0,38	0
High	Q9Y4F1-2	Isoform 2 of FERM, RhoGEF and pleckstrin domain-containing protein 1 [OS=Ho	20,6624913	6,87732342	7	8	7	1076	122,037		-3,81	-4,68	0,87	0
High	Q15154-1	Pericentriolar material 1 protein [OS=Homo sapiens]	96,271205	14,7727273	25	38	24	2024	228,392	PCM1	-4,06	-4,78	0,71	1
High	P35579-1	Myosin-9 [OS=Homo sapiens]	886,61125	65,1530612	143	375	123	1960	226,392	MYH9	-5,55	-4,93	-0,62	14
Low	Q02413	Desmoglein-1 [OS=Homo sapiens]	1,67778071	0,95328885	1	1	1	1049	113,676	DSG1	-5,24	-5,12	-0,12	0
High	Q9UPS8-3	Isoform 3 of Ankyrin repeat domain-containing protein 26 [OS=Homo sapiens]	288,748634	40,7602339	65	123	65	1710	196,289	ANKRD26	-5,04	-5,25	0,21	0
High	Q9HC84	Mucin-5B [OS=Homo sapiens]	11,2083978	2,09996529	4	5	4	5762	595,96	MUC5B	-5,37	-5,25	-0,12	0
High	Q6P1M3-1	Lethal(2) giant larvae protein homolog 2 [OS=Homo sapiens]	79,8682486	25,6862745	19	31	19	1020	113,377	LLGL2	-5,34	-5,36	0,02	0
High	O15042	U2 snRNP-associated SURP motif-containing protein [OS=Homo sapiens]	19,9016046	6,80272109	7	10	6	1029	118,219	U2SURP	-5,86	-6,03	0,17	0
High	Q15334	Lethal(2) giant larvae protein homolog 1 [OS=Homo sapiens]	104,052738	30,7330827	25	43	25	1064	115,346	LLGL1	-6,3	-6,21	-0,09	0
Medium	O00178	GTP-binding protein 1 [OS=Homo sapiens]	4,42355176	2,3916293	1	2	1	669	72,408	GTPBP1	1,31	-6,31	7,62	0
Low	Q96F15-2	Isoform 2 of GTPase IMAP family member 5 [OS=Homo sapiens]	1,33114835	5,76368876	1	2	1	347	39,559	GIMAP5	-6,46	-6,41	-0,06	0
Medium	Q9HBE1-1	POZ-, AT hook-, and zinc finger-containing protein 1 [OS=Homo sapiens]	3,34263419	3,34788937	2	2	2	687	74,013	PATZ1	-6,83	-6,65	-0,17	0

Low	Q13123	Protein Red [OS=Homo sapiens]	1,53595779	1,61579892	1	1	1	557	65,562	IK	-6,82	-6,65	-0,17	0
Medium	Q5T749	Keratinocyte proline-rich protein [OS=Homo sapiens]	3,38053481	3,45423143	2	3	2	579	64,093	KPRP	-7,15	-7,02	-0,12	0
Medium	O15344-1	E3 ubiquitin-protein ligase Midline-1 [OS=Homo sapiens]	4,49972043	5,09745127	2	2	2	667	75,203	MID1	-7,21	-7,07	-0,13	0
Medium	P06702	Protein S100-A9 [OS=Homo sapiens]	3,60240757	13,1578947	1	1	1	114	13,234	S100A9	-7,48	-7,35	-0,13	0
Medium	Q13617-2	Isoform 2 of Cullin-2 [OS=Homo sapiens]	2,77607553	2,87958115	2	2	2	764	89,434	CUL2	-7,54	-7,37	-0,17	0
Low	Q8IWU5-1	Extracellular sulfatase Sulf-2 [OS=Homo sapiens]	1,41240127	1,14942529	1	2	1	870	100,39	SULF2	-7,52	-7,39	-0,13	0
Medium	P35637-1	RNA-binding protein FUS [OS=Homo sapiens]	4,49599018	5,89353612	2	2	2	526	53,394	FUS	-7,77	-7,64	-0,13	0
Medium	P52292	Importin subunit alpha-1 [OS=Homo sapiens]	2,46205504	3,78071834	1	1	1	529	57,826	KPNA2	-7,82	-7,68	-0,13	0
High	P02545	Prelamin-A/C [OS=Homo sapiens]	6,43280034	4,81927711	3	3	2	664	74,095	LMNA	-7,82	-7,69	-0,13	0
Low	P14923	Junction plakoglobin [OS=Homo sapiens]	1,9633711	1,61073826	1	1	1	745	81,693	JUP	-8,14	-7,97	-0,17	0
High	Q9P2Y4	Zinc finger protein 219 [OS=Homo sapiens]	12,7969393	9,41828255	5	5	5	722	76,83	ZNF219	-8,27	-8,1	-0,17	0
High	Q9UGM3-4	Isoform 4 of Deleted in malignant brain tumors 1 protein [OS=Homo sapiens]	10,4731051	6,8762279	3	4	3	1527	166,395		-8,26	-8,14	-0,12	0
Medium	Q5SRE5	Nucleoporin NUP188 homolog [OS=Homo sapiens]	2,86043573	0,91480846	1	1	1	1749	195,917	NUP188	-8,37	-8,17	-0,2	0
High	Q86YZ3	Hornerin [OS=Homo sapiens]	29,5309549	9,75438596	9	28	9	2850	282,228	HRNR	-8,37	-8,23	-0,14	0
Medium	O95985	DNA topoisomerase 3-beta-1 [OS=Homo sapiens]	3,53549913	1,85614849	2	2	2	862	96,599	TOP3B	-0,03	-8,27	8,24	0
High	Q9H089	Large subunit GTPase 1 homolog [OS=Homo sapiens]	5,14549848	4,7112462	2	3	2	658	75,178	LSG1	-8,68	-8,5	-0,17	0
Low	P55201-2	Isoform 2 of Peregrin [OS=Homo sapiens]	1,30644891	0,49180328	1	1	1	1220	138,099	BRPF1	-8,75	-8,55	-0,2	0
High	P02533	Keratin, type I cytoskeletal 14 [OS=Homo sapiens]	59,7140561	26,9067797	15	146	9	472	51,529	KRT14	-8,7	-8,57	-0,13	0
High	O43824	Putative GTP-binding protein 6 [OS=Homo sapiens]	21,310887	9,49612403	4	6	4	516	56,848	GTPBP6	0	-8,58	8,58	0
High	Q9NVI1-3	Fanconi anemia group I protein [OS=Homo sapiens]	4,70590131	2,10843373	3	5	3	1328	149,229	FANCI	-8,79	-8,58	-0,2	0
Medium	Q8IXM3	39S ribosomal protein L41, mitochondrial [OS=Homo sapiens]	2,74328225	7,29927007	1	1	1	137	15,373	MRPL41	-8,81	-8,75	-0,06	0
High	O14617-5	Isoform 5 of AP-3 complex subunit delta-1 [OS=Homo sapiens]	6,36997915	1,06995885	1	2	1	1215	136,565	AP3D1	-9,04	-8,83	-0,2	0
High	P61204	ADP-ribosylation factor 3 [OS=Homo sapiens]	22,4366542	28,7292818	3	6	2	181	20,588	ARF3	-9,07	-9,01	-0,06	0
Low	Q9UM00-1	Transmembrane and coiled-coil domain-containing protein 1 [OS=Homo sapien	1,91901295	7,9787234	1	1	1	188	21,161	TMCO1	-9,13	-9,07	-0,06	0
High	P62316	Small nuclear ribonucleoprotein Sm D2 [OS=Homo sapiens]	9,26388775	24,5762712	2	2	2	118	13,518	SNRPD2	-9,16	-9,1	-0,06	0
Low	P42345	Serine/threonine-protein kinase mTOR [OS=Homo sapiens]	1,66695597	0,43154178	1	1	1	2549	288,707	MTOR	-9,32	-9,15	-0,17	0
Low	Q53HL2	Borealin [OS=Homo sapiens]	1,61403643	3,57142857	1	1	1	280	31,304	CDCA8	-9,44	-9,28	-0,16	0
High	Q9NTW7	Zinc finger protein 64 homolog, isoforms 3 and 4 [OS=Homo sapiens]	9,42200071	6,66666667	3	5	1	645	72,17	ZFP64	-9,52	-9,33	-0,19	0
Medium	Q9NSI2-1	protein FAM207A [OS=Homo sapiens]	3,31497521	5,2173913	1	1	1	230	25,441	FAM207A	-9,53	-9,46	-0,07	0
Medium	P14618	Pyruvate kinase PKM [OS=Homo sapiens]	2,35704112	2,44821092	1	1	1	531	57,9	PKM	-9,64	-9,51	-0,13	0
Low	Q14240-2	Isoform 2 of Eukaryotic initiation factor 4A-II [OS=Homo sapiens]	1,84771166	1,96078431	1	1	1	408	46,46	EIF4A2	-9,73	-9,54	-0,19	0
Medium	P62937	peptidyl-prolyl cis-trans isomerase A [OS=Homo sapiens]	3,1283687	8,48484848	1	1	1	165	18,001	PPIA	-9,62	-9,56	-0,06	0
Medium	Q8WVK2	U4/U6.U5 small nuclear ribonucleoprotein 27 kDa protein [OS=Homo sapiens]	3,0790944	6,4516129	1	1	1	155	18,849	SNRNP27	-9,67	-9,62	-0,06	0
High	P01605	Ig kappa chain V-I region Lay [OS=Homo sapiens]	21,7900992	25	2	19	1	108	11,827		-9,69	-9,63	-0,07	0
Medium	P00747	Plasminogen [OS=Homo sapiens]	3,34852815	0,98765432	1	4	1	810	90,51	PLG	-9,82	-9,65	-0,17	0
High	Q9UH99-2	Isoform 2 of SUN domain-containing protein 2 [OS=Homo sapiens]	12,9573322	6,6395664	5	6	5	738	82,452	SUN2	-9,83	-9,66	-0,17	0
High	P02768-1	Serum albumin [OS=Homo sapiens]	15,5806401	9,68801314	6	21	6	609	69,321	ALB	-9,89	-9,73	-0,16	0
Low	Q96T58	Msx2-interacting protein [OS=Homo sapiens]	1,91364017	0,27292576	1	6	1	3664	402,004	SPEN	-9,92	-9,78	-0,13	0
Medium	Q96NB2	Sideroflexin-2 [OS=Homo sapiens]	2,76170293	3,72670807	1	1	1	322	36,208	SFXN2	-9,87	-9,8	-0,07	0
Medium	P00736	Complement C1r subcomponent [OS=Homo sapiens]	3,35575841	1,27659574	1	1	1	705	80,067	C1R	-9,95	-9,88	-0,07	0
High	P07355-2	Isoform 2 of Annexin A2 [OS=Homo sapiens]	55,2638992	42,8571429	12	43	12	357	40,386	ANXA2	-9,96	-9,89	-0,07	0
High	E9PAV3	Nascent polypeptide-associated complex subunit alpha, muscle-specific form [(	9,7574984	1,63618864	3	3	3	2078	205,295	NACA	-9,96	-9,9	-0,06	0
High	P0C0S5	Histone H2A.Z [OS=Homo sapiens]	27,2148646	31,25	4	26	2	128	13,545	H2AFZ	0,37	-9,92	10,29	0
High	P01764	Ig heavy chain V-III region 23 [OS=Homo sapiens]	7,40077214	16,2393162	1	2	1	117	12,574	IGHV3-23	-10,13	-9,94	-0,19	0
High	Q9GZT4	serine racemase [OS=Homo sapiens]	5,79661264	8,23529412	2	2	2	340	36,543	SRR	-10,23	-10,07	-0,16	0
Medium	O95373	Importin-7 [OS=Homo sapiens]	3,65329684	2,69749518	2	2	2	1038	119,44	IPO7	-10,12	-10,11	0	0
High	P0C0L4-1	Complement C4-A [OS=Homo sapiens]	18,7308884	2,80963303	5	16	5	1744	192,664	C4A	-10,34	-10,18	-0,16	0
High	P13645	Keratin, type I cytoskeletal 10 [OS=Homo sapiens]	313,314096	66,609589	46	630	40	584	58,792	KRT10	-9,73	-10,19	0,46	7
Low	P42285	Superkiller viralicidic activity 2-like 2 [OS=Homo sapiens]	1,61475132	0,67178503	1	1	1	1042	117,729	SKIV2L2	-10,21	-10,2	0	0
High	Q9HCS7	Pre-mRNA-splicing factor SYF1 [OS=Homo sapiens]	8,14359667	3,2748538	3	3	3	855	99,946	XAB2	-10,26	-10,25	0	0
High	P02746	Complement C1q subcomponent subunit B [OS=Homo sapiens]	15,0241623	5,53359684	1	15	1	253	26,704	C1QB	-10,4	-10,26	-0,14	0
Low	Q9UNL2-2	Isoform 2 of Translocon-associated protein subunit gamma [OS=Homo sapiens]	1,60153915	7,07070707	1	1	1	198	22,596	SSR3	-10,4	-10,34	-0,06	0
Medium	P17482	Homeobox protein Hox-B9 [OS=Homo sapiens]	3,22380749	5,2	1	1	1	250	28,041	HOXB9	-10,49	-10,43	-0,07	0
High	P07477	Trypsin-1 [OS=Homo sapiens]	6,81232138	11,3360324	2	15	2	247	26,541	PRSS1	-10,69	-10,56	-0,13	0
Low	Q9HC10	Otoferlin [OS=Homo sapiens]	1,33451282	0,75112669	1	3	1	1997	226,61	OTOF	-10,79	-10,59	-0,2	0
High	P35580-3	Isoform 3 of Myosin-10 [OS=Homo sapiens]	458,232604	49,9248873	97	189	78	1997	231,226	MYH10	-10,87	-10,67	-0,2	0
High	P35527	Keratin, type I cytoskeletal 9 [OS=Homo sapiens]	280,682081	68,0577849	38	494	37	623	62,027	KRT9	-10,81	-10,7	-0,11	0
Medium	Q6X4T0	Uncharacterized protein C12orf54 [OS=Homo sapiens]	2,29946934	13,3858268	1	1	1	127	14,476	C12orf54	-10,81	-10,75	-0,06	0
High	P01859	Ig gamma-2 chain C region [OS=Homo sapiens]	7,04613134	10,7361963	2	15	2	326	35,878	IGHG2	-10,92	-10,77	-0,15	0
High	O60264	SWI/SNF-related matrix-associated actin-dependent regulator of chromatin sut	4,99566813	2,18631179	2	2	2	1052	121,828	SMARCA5	-10,88	-10,87	0	0
High	Q8TF09	Dynein light chain roadblock-type 2 [OS=Homo sapiens]	4,94692156	12,5	1	2	1	96	10,848	DYNLRB2	-10,94	-10,88	-0,06	0

High	P02745	Complement C1q subcomponent subunit A [OS=Homo sapiens]	7,07746698	4,48979592	1	8	1	245	26	C1QA	-11,11	-10,92	-0,19	0
Low	P23435	Cerebellin-1 [OS=Homo sapiens]	1,85604888	3,62694301	1	12	1	193	21,084	CBLN1	-11,17	-11,01	-0,16	0
High	P06753-2	Isoform 2 of Tropomyosin alpha-3 chain [OS=Homo sapiens]	19,4267759	26,6129032	6	7	4	248	29,015	TPM3	-11,15	-11,09	-0,07	0
High	P35908	Keratin, type II cytoskeletal 2 epidermal [OS=Homo sapiens]	314,418826	78,4037559	57	465	42	639	65,393	KRT2	-11,32	-11,18	-0,14	5
High	Q8N9E0	Protein FAM133A [OS=Homo sapiens]	26,4183991	18,1451613	5	26	2	248	28,923	FAM133A	-11,42	-11,29	-0,12	0
High	P06310	Ig kappa chain V-II region RPMI 6410 [OS=Homo sapiens]	6,21360354	9,77443609	1	9	1	133	14,697		-11,44	-11,38	-0,06	0
High	O94832	Unconventional myosin-Id [OS=Homo sapiens]	32,5981977	10,7355865	11	11	11	1006	116,129	MYO1D	-11,44	-11,44	0	0
Low	Q8IYJ1	Copine-9 [OS=Homo sapiens]	1,9722428	5,06329114	1	4	1	553	61,825	CPNE9	-11,69	-11,57	-0,11	0
High	O14950	Myosin regulatory light chain 12B [OS=Homo sapiens]	10,835737	18,0232558	3	4	3	172	19,767	MYL12B	-11,7	-11,63	-0,06	0
Medium	P04434	Ig kappa chain V-III region VH [OS=Homo sapiens]	4,18002199	12,9310345	2	5	1	116	12,749	IGKV3-7	-11,76	-11,7	-0,07	1
Low	Q9H0J9	Poly [ADP-ribose] polymerase 12 [OS=Homo sapiens]	1,22380749	2,28245364	1	1	1	701	79,013	PARP12	-11,89	-11,7	-0,19	0
Low	Q5JU67-1	Uncharacterized protein C9orf117 [OS=Homo sapiens]	1,93330145	2,11538462	1	1	1	520	60,496	)orf117; CFAP1	-11,77	-11,71	-0,06	0
High	O43795	Unconventional myosin-Ib [OS=Homo sapiens]	27,2572044	11,7077465	9	9	9	1136	131,902	MYO1B	-11,79	-11,78	0	0
High	P06314	Ig kappa chain V-IV region B17 [OS=Homo sapiens]	10,7214567	23,1343284	3	33	3	134	14,956		-12,04	-11,88	-0,17	0
High	Q86Y91-4	Isoform 4 of Kinesin-like protein KIF18B [OS=Homo sapiens]	7,70150584	2,29095074	2	3	2	873	95,069		-11,93	-11,93	0	0
High	P04264	Keratin, type II cytoskeletal 1 [OS=Homo sapiens]	404,093232	63,5093168	53	806	44	644	65,999	KRT1	-12,14	-12,03	-0,11	1
Medium	P62314	Small nuclear ribonucleoprotein Sm D1 [OS=Homo sapiens]	4,39340369	10,9243697	1	1	1	119	13,273	SNRPD1	-12,09	-12,03	-0,06	0
High	P01876	Ig alpha-1 chain C region [OS=Homo sapiens]	16,5093344	17,8470255	5	9	5	353	37,631	IGHA1	-12,23	-12,23	0	0
Medium	P01023	alpha-2-macroglobulin [OS=Homo sapiens]	3,82179886	1,01763908	2	6	2	1474	163,188	A2M	-12,39	-12,33	-0,06	0
High	P60660	Myosin light polypeptide 6 [OS=Homo sapiens]	36,266481	47,0198675	7	14	7	151	16,919	MYL6	-12,71	-12,65	-0,06	0
High	P01024	Complement C3 [OS=Homo sapiens]	33,2572719	4,99098016	6	18	6	1663	187,03	C3	-12,8	-12,71	-0,09	0
High	O00159-1	Unconventional myosin-Ic [OS=Homo sapiens]	55,8664137	18,2502352	20	24	20	1063	121,606	MYO1C	-12,73	-12,72	0	0
Low	Q3V6T2-1	Girdin [OS=Homo sapiens]	1,43711262	0,64136825	1	2	1	1871	215,909	CCDC88A	-13,19	-13,14	-0,06	0
High	P01765	Ig heavy chain V-III region TIL [OS=Homo sapiens]	5,10934044	7,82608696	1	4	1	115	12,348		-13,43	-13,24	-0,19	0
Low	O15247	Chloride intracellular channel protein 2 [OS=Homo sapiens]	1,60380065	6,07287449	1	5	1	247	28,338	CLIC2	-14,74	-14,55	-0,19	0

Annex Table IV: Liquid chromatography-tandem mass spectrometry (LC-MS/MS) data from SILAC (MMC treatment). The data were analyzed using SEQUEST in Proteome Discoverer 2.1 and searched in the complete human proteome database (Swiss-Prot). Peptide identification was filtered at a false discovery rate (FDR) < 1%. Coverage: percentage of the protein sequence covered by identified peptides (confident coverage threshold >1). Peptides: total number of distinct peptide sequences identified in the protein group. PSMs: total number of identified peptide spectra matched for the protein. Unique peptides: The number of peptide sequences that are unique to a protein group. MW: molecular weight. Abundance ratios are calculated based on light (for XPF-KO cells untreated), medium (for XPF-KO + XPF-Wt treated with MMC 0.5mg/mL during 21h), heavy (for XPF-KO + XPF-Wt untreated) forms of lysine and arginine. Razor peptides: peptides that can be assigned to more than one protein.